Elucidation of *Aegilops tauschii* contribution to heat and drought tolerance diversity in bread wheat through genomics and metabolomics

(ゲノミクスとメタボロミクスに基づく
タルホコムギのパンコムギ耐暑・耐乾性変異への貢献解明**)**

Itam, Michael Okoi

2021

Elucidation of *Aegilops tauschii* contribution to heat and drought tolerance diversity in bread wheat through genomics and metabolomics

(ゲノミクスとメタボロミクスに基づく
タルホコムギのパンコムギ耐暑・耐乾性変異への貢献解明**)**

A thesis submitted to the United Graduate School of Agricultural Sciences, Tottori University in partial fulfilment of the requirements for the award of Doctor of Philosophy (PhD) in Dryland Agriculture (Plant Molecular Breeding)

By

Itam, Michael Okoi

Approved by:

Prof. **Dr Motoichiro Kodama** ……

Dean, United Graduate School of Agricultural Sciences, Tottori University

Prof. **Dr Hisashi Tsujimoto**…….……....

Chairman, supervisory committee

The United Graduate School of Agricultural Sciences, Tottori University

2021

Dedication

This work is dedicated to all young people who have the audacity to dream big and the determination to make it come true, despite the odds.

Acknowledgements

I am grateful to the Ministry of Education, Culture, Sports, Science and Technology (MEXT) for awarding me a scholarship to study and fulfil my dreams.

My profound gratitude goes to my supervisor, Prof. H. Tsujimoto for his guidance, compassion and motivation, without which I would not have had the courage to complete this work.

I am indebted to my co-supervisors: Prof. M. Shigyo (Yamaguchi University) and Prof. K. Akashi for their guidance and willingness to offer assistance at all times, and for thoroughly correcting this work.

I am very grateful to Prof. B. E. Ubi (Ebonyi State University, Nigeria) for his mentorship and support for my career growth.

My special thanks go to the students and staff of the Laboratory of Molecular Breeding, Arid Land Research Center for their kindness and support especially Dr Y. S. A. Gorafi, Dr T. Ishii, Dr Y. Yamasaki, and Dr R. Mega (now in Yamaguchi University) for their collaboration and scientific appraisal which has helped to improve this work.

I appreciate the management and staff of Agricultural Research Corporation, Wad Medani, Sudan, especially Dr I. S. A. Tahir and Dr A. A. M. Idris for their technical support and hospitality during the field study. I also thank the technical staff of Arid Land Research Center, Tottori University for their tremendous support in making my work a success.

Finally, I would like to thank my family in Nigeria especially my parents, Mr and Mrs F. Itam for their love, prayers and support, and for raising me to believe in my abilities. My very special thanks go to the father of knowledge and giver of life, God almighty.

Table of contents

General Introduction

Wheat (*Triticum aestivum* L.) is one of the most important staple-food crops and key sources of food calories in the world, with high demand in developing countries (Shiferaw *et al.* 2011). However, drought and heat stresses have been a persistent problem hindering global wheat production. This problem has been exacerbated by climate change and rising global population. Therefore, it is necessary to develop new methods to ensure sustainable wheat production.

One of such methods is the use of wheat wild relatives known to possess desirable abiotic stress resilience genes. One of such relatives is *Aegilops Tauschii* (Coss.), the D genome progenitor of bread wheat. *Ae. tauschii* has been widely utilized in introgressions with durum wheat or in direct hybridization with elite bread wheat cultivars (Tsujimoto *et al.* 2015; Cox *et al.* 2017). Thus, if a large number of *Ae. tauschii* accessions is used in such crosses, a high diversity population of bread wheat will be formed, paving the way for in-depth exploration of the diversity in *Ae. tauschii* for breeding heat and drought-resilient wheat lines.

In this study, a bread wheat diversity panel previously developed using 43 accessions of *Ae. tauschii* (Tsujimoto *et al.* 2015; Gorafi *et al.* 2018) was studied to elucidate the diversity in heat and drought stress resilience, understand the mechanism of heat and drought stress resilience, and select candidate lines for climate resilience breeding.

This thesis is partitioned into six chapters. Chapter 1 was conducted in Wad Medani, Sudan to identify quantitative trait loci (QTLs) associated with heat and combined heat-drought resilience in bread wheat under field conditions. Chapter 2 and 3 were conducted in greenhouses in Tottori, Japan to validate selected candidate lines and to characterize their water conservation traits using physiological methods. Chapter 4 and 5 were conducted in growth chambers to elucidate the physiological and metabolic responses of bread wheat to drought stress at the reproductive (Chapter 4) and seedling (Chapter 5) stages. For emphasis, the introductions to Chapters 1, 2, 3, and 5 each highlights the use of *Ae. tauschii* for increasing wheat diversity. Finally, Chapter 6 is general discussion and conclusion. Study overview is shown in Figure 1.0.

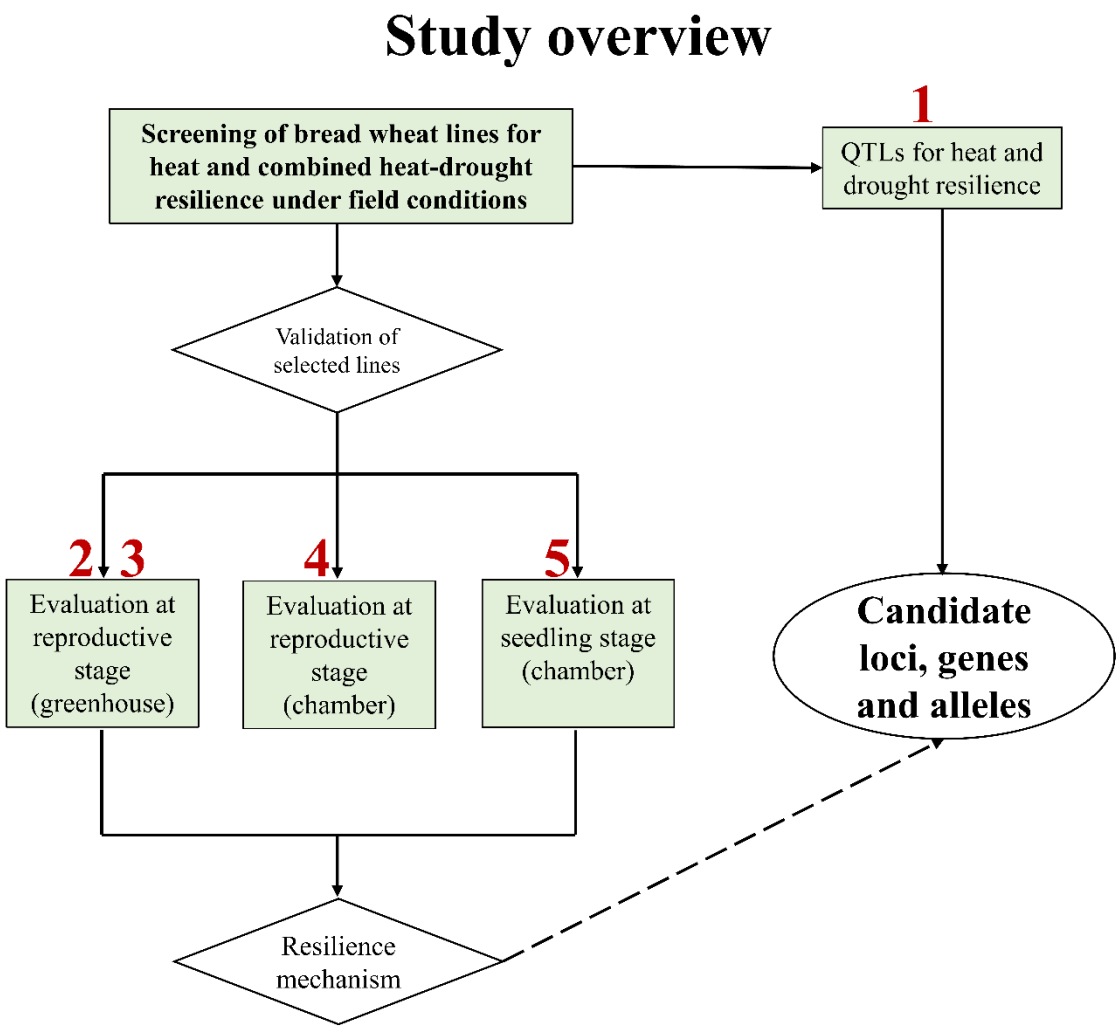

Figure 1.0. Study overview showing the sequence of studies from the field through greenhouses to growth chambers and laboratory. The numbers in red correspond to the chapters in this thesis.

Chapter 1

Genomic analysis for heat and combined heat-drought resilience in bread wheat under field conditions

1.1 Introduction

In many wheat-growing regions, heatwaves and drought episodes occur concurrently and are considered the most damaging climatic stressors for wheat (Zampieri *et al.* 2017). In the current climate change scenario, every 1°C rise in global mean temperature results in a 6% reduction in wheat yield, and a 17% increase in agricultural water supply is needed to prevent drought stress (Pennisi 2008; Zhao *et al.* 2017). This implies that global wheat production will continue to be lower than demand, especially as global population increases (Food and Agriculture Organization of the United Nations 2020). In semiarid regions, where heatwaves and drought episodes are common, an annual grain yield (GY) increase of up to 2.7% is needed (Iizumi *et al.* 2021). Such an increase may be difficult to achieve using the current elite germplasm, which has a narrow gene pool (Ogbonnaya *et al.* 2013). Therefore, the use of new genetic resources has the potential to facilitate wheat breeding for resilience to combined stresses (Reynolds *et al.* 2015).

Wheat wild relatives such as *Ae. tauschii*, the D genome progenitor of bread wheat, are a good source for developing new genetic materials (Tsujimoto *et al.* 2015). A wheat multiple synthetic derivative (MSD) population was developed using 43 *Ae. tauschii* accessions as a platform to explore the genetic diversity of *Ae. tauschii* for wheat improvement (Tsujimoto *et al.* 2015). This population exhibited high genetic diversity when characterized under heat (H) stress in Sudan (Elbashir *et al.* 2017a). Under drought stress in Japan, some MSD lines showed better adaptation than their backcross parent and check cultivars (Itam *et al.* 2020a, 2021). However, the genetic basis of the diversity in resilience to H, drought, and combined heat–drought (HD) stress has not been fully explored. Moreover, there are yet no reports on genome-wide association studies (GWAS) of HD in bread wheat under natural field conditions. Qaseem et al. (2019) and Schmidt et al. (2020) reported shared genomic regions across different conditions, including HD stress, in wheat cultivars and landraces grown in polytunnels. A few other GWAS conducted

under similar or more controlled environments have been extensively reviewed (Tricker *et al.* 2018). However, results from controlled environments may not be replicated in natural field conditions, and information from field conditions is needed to apply the findings to practical breeding.

The objective of this study was to identify QTLs associated with H and HD stress resilience in bread wheat under field conditions, and to assess the practicability of harnessing *Ae. tauschii* diversity for combined stress resilience breeding. I evaluated a systematically selected wheat diversity panel (consisting of 145 MSD lines) under H and HD in Wad Medani, Sudan, in 2019 and 2020, and identified novel alleles and QTLs for several traits, including GY and related traits. The loci for most leaf traits, including canopy temperature and Normalized Difference Vegetation Index (NDVI), were pleiotropic for GY and related traits. The expression patterns of the candidate genes (according to the data in a transcriptome database) indicate the role of gibberellin homeostasis in maintaining GY stability and of CaaX prenylation in regulating canopy temperature under the combined stress. This study provides new genetic materials and QTLs for breeding wheat with improved resilience to H and HD conditions.

1.2 Materials and Methods

1.2.1 Plant Materials

A diversity panel of 145 MSD lines and 5 check cultivars was used for this study (Table 1.1). The 145 lines are a subset of 400 MSD lines characterized for H tolerance in Sudan (Elbashir *et al.* 2017a). The MSD panel contained introgressions from 37 accessions of *Ae. tauschii* (DD genome) and the durum wheat cultivar 'Langdon' (AABB genome) (Matsuoka and Nasuda 2004). The *Ae. tauschii* accessions used were originally collected from HD stress–prone areas in the Middle East and Central Asia, including China and the Caucasus. The resulting synthetic hexaploid lines (AABBDD) were crossed with the Japanese bread wheat cultivar 'Norin 61' (hereafter N61, AABBDD). To reduce linkage drag, the F_1 hybrids were backcrossed to N61 (Tsujimoto *et al.* 2015). Therefore, the A and B genomes of the MSD lines are biparental (from

'Langdon' and N61), whereas the D genome is multiparental (from 37 *Ae. tauschii* accessions). A simplified breeding scheme of the MSD lines is shown in Fig. 1.1. The lines in the diversity panel were selected based on similar days to 50% heading (DH) and were evaluated under H and HD stress in Sudan during the 2018–19 (BC_1F_6 generation) and 2019–20 (BC_1F_7 generation) growing seasons.

1.2.2 Experimental Site and Design

All experiments were conducted at the Gezira Research Farm, Agricultural Research Corporation, Wad Medani, Sudan (14°24′N, 33°29′E, 407 m above sea level). The Gezira Research Farm is a dry, hot irrigated field categorized in mega-environment 5 for wheat cultivation (Gbegbelegbe *et al.* 2017). It has a heavy clay soil (pH 8.0–8.4) with low contents of organic matter (< 5%), nitrogen, and phosphorus (Elbashir *et al.* 2017a). Each experiment was designed in an alpha lattice with two replications. A total of 8 blocks per replication with 20 plots per block were used. Each plot had four rows, 1 m long and 0.2 m apart.

1.2.3 Field Management and Drought Treatment

Seeds were treated with the insecticide Gaucho (imidacloprid, 35% WP, Bayer Crop Science, Kansas City, MO, USA) at 0.75 g kg^{-1} seed to control insect pests. The treated seeds were manually sown at 120 kg ha^{-1} during the last week of November. Field management and drought treatment were as described in Elhadi et al. (2021). Before sowing, phosphorus was applied as superphosphate by furrow placement at a rate of 43 kg ha^{-1} of P_2O_5. Irrigation was applied every 10–12 days, and the plots were hand-weeded at least twice. Soil water potential was monitored every 2 h by sensors (Decagon Devices, Pullman, WA, USA) buried 20 cm in the soil. To create the HD condition, drought was imposed by withholding irrigation when 50% of all genotypes had reached flowering, while regular irrigation continued under the H condition. To avoid permanent wilting, plots under the HD condition were re-watered when the soil water potential approached −900 kPa (Fig. 1.2A and B). In Wad Medani, Sudan, there is no rain during the winter season and the relative humidity is generally low (Elsheikh *et al.* 2015). Field relative

humidity was obtained from January to March 2020 and the daytime value was between 20 and 30%. The air temperature and relative humidity of the field was obtained from the Sudan Meteorological Agency and from a weather station within the field.

1.2.4 Evaluated traits

1.2.4.1 Morphophysiological traits

Morphophysiological traits were measured according to Pask et al. (2012). Chlorophyll content (SPAD), ground cover (GC), and NDVI were measured during the grain filling stage. Canopy temperature (CT) was measured three times: at 7 days before flowering (CT1), during flowering (CT2), and during grain filling (CT3). Plant height (PH), biomass (BIO), number of spikes per m^2 (SN), number of kernels per spike (KPS), GY, thousand-kernel weight (TKW), and harvest index (HI) were determined at maturity. DH, days to maturity (DM), and grain-filling duration (GFD) were recorded.

1.2.4.2 ^{13}C isotope ($\delta^{13}C$) analysis

The ^{13}C composition of flag leaves was analysed using an elemental analyser connected to a continuous-flow isotope ratio mass spectrometer (EA/IRMS; Thermo Fisher Scientific) as described in Itam et al. (2020b). Dry flag leaf samples (1 mg) were put into tin capsules (5 mm × 9 mm, Lüdi Swiss, Switzerland) and entered into a combustion oven by an autosampler. Each sample was measured against CO_2 calibrated with an isotope standard to an accuracy of ±0.066‰ SD. Finally, the ^{13}C composition was calculated as $\delta^{13}C = [(R_{sample}/R_{standard}) - 1] \times 1000$, where R is the $^{13}C/^{12}C$ isotope ratio.

1.2.5 Genotyping-by-sequencing for association mapping

Total genomic DNA was extracted using the CTAB method (Saghai-Maroof *et al.* 1984), and DNA samples (20 µl; 50–100 ng μl^{-1}) were sent to Diversity Arrays Technology (DArT) Pty. Ltd., Australia (http://www.diversityarrays.com) for whole-genome scanning using DArT-seq markers. Complexity was reduced using a combination of restriction enzymes to obtain a subset

of restriction fragments for each sample (Sansaloni *et al.* 2011). The restriction fragments were then sequenced and aligned to the wheat_Chrom_Wheat_Norin61_v1.1 reference genome. The nucleotide polymorphisms (referred to as SNP markers) present in the restriction fragments were used for GWAS. The SNP markers are codominant in nature and were scored "0" (homozygous reference allele), "1" (homozygous SNP allele), or "2" (heterozygote). The markers were filtered on the basis of minimum reproducibility (95%), call rate (95%), and average read depth. A total of 14,383 SNP markers were used for association mapping.

1.2.6 Statistical analysis

Best linear unbiased estimates (BLUEs) were obtained for each trait under H and HD using the residual maximum likelihood (REML) method implemented in META-R (Alvarado *et al.* 2020). In BLUEs, genotypes and environments were considered as fixed factors, while replication and block were random factors. To minimize the possible confounding effect of heading date, another set of BLUEs (adjusted BLUEs) was calculated by using DH as a covariate (Sukumaran *et al.* 2018). To separate drought response (DR) from H response in the HD condition, I divided the predicted means under HD by those under H for all traits except DH (Schmidt *et al.* 2020). Analysis of variance was performed for all evaluated traits in GenStat 19th edition (http://www.genstat.co.uk). Broad-sense heritability was estimated for each trait in Plant Breeding Tools v. 1.3 (http://bbi.irri.org). To assess genotype stability across different conditions, GY stability index was calculated using the Finlay–Wilkinson regression model: $y_{ij} = \mu + G_i + \beta_i E_j + \varepsilon_{ij}$, where the regressand y_{ij} is the mean GY of the genotype, the intercept $\mu + G_i$ corresponds to the genetic main effect, the slope β_i corresponds to genotype variability in GY across environments (i.e., GY stability index), the regressor E_j is the population-wide variability in GY across environments (i.e., environmental index), and ε_{ij} is the error term (Finlay and Wilkinson 1963).

1.2.7 Genome-Wide Association Study

Genome-wide association analysis was performed with the BLUEs for H, HD, and DR in 2019 and 2020, using the generalized linear model and mixed linear model implemented in TASSEL v. 5 (Bradbury *et al.* 2007). The generalized linear model was fitted with principal components, and the mixed linear model was fitted with principal components and a kinship matrix (Yu *et al.* 2006). The best-fit model for each dataset was selected using quantile–quantile plots. Significant marker–trait associations (MTAs) were determined at a threshold of $-\log(p) = 3$, and the quantile–quantile and Manhattan plots were generated in the R package "qqman" (Turner 2018). Then, the *p*-values were adjusted for multiple testing using false discovery rate (FDR) (Benjamini and Hochberg 1995) at the 0.05 and 0.2 thresholds. To better explore the contribution of the *Ae. tauschii* D genome, I also conducted a D genome–wide analysis using only the D genome markers. Because the A and B genomes in this panel are biparental whereas the D genome is multiparental, conducting an additional GWAS on the D genome increased the statistical power of the analysis. Stable MTAs were found in two or more conditions, and pleiotropic MTAs were found for two or more traits. To identify candidate genes, I conducted a BLASTN search of significant markers against the IWGSC RefSeq v. 1.0 (https://urgi.versailles.inra.fr/blast/), and the expression patterns of two candidate genes were investigated in the Genevestigator software (www.genevestigator.com).

1.3 Results

1.3.1 Field condition in 2019 and 2020

The average air temperature at the Gezira Research Farm ranged from 21.6 to 33.1°C in 2019 and from 17.4 to 28.0°C in 2020. The maximum temperature ranged from 30.8 to 43.0°C in 2019 and from 27.0 to 43.5°C in 2020. As expected, the highest air temperatures were recorded towards the end of the growing season which corresponds to the reproductive stages in both years (Fig. 1.2A and B). Soil water potential decreased from near 0 before drought stress to near −900 kPa during severe HD stress in both seasons (Fig. 1.2C and D).

1.3.2 Heat and combined heat-drought effect on trait variability under field conditions

Plants in the two treatments (H and HD) were grown under the natural heat condition with regular irrigation until anthesis. Irrigation was then withheld in the HD condition to induce combined stress, whereas, the H treatment was regularly irrigated to ensure that only heat stress was imposed (Fig. 1.2). This resulted in H and post-anthesis HD stress. Highly significant differences were observed between the main effects of genotype and environment for most of the evaluated traits in each year. The genotype by environment (G×E) interaction effects were significant for DM, GFD, GY, KPS, SPAD and TKW in 2019, and for GY, HI, and KPS in 2020 (Table 1.2).

Heritability estimates were similar between 2019 and 2020. DH, HI, and PH had consistently higher heritability values (ranging from 0.70 to 0.89) than other traits, whereas BIO, CT1, CT2, CT3, SN, and SPAD had relatively lower heritability estimates (Table 1.3). CT2 had moderate heritability, indicating a significant genetic control, whereas under H condition heritability was low, indicating low genetic control (Table 1.3). Except for CT2 in 2019, mean CT values tended to be lower under HD than under H condition. The DM, GFD, HI, and TKW values were also lower under HD than under H condition in both years. Consequently, GY was lower under HD than under H, indicating a more severe effect of the HD condition (Table 1.3). The mean GY was 2735 kg ha^{-1} under H and 1588 kg ha^{-1} under HD in 2019, and 3116 and 2297 kg ha^{-1}, respectively, in 2020, indicating higher performance ($p < 0.05$) in 2020.

GY correlated significantly ($p < 0.05$) with most of the evaluated traits in both conditions in both years (Table 1.4). The GY–BIO and GY–HI correlations were consistently high, with correlation coefficients (r) ranging from 0.564 to 0.742 ($p < 0.01$) in both conditions in both years. In contrast, all CT values were negatively correlated with most traits, including GY and BIO, under H in 2019 and under both conditions in 2020 (Table 1.4). Similarly, $\delta^{13}C$ was negatively correlated with GY in both conditions, and with BIO, HI, and SPAD under HD in 2019. DH and GFD were negatively correlated in both conditions in both years (Table 1.4). Additionally, I found

low positive correlations between the two conditions for most traits, except DH and PH which had high correlations (r = 0.619–0.806, Table 1.4) likely because the combined stress was imposed after heading.

Some MSD lines had higher average yield performance under H and HD conditions than the check cultivars, indicating significant genetic gains (Fig. 1.3A). Also, some MSD lines had higher DR values than the check cultivars in both years (Fig. 1.3B). The decreasing yield trend under HD conditions is shown in Fig. 1.3C. Yield stability index was higher in some MSD lines than in the check cultivars, including N61 and 'Imam' (Fig. 1.3D). A list of the lines with high GY and considerable GY stability is shown in Table 1.5.

1.3.3 MTAs

Many significant MTAs were identified for various traits, with 12% and 27% of the MTAs passing the FDR 0.05 and 0.2 thresholds, respectively. In 2019, 75 MTAs for H, 4 for HD, and 25 for DR passed the FDR tests; in 2020, 23 MTAs for H, 62 for HD, and 123 for DR passed (Fig. 1.4A). In total, 100 highly significant MTAs (FDR < 0.2) were associated with H, 68 with HD, and 150 with DR in both years (including MTAs for GY stability index, Table 1.6). About 70% of all MTAs were for GY, KPS, NDVI, and CT (Fig. 1.4B). The MTAs were found on 19 chromosomes, and 56.6% of all MTAs were found on chromosomes (Chromosomes) 2D, 3D, 5D, and 7D (Fig. 1.4C). The MTAs identified for CT1, CT3, GY, KPS, and PH had the highest variation in allelic effect, which ranged from 6.7% to 52.1% (Fig. 1.4D). All identified MTAs are listed in Table 1.6. A summary of the MTAs (except those for GC, SPAD, and $\delta^{13}C$) and chromosomal positions is shown in Fig. 1.5. Representative Manhattan plots are shown in Fig. 1.6, and those for GY in the D genome alone are shown in Fig. 1.7. Forty-one stable or pleiotropic MTAs were identified (Table 1.7). Further analysis of some of the stable MTAs revealed the source of the SNP alleles (*Ae. tauschii*, 'Langdon', or N61) and the possible effect of the alleles on individual traits (Fig. 1.8)

1.3.3.1 MTAs under H

Under H, 88.5% of the MTAs identified were for CT1, CT3, PH, NDVI, or GFD (Table 1.6). Ten MTAs for CT3 explained between 19.8% and 35.1% of the variation, and six of them were collocated between 710 and 718 Mbp on Chromosome 3A (Table 1.6). Two MTAs for GY (7940688|F|0-16 and 998513|F|0-66), located between 508 and 522 Mbp on Chromosome 3D, explained 10.6% and 11.8%, respectively, of the phenotypic variation (Fig. 1.4, Table 1.6).

1.3.3.2 MTAs under HD

Under HD, 55% of the MTAs identified were for CT1, NDVI, PH, and KPS. Nine MTAs on Chromosomes 1D, 3D, 5D, and 7D were identified for CT1, seven of which were on 3D and 7D and explained 7.4%–11.4% of the variation (Fig. 1.4, Table 1.6). Among nine MTAs for NDVI, six were collocated on Chromosome 2D (606–618 Mbp) and explained 9.2%–15.4% of the variation. Twelve MTAs were identified for KPS, three of which were collocated on Chromosome 7D (345–384 Mbp) and explained on average 9.9% of the variation. Six MTAs for GY explained 7.8%–14.5% of the variation (Fig. 1.4, Table 1.6).

1.3.3.3 MTAs for DR

To estimate DR, the ratio of BLUEs obtained under HD to those obtained under H were used for GWAS. The MTAs obtained for DR explained, on average, 14.7% of phenotypic variations, and 51.8% of the MTAs controlled GY and KPS. The MTAs controlling GY explained 7.2%–24.1% of the variation, whereas MTAs for KPS elucidated 7.10%–40.4% of the variation. Six MTAs for KPS were collocated: 7351923|F|0-56 and 1230357|F|0-39 were located at 240.6 Mbp on Chromosome 3B, 1056569|F|0-52 and 981730|F|0-67 at 333.1 Mbp on Chromosome 5D, and 2252899|F|0-22 and 3024415|F|0-22 at 408.0–408.6 Mbp on Chromosome 5D (Fig. 1.4, Table 1.6). Two MTAs for GY (1125420|F|0-29 and 1072095|F|0-54) were collocated on Chromosome 3D and explained 21.5% and 9.6%, respectively, of the variation.

1.3.4 Loci controlling plant phenology

MTAs for PH were identified on Chromosomes 4A and 3D–7D. Two MTAs (1001495|F|0-20 and 1042486|F|0-52) were collocated between 577.5 and 577.7 Mbp on Chromosome 4A and explained 7.2%–9.7% of the variation under H and HD conditions. Four MTAs controlling PH were found between 25 and 37 Mbp on Chromosome 4D. Two of them were stable across H and HD: 1079306|F|0-62 was stable in both years and explained 9.5%–25.7% of the variation, whereas 4005784|F|0-33 was stable in 2020 and explained 7.2%–9.7% of the variation in PH (Table 1.7).

Eleven MTAs were identified for GFD and explained, on average, 10.3% of the variation. An MTA on Chromosome 3D (991772|F|0-64) was pleiotropic for DM in the DR in 2020, and an MTA on Chromosome 6D (1120327|F|0-5) was pleiotropic for GY under H in 2020 (Table 1.7).

1.3.5 Loci controlling leaf traits associated with GY traits

Because leaf traits were correlated with GY and related traits (Table 1.4), I investigated the loci controlling CT, NDVI, and $\delta^{13}C$. Most of the MTAs for leaf traits were found on Chromosomes 2D, 3D, and 5D. Three loci were identified on Chromosome 2D: the first locus (23–96 Mbp) harboured MTAs for $\delta^{13}C$, CT3, NDVI, and HI, which explained 7.6%–30.6% of the variation; the second locus (511–554 Mbp) harboured MTAs for CT1, NDVI, KPS, and GY, which explained 7.6–17.7%; and the third locus (606–614 Mbp) harboured MTAs for NDVI, TKW, and GY, which explained 7.1%–16.2%. The locus on Chromosome 3D (155–171 Mbp) harboured MTAs for CT1, CT3, and NDVI, which explained on average 9.9% of the variation. The locus on Chromosome 5D (407–413 Mbp) contained MTAs for CT1, CT2, CT3, NDVI, and BIO, which explained 7.7%–32.8% of the variation. As all these loci on Chromosomes 2D, 3D, and 5D also harboured MTAs for GY and related traits under H, HD, and DR (Fig. 1.4, Table 1.6).

1.3.6 Loci controlling GY, KPS, and TKW

I identified a locus on Chromosome 3D (521–549 Mbp) controlling GY and explaining 9.6%–21.5% of the variation under H and DR, and another locus on Chromosome 3D (79–90 Mbp) common to KPS and TKW explaining 9.3%–22.4% of the variation under H and DR. Also,

I identified a locus common to KPS and TKW on Chromosome 5D (240.6 Mbp) which explained on average 8.5% of the variation in DR, and a locus controlling GY and KPS on Chromosome 7A (517–556 Mbp) explaining a relatively high (21.0%–40.3%) proportion of the variation under DR (Table 1.7).

1.3.7 Candidate genes

A candidate gene for GY, GY stability, and NDVI was identified as a gibberellin-regulating gene (*GA20ox* TraesCS3D02G393900) on Chromosome 3D (998513|F|0-66, 508.3 Mbp). A candidate gene for CT3 was identified as a gene involved in CaaX prenylation (*CaaX prenyl protease 2*, TraesCS1D02G228400) on Chromosome 1D (12002285|F|0-11, 315.1 Mbp). Both candidate genes had similar expression patterns, with highest expression in the endosperm (*GA20ox,* Fig. 1.9) and in the roots, shoots and inflorescences (*CaaX prenyl protease 2*, Fig. 1.10). Other candidate genes are shown in Table 1.8.

1.4 Discussion

In this study, I subjected a high diversity bread wheat panel to H and HD stress under field conditions, to identify QTLs controlling combined stress resilience. The strong G×E interaction effect ($p < 0.001$, Table 1.2) on most traits confirmed the high genetic diversity of the panel. Under HD, GY was drastically reduced (up to 58% of that under H), highlighting the detrimental effect of HD under natural field conditions. Similar observations have been reported under field (Pradhan *et al.* 2012; Liu *et al.* 2019) and controlled conditions (Prasad *et al.* 2011; Schmidt *et al.* 2020). The moderate to high heritability estimates for most of the traits were similar to those reported under separate H, drought stress, and yield potential conditions in Mexico (Sukumaran *et al.* 2018), reflecting the genetic control of these traits across environments. The correlations observed between most of the evaluated traits suggest an association among these traits at the genetic level, which improves selection efficiency (Shimelis and Shiringani 2010). The weak positive correlations of individual traits between H and HD indicate that genotypes that performed

well under H were strongly affected by HD (Table 1.4). However, some genotypes performed relatively well under both conditions and are promising for further breeding (Fig. 1.3). Their good performance may be attributed to the effect of different SNP alleles. For example, genotypes with the R allele for 1218720|F|0-55 on Chromosome 7A, C allele for 18732940|F|0-36 on Chromosome 6B, and Y allele for 1076657|F|0-26 on Chromosome 3D had higher GY across the environments than that of other genotypes, including N61 (Fig. 1.8).

Among the leaf traits, CT1–CT3 and $\delta^{13}C$ were negatively correlated with GY and related traits, whereas NDVI was positively correlated, especially with BIO (Table 1.4). Similar results have been reported under field conditions (Rutkoski *et al.* 2016; Sukumaran *et al.* 2018), indicating the effectiveness of these traits for improving selection efficiency for GY. Rutkoski *et al.* (2016) reported the use of CT and NDVI measurements to improve GY prediction accuracy by up to 70%, whereas an earlier study in Spain (Royo *et al.* 2002) reported that carbon isotope discrimination was more effective than canopy temperature depression in assessing genotypic variation in GY. Similarly, Itam et al. (2020) reported an increasing trend of CT and $\delta^{13}C$ under progressive drought stress due to stomatal regulation. Overall, a combination of CT, NDVI, and $\delta^{13}C$ may be useful for breeding for improved GY under H and HD conditions.

The genetic basis of quantitative traits such as H and HD resilience is complex and requires detailed genomic analyses. In GWAS, I set DH as a covariate to minimize any possible confounding effect of plant phenology. Many MTAs are reportedly dependent on DH (Sukumaran *et al.* 2018; Schmidt *et al.* 2020), but 99% of the MTAs identified in this study were independent of DH, mainly because selection of the wheat panel was based on similar DH. No significant correlation was found between DH and GY (Table 1.4). Therefore, I consider this wheat panel to be suitable for mining novel QTLs for H and HD stress resilience without the confounding effect of plant phenology. I found stable MTAs across two or more conditions and pleiotropic MTAs controlling more than one trait, indicating the stability of the associated QTLs across environments and common regulation of these traits (Table 1.7, Table 1.6). A plot of stable MTAs

showed the effect of SNP alleles on the evaluated traits, indicating that positive alleles for GY on Chromosomes 6B and 7A were derived from 'Langdon', the durum wheat cultivar used as a bridge during the crosses (Fig. 1.8). Itam et al. (2021) reported that the introgressed segments from 'Langdon' (AABB) contribute to the A and B genome diversity of the panel. Conversely, the positive alleles in the D genome derived from *Ae. tauschii* were associated with high GY stability index and GY under H and HD (Fig. 1.8). Some MSD lines and N61 contained a negative allele for PH, supporting the fact that N61 harbours the dwarfing genes that were important for the Green Revolution (Shimizu *et al.* 2021; Tsujimoto 2021). Overall, genotypes carrying the positive alleles for GY and GY stability index and negative alleles for PH may be selected for future breeding.

1.4.1. Genetic control of leaf traits

QTLs on Chromosomes 2D (23–96, 511–554, and 606–614 Mbp), 3D (155–171 Mbp), and 5D (407–413 Mbp) were identified for most leaf traits, including CT1–CT3 and NDVI. The Chromosome 2D locus at 23–96 Mbp controlled the $\delta^{13}C$ value. Two QTLs for carbon isotope discrimination have been previously reported: one on Chromosome 2DL (20.7–47.7 cM) and another on Chromosome 2DS (72.8–90.3 cM), explaining 10% and 5%, respectively, of the genetic variance in doubled haploid wheat progeny (Rebetzke *et al.* 2008). However, owing to the limitations of $\delta^{13}C$ or carbon isotope discrimination (Dixon *et al.* 2019), direct selection using carbon isotope traits alone may offer limited opportunities for wheat improvement. A combination of $\delta^{13}C$ and easy-to-measure leaf traits such as CT and NDVI will likely improve selection efficiency.

One candidate gene regulating canopy temperature at grain filling (CT3) was *CaaX prenyl protease 2* (TraesCS1D02G228400). CaaX prenyl proteases are involved in the prenylation of CaaX proteins, a step essential for protein–membrane interactions, plant development, and stress signalling, especially in abscisic acid signalling in Arabidopsis (Bracha-Drori *et al.* 2008) and wheat (Zhang *et al.* 2015). In the bread wheat lines, this gene may play a role in stress signalling

and stomatal regulation under H and HD stresses, resulting in canopy temperature regulation. Further research is needed for the applicability of this gene to wheat breeding. QTLs for CT promote downward root growth (30–90 cm) under drought stress and root spread close to the soil surface under H, a root distribution strategy for wheat adaptation to both stresses (Pinto and Reynolds 2015). However, HD would likely result in a trade-off between root elongation and spread to optimize plant–water relations. In our study, the decreasing trend of CT2 and CT3 suggests that most of the wheat lines maintained lower canopy temperature under HD than in H stress. Low canopy temperature has been linked to high GY in wheat under separate H and drought stress conditions (Pinto and Reynolds 2015). The QTLs on Chromosomes 2D, 3D, and 5D may regulate resilience to H and HD and are potentially useful for wheat breeding.

1.4.2 Genetic control of GY and related traits

In wheat, GY is the most important trait. A locus on Chromosome 3D (521–549 Mbp) controlled GY alone, a locus on Chromosome 7A (517–556 Mbp) controlled GY and KPS, and two loci on Chromosomes 3D (79–90 Mbp) and 5D (240.6 Mbp) each controlled KPS and TKW under H and HD stresses. These loci explained up to 40.3% of the variation in GY and related traits under H and HD and thus they offer great potential for improvement of wheat climate resilience. This potential reflects the importance of harnessing *Ae. tauschii* diversity for climate resilience breeding using the synthetic derivative approach (Fig. 1.1) (Tsujimoto *et al.* 2015; Itam *et al.* 2020a). Further analysis and validation of individual QTLs using a recombinant population would be needed to better understand the effects of the pleiotropic QTLs on individual traits. Also, the use of functional markers such as kompetitive allele-specific PCR (Rasheed *et al.* 2016; Fang *et al.* 2020) markers may facilitate selection and further breeding.

It is worthy of note that an MTA for GY stability index on Chromosome 3D (998513|F|0-66, 508.3 Mbp) was linked to the gene TraesCS3D02G393900, which is orthologous to *gibberellin-20-oxidase* (*GA20ox*) in *Zea may*s L. (Zm00001d007894). *GA20ox3* functions in gibberellin biosynthesis, and gibberellins play a central role in plant responses to abiotic stresses

by integrating multiple hormone signalling pathways (Colebrook *et al.* 2014). Similarly, gibberellin-sensitive *Rht* alleles (controlling plant height) have been reported to confer tolerance to heat and drought stress in wheat (Alghabari *et al.* 2016). I hypothesize that TraesCS3D02G393900 on Chromosome 3D may favourably alter gibberellin content, ultimately resulting in higher GY stability under H and HD conditions. This offers a potential for developing climate-resilient wheat cultivars by optimizing gibberellin homeostasis. However, further investigations are needed to test this hypothesis by exploiting the diversity in gibberellin-regulating genes in wheat. Our database search revealed that TraesCS3D02G393900 is mainly expressed during the late vegetative and reproductive stages, with highest expression in the endosperm (Fig. 1.9) (Pearce *et al.* 2015). Similar expression patterns were reported in its orthologs in *Z. mays* (Zm00001d007894) (Yousaf *et al.* 2019), *Oryza sativa* L. (LOC_Os07g07420) (Qin *et al.* 2013), and *Hordeum vulgare* L. (HORVU3Hr1G089980) (Betts *et al.* 2020) indicating a similar function of these genes among members of the grass family.

The wheat MSD panel used in this study represents the diversity of 37 *Ae. tauschii* accessions, and the study provides insights on the utilization of high-diversity breeding panels for wheat improvement. Since this is the first GWAS under HD in field conditions, the identified candidate genes, novel alleles, and QTLs will potentially serve as genomic landmarks for breeding to improve wheat adaptation to H and HD stresses under climate change.

Table 1.1 List of plant materials. The pedigrees of the MSD lines include the origins and lineages of donor *Ae. tauschii* accessions.

Genotypes	Cross name	Pedigree	Origin of *Ae tauschii* accession	Lineage of *Ae. tauschii* accession
Norin 61	NA	Akabouzu/Sunekiri × Shinriki//Shinchunaga	NA	NA
Imam	NA	Check cultivar	NA	NA
Gomeria	NA	Check cultivar	NA	NA
Fielder	NA	Check cultivar	NA	NA
Roelf	NA	Check cultivar	NA	NA
MSD363	Syn26	Norin 61/*T. durum* cv. Langdon × *Ae. tauschii* AE454//Norin 61	Georgia	TauL3
MSD54	Syn26	Norin 61/*T. durum* cv. Langdon × *Ae. tauschii* AE454//Norin 61	Georgia	TauL3
MSD122	Syn26	Norin 61/*T. durum* cv. Langdon × *Ae. tauschii* AE454//Norin 61	Georgia	TauL3
MSD135	Syn26	Norin 61/*T. durum* cv. Langdon × *Ae. tauschii* AE454//Norin 61	Georgia	TauL3
MSD119	Syn26	Norin 61/*T. durum* cv. Langdon × *Ae. tauschii* AE454//Norin 61	Georgia	TauL3
MSD347	Syn26	Norin 61/*T. durum* cv. Langdon × *Ae. tauschii* AE454//Norin 61	Georgia	TauL3
MSD186	Syn26	Norin 61/*T. durum* cv. Langdon × *Ae. tauschii* AE454//Norin 61	Georgia	TauL3
MSD245	Syn26	Norin 61/*T. durum* cv. Langdon × *Ae. tauschii* AE454//Norin 61	Georgia	TauL3
MSD66	Syn26	Norin 61/*T. durum* cv. Langdon × *Ae. tauschii* AE454//Norin 61	Georgia	TauL3
MSD383	Syn27	Norin 61/*T. durum* cv. Langdon × *Ae. tauschii* AE454//Norin 61	Georgia	TauL3
MSD410	Syn27	Norin 61/*T. durum* cv. Langdon × *Ae. tauschii* AE454//Norin 61	Georgia	TauL3
MSD147	Syn27	Norin 61/*T. durum* cv. Langdon × *Ae. tauschii* AE454//Norin 61	Georgia	TauL3
MSD311	Syn27	Norin 61/*T. durum* cv. Langdon × *Ae. tauschii* AE454//Norin 61	Georgia	TauL3
MSD395	Syn27	Norin 61/*T. durum* cv. Langdon × *Ae. tauschii* AE454//Norin 61	Georgia	TauL3
MSD340	Syn27	Norin 61/*T. durum* cv. Langdon × *Ae. tauschii* AE454//Norin 61	Georgia	TauL3
MSD241	Syn27	Norin 61/*T. durum* cv. Langdon × *Ae. tauschii* AE454//Norin 61	Georgia	TauL3
MSD377	Syn27	Norin 61/*T. durum* cv. Langdon × *Ae. tauschii* AE454//Norin 61	Georgia	TauL3
MSD195	Syn27	Norin 61/*T. durum* cv. Langdon × *Ae. tauschii* AE454//Norin 61	Georgia	TauL3
MSD342	Syn27	Norin 61/*T. durum* cv. Langdon × *Ae. tauschii* AE454//Norin 61	Georgia	TauL3
MSD169	Syn28	Norin 61/*T. durum* cv. Langdon × *Ae. tauschii* IG48042//Norin 61	India	TauL1
MSD5	Syn28	Norin 61/*T. durum* cv. Langdon × *Ae. tauschii* IG48042//Norin 61	India	TauL1
MSD437	Syn28	Norin 61/*T. durum* cv. Langdon × *Ae. tauschii* IG48042//Norin 61	India	TauL1
MSD114	Syn28	Norin 61/*T. durum* cv. Langdon × *Ae. tauschii* IG48042//Norin 61	India	TauL1
MSD189	Syn28	Norin 61/*T. durum* cv. Langdon × *Ae. tauschii* IG48042//Norin 61	India	TauL1
MSD226	Syn28	Norin 61/*T. durum* cv. Langdon × *Ae. tauschii* IG48042//Norin 61	India	TauL1
MSD121	Syn28	Norin 61/*T. durum* cv. Langdon × *Ae. tauschii* IG48042//Norin 61	India	TauL1
MSD330	Syn28	Norin 61/*T. durum* cv. Langdon × *Ae. tauschii* IG48042//Norin 61	India	TauL1
MSD22	Syn29	Norin 61/*T. durum* cv. Langdon × Ae. tauschii IG126387//Norin 61	Turkmenistan	TauL1
MSD53	Syn29	Norin 61/*T. durum* cv. Langdon × Ae. tauschii IG126387//Norin 61	Turkmenistan	TauL1
MSD61	Syn29	Norin 61/*T. durum* cv. Langdon × Ae. tauschii IG126387//Norin 61	Turkmenistan	TauL1
MSD217	Syn29	Norin 61/*T. durum* cv. Langdon × Ae. tauschii IG126387//Norin 61	Turkmenistan	TauL1
MSD496	Syn29	Norin 61/*T. durum* cv. Langdon × Ae. tauschii IG126387//Norin 61	Turkmenistan	TauL1
MSD192	Syn30	Norin 61/*T. durum* cv. Langdon × *Ae. tauschii* IG131606//Norin 61	Kyrgyzstan	TauL1
MSD84	Syn30	Norin 61/*T. durum* cv. Langdon × *Ae. tauschii* IG131606//Norin 61	Kyrgyzstan	TauL1
MSD26	Syn30	Norin 61/*T. durum* cv. Langdon × *Ae. tauschii* IG131606//Norin 61	Kyrgyzstan	TauL1
MSD289	Syn30	Norin 61/*T. durum* cv. Langdon × *Ae. tauschii* IG131606//Norin 61	Kyrgyzstan	TauL1
MSD17	Syn30	Norin 61/*T. durum* cv. Langdon × *Ae. tauschii* IG131606//Norin 61	Kyrgyzstan	TauL1
MSD394	Syn30	Norin 61/*T. durum* cv. Langdon × *Ae. tauschii* IG131606//Norin 61	Kyrgyzstan	TauL1
MSD475	Syn30	Norin 61/*T. durum* cv. Langdon × *Ae. tauschii* IG131606//Norin 61	Kyrgyzstan	TauL1
MSD250	Syn31	Norin 61/*T. durum* cv. Langdon × *Ae. tauschii* KU20-8//Norin 61	Iran	Taul2
MSD65	Syn31	Norin 61/*T. durum* cv. Langdon × *Ae. tauschii* KU20-8//Norin 61	Iran	Taul2
MSD163	Syn31	Norin 61/*T. durum* cv. Langdon × *Ae. tauschii* KU20-8//Norin 61	Iran	Taul2
MSD296	Syn32	Norin 61/*T. durum* cv. Langdon × *Ae. tauschii* KU-2039//Norin 61	Afghanistan	Taul1
MSD249	Syn32	Norin 61/*T. durum* cv. Langdon × *Ae. tauschii* KU-2039//Norin 61	Afghanistan	Taul1
MSD392	Syn32	Norin 61/*T. durum* cv. Langdon × *Ae. tauschii* KU-2039//Norin 61	Afghanistan	Taul1
MSD190	Syn32	Norin 61/*T. durum* cv. Langdon × *Ae. tauschii* KU-2039//Norin 61	Afghanistan	Taul1
MSD160	Syn32	Norin 61/*T. durum* cv. Langdon × *Ae. tauschii* KU-2039//Norin 61	Afghanistan	Taul1
MSD332	Syn33	Norin 61/*T. durum* cv. Langdon × *Ae. tauschii* KU-2074//Norin 61	Iran	TauL2
MSD7	Syn33	Norin 61/*T. durum* cv. Langdon × *Ae. tauschii* KU-2074//Norin 61	Iran	TauL2
MSD301	Syn33	Norin 61/*T. durum* cv. Langdon × *Ae. tauschii* KU-2074//Norin 61	Iran	TauL2
MSD343	Syn33	Norin 61/*T. durum* cv. Langdon × *Ae. tauschii* KU-2074//Norin 61	Iran	TauL2
MSD52	Syn34	Norin 61/*T. durum* cv. Langdon × *Ae. tauschii* KU-2075//Norin 61	Iran	TauL2
MSD132	Syn34	Norin 61/*T. durum* cv. Langdon × *Ae. tauschii* KU-2075//Norin 61	Iran	TauL2
MSD325	Syn34	Norin 61/*T. durum* cv. Langdon × *Ae. tauschii* KU-2075//Norin 61	Iran	TauL2
MSD346	Syn35	Norin 61/*T. durum* cv. Langdon × *Ae. tauschii* KU-2080//Norin 61	Iran	TauL2
MSD274	Syn35	Norin 61/*T. durum* cv. Langdon × *Ae. tauschii* KU-2080//Norin 61	Iran	TauL2
MSD406	Syn36	Norin 61/*T. durum* cv. Langdon × *Ae. tauschii* KU-2088//Norin 61	Iran	TauL2
MSD95	Syn36	Norin 61/*T. durum* cv. Langdon × *Ae. tauschii* KU-2088//Norin 61	Iran	TauL2
MSD490	Syn37	Norin 61/*T. durum* cv. Langdon × *Ae. tauschii* KU-2092//Norin 61	Iran	TauL2
MSD43	Syn38	Norin 61/*T. durum* cv. Langdon × *Ae. tauschii* KU-2096//Norin 61	Iran	TauL2
MSD371	Syn38	Norin 61/*T. durum* cv. Langdon × *Ae. tauschii* KU-2096//Norin 61	Iran	TauL2
MSD32	Syn38	Norin 61/*T. durum* cv. Langdon × *Ae. tauschii* KU-2096//Norin 61	Iran	TauL2
MSD219	Syn39	Norin 61/*T. durum* cv. Langdon × *Ae. tauschii* KU-2097//Norin 61	Iran	TauL2
MSD378	Syn39	Norin 61/*T. durum* cv. Langdon × *Ae. tauschii* KU-2097//Norin 61	Iran	TauL2
MSD162	Syn39	Norin 61/*T. durum* cv. Langdon × *Ae. tauschii* KU-2097//Norin 61	Iran	TauL2
MSD450	Syn39	Norin 61/*T. durum* cv. Langdon × *Ae. tauschii* KU-2097//Norin 61	Iran	TauL2
MSD50	Syn39	Norin 61/*T. durum* cv. Langdon × *Ae. tauschii* KU-2097//Norin 61	Iran	TauL2
MSD370	Syn40	Norin 61/*T. durum* cv. Langdon × *Ae. tauschii* KU-2098//Norin 61	Iran	TauL2
MSD455	Syn40	Norin 61/*T. durum* cv. Langdon × *Ae. tauschii* KU-2098//Norin 61	Iran	TauL2
MSD77	Syn40	Norin 61/*T. durum* cv. Langdon × *Ae. tauschii* KU-2098//Norin 61	Iran	TauL2
MSD18	Syn42	Norin 61/*T. durum* cv. Langdon × *Ae. tauschii* KU-2105//Norin 61	Iran	TauL2
MSD19	Syn42	Norin 61/*T. durum* cv. Langdon × *Ae. tauschii* KU-2105//Norin 61	Iran	TauL2
MSD427	Syn42	Norin 61/*T. durum* cv. Langdon × *Ae. tauschii* KU-2105//Norin 61	Iran	TauL2
MSD280	Syn42	Norin 61/*T. durum* cv. Langdon × *Ae. tauschii* KU-2105//Norin 61	Iran	TauL2
MSD181	Syn42	Norin 61/*T. durum* cv. Langdon × *Ae. tauschii* KU-2105//Norin 61	Iran	TauL2
MSD259	Syn42	Norin 61/*T. durum* cv. Langdon × *Ae. tauschii* KU-2105//Norin 61	Iran	TauL2

Table 1.1 continued

Genotypes	Cross name	Pedigree	Origin of *Ae tauschii* accession	Lineage of *Ae. tauschii* accession
MSD401	Syn44	Norin 61/*T. durum* cv. Langdon × *Ae. tauschii* KU-2124//Norin 61	Iran	TauL2
MSD404	Syn44	Norin 61/*T. durum* cv. Langdon × *Ae. tauschii* KU-2124//Norin 61	Iran	TauL2
MSD143	Syn44	Norin 61/*T. durum* cv. Langdon × *Ae. tauschii* KU-2124//Norin 61	Iran	TauL2
MSD265	Syn44	Norin 61/*T. durum* cv. Langdon × *Ae. tauschii* KU-2124//Norin 61	Iran	TauL2
MSD81	Syn44	Norin 61/*T. durum* cv. Langdon × *Ae. tauschii* KU-2124//Norin 61	Iran	TauL2
MSD177	Syn44	Norin 61/*T. durum* cv. Langdon × *Ae. tauschii* KU-2124//Norin 61	Iran	TauL2
MSD108	Syn45	Norin 61/*T. durum* cv. Langdon × *Ae. tauschii* KU-2126//Norin 61	Iran	TauL2
MSD8	Syn45	Norin 61/*T. durum* cv. Langdon × *Ae. tauschii* KU-2126//Norin 61	Iran	TauL2
MSD254	Syn45	Norin 61/*T. durum* cv. Langdon × *Ae. tauschii* KU-2126//Norin 61	Iran	TauL2
MSD247	Syn47	Norin 61/*T. durum* cv. Langdon × *Ae. tauschii* KU-2159//Norin 61	Iran	TauL2
MSD131	Syn47	Norin 61/*T. durum* cv. Langdon × *Ae. tauschii* KU-2159//Norin 61	Iran	TauL2
MSD413	Syn48	Norin 61/*T. durum* cv. Langdon × *Ae. tauschii* KU-2829A//Norin 61	Georgia	TauL3
MSD345	Syn48	Norin 61/*T. durum* cv. Langdon × *Ae. tauschii* KU-2829A//Norin 61	Georgia	TauL3
MSD384	Syn48	Norin 61/*T. durum* cv. Langdon × *Ae. tauschii* KU-2829A//Norin 61	Georgia	TauL3
MSD368	Syn48	Norin 61/*T. durum* cv. Langdon × *Ae. tauschii* KU-2829A//Norin 61	Georgia	TauL3
MSD130	Syn50	Norin 61/*T. durum* cv. Langdon × *Ae. tauschii* AT55//Norin 61	China	TauL1
MSD453	Syn50	Norin 61/*T. durum* cv. Langdon × *Ae. tauschii* AT55//Norin 61	China	TauL1
MSD470	Syn50	Norin 61/*T. durum* cv. Langdon × *Ae. tauschii* AT55//Norin 61	China	TauL1
MSD123	Syn50	Norin 61/*T. durum* cv. Langdon × *Ae. tauschii* AT55//Norin 61	China	TauL1
MSD55	Syn51	Norin 61/*T. durum* cv. Langdon × *Ae. tauschii* AT76//Norin 61	China	TauL1
MSD112	Syn52	Norin 61/*T. durum* cv. Langdon × *Ae. tauschii* AT80//Norin 61	China	TauL1
MSD335	Syn52	Norin 61/*T. durum* cv. Langdon × *Ae. tauschii* AT80//Norin 61	China	TauL1
MSD434	Syn52	Norin 61/*T. durum* cv. Langdon × *Ae. tauschii* AT80//Norin 61	China	TauL1
MSD117	Syn52	Norin 61/*T. durum* cv. Langdon × *Ae. tauschii* AT80//Norin 61	China	TauL1
MSD92	Syn52	Norin 61/*T. durum* cv. Langdon × *Ae. tauschii* AT80//Norin 61	China	TauL1
MSD317	Syn53	Norin 61/*T. durum* cv. Langdon × *Ae. tauschii* AE1090//Norin 61	Kazakhstan	TauL1
MSD91	Syn54	Norin 61/*T. durum* cv. Langdon × *Ae. tauschii* IG47259//Norin 61	Syria	TauL1
MSD205	Syn54	Norin 61/*T. durum* cv. Langdon × *Ae. tauschii* IG47259//Norin 61	Syria	TauL1
MSD487	Syn54	Norin 61/*T. durum* cv. Langdon × *Ae. tauschii* IG47259//Norin 61	Syria	TauL1
MSD62	Syn55	Norin 61/*T. durum* cv. Langdon × *Ae. tauschii* KU-20-10//Norin 61	Iran	TauL2
MSD257	Syn55	Norin 61/*T. durum* cv. Langdon × *Ae. tauschii* KU-20-10//Norin 61	Iran	TauL2
MSD360	Syn57	Norin 61/*T. durum* cv. Langdon × *Ae. tauschii* KU-2078//Norin 61	Iran	TauL2
MSD313	Syn57	Norin 61/*T. durum* cv. Langdon × *Ae. tauschii* KU-2078//Norin 61	Iran	TauL2
MSD31	Syn57	Norin 61/*T. durum* cv. Langdon × *Ae. tauschii* KU-2078//Norin 61	Iran	TauL2
MSD222	Syn58	Norin 61/*T. durum* cv. Langdon × *Ae. tauschii* KU-2079//Norin 61	Iran	TauL2
MSD284	Syn59	Norin 61/*T. durum* cv. Langdon × *Ae. tauschii* KU-20-9//Norin 61	Iran	TauL2
MSD255	Syn60	Norin 61/*T. durum* cv. Langdon × *Ae. tauschii* KU-2090//Norin 61	Iran	TauL2
MSD275	Syn60	Norin 61/*T. durum* cv. Langdon × *Ae. tauschii* KU-2090//Norin 61	Iran	TauL2
MSD476	Syn61	Norin 61/*T. durum* cv. Langdon × *Ae. tauschii* KU-2091//Norin 61	Iran	TauL2
MSD397	Syn62	Norin 61/*T. durum* cv. Langdon × *Ae. tauschii* KU-2092//Norin 61	Iran	TauL2
MSD141	Syn62	Norin 61/*T. durum* cv. Langdon × *Ae. tauschii* KU-2092//Norin 61	Iran	TauL2
MSD165	Syn62	Norin 61/*T. durum* cv. Langdon × *Ae. tauschii* KU-2092//Norin 61	Iran	TauL2
MSD426	Syn62	Norin 61/*T. durum* cv. Langdon × *Ae. tauschii* KU-2092//Norin 61	Iran	TauL2
MSD304	Syn62	Norin 61/*T. durum* cv. Langdon × *Ae. tauschii* KU-2092//Norin 61	Iran	TauL2
MSD278	Syn62	Norin 61/*T. durum* cv. Langdon × *Ae. tauschii* KU-2092//Norin 61	Iran	TauL2
MSD159	Syn63	Norin 61/*T. durum* cv. Langdon × *Ae. tauschii* KU-2103//Norin 61	Iran	TauL2
MSD389	Syn63	Norin 61/*T. durum* cv. Langdon × *Ae. tauschii* KU-2103//Norin 61	Iran	TauL2
MSD145	Syn64	Norin 61/*T. durum* cv. Langdon × *Ae. tauschii* KU-2109//Norin 61	Iran	TauL2
MSD24	Syn64	Norin 61/*T. durum* cv. Langdon × *Ae. tauschii* KU-2109//Norin 61	Iran	TauL2
MSD361	Syn64	Norin 61/*T. durum* cv. Langdon × *Ae. tauschii* KU-2109//Norin 61	Iran	TauL2
MSD488	Syn64	Norin 61/*T. durum* cv. Langdon × *Ae. tauschii* KU-2109//Norin 61	Iran	TauL2
MSD106	Syn65	Norin 61/*T. durum* cv. Langdon × *Ae. tauschii* KU-2132//Norin 61	Turkey	TauL1
MSD270	Syn65	Norin 61/*T. durum* cv. Langdon × *Ae. tauschii* KU-2132//Norin 61	Turkey	TauL1
MSD148	Syn65	Norin 61/*T. durum* cv. Langdon × *Ae. tauschii* KU-2132//Norin 61	Turkey	TauL1
MSD6	Syn65	Norin 61/*T. durum* cv. Langdon × *Ae. tauschii* KU-2132//Norin 61	Turkey	TauL1
MSD366	Syn66	Norin 61/*T. durum* cv. Langdon × *Ae. tauschii* KU-2136//Norin 61	Turkey	TauL1
MSD128	Syn67	Norin 61/*T. durum* cv. Langdon × *Ae. tauschii* KU-2155//Norin 61	Iran	TauL2
MSD178	Syn68	Norin 61/*T. durum* cv. Langdon × *Ae. tauschii* KU-2156//Norin 61	Iran	TauL2
MSD414	Syn68	Norin 61/*T. durum* cv. Langdon × *Ae. tauschii* KU-2156//Norin 61	Iran	TauL2
MSD187	Syn68	Norin 61/*T. durum* cv. Langdon × *Ae. tauschii* KU-2156//Norin 61	Iran	TauL2
MSD215	Syn68	Norin 61/*T. durum* cv. Langdon × *Ae. tauschii* KU-2156//Norin 61	Iran	TauL2
MSD41	Syn68	Norin 61/*T. durum* cv. Langdon × *Ae. tauschii* KU-2156//Norin 61	Iran	TauL2
MSD307	Syn68	Norin 61/*T. durum* cv. Langdon × *Ae. tauschii* KU-2156//Norin 61	Iran	TauL2
MSD298	Syn68	Norin 61/*T. durum* cv. Langdon × *Ae. tauschii* KU-2156//Norin 61	Iran	TauL2
MSD485	Syn68	Norin 61/*T. durum* cv. Langdon × *Ae. tauschii* KU-2156//Norin 61	Iran	TauL2
MSD88	Syn68	Norin 61/*T. durum* cv. Langdon × *Ae. tauschii* KU-2156//Norin 61	Iran	TauL2
MSD44	Syn71	Norin 61/*T. durum* cv. Langdon × *Ae. tauschii* PI499262//Norin 61	China	TauL1
MSD12	Syn71	Norin 61/*T. durum* cv. Langdon × *Ae. tauschii* PI499262//Norin 61	China	TauL1
MSD133	Syn72	Norin 61/*T. durum* cv. Langdon × *Ae. tauschii* PI508262//Norin 61	China	TauL1

Table 1.2 Mean sums of squares for traits evaluated under heat and combined heat–drought stress in 2019 and 2020.

	2019					2020				
Trait	**G**	**E**	**G×E**	**Residual**	**Total**	**G**	**E**	**G×E**	**Residual**	**Total**
BIO	5167994***	1251009401***	2757435	2525932	6058830	11019120***	302820432***	4077099	3469217	6545702
CT1	3.43	10.35	3.86	4.38	4.77	5.96	154.34***	4.92	4.98	5.75
CT2	3.28	500.32***	5.44	5.40	8.28	2.42	973.34***	1.91	2.24	5.50
CT3	3.47	366.05**	2.85	4.67	6.00	3.50***	627.10**	2.49	2.61	4.30
DH	26***	18	7*	5	12	54***	256***	9	8	22
DM	16***	970***	5	4	10	61.57***	850***	19*	15	32
GC	0.29	11.95***	0.24	0.29	0.34	NA	NA	NA	NA	NA
GFD	18***	726***	8*	6	11	37***	2039***	17	16	25
GY	1016560***	197535241***	441017***	263335	897450	1460928***	101934817***	529329***	326270	871589
HI	88.62***	3196.01***	32.68	27.92	52.47	85.46***	3223.96***	40.28***	22.31	51.32
KPS	63***	73	43**	30	45	111***	129	61*	47	69
NDVI	0.0100***	1.5500***	0.0043	0.0035	0.0090	0.0064***	0.0060	0.0027	0.0028	0.0041
PH	102.0***	3578.5***	31.2	27.3	66.3	194.3***	1102.5***	24.3	23.7	75.1
SN	6222	1896188***	8813	7275	13531	15889**	383043***	11782	10898	14053
SPAD	12.94***	9.93	7.35*	5.45	8.05	176.90	50.30	178.60	175.90	178.00
TKW	35.3***	3634.9***	21.8**	14.9	28.9	44.8***	819.3***	20.7	25.6	30.5
$\delta^{13}C$	0.67***	50.42***	0.45	0.45	0.66	NA	NA	NA	NA	NA

Table 1.3 Descriptive statistics and heritability (h^2) estimates of the bread wheat panel under heat and combined heat–drought stress in 2019 and 2020 and predicted means of 'Norin 61' (the backcross parent of the MSD lines) and 'Imam' (a popular Sudanese cultivar).

	H2019				H2020					HD2019				HD2020				
Traits	**Range**	**Mean**	**N61**	**Imam**	**Range**	**Mean**	**N61**	**Imam**	h^2	**Range**	**Mean**	**N61**	**Imam**	**Range**	**Mean**	**N61**	**Imam**	h^2
BIO	4312–13812	9180	11625	10125	4456–16926	10103	10017	12339	0.30	2125–11125	6292	5625	7062	2798–15196	8682	8204	10526	0.2
CT1	18.47–30.49	28.01	29.25	25.9	19.00–30.24	23.04	21.08	20.12	0.00	22.16–32.76	27.75	27.75	29.35	18.50–27.58	22.02	22.03	19.52	0.32
CT2	15.85–25.4	20.84	18.15	19.55	23.42–29.66	26.07	25.91	25.17	0.00	19.4–26.15	22.67	21.70	21.75	20.52–26.27	23.53	25.46	21.42	0.45
CT3	22.94–35.41	27.15	27.17	24.77	23.34–29.46	26.04	26.45	24.01	0.33	22.82–29.57	25.59	26.72	25.52	21.7–29.84	23.99	25.15	24.01	0.13
DH	50–64	58	59	64	53–72	61.71	58	64	0.70	51–65	57	58	63	49–74	63	57	68	0.77
DM	80–90	87	87	90	87–108	98	89	105	0.66	74–91	84	83	89	85–106	95	89	96	0.59
GC	2.25–4.50	3.60	3.75	3.25	NA	NA	NA	NA	NA	1.75–4.25	3.32	3.75	3.25	NA	NA	NA	NA	NA
GFD	23–38	29	29	26	29–50	36	31	41	0.32	23–37	27	25	26	24–42	32	32	28	0.75
GY	1032–5094	2735	2626	3594	1171–4687	3116	3735	4586	0.62	469–3706	1588	1375	1775	408–4014	2297	3358	2861	0.44
HI	8.75–42.75	30.07	22.40	35.60	16.9–45.46	31.32	40.22	36.14	0.77	8.17–41.84	25.45	24.49	25.89	11.73–48.07	26.74	44.46	26.57	0.63
KPS	17–47	29	27	34	10–49	29	29	42	0.64	14–42	29	25	23	4–51	30	30	45	0.58
NDVI	0.30–0.74	0.57	0.57	0.63	0.43–0.74	0.65	0.66	0.66	0.29	0.2–0.65	0.46	0.43	0.56	0.50–0.73	0.64	0.63	0.69	0.59
PH	57.1–94.0	73.9	78.5	75.0	65.3–106.8	87.5	84.6	88.1	0.89	53.0–90.0	69.0	67.5	65.0	62.6–103.2	84.8	83.8	79.8	0.82
SN	200–515	301	275	440	223–712	488	473	662	0.18	305–620	414	500	495	219–707	437	328	707	0
SPAD	42.55–56.00	49.52	48.90	49.55	19.94–44.96	34.49	37.44	36.82	0.00	43.95–56.30	49.77	45.80	49.20	16.09–45.64	32.87	35.09	30.37	0
TKW	20.2–45.4	30.1	32.2	36.8	20.3–49.3	34.2	34.7	28.6	0.56	16.4–37.1	25.2	23.1	28.8	20.9–41.4	31.9	28.2	30.1	0.42
$\delta^{13}C$	-29.97– (-26.89)	-28.28	-28.32	-29.32	NA	NA	NA	NA	NA	-29.07– (-26.28)	-27.70	-27.86	-27.87	NA	NA	NA	NA	NA

BIO, biomass; CT1, canopy temperature 7 days before flowering; CT2, canopy temperature at flowering; CT3, canopy temperature at grain filling; DH, days to 50% heading; DM, days to maturity; GC, ground cover; GFD, grain-filling duration; GY, grain yield; HI, harvest index; KPS, kernel number per spike; NDVI, normalized difference vegetation index; PH, plant height; SN, number of spikes per m^2; SPAD, chlorophyll content; TKW, thousand-kernel weight; $\delta^{13}C$, delta carbon-13 value.

Table 1.4 Correlation coefficients of the evaluated traits in 2019 and 2020.

Trait	Year	BIO	CT1	CT2	CT3	DH	DM	GC	GFD	GY	HI	KPS	NDVI	PH	SN	SPAD	TKW	$\delta^{13}C$
BIO	2019	**.458****	-.044	-.253**	-.227**	.181*	.356**	.291**	.063	.647**	-.116	.249**	.532**	.457**	.082	-.081	.154	-.156
	2020	**.504****	-.421**	-.374**	-.409**	.026	-.202*	NA	-.281**	.641**	-.114	.170*	.439**	.285**	.165*	-.097	.018	NA
CT1	2019	-.104	**-.003**	.129	.081	-.092	-.090	.074	.036	.042	.044	-.021	-.160	-.035	.225**	-.066	-.013	.057
	2020	-.477**	**.171***	.202*	.269**	.106	.177*	NA	.115	-.362**	-.032	-.145	-.176*	-.166*	-.313**	-.153	-.059	NA
CT2	2019	-.215**	-.154	**.084**	.048	.034	-.050	.090	-.076	-.257**	-.118	-.290**	-.220**	-.216**	.145	-.029	-.114	.061
	2020	-.329**	.340**	**.194***	.297**	-.237**	-.120	NA	.077	-.283**	.012	-.154	-.249**	-.134	-.199*	-.056	.053	NA
CT3	2019	-.134	.081	-.060	**.205***	-.202*	-.178*	-.101	.094	-.180*	-.033	-.019	-.161*	-.077	-.182*	.075	-.036	.055
	2020	-.272**	.220**	.297**	**.267****	-.086	.061	NA	.155	-.358**	-.036	-.171*	-.236**	-.215**	-.255**	-.079	-.190*	NA
DH	2019	.190*	.043	-.080	-.130	**.632****	.496**	-.143	-.757**	.097	-.033	.086	.299**	.070	.049	.084	-.085	-.030
	2020	.028	-.145	-.201*	-.163*	**.752****	.592**	NA	-.222**	-.011	-.046	.127	.338**	.168*	.014	-.050	-.172*	NA
DM	2019	.218**	.007	.091	-.124	.584**	**.598****	-.130	.191*	.130	-.155	.178*	.537**	.179*	.190*	-.021	-.072	.069
	2020	.071	.102	-.014	-.012	.674**	**.590****	NA	.655**	.003	-.086	.019	.262**	.055	-.136	-.117	-.173*	NA
GC	2019	.162*	-.043	-.002	.048	-.145	-.271**	**.244****	.064	.185*	-.074	.110	.063	.263**	.177*	-.083	.100	-.046
	2020	NA	NA	NA	NA	NA	NA	**NA**	NA	NA	NA	NA	NA	NA	NA	NA	NA	NA
GFD	2019	.013	-.041	.186*	.017	-.521**	.388**	-.120	**.436****	-.011	-.080	.036	.066	.055	.088	-.110	.042	.086
	2020	.060	.306**	.232**	.188*	-.413**	.394**	NA	**.446****	.014	-.061	-.096	-.001	-.091	-.177*	-.095	-.048	NA
GY	2019	.701**	-.109	-.057	-.099	.082	.000	.196*	-.093	**.505****	.667**	.351**	.269**	.204*	.050	.058	.230**	-.182*
	2020	.687**	-.361**	-.290**	-.275**	.010	-.149	NA	-.196*	**.485****	.564**	.294**	.128	-.101	.246**	.131	.064	NA
HI	2019	.074	-.059	.098	-.046	-.064	-.190*	.098	-.127	.742**	**.507****	.215**	-.146	-.193*	-.023	.132	.156	-.076
	2020	-.187*	-.016	-.036	-.136	-.017	-.028	NA	-.014	.657**	**.397****	.326**	-.196*	-.302**	-.080	.009	.020	NA
KPS	2019	.045	-.055	.088	-.075	-.027	-.066	.025	-.039	.324**	.412**	**.265****	.291**	.175*	.052	.049	-.105	-.037
	2020	.082	-.284**	-.255**	-.182*	.143	.103	NA	-.050	.425**	.381**	**.387****	-.001	.108	.042	-.002	-.199*	NA
NDVI	2019	.206*	.076	-.162*	-.187*	.559**	.612**	-.255**	.009	.094	-.036	-.003	**.506****	.407**	.016	-.058	-.052	-.134
	2020	.354**	-.374**	-.451**	-.324**	.523**	.296**	NA	-.286**	.320**	.007	.203*	**.447****	.193*	.269**	.071	-.096	NA
PH	2019	.227**	-.124	-.181*	-.121	.032	-.036	.068	-.074	.073	-.122	-.001	.131	**.619****	-.016	.015	.130	.017
	2020	.164*	-.366**	-.016	-.198*	.084	-.058	NA	-.176*	.107	-.126	.064	.254**	**.806****	.100	-.130	-.018	NA
SN	2019	.181*	.047	-.088	-.145	.182*	.135	.089	-.065	.104	-.004	-.141	.181*	-.107	**.144**	-.055	-.062	.160
	2020	.368**	-.062	-.183*	-.129	-.043	-.110	NA	-.083	.137	.025	.084	.137	.134	**.309****	.303**	.031	NA
SPAD	2019	.152	.028	-.037	-.133	-.113	-.150	.102	-.030	.149	.059	.142	-.103	.187*	.012	**.311****	.072	-.017
	2020	.110	.022	.071	.138	.179*	.056	NA	-.153	-.068	.000	-.014	.122	-.100	.007	**.675****	.071	NA
TKW	2019	.016	-.131	.137	.076	.117	.094	-.055	-.033	.188*	.219**	.037	.213**	.051	-.131	-.061	**.285****	.072
	2020	.094	.032	.079	-.032	-.245**	-.175*	NA	.089	.092	.134	.061	-.124	.019	.072	.032	**.477****	NA
$\delta^{13}C$	2019	-.212**	.070	.215**	.041	.233**	.156	-.080	-.101	-.238**	-.177*	-.078	.076	-.093	.021	-.220**	.153	**.250****
	2020	NA	NA	NA	NA	NA	NA	NA	NA	NA	NA	NA	NA	NA	NA	NA	NA	NA

Asterisks: significant at the *0.05 and **0.01 levels (2-tailed). BIO, biomass; CT1, canopy temperature 7 days before flowering; CT2, canopy temperature at flowering; CT3, canopy temperature at grain filling; DH, days to 50% heading; DM, days to maturity; GC, ground cover; GFD, grain-filling duration; GY, grain yield; HI, harvest index; KPS, kernel number per spike; NDVI, normalized difference vegetation index; PH, plant height; SN, number of spikes per m^{-2}; SPAD, chlorophyll content; TKW, thousand-kernel-weight; $\delta^{13}C$, delta carbon-13 value. Numbers in bold arranged diagonally represent individual trait correlations between two field conditions; the diagonal separates the two field conditions: Left to right, heat stress; top to bottom, combined heat and drought stress.

Table 1.5 MSD lines selected on the basis of grain yield (GY) and its stability under heat (H) and combined heat–drought (HD) stress in comparison with their backcross parent (Norin 61) and a Sudanese check cultivar (Imam).

Genotypes	Cross name	Mean GY under H	Mean GY under HD	Drought response	Stability index
MSD280	Syn42	2966	2791	0.68	0.09
MSD345	Syn48	2013	2162	0.90	0.16
MSD401	Syn44	3645	3295	0.60	0.25
MSD189	Syn28	3261	2775	0.72	0.38
MSD254	Syn45	2990	2966	0.98	0.42
MSD298	Syn68	3084	2579	0.77	0.55
MSD53	Syn29	4355	2575	0.51	0.70
MSD165	Syn62	3437	2918	0.75	0.95
MSD181	Syn42	4416	2865	0.65	1.03
MSD6	Syn65	3449	2807	0.74	1.09
MSD342	Syn27	3316	2744	0.93	1.10
Norin 61	Parent	3181	2367	0.75	1.33
MSD17	Syn30	4216	2632	0.82	1.44
MSD117	Syn52	4013	2822	0.66	1.47
MSD26	Syn30	4282	2662	0.82	1.51
Imam	Check	4090	2318	0.53	1.79

Table 1.6 Marker–trait associations detected under heat (H) and combined heat–drought (HD) conditions, and in the drought response (DR) in 2019 and 20200.

Environment	Year	FDR threshold	Trait	Marker	Chr	Position (Mbp)	Allelic effect (%)
DR	2020	0.05	BIO	978457|F|0-57	1D	22.2894	15.0
DR	2020	0.2	BIO	979533|F|0-6	1D	473.0129	7.1
DR	2020	0.2	BIO	5332288|F|0-5	1D	480.2929	8.8
DR	2019	0.2	BIO	5579634|F|0-41	2D	428.0024	12.7
DR	2020	0.2	BIO	991074|F|0-56	3D	43.3822	9.0
HD	2020	0.2	BIO	1027779|F|0-8	3D	100.6292	9.9
HD	2020	0.2	BIO	1082224|F|0-42	3D	122.6131	9.9
HD	2020	0.2	BIO	2248892|F|0-33	3D	390.2810	7.7
DR	2020	0.2	BIO	34876945|F|0-25	3D	415.2178	9.2
DR	2020	0.2	BIO	2256582|F|0-65	4D	337.6461	7.4
DR	2020	0.2	BIO	2256582|F|0-26	4D	337.6461	7.1
DR	2020	0.05	BIO	3942413|F|0-13	4D	372.3598	14.0
DR	2020	0.05	BIO	5580487|F|0-25	5D	262.3193	11.3
DR	2020	0.2	BIO	986326|F|0-60	5D	359.1114	9.3
DR	2020	0.05	BIO	3028230|F|0-33	5D	413.7144	9.0
HD	2019	0.2	BIO	18732940|F|0-36	6B	118.8663	12.9
DR	2020	0.2	BIO	1042596|F|0-41	7D	452.2852	9.5
DR	2020	0.2	BIO	1012073|F|0-63	7D	556.3443	8.9
H	2019	0.2	CT1	1208625|F|0-68	1A	489.6421	19.4
H	2019	0.2	CT1	1019639|F|0-61	1D	39.0578	20.2
H	2020	0.2	CT1	1100678|F|0-9	1D	218.9722	9.2
H	2020	0.2	CT1	1100678|F|0-9	1D	218.9722	8.7
H	2020	0.2	CT1	1053877|F|0-54	1D	235.2711	8.7
H	2020	0.2	CT1	2256575|F|0-47	1D	379.6019	6.9
H	2020	0.2	CT1	983585|F|0-55	1D	456.8339	8.3
H	2019	0.05	CT1	1400644|F|0-12	2A	4.1489	26.3
H	2019	0.05	CT1	1204582|F|0-30	2A	741.1086	24.3
H	2019	0.05	CT1	1117704|F|0-29	2A	743.7529	52.1
H	2019	0.05	CT1	1225998|F|0-21	2A	744.7130	51.8
H	2019	0.05	CT1	1022058|F|0-20	2A	747.5276	50.3
H	2019	0.05	CT1	1250340|F|0-51	2A	768.5119	49.3
H	2019	0.05	CT1	1203799|F|0-13	2A	769.8551	23.7
H	2019	0.05	CT1	983095|F|0-31	2A	774.0126	21.1
H	2019	0.05	CT1	1100834|F|0-47	2A	775.6323	31.9
H	2019	0.05	CT1	1125759|F|0-23	2B	700.9360	29.0
H	2019	0.05	CT1	999645|F|0-14	2D	181.7422	51.0
H	2019	0.05	CT1	999645|F|0-14	2D	181.7422	27.4
H	2020	0.2	CT1	994213|F|0-21	2D	511.7080	13.3
H	2019	0.05	CT1	12775250|F|0-28	2D	645.3833	45.7
H	2019	0.05	CT1	12775250|F|0-28	2D	645.3833	27.5
H	2019	0.05	CT1	1095302|F|0-12	2D	647.8139	49.3
H	2019	0.05	CT1	1095302|F|0-12	2D	647.8139	27.9
H	2020	0.2	CT1	1027779|F|0-8	3D	100.6292	8.8
H	2019	0.2	CT1	1695255|F|0-8	3D	155.5501	11.5
H	2019	0.05	CT1	1123716|F|0-7	3D	344.5745	31.8
H	2020	0.2	CT1	1180381|F|0-15	3D	375.6582	13.6
H	2020	0.2	CT1	1180381|F|0-15	3D	375.6582	11.1
H	2019	0.05	CT1	2248241|F|0-53	3D	438.7934	50.1
H	2019	0.05	CT1	2248241|F|0-53	3D	438.7934	28.0
H	2019	0.05	CT1	1864955|F|0-22	3D	462.6768	14.3
H	2019	0.05	CT1	1041486|F|0-68	3D	487.3081	13.6
H	2019	0.2	CT1	985748|F|0-43	3D	550.7138	14.4
H	2019	0.2	CT1	1000555|F|0-21	4D	329.5449	20.8
H	2019	0.2	CT1	1218080|F|0-5	5A	333.9827	19.7
H	2019	0.2	CT1	4005828|F|0-25	5A	687.0349	17.8
H	2019	0.05	CT1	3934675|F|0-8	5A	697.2535	48.8
H	2019	0.2	CT1	4990799|F|0-17	5B	530.5696	19.0
H	2020	0.2	CT1	1201131|F|0-43	5D	407.0293	9.1
H	2020	0.2	CT1	1201131|F|0-43	5D	407.0293	8.6
H	2019	0.05	CT1	2249157|F|0-24	6D	394.0044	25.6
H	2019	0.2	CT1	1022746|F|0-47	7B	605.4248	19.8
H	2020	0.2	CT1	3030599|F|0-20	7D	4.5102	7.4
H	2019	0.05	CT1	981402|F|0-35	7D	178.6614	29.3
H	2019	0.05	CT1	981402|F|0-35	7D	178.6614	22.3
H	2020	0.05	CT1	1036583|F|0-40	7D	190.5332	12.5
H	2020	0.05	CT1	1036583|F|0-40	7D	190.5332	11.4
H	2020	0.05	CT1	1019161|F|0-13	7D	223.2847	12.5
H	2020	0.05	CT1	1019161|F|0-13	7D	223.2847	11.4
H	2020	0.2	CT1	3030400|F|0-17	7D	565.4297	9.1
DR	2020	0.05	CT2	991074|F|0-56	3D	43.3822	12.6
DR	2020	0.05	CT2	2251455|F|0-29	3D	55.1356	12.6
HD	2020	0.05	CT2	2251455|F|0-29	3D	55.1356	14.7
DR	2020	0.2	CT2	986326|F|0-60	5D	359.1114	10.8
HD	2020	0.2	CT2	986326|F|0-60	5D	359.1114	9.8
DR	2020	0.05	CT2	3028230|F|0-33	5D	413.7144	10.7
HD	2020	0.2	CT2	3028230|F|0-33	5D	413.7144	7.7

Table 1.6 continued

Environment	Year	FDR threshold	Trait	Marker	Chr	Position (Mbp)	Allelic effect (%)
DR	2020	0.05	CT2	1012073|F|0-63	7D	556.3443	10.7
HD	2020	0.2	CT2	1012073|F|0-63	7D	556.3443	7.6
H	2019	0.05	CT3	1082710|F|0-59	1A	28.7540	25.4
H	2019	0.05	CT3	3027292|F|0-37	1A	34.3785	30.9
H	2019	0.2	CT3	1129476|F|0-18	1A	38.4376	20.2
H	2019	0.05	CT3	1266478|F|0-10	1A	50.4536	30.9
H	2019	0.05	CT3	5578033|F|0-26	1B	260.3785	35.5
H	2019	0.05	CT3	39465884|F|0-7	1B	633.7054	30.6
DR	2020	0.2	CT3	977232|F|0-68	1D	13.2114	6.9
HD	2020	0.05	CT3	14822559|F|0-33	1D	308.5262	11.2
DR	2020	0.05	CT3	14822559|F|0-33	1D	308.5262	10.9
HD	2020	0.2	CT3	12002285|F|0-11	1D	315.1118	10.6
DR	2020	0.05	CT3	12002285|F|0-11	1D	315.1118	12.3
DR	2020	0.2	CT3	1104269|F|0-13	1D	394.4788	7.5
H	2019	0.05	CT3	2367294|F|0-52	1D	397.0893	27.9
DR	2020	0.2	CT3	1219506|F|0-62	1D	476.9119	8.6
H	2019	0.05	CT3	2251827|F|0-27	1D	482.0382	24.3
H	2019	0.2	CT3	3955635|F|0-50	1D	489.0957	10.7
H	2019	0.2	CT3	15322778|F|0-26	2D	50.6058	18.1
H	2019	0.05	CT3	1862989|F|0-7	2D	61.5520	30.6
H	2019	0.05	CT3	1095082|F|0-64	2D	136.9053	27.9
DR	2020	0.2	CT3	3222134|F|0-18	2D	220.5234	9.5
H	2019	0.05	CT3	5580230|F|0-26	3A	198.2549	24.5
H	2019	0.05	CT3	2277485|F|0-63	3A	699.9934	35.1
H	2019	0.05	CT3	1064764|F|0-14	3A	709.6537	31.6
H	2019	0.2	CT3	985381|F|0-20	3A	710.9380	20.4
H	2019	0.05	CT3	1090686|F|0-37	3A	712.3853	30.6
H	2019	0.2	CT3	1203001|F|0-61	3A	715.1586	19.9
H	2019	0.2	CT3	3024755|F|0-41	3A	715.1991	19.9
H	2019	0.2	CT3	1065425|F|0-44	3A	715.9048	19.8
H	2019	0.2	CT3	2256792|F|0-61	3A	716.2733	19.8
H	2019	0.2	CT3	2254238|F|0-9	3A	718.7174	19.8
H	2019	0.05	CT3	1218356|F|0-42	3B	449.7833	30.7
H	2019	0.2	CT3	3022046|F|0-15	3B	774.4936	21.3
HD	2020	0.2	CT3	1015501|F|0-10	3D	164.8254	10.2
DR	2020	0.2	CT3	4005454|F|0-33	3D	170.8416	7.2
H	2019	0.2	CT3	2245285|F|0-11	4D	301.8567	20.7
H	2019	0.05	CT3	3027828|F|0-27	4D	366.1985	15.4
H	2019	0.2	CT3	2250763|F|0-61	5D	410.7371	11.8
H	2019	0.05	CT3	1694818|F|0-5	5D	413.3888	32.8
H	2019	0.05	CT3	1066627|F|0-41	5D	441.2354	30.7
H	2019	0.05	CT3	1012707|F|0-49	5D	538.9146	17.1
H	2019	0.2	CT3	1106487|F|0-6	6D	92.6181	13.5
H	2019	0.05	CT3	2261024|F|0-26	6D	359.0751	28.8
H	2019	0.05	CT3	3025223|F|0-14	7D	455.6705	15.8
H	2019	0.2	DH	1280070|F|0-32	1A	23.3047	21.2
H	2019	0.2	DM	1072074|F|0-40	1D	348.1509	10.2
DR	2020	0.2	DM	991772|F|0-64	3D	507.1450	7.9
HD	2020	0.2	DM	3944690|F|0-29	5D	203.7861	7.9
DR	2019	0.2	DM	1040939|F|0-46	7D	196.7994	12.2
HD	2019	0.2	G_C	3948039|F|0-20	1D	236.2379	15.0
HD	2020	0.05	GFD	1228823|F|0-17	2D	354.3297	12.9
HD	2020	0.2	GFD	1201290|F|0-33	3D	374.0499	9.8
HD	2020	0.2	GFD	1129525|F|0-13	3D	444.1162	9.3
DR	2020	0.2	GFD	991772|F|0-64	3D	507.1450	8.0
DR	2020	0.2	GFD	4261480|F|0-22	5D	421.6186	8.2
H	2020	0.2	GFD	1090466|F|0-31	6D	37.1887	12.1
H	2020	0.2	GFD	1167866|F|0-33	6D	118.8877	12.1
H	2020	0.2	GFD	983854|F|0-28	6D	151.0065	11.4
H	2020	0.2	GFD	1120327|F|0-5	6D	295.3397	11.4
H	2019	0.05	GFD	3027860|F|0-38	7D	108.3397	11.8
HD	2020	0.05	GFD	1027554|F|0-17	7D	431.8969	12.9
HD	2020	0.2	GFD	1155271|F|0-34	7D	587.1039	9.5
DR	2019	0.2	GY	3937862|F|0-24	1D	58.7242	12.8
DR	2020	0.2	GY	3934484|F|0-17	1D	394.1505	7.8
DR	2020	0.2	GY	3936699|F|0-5	1D	437.3718	7.4
DR	2020	0.2	GY	1102235|F|0-11	1D	483.2768	7.3
DR	2019	0.2	GY	3028687|F|0-7	2A	93.3807	23.7
DR	2019	0.2	GY	4002222|F|0-30	2B	727.0959	22.7
HD	2020	0.2	GY	3020847|F|0-49	2D	23.1102	7.6
DR	2019	0.05	GY	2244489|F|0-10	2D	411.5232	16.1
DR	2020	0.2	GY	3940297|F|0-5	2D	521.6837	9.0
DR	2020	0.05	GY	1221747|F|0-26	2D	553.2400	17.7
DR	2019	0.05	GY	1702486|F|0-35	2D	574.0426	16.1
DR	2019	0.05	GY	981901|F|0-9	2D	607.2500	16.2
DR	2019	0.2	GY	1229938|F|0-14	3B	68.1182	21.7
DR	2020	0.2	GY	4538129|F|0-30	3D	7.6912	9.4
DR	2020	0.05	GY	982662|F|0-31	3D	73.8790	15.6

Table 1.6 continued

Environment	Year	FDR threshold	Trait	Marker	Chr	Position (Mbp)	Allelic effect (%)
H	2020	0.2	GY	998513|F|0-66	3D	508.3279	11.8
H	2020	0.2	GY	7940688|F|0-16	3D	521.7681	10.6
DR	2019	0.2	GY	1125420|F|0-29	3D	548.3149	21.5
DR	2020	0.2	GY	1072095|F|0-54	3D	549.4055	9.6
DR	2020	0.05	GY	1076657|F|0-26	3D	567.5813	9.7
HD	2020	0.2	GY	1076657|F|0-26	3D	567.5813	7.8
DR	2019	0.2	GY	2276594|F|0-47	5B	112.6573	21.1
DR	2019	0.2	GY	6044207|F|0-13	5B	377.6620	21.3
DR	2020	0.2	GY	1023486|F|0-67	5D	61.3813	9.2
DR	2020	0.05	GY	2256906|F|0-13	5D	356.6147	13.5
HD	2020	0.2	GY	2256906|F|0-13	5D	356.6147	8.5
DR	2020	0.2	GY	7913266|F|0-32	5D	456.6315	7.2
DR	2020	0.2	GY	7913266|F|0-37	5D	456.6315	7.2
DR	2019	0.2	GY	18732940|F|0-36	6B	69.3127	22.1
HD	2019	0.2	GY	18732940|F|0-36	6B	69.3127	14.4
DR	2019	0.05	GY	1120327|F|0-5	6D	295.3397	15.5
DR	2020	0.05	GY	988652|F|0-39	6D	452.8791	19.3
HD	2020	0.2	GY	988652|F|0-39	6D	452.8791	8.5
DR	2019	0.2	GY	2280684|F|0-22	7A	517.0785	22.3
DR	2019	0.2	GY	2295102|F|0-20	7A	556.9312	21.9
DR	2019	0.2	GY	1218720|F|0-55	7A	557.2462	22.1
DR	2019	0.2	GY	1075160|F|0-13	7A	601.3921	24.1
DR	2019	0.2	GY	1112580|F|0-49	7A	632.6262	21.0
HD	2020	0.2	GY	3064942|F|0-34	7B	284.5448	14.5
DR	2019	0.2	GY	989685|F|0-12	7B	605.8777	21.4
DR	2019	0.2	GY	3064670|F|0-45	7B	633.4278	21.4
DR	2019	0.05	GY	3961023|F|0-32	7D	5.0627	15.3
DR	2020	0.05	GY	7351646|F|0-20	7D	592.3659	12.3
DR	2019	0.2	HI	3937862|F|0-24	1D	58.7242	13.8
H	2019	0.2	HI	4983856|F|0-56	2A	31.6385	18.6
HD	2020	0.2	HI	3020847|F|0-49	2D	23.1102	8.5
HD	2020	0.2	HI	1051868|F|0-51	2D	329.2793	7.6
DR	2020	0.05	HI	3022387|F|0-13	3D	310.6874	11.0
DR	2020	0.2	HI	1004442|F|0-37	5D	454.1256	9.8
DR	2020	0.2	HI	4009212|F|0-6	6D	406.0862	7.2
HD	2020	0.05	HI	12470469|F|0-28	6D	444.6109	14.2
DR	2019	0.2	HI	7930420|F|0-6	7D	63.0088	13.8
DR	2020	0.2	HI	1025259|F|0-41	7D	175.6386	7.1
DR	2020	0.05	KPS	2281182|F|0-22	1B	589.9174	39.6
DR	2020	0.05	KPS	1082855|F|0-31	1B	676.8726	39.3
HD	2020	0.2	KPS	7491847|F|0-11	1D	111.8955	8.7
DR	2020	0.2	KPS	2251549|F|0-38	1D	204.8098	10.2
HD	2020	0.05	KPS	3024574|F|0-11	1D	437.0821	9.8
HD	2020	0.2	KPS	2256681|F|0-65	1D	471.0102	9.7
DR	2020	0.05	KPS	3939561|F|0-7	2A	750.5348	38.8
DR	2020	0.05	KPS	9724257|F|0-11	2B	548.7828	40.4
DR	2020	0.2	KPS	1028905|F|0-46	2B	595.5288	20.7
DR	2020	0.2	KPS	2241754|F|0-65	2D	448.6926	8.0
HD	2020	0.2	KPS	994213|F|0-21	2D	511.7080	11.2
DR	2020	0.2	KPS	3954462|F|0-18	2D	554.1597	7.1
DR	2020	0.05	KPS	1142851|F|0-23	2D	583.9378	34.9
DR	2020	0.05	KPS	2254347|F|0-61	2D	632.5982	17.4
DR	2020	0.05	KPS	3064854|F|0-28	3B	692.8034	38.9
DR	2020	0.2	KPS	7165313|F|0-16	3B	694.0363	19.9
DR	2020	0.2	KPS	1029529|F|0-51	3D	79.0855	22.4
DR	2020	0.05	KPS	2244538|F|0-18	3D	88.0099	12.0
DR	2020	0.05	KPS	1057222|F|0-51	3D	90.2898	18.9
DR	2020	0.05	KPS	1120667|F|0-53	3D	112.8914	24.4
DR	2020	0.05	KPS	1120667|F|0-53	3D	112.8914	13.4
DR	2020	0.2	KPS	1219209|F|0-42	3D	355.7334	20.9
DR	2020	0.05	KPS	3937529|F|0-7	3D	396.4758	26.1
DR	2020	0.05	KPS	3937529|F|0-7	3D	396.4758	15.7
DR	2020	0.05	KPS	985748|F|0-43	3D	550.7138	15.3
DR	2020	0.2	KPS	1268903|F|0-29	4A	163.9526	21.8
DR	2020	0.2	KPS	5346492|F|0-14	4D	374.9368	7.1
DR	2020	0.2	KPS	4910519|F|0-19	4D	505.8963	7.2
DR	2020	0.2	KPS	1050802|F|0-46	5A	420.0481	19.9
DR	2020	0.2	KPS	3032576|F|0-19	5A	522.7827	16.4
DR	2020	0.05	KPS	1068618|F|0-28	5B	335.9755	21.0
DR	2020	0.05	KPS	7351923|F|0-56	5D	240.6867	9.6
DR	2020	0.05	KPS	1230357|F|0-39	5D	240.6867	9.6
DR	2020	0.2	KPS	1056569|F|0-52	5D	333.1162	7.2
DR	2020	0.05	KPS	981730|F|0-67	5D	333.5014	34.9
DR	2020	0.2	KPS	1147918|F|0-8	5D	335.3534	20.1
DR	2020	0.05	KPS	2295453|F|0-32	5D	351.9524	35.3
DR	2020	0.2	KPS	1050815|F|0-41	5D	399.1483	10.1
DR	2020	0.05	KPS	2252899|F|0-22	5D	408.0288	9.6
DR	2020	0.2	KPS	3024415|F|0-22	5D	408.6572	9.1

Table 1.6 continued

Environment	Year	FDR threshold	Trait	Marker	Chr	Position (Mbp)	Allelic effect (%)
DR	2020	0.2	KPS	3023148|F|0-12	5D	421.7364	8.9
DR	2020	0.2	KPS	12770582|F|0-5	5D	526.2812	8.6
DR	2020	0.2	KPS	1203503|F|0-26	6B	17.9132	20.6
H	2019	0.2	KPS	2291659|F|0-35	6D	91.6709	16.3
DR	2020	0.05	KPS	1044960|F|0-37	6D	404.6068	16.3
DR	2020	0.05	KPS	986959|F|0-25	7A	146.7970	40.3
DR	2020	0.05	KPS	10984056|F|0-9	7A	517.1089	39.1
DR	2020	0.05	KPS	3949858|F|0-7	7D	39.0252	12.7
HD	2020	0.2	KPS	22841076|F|0-20	7D	92.3689	10.5
HD	2020	0.2	KPS	1020172|F|0-12	7D	118.8356	9.6
HD	2020	0.2	KPS	1024554|F|0-10	7D	153.6798	11.8
DR	2020	0.2	KPS	2243298|F|0-67	7D	257.6928	11.1
HD	2020	0.2	KPS	2248959|F|0-26	7D	345.3421	9.6
DR	2020	0.05	KPS	1144732|F|0-47	7D	379.9396	17.8
HD	2020	0.2	KPS	1144732|F|0-47	7D	379.9396	10.8
HD	2020	0.2	KPS	3025839|F|0-21	7D	384.1649	9.6
HD	2020	0.2	KPS	1059871|F|0-13	7D	418.3697	9.6
HD	2020	0.2	KPS	1005586|F|0-41	7D	519.9590	9.2
DR	2020	0.2	KPS	1696595|F|0-43	7D	592.1031	10.3
DR	2020	0.2	NDVI	2242928|F|0-11	1D	23.3051	7.5
H	2020	0.2	NDVI	1073622|F|0-6	1D	475.7898	12.9
DR	2020	0.05	NDVI	1017634|F|0-37	2D	47.0812	10.5
HD	2020	0.2	NDVI	994213|F|0-21	2D	511.7080	11.4
DR	2020	0.05	NDVI	1072470|F|0-26	2D	553.3073	10.7
HD	2020	0.05	NDVI	1385391|F|0-63	2D	606.4292	15.5
HD	2020	0.2	NDVI	1228058|F|0-36	2D	607.1657	9.7
HD	2020	0.05	NDVI	1161247|F|0-23	2D	614.0180	12.3
HD	2020	0.2	NDVI	4734029|F|0-28	2D	614.1774	9.2
HD	2020	0.2	NDVI	2243702|F|0-5	2D	615.0569	11.2
HD	2020	0.05	NDVI	3027000|F|0-12	2D	618.0410	15.4
H	2019	0.2	NDVI	3945625|F|0-14	3A	608.1538	18.4
HD	2020	0.2	NDVI	4999631|F|0-16	3D	6.7293	9.2
HD	2020	0.2	NDVI	1165624|F|0-46	3D	18.0539	9.3
H	2020	0.2	NDVI	1015501|F|0-10	3D	164.8254	12.6
DR	2020	0.05	NDVI	1080037|F|0-25	3D	192.9016	10.6
DR	2020	0.2	NDVI	997530|F|0-63	3D	437.8283	8.3
DR	2020	0.05	NDVI	1022931|F|0-7	3D	466.7390	10.7
DR	2020	0.05	NDVI	998513|F|0-66	3D	508.3279	11.2
DR	2020	0.05	NDVI	39678720|F|0-15	5D	47.0960	10.6
DR	2020	0.2	NDVI	1863353|F|0-35	5D	371.2321	23.5
DR	2020	0.05	NDVI	1095120|F|0-15	5D	408.0284	10.3
DR	2020	0.2	NDVI	2250763|F|0-61	5D	410.7371	9.0
DR	2020	0.2	NDVI	1694818|F|0-11	5D	413.3888	8.7
DR	2020	0.2	NDVI	1201507|F|0-56	5D	489.8934	8.1
H	2019	0.2	NDVI	986239|F|0-26	6D	394.8296	9.9
H	2019	0.2	NDVI	1016778|F|0-52	6D	402.4929	10.5
DR	2020	0.05	NDVI	1021994|F|0-55	7D	287.8062	13.1
DR	2020	0.2	PH	1038325|F|0-42	3D	416.2526	8.4
DR	2020	0.2	PH	6026258|F|0-10	3D	416.6197	8.4
H	2019	0.05	PH	1042486|F|0-52	4A	577.5632	23.9
HD	2020	0.2	PH	1001495|F|0-20	4A	577.7311	21.2
HD	2020	0.05	PH	3222279|F|0-26	4D	0.8496	9.5
HD	2020	0.05	PH	1079306|F|0-62	4D	25.7018	25.7
H	2020	0.05	PH	1079306|F|0-62	4D	25.7018	19.1
HD	2019	0.2	PH	1079306|F|0-62	4D	25.7018	16.6
H	2019	0.05	PH	1079306|F|0-62	4D	25.7018	15.2
H	2020	0.2	PH	4005784|F|0-33	4D	36.8667	9.7
HD	2020	0.2	PH	4005784|F|0-33	4D	36.8667	7.2
HD	2020	0.2	PH	993587|F|0-12	4D	210.1766	10.0
HD	2020	0.2	PH	1022761|F|0-32	4D	337.3152	8.8
HD	2020	0.2	PH	3937707|F|0-14	5D	209.1281	8.5
HD	2020	0.2	PH	995342|F|0-48	5D	514.8222	6.7
HD	2020	0.2	PH	3027201|F|0-17	6D	442.2847	9.3
DR	2020	0.2	PH	1046126|F|0-14	6D	465.1571	8.4
HD	2020	0.2	PH	2249760|F|0-32	7D	390.7814	8.4
DR	2020	0.2	PH	2249077|F|0-37	7D	567.9780	7.3
ALL	ALL	0.05	SI	998513|F|0-66	3D	508.3279	20.3
ALL	ALL	0.2	SI	988144|F|0-65	6D	454.7564	12.5
DR	2020	0.2	SN	1696345|F|0-38	1D	421.8725	9.3
DR	2020	0.2	SN	2245733|F|0-34	3D	291.0051	9.4
DR	2020	0.05	SN	5340160|F|0-18	3D	512.0049	11.2
DR	2020	0.05	SN	1085853|F|0-11	4D	388.4887	11.8
H	2019	0.2	SN	1059847|F|0-61	5D	57.5152	11.9
DR	2020	0.2	SN	1083351|F|0-31	6D	292.9532	9.7
DR	2020	0.05	SN	4005686|F|0-16	6D	346.9821	9.7
DR	2020	0.2	SN	2259985|F|0-12	6D	386.8372	10.8
DR	2020	0.2	SN	1672718|F|0-29	6D	402.3285	7.5
DR	2020	0.05	SN	7491478|F|0-13	6D	425.5487	15.5

Table 1.6 continued

Environment	Year	FDR threshold	Trait	Marker	Chr	Position (Mbp)	Allelic effect (%)
HD	2020	0.05	SPAD	1236663|F|0-12	5D	344.2854	17.3
DR	2020	0.05	SPAD	1236663|F|0-12	5D	344.2854	16.8
HD	2020	0.2	TKW	1385391|F|0-63	2D	606.4292	10.9
HD	2020	0.05	TKW	1228058|F|0-36	2D	607.1657	10.5
HD	2020	0.2	TKW	1161247|F|0-23	2D	614.0180	7.7
HD	2020	0.2	TKW	4734029|F|0-28	2D	614.1774	7.1
H	2019	0.2	TKW	1057222|F|0-51	3D	90.2898	9.3
HD	2020	0.2	TKW	985748|F|0-43	3D	550.7138	9.1
HD	2020	0.2	TKW	1167421|F|0-66	5D	7.9770	8.3
DR	2020	0.2	TKW	7351923|F|0-56	5D	240.6867	7.4
DR	2020	0.2	TKW	1230357|F|0-39	5D	240.6867	7.3
H	2020	0.2	TKW	3943127|F|0-20	7D	531.7219	10.1
H	2019	0.2	$\delta^{13}C$	1020943|F|0-38	2D	96.6961	10.1

Table 1.7 Stable and pleiotropic MTAs under heat (H) and combined heat–drought (HD) conditions, and in the drought response (DR) in 2019 and 2020.

Environment	Year	FDR threshold	Trait (Specific environment)	Marker	Chr.	Position (Mbp)	Allelic effect (%)
DR	2019	0.2	GY, HI	3937862|F|0-24	1D	58.724191	12.8–13.7
HD	2020	0.2	GY, HI	3020847|F|0-49	2D	23.110173	7.6–8.5
H, HD, DR	2020	0.05	GY, SI, NDVI	998513|F|0-66	3D	508.32788	11.2–20.3
HD, DR	2020	0.05	GY	1076657|F|0-26	3D	567.58126	7.7–9.7
HD, DR	2020	0.05	GY	2256906|F|0-13	5D	356.61467	8.5–13.5
H, DR	2019, 2020	0.2	GY (DR2019), GFD(H2020)	1120327|F|0-5	6D	295.33974	11.4–15.5
HD, DR	2020	0.05	GY	988652|F|0-39	6D	452.87905	8.5–19.3
H, HD	2019	0.2	GY	1218720|F|0-55	7A	557.24618	14.6–22.1
HD, DR	2019	0.2	GY, BIO (HD2019)	18732940|F|0-36	6B	69.312667	12.9–22.1
HD	2020	0.05	TKW, NDVI	1161247|F|0-23	2D	614.01796	7.7–12.3
HD	2020	0.2	TKW, NDVI	4734029|F|0-28	2D	614.17744	7.1–9.2
H, DR	2019, 2020	0.05	TKW (H2019), KPS (DR2020)	1057222|F|0-51	3D	90.289806	9.3–18.9
HD, DR	2019, 2020	0.2	TKW (HD2020), KPS (DR2020), CT1(HD2019)	985748|F|0-43	3D	550.71378	9.1–15.3
DR	2020	0.05	TKW, KPS	7351923|F|0-56	5D	240.6867	7.4–9.6
DR	2020	0.05	TKW, KPS	1230357|F|0-39	5D	240.6867	7.3–9.6
HD	2020	0.05	TKW, NDVI	1385391|F|0-63	2D	606.42916	10.9–15.5
HD	2020	0.2	TKW, NDVI	1228058|F|0-36	2D	607.16567	9.7–10.5
HD	2020	0.05	TKW, NDVI	1161247|F|0-23	2D	614.01796	7.7–12.3
HD	2020	0.2	TKW, NDVI	4734029|F|0-28	2D	614.17744	7.1–9.2
HD	2020	0.05	TKW, NDVI	1385391|F|0-63	2D	606.42916	10.8–15.521
H, HD	2020	0.2	KPS, CT1, NDVI	994213|F|0-21	2D	511.70796	11.2–13.3
DR	2020	0.2	BIO, CT2	991074|F|0-56	3D	43.382158	8.9–12.6
HD, DR	2020	0.2	BIO (DR), CT2	986326|F|0-60	5D	359.1114	9.3–10.8
HD, DR	2020	0.05	BIO (DR), CT2	3028230|F|0-33	5D	413.71439	7.7–10.7
HD, DR	2020	0.2	BIO (DR), CT2	1012073|F|0-63	7D	556.34431	8.9–10.7
H, HD, DR	2019, 2020	0.05	PH	1079306|F|0-62	4D	25.701834	15.2–27.3
H, HD	2020	0.2	PH	4005784|F|0-33	4D	36.86672	7.2–9.7
DR	2020	0.2	DM, GFD	991772|F|0-64	3D	507.14502	7.9–8.0
HD, DR	2020	0.05	CT2	2251455|F|0-29	3D	55.135592	12.6–14.7
HD, DR	2020	0.05	CT3	12002285|F|0-11	1D	315.11177	10.6–12.3
H, HD	2020	0.2	CT3, NDVI	1015501|F|0-10	3D	164.82545	10.2–12.6
H, DR	2019, 2020	0.2	CT3, NDVI	2250763|F|0-61	5D	410.7371	9.0–11.8
HD, DR	2020	0.05	SPAD	1236663|F|0-12	5D	344.28537	16.8–17.3
HD	2020	0.2	NDVI	1228058|F|0-36	2D	607.16567	9.7–10.5

Traits without an environment in parenthesis were identified in the environment(s) and year(s) listed in the first and second columns, respectively. BIO, biomass; CT1, canopy temperature 7 days before flowering; CT2, canopy temperature at flowering; CT3, canopy temperature at grain filling; DM, days to maturity; GFD, grain-filling duration; GY, grain yield; HI, harvest index; KPS, kernel number per spike; NDVI, normalized difference vegetation index; PH, plant height; SI, GY stability index; SPAD, chlorophyll content; TKW, thousand-kernel weight.

Table 1.8 Selected candidate genes for marker–trait associations and their locations and functions.

Condition	Year	FDR	Trait	Marker	Chr	Pos (Mbp)	Allelic effect (%)	Candidate gene	Candidate gene location	Gene function
H, HD	2019 (H), 2020 (HD)	0.05	PH	1042486|F|0-52	4A	577.563158	23.892	TraesCS4A02G274300	chr4A:584388335..584388391	Probable ethylene response sensor 1 (OsERS1) in rice, based on seuquence prediction.
H, HD	2019 (H), 2020 (H, HD)	0.2	PH	1001495|F|0-20	4A	577.731119	21.222	TraesCS4A02G276600	chr4A:584553204..584553272	ATCES1; Hydrolyses only phytoceramide into phytosphingosine and free fatty acid (PubMed:25619405). Does not have reverse activity (By similarity). Affects plant morphogenesis. Required for the formation of wax layer that ensure cuticle permeability. Implicated in abscisic acid (ABA)-mediated stomatal closure. Involved in both biotic and abiotic stresses. Promotes salt resistance and defense responses toward pathogenic bacteria (e.g. *P.syringae*) and against the fungal toxin fumonisin B1 (FB1)
H, HD, DR	2019, 2020	0.2	PH	1079306|F|0-62	4D	25.701834	27.269	TraesCS4D02G049700	chr4D:25193438..25193506	Protein POLLEN DEFECTIVE IN GUIDANCE 1
H, HD	2020	0.2	PH	4005784|F|0-33	4D	36.86672	9.684	TraesCS4D02G060900	chr4D:36446783..36446826	Calcium-transporting ATPase
DR, HD	2020	0.05	GY	2256906|F|0-13	5D	356.614667	13.473	TraesCS5D02G248600	chr5D:355677599..355677667	Glycosyltransferase
DR, HD	2020	0.05	GY	1076657|F|0-26	3D	567.581264	9.749	TraesCS3D02G466100	chr3D:569516179..569516247	E3 ubiquitin protein ligase
H, HD, DR	2019, 2020	0.05	SI, GY (H2020), NDVI (DR2020)	998513|F|0-66	3D	508.327883	20.304	TraesCS3D02G394000	chr3D:509245722..509245789	GA20ox-D3 protein (Catalyses the formation of bioactive gibberellins (GAs) via a three-step oxidation at C-20 of the GA skeleton). In Barley, GA20ox3 (HORVU3Hr1G089980) is expressed in aleurone layers during germination. In rice, GA20ox3 decrease in the developing anthers by exposure to low temperature.
HD, DR	2020	0.05	CT3	12002285|F|0-11	1D	315.111774	15.041	TraesCS1D02G228400	chr1D:316235578..316235646	CAAX prenyl protease 2 (Finding CAAX motif and proteolyzing target ->Prenylation of CAAX proteins -> anchoring to cellular membrane -> ABA response)

H, heat stress; HD, combined heat–drought stress; DR, drought response under heat stress; FDR, False Discovery Rate threshold.

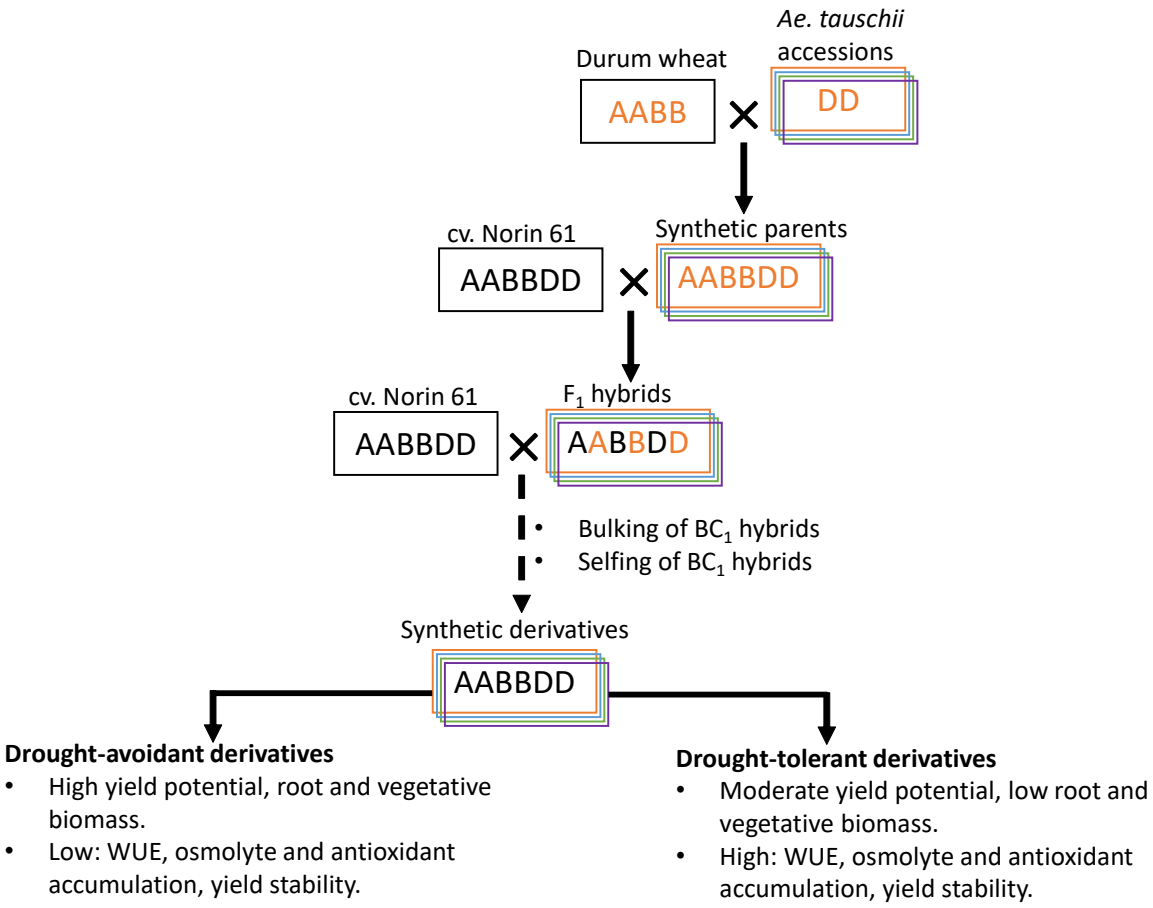

Figure 1.1 Schematic diagram of a diversity breeding scheme showing wide hybridization, selection and characterization for drought resilience in wheat (adapted from Tsujimoto et al. (2015)).

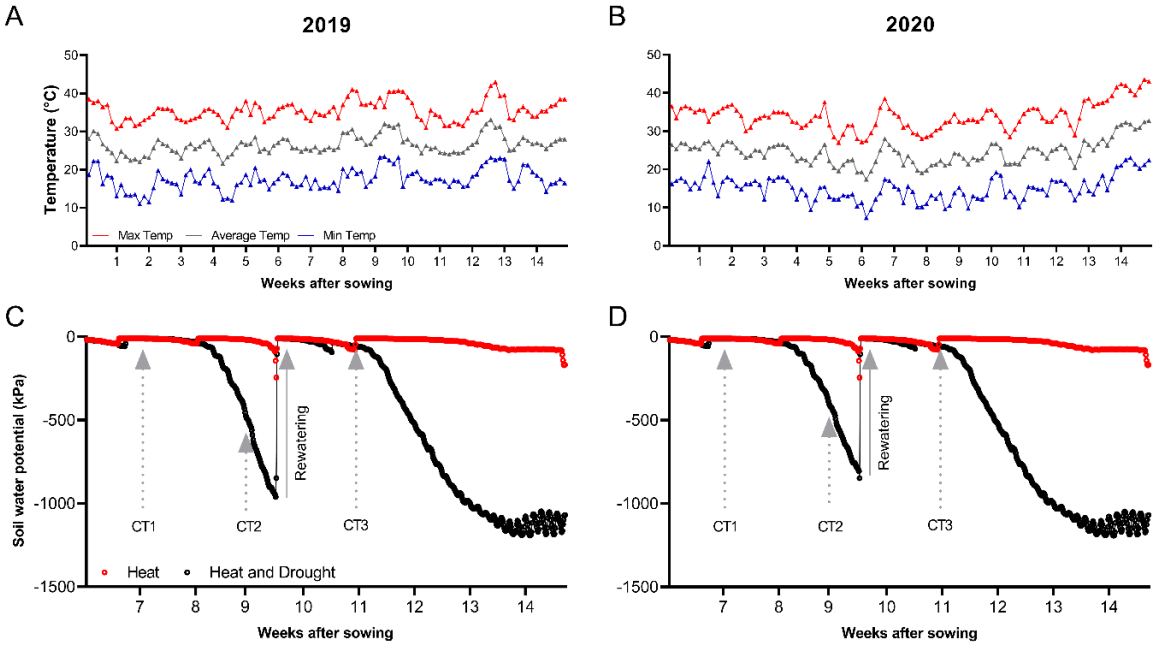

Figure 1.2 Field conditions. (A, B) Daily air temperature in (A) 2019 and (B) 2020. (C, D) Soil water potential in heat and combined heat–drought conditions in (C) 2019 and (D) 2020. The dotted arrows indicate the time points when the three canopy temperature measurements (CT1, CT2, and CT3) were taken.

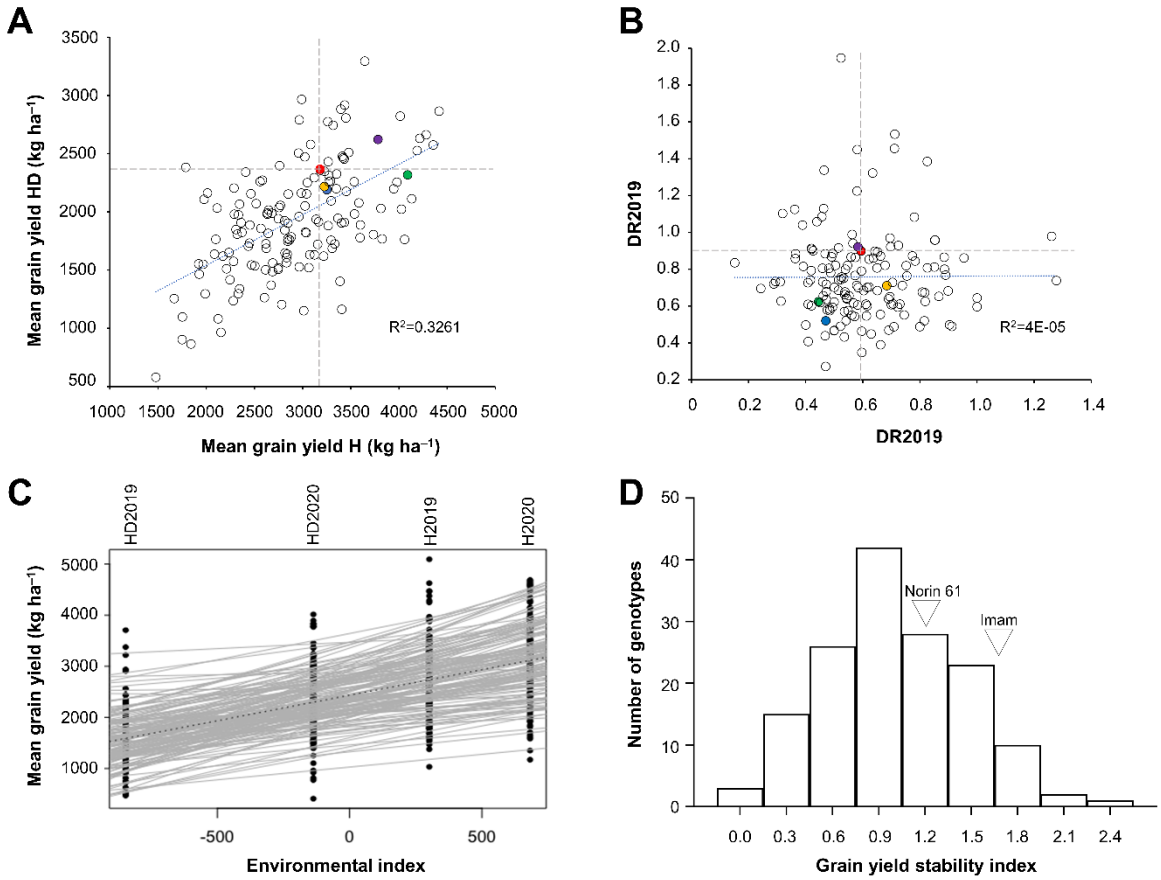

Figure 1.3 Grain yield parameters of the investigated genotypes. (A) Average grain yield under heat (H) and heat–drought (HD) conditions, (B) drought response under heat stress (DR) in 2019 and 2020. Dashed grey lines intersect on 'Norin 61' (red circle), the backcross parent. Check cultivars: green circles, 'Imam'; blue circles, 'Fielder'; violet circles, 'Roelf'; and yellow circles, 'Gomria' (C, D) yield stability index across the four environments. (C) Each line represents mean grain yield for each genotype. The dashed line represents the population mean. Most of the genotypes showed a decreasing trend in grain yield under HD. (D) The most stable lines have a lower stability index (< 1.0) compared with the less stable lines. Some genotypes are more stable than 'Norin 61' and 'Imam'.

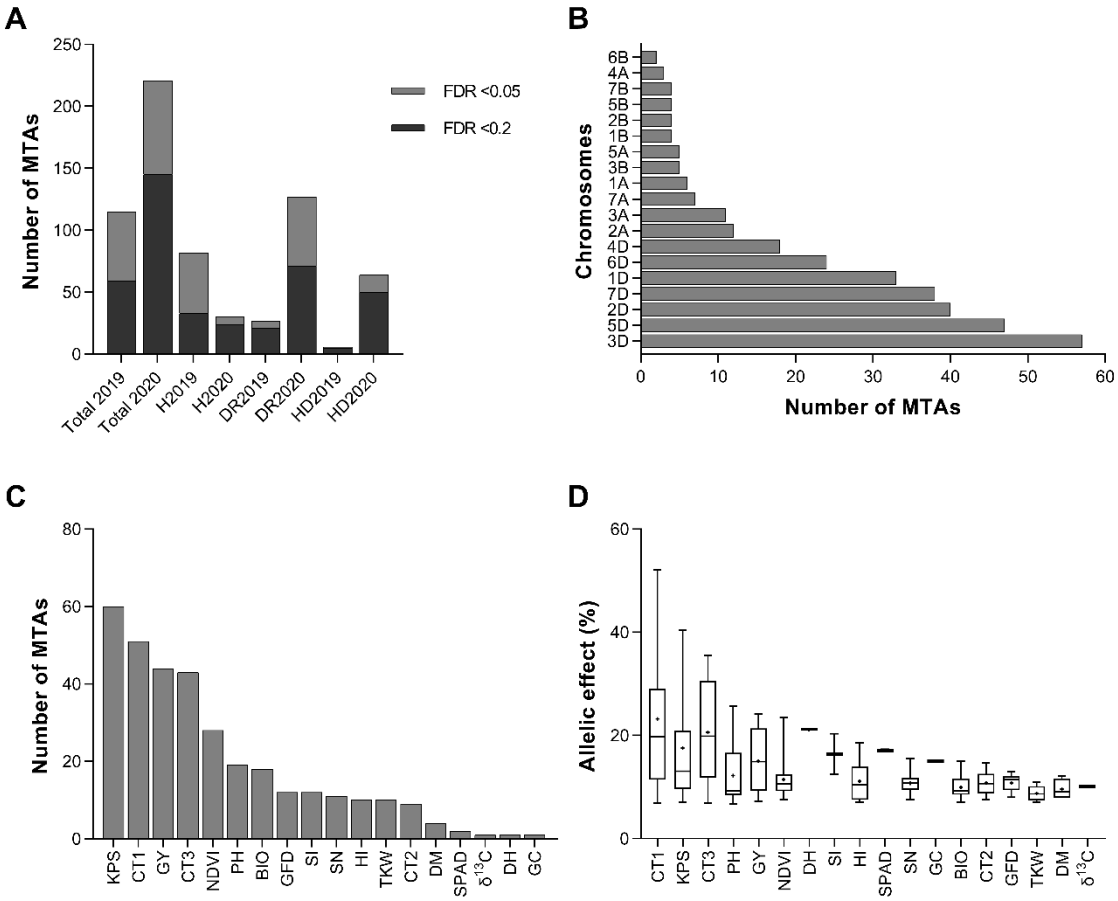

Figure 1.4 Summary of marker–trait associations. (A) Number of MTAs in each field condition in 2019 and 2020; (B) number of MTAs identified on each chromosome; (C) number of MTAs identified for each trait; and (D) the range of allelic effects of MTAs in each trait. BIO, biomass; CT1, canopy temperature at 7 days before flowering; CT2, canopy temperature at flowering; CT3, canopy temperature at grain filling; DH, days to 50% heading; DM, days to maturity; GC, ground cover; GFD, grain-filling duration; GY, grain yield; HI, harvest index; KPS, kernel number per spike; NDVI, normalized difference vegetation index; PH, plant height; SI, GY stability index; SN, number of spikes per m^2; SPAD, chlorophyll content; TKW, thousand-kernel weight; $\delta^{13}C$, delta carbon-13 value

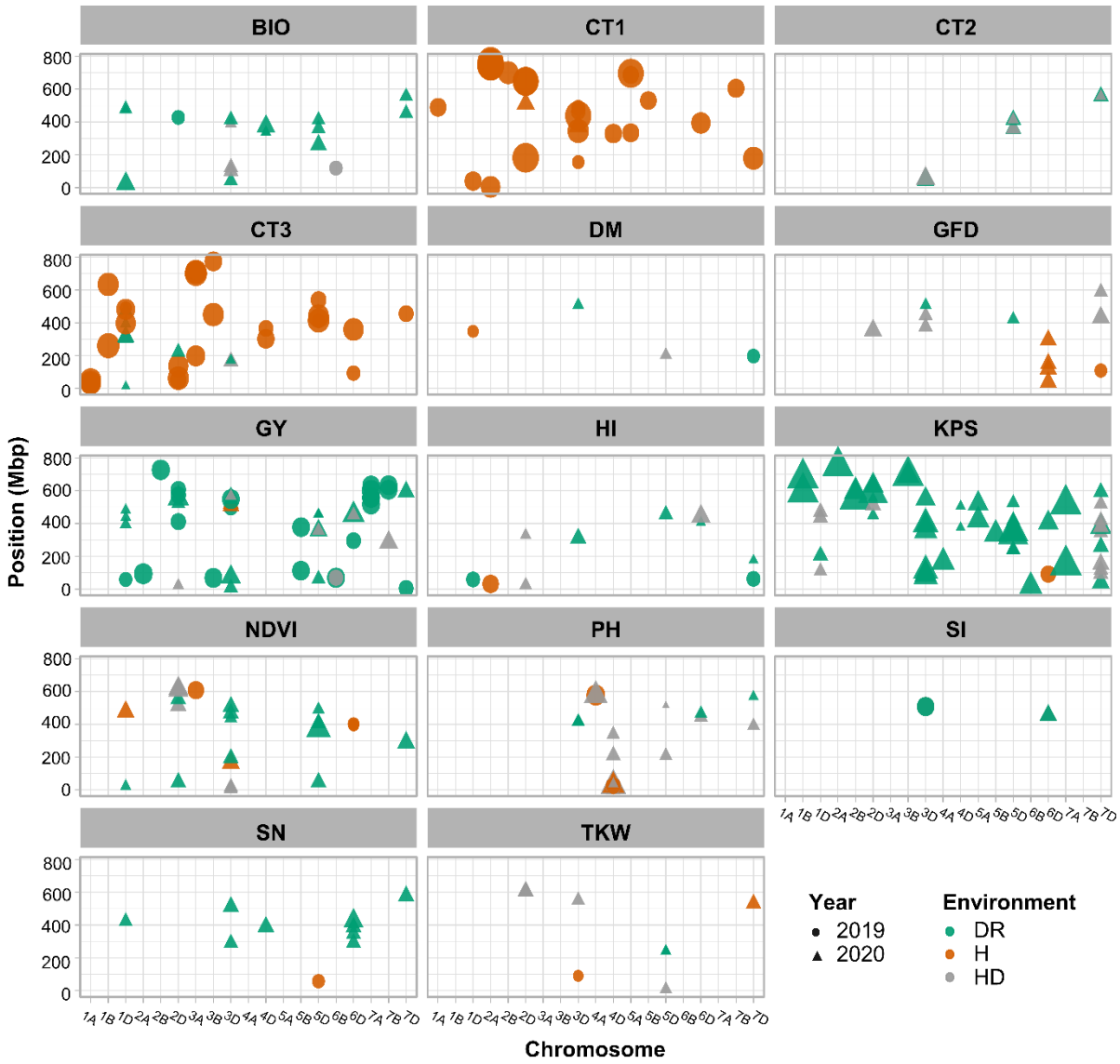

Figure 1.5 Physical positions of markers associated with evaluated traits under heat (H) and combined heat–drought (HD) conditions, and in the drought response under heat stress (DR). Symbol size corresponds to the allelic effect of each MTA. BIO, biomass; CT1, canopy temperature 7 days before flowering; CT2, canopy temperature at flowering; CT3, canopy temperature at grain filling; DM, days to maturity; GFD, grain-filling duration; GY, grain yield; HI, harvest index; KPS, kernel number per spike; NDVI, normalized difference vegetation index; PH, plant height; SI, grain yield stability index; SN, number of spikes per m^2; TKW, thousand-kernel weight.

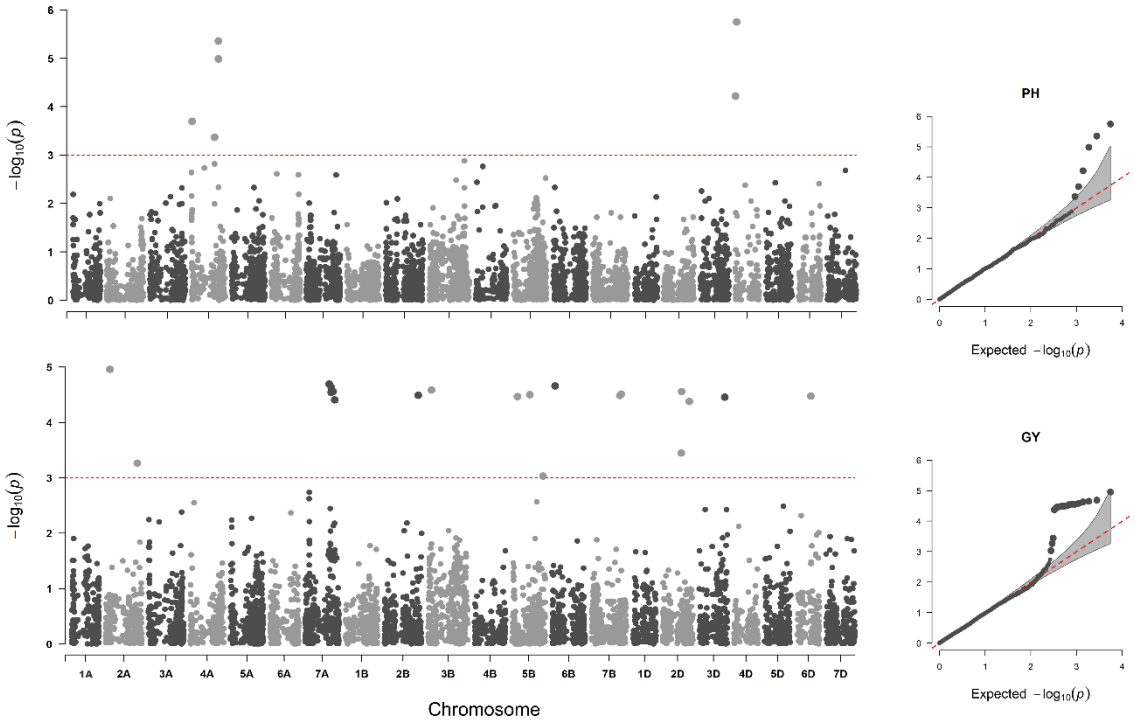

Figure 1.6 Representative Manhattan plots of plant height (PH) and grain yield (GY) showing marker–trait associations in all three subgenomes of bread wheat lines under combined heat and drought stress (for PH) and in the drought response (for GY). The quantile–quantile plots of the genome-wide analysis are shown on the right.

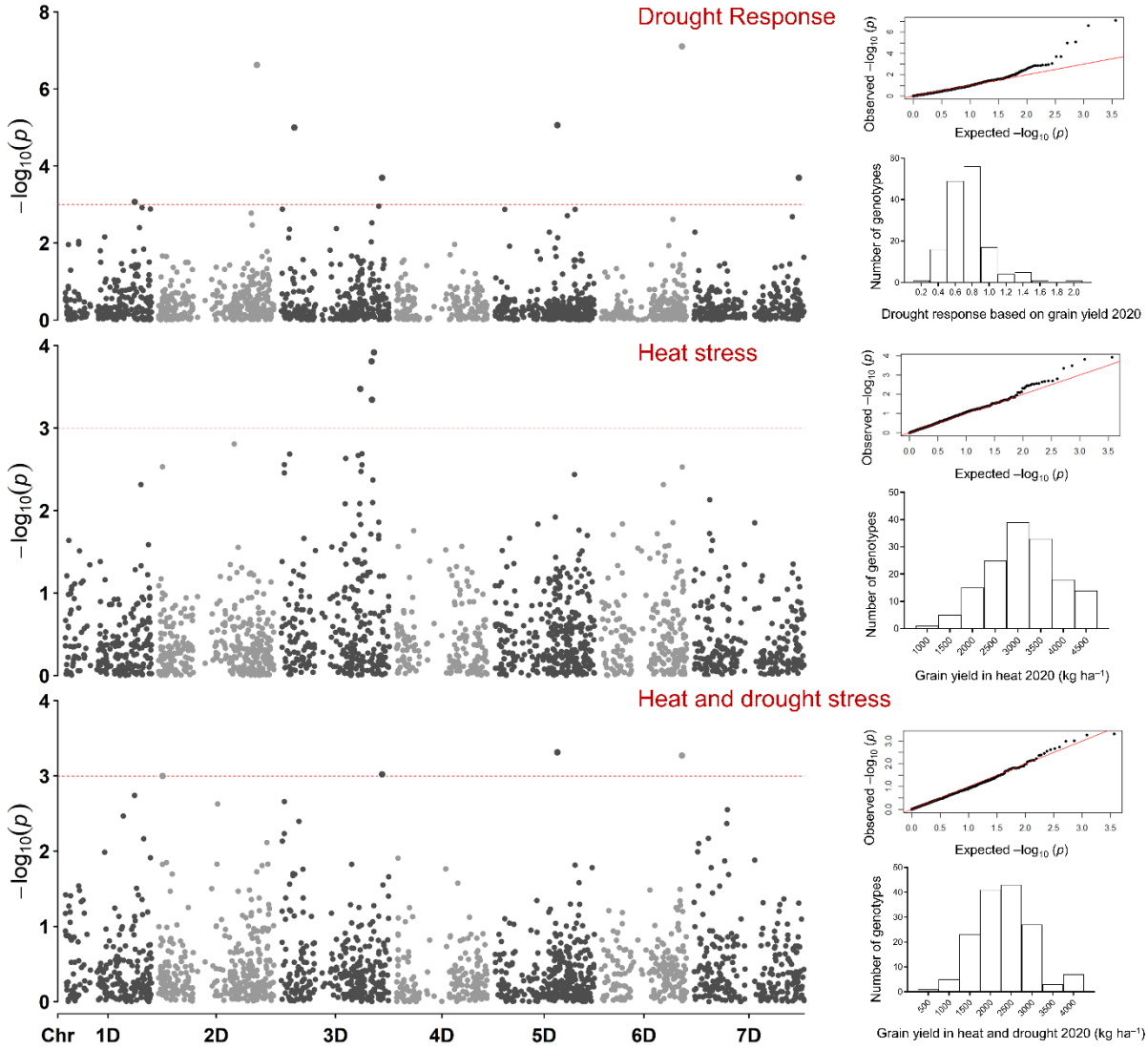

Figure 1.7 Representative Manhattan plots for grain yield showing marker–trait associations in the D genome of bread wheat lines under heat or combined heat–drought stress, and in the drought response. The distribution of grain yield and quantile–quantile plots of the genome-wide analysis are shown for each condition.

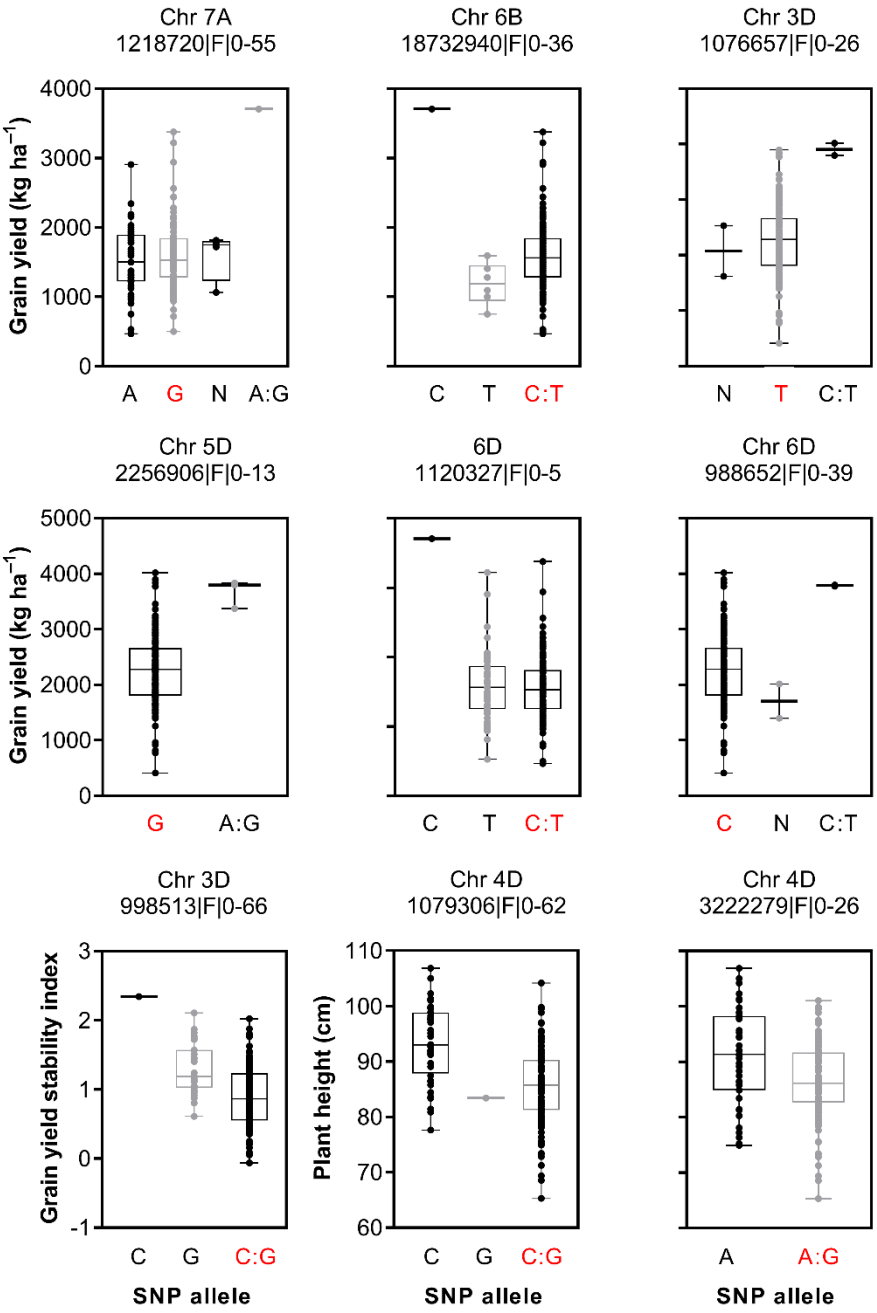

Figure 1.8 Effect of selected stable marker-trait associations on grain yield, stability index, and plant height in a bread wheat population grown under heat or combined heat–drought stress. A, adenine; C, cytosine; T, thymine; G, guanine; N, unknown. Red alleles are those of the backcross parent of the population, 'Norin 61'.

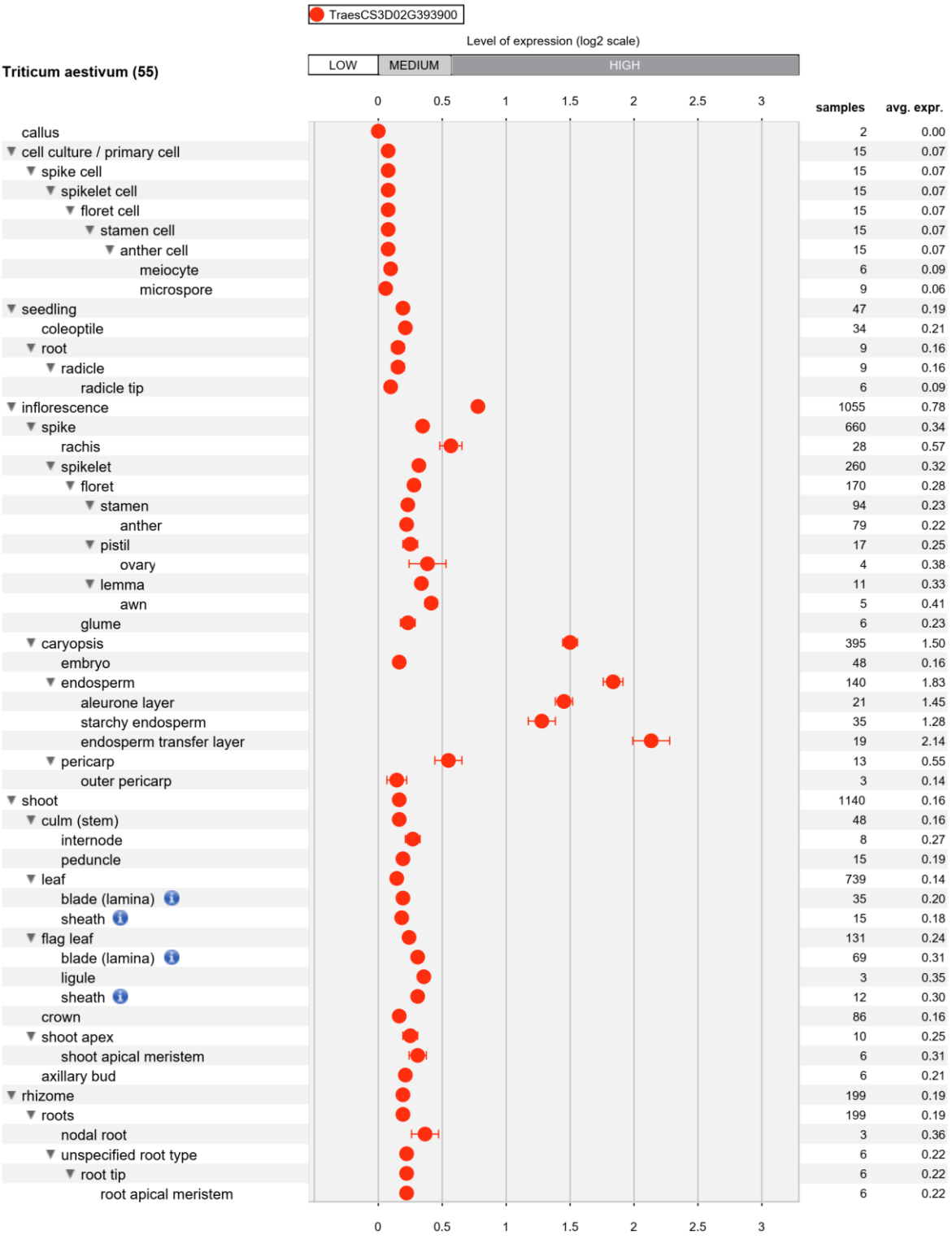

Figure 1.9 Expression pattern of *GA20ox* (TraesCS3D02G393900), the candidate gene for grain yield stability in wheat under heat and combined heat–drought conditions. Expression in 55 anatomical parts is shown on a $\log_2$ scale. The expression was high in endosperm tissues. Data were retrieved from the wheat transcriptome database implemented in Genevestigator.

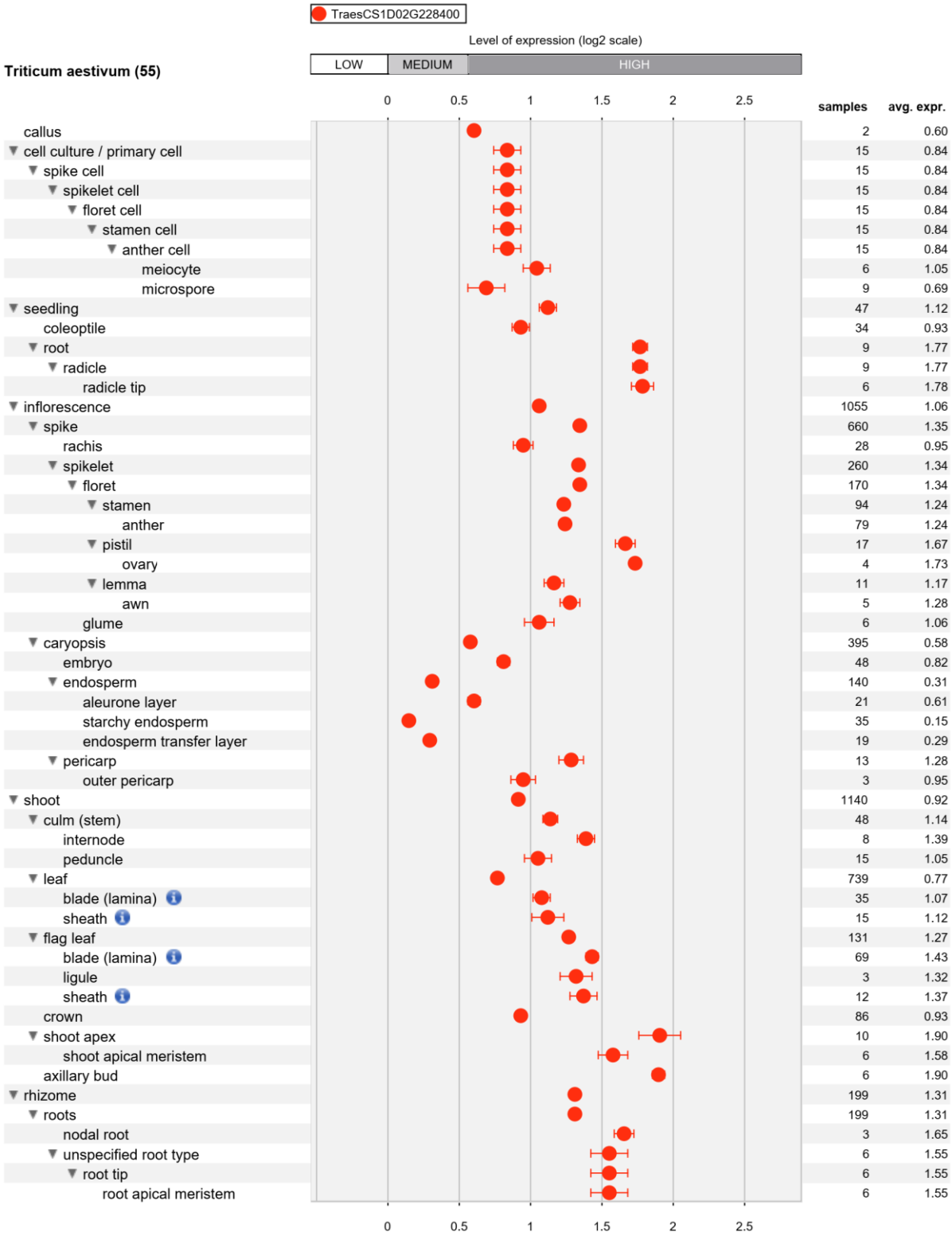

Figure 1.10 Expression pattern of *CaaX prenyl protease 2* (TraesCS1D02G228400), the candidate gene for canopy temperature at grain filling in wheat under heat and combined heat–drought conditions. Expression in 55 anatomical parts is shown on a $\log_2$ scale. Expression was high in roots, shoots, and inflorescences. Data were retrieved from the wheat transcriptome database implemented in Genevestigator.

Chapter 2

Genetic variation in drought resilience-related traits among wheat multiple synthetic derivative lines: insights for climate resilience breeding

2.1 Introduction

Wheat (*T. aestivum* L.) productivity is considerably limited by persistent drought stress. To meet global wheat demands, the current annual increase of 1% must be accelerated to at least 1.6% (GCARD 2012). This task is compounded by the current climate change scenario (Elliott *et al.* 2014), and therefore, developing climate-resilient wheat genotypes with the capacity to thrive under different abiotic stresses needs urgent attention.

Climate-resilient wheat genotypes are scarce due to the narrow genetic diversity in modern wheat cultivars (Ogbonnaya *et al.* 2013). To broaden this genetic diversity, the use of wheat wild relatives for stress resilience breeding has been widely reported (Ogbonnaya *et al.* 2013; Tsujimoto *et al.* 2015; Cox *et al.* 2017; Kishii 2019). To utilize the variation in *Ae. tauschii* for wheat breeding, synthetic hexaploid wheat lines were developed by crossing *Ae. tauschii* accessions with a durum wheat cultivar, 'Langdon' (Tsujimoto *et al.* 2015). Then, to reduce linkage drag, the synthetic hexaploid wheat lines were crossed and backcrossed with a popular bread wheat cultivar, N61 and the resulting lines were named 'multiple synthetic derivative (MSD) lines' (Tsujimoto *et al.* 2015). The MSD lines possess a wide diversity of stress tolerance-related traits (Elbashir *et al.* 2017a; Gorafi *et al.* 2018). Elbashir *et al.* (2017a) evaluated a population of 400 MSD lines under heat stress in Sudan and selected heat-tolerant candidate lines. Similarly, the same population was evaluated for salinity tolerance, and salinity-tolerant candidate lines were selected (manuscript under preparation). However, genetic analysis for drought resilience among the MSD lines is limited. Also, the role of *Ae. tauschii* in conferring multiple stress tolerance to wheat is not well understood. Since wheat response to various abiotic stresses is similar and operates through connected pathways (Abhinandan *et al.* 2018; Tounsi *et al.* 2019), I selected the previously-reported heat-tolerant (Elbashir *et al.* 2017a) and salinity-tolerant MSD lines for evaluation under a drought-rewatering-drought cycle.

The objective was to select drought-resilient MSD lines that may also possess heat or salinity resilience traits for breeding. MSD lines exhibiting high-stress tolerance index (STI) and mean productivity (MP) compared with their backcross parent and standard cultivars under drought stress were selected for further breeding.

2.2 Materials and Methods

2.2.1 Plant materials

Twenty-four MSD lines were selected based on heat stress tolerance (14 lines) (Elbashir *et al.* 2017a; b) and salinity stress tolerance (10 lines) (manuscript under preparation). Two of the MSD lines were previously named as MNH2 and MNH5 (Elbashir *et al.* 2017a). For consistency with (Elbashir *et al.* 2017a; b), the names of these two lines (MNH2 and MNH5) are retained in this chapter. Therefore, in this study, the term "MSD lines" refers to all twenty-four lines including MNH2 and MNH5. For comparison, the backcross parent of the MSD lines (N61) and three check cultivars were included in the study. The check cultivars were 'Imam' (a widely cultivated cultivar in Sudan), 'Cham 6'and 'Halberd' (elite wheat cultivars from ICARDA and CIMMYT, respectively). A list of plant materials and their pedigrees is shown in Table 2.1.

2.2.2 Experimental design and drought treatment

The experiment was conducted in a greenhouse in Arid Land Research Centre, Tottori University, Japan (coordinates: 35.5354534, 134.212066), during the 2018/2019 and 2019/2020 growing seasons. Two rectangular beds (100 m × 1.2 m each) were constructed using concrete blocks, 0.35 m deep. The beds were filled with sand-dune regosol (collected from the Tottori Sand Dunes). Four irrigation tubes (0.3 m apart) were set along the beds. Before sowing, fertilizer (NPK 366) was applied at 20 kg ha^{-1} by mixing with soil. A second application (NPK 366 + Mg) was made during the tillering stage at 50 kg ha^{-1}. Seeds were sown on rows across the beds, each row for a different genotype, with planting distance 0.2 m × 0.3 m between and within rows. At first, eight seeds were sown per row, but latter thinned to four plants at 20 d after germination. Seeds were sown on January 29th and December 15th during the first and second growing seasons,

respectively. The experiment was designed in alpha lattice with two treatment levels (well-watered and drought conditions) and three replicates per treatment. The average light intensity in the greenhouse during the reproductive stage was 37,546 lx. The corresponding day/night temperature and relative humidity were 31/18 ºC and 36/67%, respectively. The soil water potential was measured every two hours using sensors (Decagon devices, WA, USA). Automatic irrigation was performed using Aqua Pro automated irrigation controller (Netafim, Tel Aviv, Israel). When 50% of the plants had flowered, drought was imposed by withholding water supply in one bed, while the well-watered condition was maintained at 90% field capacity. To account for minor phenological differences between the genotypes, genotypes with more than 7 d of delayed flowering (compared to N61) were separated from other genotypes and exposed to drought separately. To mimic the erratic rainfall pattern common in drought-prone areas, the drought-treated bed was rewatered when soil moisture was near permanent wilting point (-1500 kPa, Fig. 2.1).

2.2.3 Traits evaluated

The number of days-to-heading (DH) was measured when 50% of the spikes had headed. Chlorophyll content (SPAD) was measured during the grain-filling stage using the Minolta SPAD-502 chlorophyll meter (Konica-Minolta, Japan). The SPAD readings were made on the penultimate leaves of 12 main tillers (four tillers per replicate). Plant height (PH), biomass per square meter (BIO), grain weight per square meter (GY), number of spikes per square meter (SN), kernel number per spike (KPS), thousand-kernel weight (TKW), and harvest index (HI) were determined at maturity. The STI was calculated as grain weight difference between drought-stressed and well-watered plants using the equation below:

$$\frac{GWsi \times GWpi}{(GWpi)^2} \qquad (1)$$

where GWsi is the grain weight under drought stress, and GWpi is the grain weight under well-watered conditions, for genotype "i" (Fernandez 1992). The MP was calculated as average yield in the well-watered and drought conditions (Rosielle and Hamblin 1981).

2.2.4 Graphical genotyping using DArTseq markers

Genomic DNA was extracted using the CTAB method (Saghai-Maroof *et al.* 1984) and sent to Diversity Arrays Technology Pty Ltd, Australia (http://www.diversityarrays.com) for whole-genome scanning using the DArT-seq platform. Complexity reduction was applied to obtain a subset of restriction fragments for each genotype using a combination of restriction enzymes (Sansaloni *et al.* 2011). The restriction fragments were then sequenced and aligned to the wheat_ChineseSpring10 reference genome and wheat_ConsensusMap_version_4. The presence or absence variation of the genomic fragments (SilicoDArT markers) were used for graphical genotyping. The SilicoDArT markers are dominant and were scored in a binary fashion: "0" or "1" representing absence or presence, respectively, of a restriction fragment containing the marker sequence. A total of 51,202 SilicoDArtT markers were obtained. The markers were then filtered on the basis of minimum reproducibility (95%), call rate (90%), and average read depth (8). Only markers that have known chromosomal positions and are polymorphic between N61 and the synthetic parents of individual MSD lines were used for genotyping. Finally, a minimum of 4,148 polymorphic markers were used for the graphical genotyping of individual genotypes. The markers were ordered according to their position within each chromosome from top to bottom, and the conditional formatting function in Microsoft Excel 2019 was used to highlight each marker.

2.2.5 Statistical analysis

ANOVA was performed for nine physio-agronomic traits for each year following the General Linear Model, using GenStat 18th edition (http://www.genstat.co.uk). The ANOVA was performed by considering genotype by water regime as Treatment Structure, and Rep/Sub-block as Blocking (Nuisance terms). Broad-sense heritability (h^2) was estimated for each trait using Plant Breeding Tools software version 1.3 (http://bbi.irri.org). The correlation coefficients for nine agronomic traits were calculated using IBM SPSS Statistics for Windows, version 23 (IBM Corp., Armonk, N.Y., USA). A principal component analysis (PCA) was conducted using the

FactoMineR package in R (Lê *et al.* 2008). Genotype-genotype comparisons for STI and MP were conducted using the Tukey Honestly Significant Difference (HSD) test, and drought-tolerant candidates were selected based on high STI and MP.

2.3 Results

2.3.1 Influence of genotype and water regime on trait variability

Bartlett's test for homogeneity of variance revealed that the error variances between the two years were heterogeneous for most traits ($F = 3, 332$; $P < 0.05$) and therefore, individual year data were used to assess drought resilience. Although the sowing dates were different between 2019 and 2020, the trend for most of the evaluated traits was the same in both years. The means and ranges of all evaluated traits for the MSD lines and N61 are shown in Table 2.2. The ANOVA table (Table 2.3) revealed highly significant differences between the main effects of genotype (G) and water regime (E) for most of the evaluated traits in each year. The DH was non-significantly affected by water regime in both years. The interaction effects of G and E (G×E) were significant ($P < 0.05$) for SPAD, GY and TKW during 2019, and for SPAD and SN during 2020. Other traits were non-significantly affected by G×E interaction in both years (Table 2. 3). In 2020, the investigated genotypes showed longer DH and higher GY and HI than in 2019 under both water regimes. Two MSD lines (MSD53 and MSD308) had later heading dates than N61 and the three check cultivars under both control and drought conditions for two years (Table 2.4, 2.5).

The PCA revealed differences in trait contribution, with GY, BIO, and PH having the strongest contribution to the PCs under drought condition (Fig. 2.2A). The first component (Dim 1) explained 35.7%, while the second component (Dim 2) explained 21.9% of the variability. Three high-yielding MSD lines were separated from other genotypes: MSD53 was close to MSD308, while MSD140 was close to the check cultivars 'Imam' and 'Cham6'. MSD140 has two sister lines that are relatively sensitive to drought stress. These two sister lines (MNH2 and MSD376) were separated from MSD140 on the PCA biplot (Fig. 2.2B).

High heritability values (above 47%) were observed for DH, PH, KPS, and TKW in both water regimes. Other traits showed medium to low heritability values (below 35%) in both water regimes, except SN (57%) under well-watered conditions (Table 2.3).

GY significantly correlated ($P < 0.05$) with most of the evaluated traits under both water regimes for two years (Table 2.6). Significant correlations were also found among other traits. Worthy of note is the positive correlation between BIO and SN (0.813), and BIO and KPS (0.623), and the negative correlations between HI and BIO (-0.869), and HI and SN (-0.855) under well-watered conditions in 2019 (Table 2.6). Similar trends were found under drought conditions in 2019, and in both water regimes in 2020 (Table 2.6). Additionally, positive correlations between different water regimes were recorded for most traits.

2.3.2 STI and MP

To select drought-resilient candidates among the wheat MSD lines, stress tolerance index (STI) and mean productivity (MP) were calculated. There was variability in STI among the evaluated genotypes with some MSD lines showing higher STI than N61 and 'Imam'. Specifically, MNH5, MSD140, and MSD308 exhibited higher STIs compared with N61 and 'Imam' for two years (Fig. 2.3A and B). Similarly, MSD308 consistently showed higher MP than N61 and 'Imam' for two years (but non-significantly higher than N61 in 2020), while MSD53 showed higher MP than N61 and 'Imam' in 2020 (Fig. 2.3C and D).

2.3.3 Graphical Genotyping

The results indicated that MNH5, MSD53, MSD140, and MSD308 had better drought resilience than N61 and the three check cultivars, including 'Imam'. Therefore, to identify the genomic regions that may be associated with drought adaptation in the selected MSD lines, I conducted graphical genotyping by comparing their genomes with those of their donor (synthetic) and backcross (N61) parents. The results showed that the MSD lines were different from their parents in several genomic regions; various recombinant portions (introgressed segments) were found in most of the 21 chromosomes (Fig. 2.4). Worthy of note, MNH5 and MSD308 showed

similar introgressed segments on chromosome 1A. All four drought-resilient lines possessed similar introgressed segments on chromosome 6B which were not found in two drought-sensitive lines (MNH2 and MSD376) (Fig. 2.4). Also, MNH5, MSD53, and MSD140 showed similar introgressed segments on chromosome 4B. Interestingly, the drought-resilient MSD53 and MSD140 and the drought-sensitive MNH2 and MSD376 were developed from the same *Ae. tauschii* accession (Table 2.1). Since these lines could be considered as sister lines, their genomes were graphically compared (Fig. 2.4). Similarly, MSD53 and MSD140 contained similar introgressed segments on chromosome 2D and 3D (Fig. 2.4). These segments were not found in the drought-sensitive lines (MNH2 and MSD376). MNH5 and MSD308 also possessed large introgressed segments on chromosome 2D and 3D. Taken together, the drought-resilient MSD lines possessed similar introgressed segments on chromosome 6B, 4B (except MSD308), 2D, and 3D (except MNH5) (Fig. 2.4).

2.4 Discussion

One way to ensure sustainable wheat production under the current climate change scenario is to develop drought-resilient wheat genotypes that can adapt to more than one abiotic stress. Drought resilience is a quantitative trait controlled by many QTLs and thus, it is difficult to use marker-assisted selection techniques for drought resilience breeding. Therefore, a first step in breeding drought-resilient wheat lines may be to broaden the wheat gene pool using wild introgressions. In the present study, the investigated MSD lines were developed from wild (*Ae. tauschii*) introgressions, and had been previously selected as heat (Elbashir *et al.* 2017a) and salinity-tolerant candidates (Table 2.1).

The significant genotypic differences ($P < 0.001$) observed for the investigated traits (Table 2.3) indicated high genetic diversity among the MSD lines. This diversity is mainly due to the introgressions with individual *Ae. tauschii* accessions and may, therefore, be useful for further breeding for drought-resilient wheat lines. Significant differences due to water regime were observed in all evaluated traits except DH (Table 2.3). These differences may have resulted from

the profound effect of drought on yield and yield components (Fischer and Maurer 1978). The non-significant effect of water regime on DH was expected since the drought stress was imposed after heading. The significant G×E interaction effects on SPAD, yield and yield components for two years reflect the variation in drought adaptation among the investigated genotypes.

The high heritability estimates for most of the investigated traits for two years point to a possible effect of genes or major QTL on these traits. Low heritability estimates are often reported for yield and yield components under drought conditions (Eid 2009; Yaqoob 2016). Moreover, heritability values are subject to specific sets of genotypes and target environments (Mwadzingeni *et al.* 2017). Therefore, the heritability estimates in this study may have been influenced by the small population size and the amount of genetic variance present in the investigated lines. Overall, the heritability estimates indicated that these traits are highly influenced by genetic factors and may be useful for cultivar development. Also, there were high correlations between most of the evaluated traits, suggesting a strong inherent association among these traits at the genetic level. Highly heritable traits exhibiting strong correlations with other quantitative traits improve selection efficiency (Shimelis and Shiringani 2010; Mwadzingeni *et al.* 2017). Furthermore, the positive and highly significant correlations between traits under different water regimes (Table 2.6) suggest that these traits were consistent in both conditions. Similar correlations have been reported in bread wheat under different drought intensities in Morocco (Bennani *et al.* 2017).

The high STI exhibited by three MSD lines (MNH5, MSD308, and MSD140) suggests better adaptation of the MSD lines to post-anthesis drought stress compared with practical cultivars, N61 and 'Imam' (Fig. 2.3A and B). This points to the potential of the MSD lines in outperforming popular elite cultivars including 'Imam' which is widely cultivated in stress-prone areas in Sudan. STI is a reliable selection criterion that has been used for selecting drought-resilient wheat (Bennani *et al.* 2017) and rice genotypes (Mau *et al.* 2019). Similarly, some MSD lines showed higher MP compared with N61 and 'Imam', reflecting the higher productivity of the MSD lines in both water regimes (Fig. 2.3C and D). These MSD lines present an opportunity to

develop new cultivars with high yield under well-watered and marginal rainfall-growing regions. Based on STI and MP fortwo years, MSD308 was the best performing, and therefore, selected alongside MNH5, MSD53, and MSD140 (Fig. 2.3) for further breeding for drought resilience. These MSD lines (except MNH5) were separated from other lines in the PCA (Fig. 2.2B), suggesting unique drought resilience traits which may be due to similar effects of introgression. Additionally, MSD53 was recently reported to have an efficient water conservation capacity under dry down conditions (Itam *et al.* 2020a).

Genotyping with polymorphic markers ensured that the variation in each MSD line was due to introgressed segments from its synthetic parent (containing *Ae. tauschii* genome). The presence of such introgressed segments indicates the effectiveness of the synthetic derivative approach for utilizing the variation in *Ae. tauschii* for wheat breeding (Tsujimoto *et al.* 2015; Cox *et al.* 2017). These acquired genomic segments are likely the source of variation in drought resilience traits among the MSD lines and between the MSD lines and N61. For example, chromosome 1A harbours many plant height-regulating genes, including *Rht-B1* and *Rht-D1* (Zanke *et al.* 2014; Daba *et al.* 2020). Plant height is strongly associated with yield and yield components and has been a major target for selection for high yield in wheat (Rebetzke *et al.* 2011). This suggests that the introgressed chromosome 1A segments in MNH5 and MSD308 may have yield-related functions. Similarly, chromosomes 4B and 6B introgressions may have drought-resilience functions. Chromosome 4BS harbours the QTL qDSI.4B.1 which is associated with drought susceptibility index, GY, HI, and root biomass in bread wheat under drought stress (Kadam *et al.* 2012), whereas chromosome 6B harbours the QTL QYld.aww-6B.1 which is associated with increased GY, leaf biomass, and chlorophyll index under combined drought and heat stress (Schmidt *et al.* 2020). The introgressions in the A and B subgenomes are likely from durum wheat ('Langdon') which is the source of the A and B subgenomes in the synthetic parents (Table 2.1, Fig. 2.4). This reflects the presence of important durum wheat genes in the MSD lines for bread wheat improvement. Furthermore, three drought-resilient lines (MSD53, MSD308, and

MSD140) contained introgressed segments on chromosome 2D. Chromosome 2D bears the photoperiod sensitivity gene, *Ppd-D1* (Hanocq *et al.* 2004) which is associated with multiple traits including HI, spike length and chlorophyll content under drought conditions (Dodig *et al.* 2012), and canopy temperature at grain filling under optimal conditions (Sukumaran *et al.* 2014). Similarly, chromosome 3D is associated with chlorophyll and carotenoid properties and increased GY under drought stress (Czyczyło-Mysza *et al.* 2011). Furthermore, since the synthetic parents were developed with 37 different accessions of *Ae. tauschii*, the presence of similar introgressed segments among unrelated drought-resilient MSD lines is interesting; the introgressed segments on chromosome 2D were not present in the drought-sensitive sister lines of the same synthetic parent, emphasizing their (2D donations) possible role in drought adaptation and the potential for utilization in drought resilience breeding. These results are in agreement with those obtained in Chapter 1 where novel QTLs, candidate genes, and alleles were found especially on chromosome 2D and 3D, further suggesting their role in drought resilience in wheat.

In this study, the screening of the MSD lines under a drought-rewatering-drought cycle ensured that selected lines are able to not only survive the erratic rainfall pattern common in natural field conditions, but to maintain high yield under prolonged drought spells nearing wilting point. Under the test environment, high heritability values were obtained for some of the evaluated traits indicating that selection based on such traits can result in genetic gain for drought resilience. Since the investigated lines had been evaluated under separate heat (Elbashir *et al.* 2017a; b) and salinity stresses, they are a useful genetic resource for further breeding for climate-resilient wheat that may thrive under different abiotic stresses.

Table 2.1 List of selected plant materials showing heat or salinity-tolerant lines.

Genotype	Traits	Synthetic family	Pedigree
Norin 61	Control		Akabouzu/Sunekiri × Shinriki//Shinchunaga (Japan)
Imam	Check		Sudan, Turkey, CIMMYT
Halberd	Check		CIMMYT
Cham 6	Check		ICARDA, Syria
MSD006	Heat tolerant	Syn65	Norin 61/*T. durum* cv. Langdon × *Ae. tauschii* KU-2132//*Norin 61
MSD084	Heat tolerant	Syn30	Norin 61/*T. durum* cv. Langdon × *Ae. tauschii* IG131606//*Norin 61
MSD108	Heat tolerant	Syn45	Norin 61/*T. durum* cv. Langdon × *Ae. tauschii* KU-2126//*Norin 61
MSD186	Heat tolerant	Syn30	Norin 61/*T. durum* cv. Langdon × *Ae. tauschii* IG131606//*Norin 61
MSD265	Heat tolerant	Syn44	Norin 61/*T. durum* cv. Langdon × *Ae. tauschii* KU-2124//*Norin 61
MSD296	Heat tolerant	Syn32	Norin 61/*T. durum* cv. Langdon × *Ae. tauschii* KU-2039//*Norin 61
MSD345	Heat tolerant	Syn48	Norin 61/*T. durum* cv. Langdon × *Ae. tauschii* KU-2829A//*Norin 61
MSD360	Heat tolerant	Syn57	Norin 61/*T. durum* cv. Langdon × *Ae. tauschii* KU-2078//*Norin 61
MSD054	Heat tolerant	Syn26	Norin 61/*T. durum* cv. Langdon × *Ae. tauschii* AE454//*Norin 61
MSD208	Heat tolerant	Syn26	Norin 61/*T. durum* cv. Langdon × *Ae. tauschii* AE454//*Norin 61
MSD453	Heat tolerant	Syn50	Norin 61/*T. durum* cv. Langdon × *Ae. tauschii* AT55//*Norin 61
MSD367	Heat tolerant	Syn57	Norin 61/*T. durum* cv. Langdon × *Ae. tauschii* KU-2078//*Norin 61
MNH2	Heat tolerant	Syn68	Norin 61/*T. durum* cv. Langdon × *Ae. tauschii* KU-2156//*Norin 61
MNH5	Heat tolerant	Syn29	Norin 61/*T. durum* cv. Langdon × Ae. tauschii IG126387//*Norin 61
MSD308	Salinity tolerant	Syn60	Norin 61/*T. durum* cv. Langdon × *Ae. tauschii* KU-2090//*Norin 61
MSD366	Salinity tolerant	Syn66	Norin 61/*T. durum* cv. Langdon × *Ae. tauschii* KU-2136//*Norin 61
MSD254	Salinity tolerant	Syn45	Norin 61/*T. durum* cv. Langdon × *Ae. tauschii* KU-2126//*Norin 61
MSD53	Salinity tolerant	Syn68	Norin 61/*T. durum* cv. Langdon × *Ae. tauschii* KU-2156//*Norin 61
MSD376	Salinity tolerant	Syn68	Norin 61/*T. durum* cv. Langdon × *Ae. tauschii* KU-2156//*Norin 61
MSD273	Salinity tolerant	Syn30	Norin 61/*T. durum* cv. Langdon × *Ae. tauschii* IG131606//*Norin 61
MSD386	Salinity tolerant	Syn72	Norin 61/*T. durum* cv. Langdon × *Ae. tauschii* PI508262//*Norin 61
MSD55	Salinity tolerant	Syn51	Norin 61/*T. durum* cv. Langdon × *Ae. tauschii* AT76//*Norin 61
MSD140	Salinity tolerant	Syn68	Norin 61/*T. durum* cv. Langdon × *Ae. tauschii* KU-2156//*Norin 61
MSD044	Salinity tolerant	Syn71	Norin 61/*T. durum* cv. Langdon × *Ae. tauschii* PI499262//*Norin 61

Table 2.2 Means and ranges of traits for the investigated genotypes and the backcross parent of the MSD lines, Norin 61 (N61), under two contrasting water regimes for two years.

	Well-watered 2019			**Drought 2019**			**Well-watered 2020**			**Drought 2020**		
	Range	**Mean**	**N61**	**Range**	**Mean**	**N61**	**Range**	**Mean**	**N61**	**Range**	**Mean**	**N61**
DH	80.0–97.0	84.6	82.0	80.0–97.0	84.6	82.0	117.6–137.7	122.6	119.6	116.0–138.0	122.6	119.6
SPAD	34.0–50.0	42.3	42.8	16.8–25.6	21.2	21.4	37.1–54.7	45.9	47.6	31.0–52.2	40.2	39.9
PH	70.0–130.0	95.4	87.3	66.0–122.0	88.9	83.0	60.0–120.0	84.4	83.3	58.0–112.0	80.7	74.0
GY	93.6–181.2	126.7	124.8	78.0–160.8	113.6	111.0	249.0–1038.0	516.3	668.6	35.6–626.4	290.7	340.2
BIO	480.0–1740.0	1114.2	1200.0	240.0–1140.0	767.1	780.0	504.0–2346.0	1062.4	1256.0	336.0–1422.0	654.8	682.0
SN	150.0–420.0	275.9	328.0	78.0–324.0	221.7	256.0	156.0–474.0	283.3	348.0	120.0–342.0	202.5	260.0
KPS	39.5–58.1	46.6	50.1	37.0–52.5	45.49	49.3	32.1–59.4	42.2	48.5	28.3–50.5	39.1	40.7
TKW	39.1–53.8	45.3	41.5	37.4–48.4	41.7	37.4	34.7–53.6	43.0	39.4	3.4–44.1	36.6	32.4
HI	0.06–0.21	0.1	0.1	0.09–0.38	0.2	0.2	0.40–0.62	0.5	0.5	0.05–0.50	0.4	0.5

DH, days to 50% heading; SPAD, chlorophyll content; PH, plant height; GY, grain yield; BIO, biomass; HI, harvest index; SN, number of spikes per square meter; KPS, kernel number per spike; TKW, thousand-kernel weight.

Table 2.3 Mean sum of squares for evaluated traits under two contrasting water regimes for two years.

	2019						2020							
Trait	**G**	**E**	**G×E**	**Residual**	**Total**	**CV (%)**	**G**	**E**	**G×E**	**Residual**	**Total**	**CV (%)**	**h^2 well-watered**	**h^2 drought**
DH	135.7***	0.0	0.0	0.0	21.9	0.1	130.8***	0.0	0.0	3.3	25.4	1.5	0.84	0.84
SPAD	27.9***	18757.9***	16.3***	0.8	120.0	2.8	39.8*	1401.8***	11.1***	9.3	23.2	7.1	0.14	0.14
PH	975.3***	1761.5***	16.4	12.8	180.1	3.9	648.6***	575.7**	49.5	65.6	160.8	9.8	0.83	0.81
GY	847.8***	7227.3***	205.0*	112.0	291.2	8.8	49632.0***	2136793.0***	10465.0	8389.0	31781.0	22.7	0.00	0.19
BIO	203375.0***	5061343.0***	28010.0	28001.0	88526.0	17.8	281263.0***	6977052.0***	48669.0	37076.0	137849.0	22.4	0.16	0.20
SN	11481.0***	123446.0***	1148.0	1522.0	3846.0	15.7	10728.0***	274106.0***	1740.0***	2163.0	5635.0	19.1	0.57	0.21
KPS	99.3*	53.2	19.9	14.8	30.2	8.4	78.7***	399.7***	13.5	17.7	31.5	10.4	0.48	0.67
TKW	50.6***	537.0***	5.1**	2.5	14.0	3.7	92.4***	1719.6***	11.7	8.0	32.8	7.1	0.92	0.91
HI	0.003***	0.06***	0.0007	0.0007	0.001	20.3	0.004***	0.08***	0.0	0.0	0.0	8.6	0.00	0.35
df	110	27	1	27	167		110	27	1	27	167			

*, **, and ***, represent F-probability values less than 0.05, 0.01, and 0.001, respectively. DH, days to 50% heading; SPAD, chlorophyll content; PH, plant height; GY, grain yield; BIO, biomass; SN, number of spikes per square meter; KPS, kernel number per spike; TKW, thousand-kernel weight; HI, harvest index; df, degrees of freedom. G, genotypic main effect; E, water regime main effect; G×E, genotype by water regime interaction effect; h^2, broad sense heritability; CV, coefficient of variation.

Table 2.4 Predicted means for investigated traits under two contrasting water regimes in 2019.

			Well-watered control 2019									Drought 2019								
Genotype	STI	MP	DH	SPAD	PH	GY	BIO	SN	KPS	TKW	HI	DH	SPAD	PH	GY	BIO	SN	KPS	TKW	HI
Norin 61	0.76	117.90	82.00	42.80	87.33	124.80	1200.00	328.00	50.07	41.56	0.10	82.00	21.43	83.00	111.00	780.00	256.00	49.30	37.48	0.15
Cham6	0.84	105.90	89.00	38.57	73.67	99.40	600.00	170.00	40.10	41.32	0.17	89.00	22.27	68.00	112.40	500.00	156.00	45.00	41.58	0.23
Halberd	0.99	111.30	87.00	41.60	97.67	118.60	820.00	202.00	42.67	46.33	0.14	87.00	20.20	90.33	104.00	540.00	166.00	39.40	43.95	0.20
Imam	0.94	111.10	87.00	45.00	80.67	118.00	860.00	228.00	42.33	46.48	0.14	87.00	24.20	73.00	104.20	500.00	154.00	41.97	41.35	0.24
MNH2	0.85	137.90	82.00	38.60	123.67	151.40	1360.00	298.00	58.13	43.38	0.11	82.00	21.20	118.33	124.40	920.00	226.00	51.63	40.14	0.14
MNH5	1.14	148.50	81.00	44.43	109.00	164.60	1260.00	266.00	51.57	53.22	0.13	81.00	21.33	101.00	132.40	860.00	224.00	50.23	44.14	0.16
MSD006	1.06	116.90	80.00	47.50	102.67	131.20	1180.00	280.00	44.53	49.14	0.11	80.00	21.33	93.00	102.60	760.00	234.00	38.53	44.43	0.16
MSD044	0.92	110.40	80.00	43.83	81.00	118.80	1180.00	348.00	42.47	46.61	0.10	80.00	19.50	79.00	102.00	900.00	296.00	41.97	40.48	0.12
MSD054	0.77	114.60	83.00	41.63	78.67	124.00	900.00	244.00	49.40	41.83	0.14	83.00	18.67	77.33	105.20	620.00	196.00	46.80	37.55	0.17
MSD084	0.98	120.30	83.00	34.53	103.00	121.00	1040.00	226.00	42.43	47.54	0.12	83.00	19.87	95.33	119.60	760.00	204.00	47.17	42.25	0.16
MSD108	0.99	120.90	94.00	42.40	84.33	128.80	980.00	234.00	45.77	46.91	0.13	94.00	20.57	81.67	113.00	660.00	208.00	43.63	43.20	0.17
MSD140	1.19	131.10	82.00	49.47	85.00	141.00	860.00	216.00	45.43	51.69	0.17	82.00	22.03	81.67	121.20	700.00	192.00	42.63	47.41	0.17
MSD186	0.99	108.40	83.00	43.10	94.00	116.60	1020.00	274.00	41.70	46.58	0.12	83.00	20.20	88.00	100.20	580.00	194.00	38.43	43.64	0.18
MSD208	0.80	106.95	83.00	41.70	80.67	114.00	920.00	304.00	44.47	42.74	0.13	83.00	20.67	78.33	99.90	680.00	228.00	43.35	38.49	0.15
MSD254	0.81	125.40	81.00	43.20	88.33	133.60	1320.00	340.00	51.73	43.00	0.10	81.00	22.27	82.33	117.20	880.00	266.00	50.73	38.50	0.13
MSD265	0.94	123.50	84.00	44.67	101.67	134.60	1400.00	336.00	48.33	46.40	0.10	84.00	22.07	91.67	112.40	900.00	270.00	44.90	41.74	0.13
MSD273	0.96	121.60	88.00	45.30	92.67	123.00	1540.00	356.00	44.90	45.66	0.08	88.00	24.60	83.00	120.20	880.00	242.00	46.50	43.10	0.14
MSD296	0.89	121.80	81.00	39.30	126.67	132.40	1240.00	262.00	50.60	43.60	0.11	81.00	24.00	116.67	111.20	900.00	232.00	44.40	41.83	0.13
MSD308	1.21	149.90	97.00	41.53	95.33	158.40	1500.00	276.00	51.40	51.20	0.11	97.00	22.37	85.00	141.40	760.00	168.00	48.67	48.40	0.19
MSD345	0.87	97.10	83.00	43.00	87.33	105.20	620.00	184.00	39.47	44.45	0.17	83.00	23.03	78.33	89.00	440.00	138.00	36.97	40.09	0.21
MSD360	1.05	119.70	84.00	38.37	115.33	128.00	1240.00	282.00	45.07	47.27	0.11	84.00	19.43	107.00	111.40	960.00	246.00	40.73	45.57	0.12
MSD366	0.95	118.90	81.00	38.10	105.67	116.00	1160.00	298.00	42.70	45.29	0.10	81.00	22.77	105.33	121.80	840.00	214.00	47.20	43.01	0.15
MSD367	0.80	124.70	88.00	38.73	110.67	139.60	1220.00	272.00	54.60	42.62	0.11	88.00	20.03	100.33	109.80	820.00	244.00	47.47	38.61	0.14
MSD376	0.86	118.30	86.00	39.67	98.33	118.20	1100.00	294.00	44.97	43.84	0.11	86.00	17.30	87.33	118.40	760.00	224.00	48.77	40.45	0.17
MSD386	0.76	109.40	82.00	48.13	84.67	108.00	1100.00	320.00	43.77	41.12	0.10	82.00	23.03	78.33	110.80	800.00	260.00	49.17	37.88	0.14
MSD453	0.84	131.90	81.00	46.47	90.00	138.40	1260.00	360.00	52.83	43.66	0.11	81.00	21.33	87.33	125.40	940.00	276.00	52.57	39.73	0.14
MSD53	0.80	117.00	97.00	42.97	100.33	111.40	1200.00	258.00	46.10	40.27	0.11	97.00	18.87	89.00	122.60	940.00	236.00	50.23	40.71	0.13
MSD55	0.94	123.20	81.00	41.20	93.00	129.20	1120.00	270.00	47.83	44.98	0.12	81.00	19.50	90.33	117.20	900.00	258.00	45.50	42.86	0.13

DH, days to 50% heading; SPAD, chlorophyll content; PH, plant height; GY, grain yield; BIO, biomass; HI, harvest index; SN, number of spikes per square meter; KPS, kernel number per spike; TKW, thousand-kernel weight.

Table 2.5 Predicted means for investigated traits under two contrasting water regimes in 2020.

			Well-watered control 2020									Drought 2020								
Genotype	STI	MP	DH	SPAD	PH	GY	BIO	SN	KPS	TKW	HI	DH	SPAD	PH	GY	BIO	SN	KPS	TKW	HI
Norin 61	0.69	504.40	119.70	47.67	83.33	668.60	1256.00	348.00	48.56	39.41	0.54	119.70	39.93	74.00	340.20	682.00	260.00	40.73	32.43	0.50
Cham6	0.94	405.50	125.30	51.33	69.67	472.00	994.00	234.00	45.49	43.72	0.47	125.30	48.23	70.00	339.00	704.00	214.00	39.20	39.95	0.48
Halberd	1.05	522.30	123.30	47.23	92.33	702.20	1572.00	352.00	42.99	46.56	0.45	123.30	44.00	78.00	342.40	786.00	230.00	35.71	41.64	0.43
Imam	0.93	338.60	124.40	46.18	72.38	437.90	842.80	225.60	39.77	48.32	0.52	124.40	42.68	71.71	239.30	524.80	169.60	38.91	35.78	0.46
MNH2	0.75	289.50	123.00	46.97	104.00	355.80	736.00	196.00	44.73	40.28	0.49	123.00	38.40	100.00	223.20	520.00	160.00	39.97	34.35	0.43
MNH5	1.13	346.10	119.40	43.82	96.71	413.50	804.80	209.60	39.43	50.23	0.52	119.40	38.88	102.71	278.70	590.80	179.60	37.39	41.75	0.48
MSD006	0.96	404.60	118.70	49.47	80.33	554.20	1146.00	330.00	36.39	46.18	0.48	118.70	41.40	69.67	255.00	636.00	202.00	32.71	38.49	0.42
MSD044	0.90	415.80	119.00	48.50	70.67	545.60	1056.00	350.00	35.65	43.78	0.52	119.00	42.50	67.33	286.00	596.00	234.00	32.38	38.22	0.48
MSD054	0.70	366.30	121.40	48.08	71.04	466.10	860.80	255.60	46.03	39.38	0.55	121.40	46.02	68.04	266.50	560.80	187.60	43.46	33.11	0.48
MSD084	1.00	315.40	120.70	47.67	86.33	400.20	846.00	224.00	39.07	45.83	0.47	120.70	38.03	79.33	230.60	556.00	158.00	36.01	40.45	0.42
MSD108	0.92	359.10	119.30	43.40	83.33	439.60	880.00	244.00	41.98	42.72	0.49	119.30	32.10	80.00	278.60	595.80	180.00	38.56	39.97	0.46
MSD140	1.20	301.00	118.00	48.37	69.00	393.00	744.00	214.00	35.97	50.97	0.53	118.00	41.70	73.00	209.00	454.00	146.00	33.38	43.55	0.46
MSD186	0.92	442.60	129.70	44.03	95.33	614.80	1324.00	320.00	42.37	44.73	0.46	129.70	36.63	84.00	270.40	602.00	192.00	37.63	37.99	0.45
MSD208	0.76	363.50	122.30	44.87	71.00	478.20	928.00	294.00	39.98	40.44	0.51	122.30	37.53	77.00	248.80	550.00	214.00	33.21	34.90	0.45
MSD254	0.51	413.40	122.30	46.43	80.00	617.40	1096.00	312.00	49.61	40.02	0.56	122.30	41.70	75.67	209.40	624.00	232.00	40.02	23.51	0.35
MSD265	0.83	294.00	120.00	44.20	83.00	386.60	812.00	240.00	38.89	42.60	0.47	120.00	38.70	82.33	201.40	458.00	148.00	37.46	36.04	0.44
MSD273	0.88	465.40	123.30	45.77	79.67	572.60	1202.00	316.00	41.07	43.66	0.47	123.30	40.33	77.67	358.20	778.00	248.00	39.14	37.25	0.46
MSD296	0.82	339.30	122.30	44.47	106.33	404.20	900.00	234.00	40.79	42.50	0.45	122.30	37.10	95.33	274.40	678.00	188.00	40.38	35.84	0.40
MSD308	1.20	685.80	137.30	45.80	90.67	795.40	1748.00	334.00	47.06	51.05	0.45	137.30	38.23	83.67	576.20	1298.00	284.00	46.75	43.59	0.43
MSD345	0.77	402.10	122.30	45.60	109.33	529.60	1234.00	276.00	46.55	41.08	0.43	122.30	37.23	98.00	274.60	656.00	182.00	43.54	34.85	0.42
MSD360	1.02	353.30	124.30	45.08	97.29	419.10	899.20	232.40	39.38	45.80	0.47	124.30	37.98	88.96	287.50	691.20	202.40	34.64	41.41	0.42
MSD366	0.77	417.10	119.70	44.97	90.00	526.80	1162.00	330.00	39.76	39.56	0.45	119.70	42.90	93.00	307.40	696.00	220.00	38.75	36.27	0.44
MSD367	0.71	377.10	120.70	44.23	75.33	452.80	852.00	258.00	44.27	39.71	0.53	120.70	40.13	73.33	301.40	630.00	202.00	45.67	32.97	0.48
MSD376	0.69	339.20	121.00	38.97	83.67	443.00	936.00	270.00	43.01	38.02	0.47	121.00	39.50	83.33	235.40	572.00	182.00	38.77	33.41	0.41
MSD386	0.56	351.80	121.60	44.62	69.62	438.90	839.20	304.40	41.41	35.19	0.53	121.60	43.32	73.62	264.70	559.20	196.40	46.37	29.28	0.48
MSD453	0.74	361.70	117.60	46.68	74.96	487.10	913.20	294.40	40.49	41.03	0.54	117.60	40.95	75.96	236.30	521.20	188.40	36.88	33.48	0.45
MSD53	0.83	750.80	137.70	42.37	94.00	963.40	2160.00	454.00	51.22	41.41	0.44	137.70	37.30	82.67	538.20	1230.00	302.00	47.56	37.36	0.43
MSD55	0.86	373.10	120.70	50.87	84.67	478.00	1004.00	282.00	40.69	41.36	0.48	120.70	42.43	82.00	268.20	586.00	170.00	41.02	38.53	0.46

DH, days to 50% heading; SPAD, chlorophyll content; PH, plant height; GY, grain yield; BIO, biomass; HI, harvest index; SN, number of spikes per square meter; KPS, kernel number per spike; TKW, thousand-kernel weight.

Table 2.6 Correlation coefficients of the evaluated traits in 2019 and 2020.

	2019									2020								
	DH	SPAD	PH	GY	BIO	SN	KPS	TKW	HI	DH	SPAD	PH	GY	BIO	SN	KPS	TKW	HI
DH	**1.000****	-.122	-.112	-.028	.027	-.244*	-.386	-.029	.042	**1.000****	-.168	.268*	.509**	.579**	.311**	.334**	.183	-.390**
SPAD	-.070	**.297****	-.390**	.049	.014	.187	-.056	.195	.018	-.081	**.388****	-.082	.131	.070	.126	.037	.150	.170
PH	-.224*	-.058	**.930****	.422**	.484**	.156	.470*	.157	-.347**	.086	-.271*	**.605****	.243*	.350**	.132	.264*	.057	-.551**
GY	.237*	-.013	.228*	**.523****	.541**	.273*	.784**	.541**	-0.102	.632**	.094	.063	**.646****	.974**	.905**	.586**	-.005	-.167
BIO	-0.130	-.138	.471**	.529**	**.567****	.813**	.623**	.129	-.843**	.659**	.009	.137	.930**	**.725****	.871**	.544**	.026	-.377**
SN	-.286**	-.164	.232*	.256*	.867**	**.562****	.405*	-.105	-.805**	.437**	.193	-.058	.794**	.831**	**.559****	.345**	-.216*	-.123
KPS	.333**	.234*	-.279*	.035	-.686**	.416*	**.669****	-.055	-0.366	.343**	-.001	.161	.457**	.453**	.177	**.444****	-.336**	.009
TKW	.232*	.057	.152	.330**	-.082	-.340**	-.341	**.696****	0.144	.187	-.042	.058	.362**	.176	-.051	-.247*	**.598****	-0.104
HI	.233*	.196	-.424**	-.199	-.869**	-.855**	-.378	.208	**.418****	-.0109	.235*	-.209	.288**	-.080	.005	.045	.519**	**.180**

*, **, significant at the 0.05 and 0.01 levels, respectively (2-tailed). DH, days to 50% heading; SPAD, chlorophyll content; PH, plant height; GY, grain yield; BIO, biomass; HI, harvest index; SN, number of spikes per square meter; KPS, kernel number per spike; TKW, thousand-kernel weight. The bold numbers arranged diagonally represent individual trait correlations between water regimes. The diagonal separates the two water regimes: well-watered (left to right) and drought conditions (top to bottom).

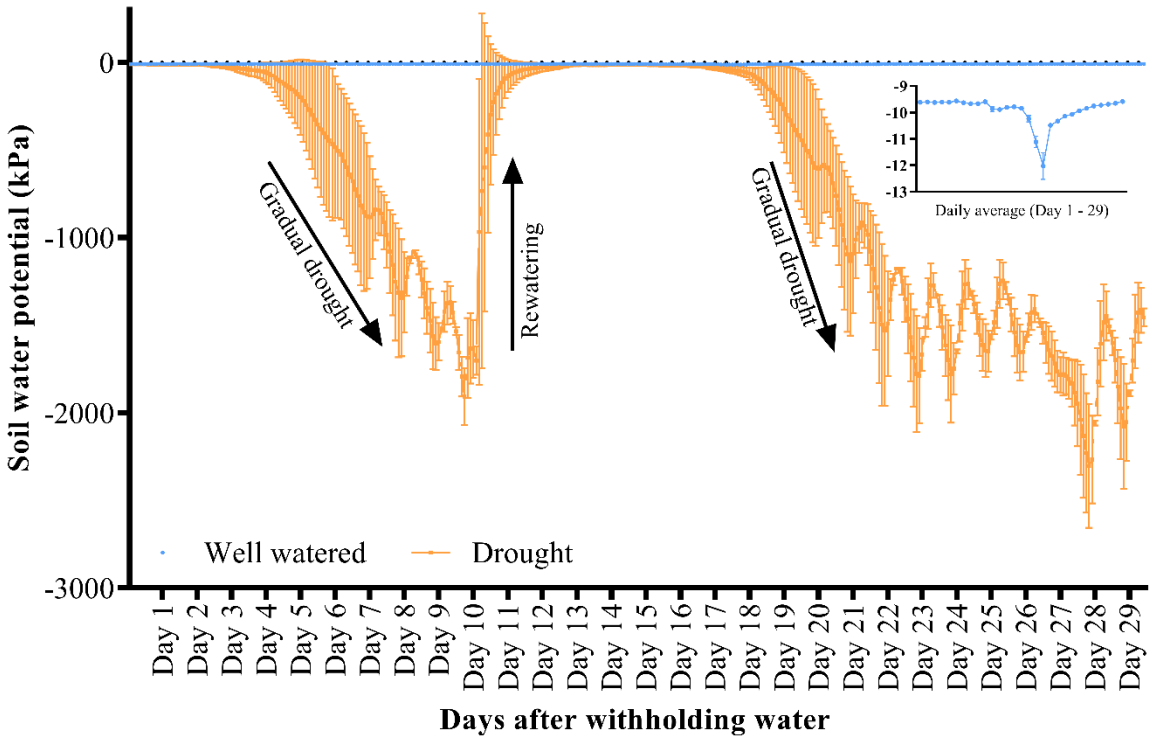

Figure 2.1 Changes in soil water potential under well-watered, drought, and rewatering periods. Data represent the mean ± standard deviation for two years. The inset graph represents daily average for the well-watered condition from day 1 to day 29 during drought treatment.

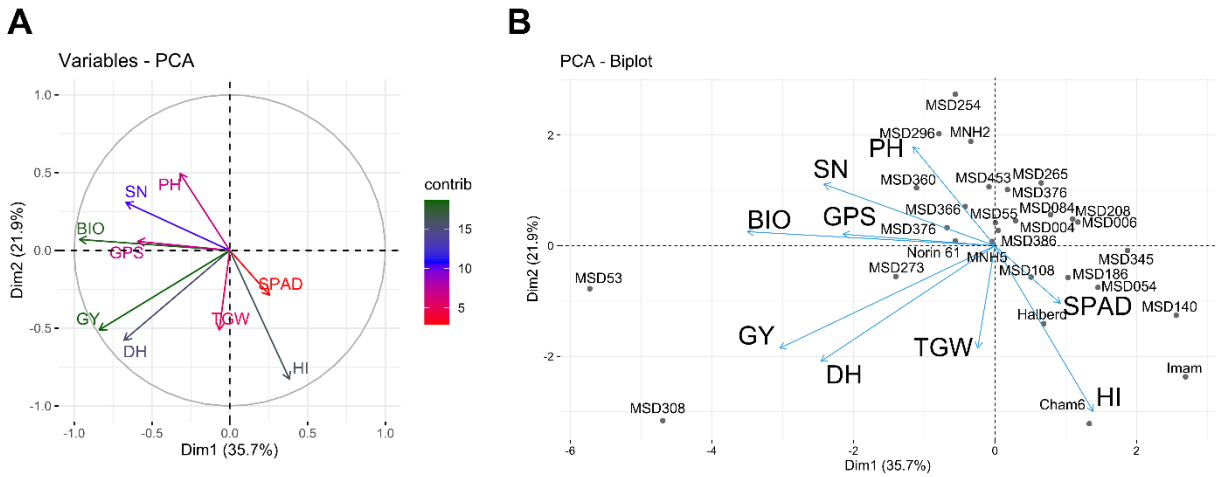

Figure 2.2 Principal component analysis (PCA) of the multiple synthetic derivative (MSD) lines, the backcross parent (Norin 61) and check cultivars (Imam, Cham6, and Halberd). (A) Variables PCA plot of the evaluated traits. Traits with high contribution to the principal components are shown in green. (B) PCA biplot showing the trends of different genotypes and evaluated traits. MSD53, MSD308, and MSD140 are separated from other MSD lines, indicating differences in drought resilience. The best linear unbiased predictors of genotypes for two years were used for the PCA. DH, days to 50% heading; SPAD, chlorophyll content; PH, plant height; GY, grain yield; BIO, biomass; HI, harvest index; SN, number of spikes per square meter; KPS, kernel number per spike; TKW, thousand-kernel weight.

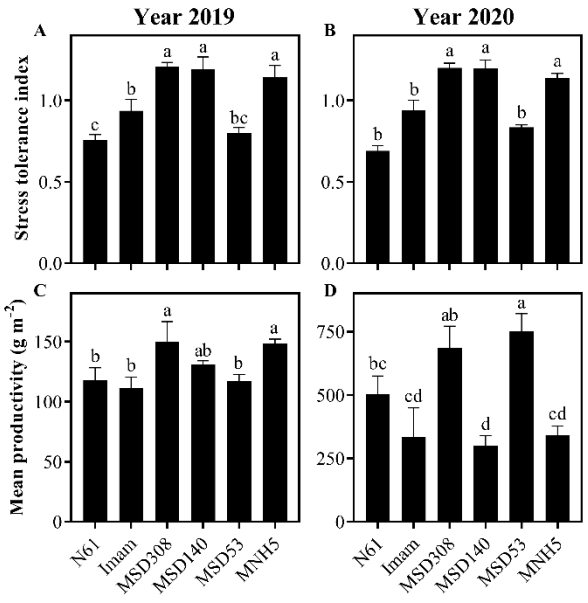

Figure 2.3 Stress tolerance index and mean productivity of selected MSD lines compared with their backcross parent, Norin 61 (N61), and a Sudanese commercial cultivar, 'Imam'. Stress tolerance index in 2019 (A) and 2020 (B). Mean productivity in 2019 (C) and 2020 (D). Data represent the mean ± standard deviation of three independent biological replicates. Bars marked with the same letter are not significantly different ($P < 0.05$), according to the Tukey HSD test.

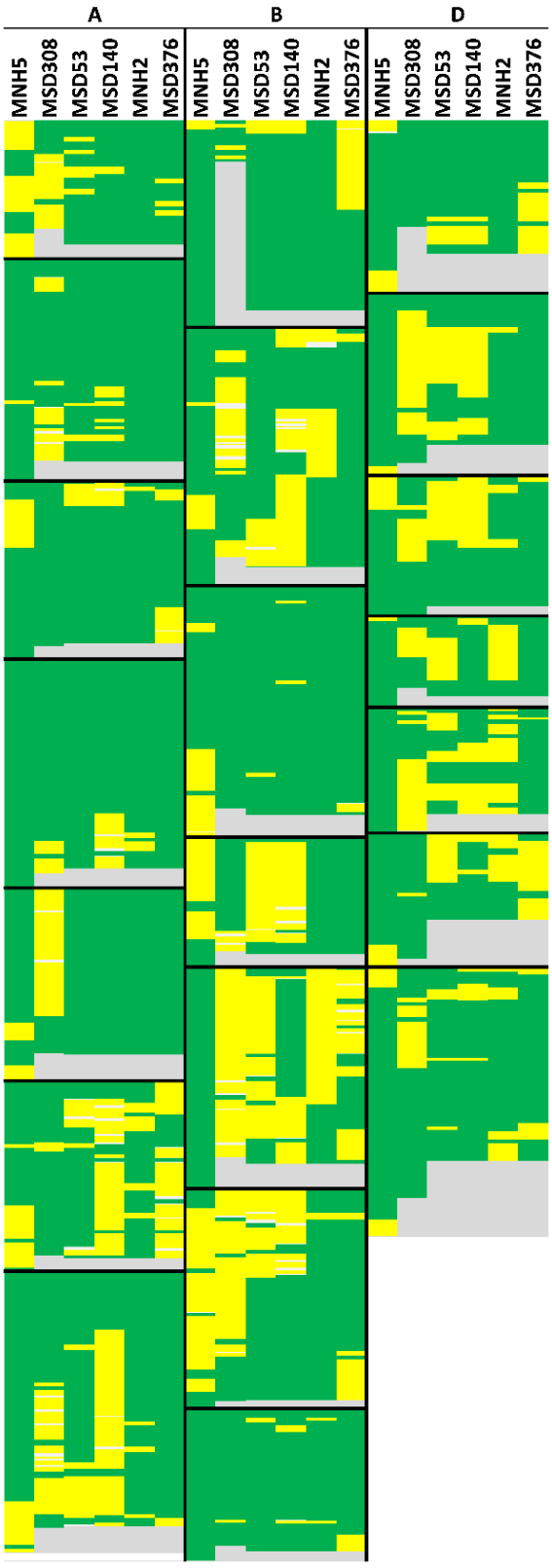

Figure 2.4 Graphical genotyping showing introgressed segments in drought-resilient (MNH5, MSD53 MSD140, and MSD308) and drought-sensitive lines (MNH2 and MSD367). Genotyping was done using Silico-DArT markers polymorphic between the backcross parent (Norin 61, green) and the synthetic parents (yellow). Missing markers are shown in grey. The chromosomes are arranged from top (1) to bottom (7) in each subgenome (A, B, D). Solid black horizontal and vertical lines denote the border between chromosomes and subgenomes, respectively.

Chapter 3

Transpiration response of two synthetic derivative wheat lines differing in drought resilience under dry-down conditions

3.1 Introduction

The reduction in global water availability has caused at least a 20.6% reduction in bread wheat yield within the last 40 years (Daryanto *et al.* 2016). Such drought-induced yield losses have been predicted to worsen in the future because of climate change (Elliott *et al.* 2014). Therefore, there is an urgent need to develop drought-resilient wheat cultivars with improved water conservation traits (World Health Organization 2018).

Drought occurs in different forms across different climatic zones and, as a result, plants need to adapt to region-specific drought conditions (Sherval *et al.* 2014). Such conditions include prolonged drought stress, erratic rainfall, and different groundwater levels. Therefore, to effectively breed drought-resilient wheat varieties, regional climatic and soil peculiarities need consideration. For example, in regions with reachable groundwater table, breeding for long root traits may be beneficial, whereas, in regions with prolonged drought stress and unreachable groundwater table, breeding for water conservation traits may be more meaningful.

Water conservation traits refer to physiological traits that enable plants to optimize water capture and/or use in order to maximize yield under water deficit. These traits are important for increasing water availability to sustain physiological activities, especially during critical stages of development (Gholipoor *et al.* 2012). Many studies have demonstrated the importance of water conservation traits for increasing yield under drought and high vapor pressure deficit in crop plants, including 0.20 t ha^{-1} in sorghum (Kholová *et al.* 2014), 2.50 t ha^{-1} in lentil (Guiguitant *et al.* 2017), and 1.35 t ha^{-1} in maize (Messina *et al.* 2015). Two main water conservation traits have been identified in crop plants: (a) low transpiration rate due to constitutively low plant hydraulic conductance under elevated vapor pressure deficits (Kholová *et al.* 2010), also referred to as water-saving, and (b) early partial stomatal closure when the soil begins to dry (Sinclair 2017), which results in effective water use.

In wheat, Mega *et al.* (2019) reported that water-saving plants overexpressing an ABA receptor (*TaPYL4*) reduced water consumption by up to 20% compared with non-transformed plants, resulting in increased yield per liter of water used. Water-saving wheat cultivars are often grown in drylands, sometimes unintentionally. Schoppach *et al.* (2017) reported that 23 South Australian cultivars conserve water by limiting transpiration, indicating that selection over 100 years resulted in cryptic selection for the limited-transpiration trait. Recent geospatial simulations across Tunisia found yield increases of up to 1.20 t ha^{-1} in wheat genotypes exhibiting water saving traits (Sadok *et al.* 2019). Conversely, the early partial stomatal closure trait ensures that the plant maintains a high transpiration rate when water is available, but quickly reduces transpiration at a relatively high soil water content when the soil begins to dry. That is, the fraction of transpirable soil water threshold ($FTSW_{Th}$) – the soil water content which triggers a drastic reduction in plant transpiration– is higher than in water-saving plants. This trait promotes maximum capture of available soil water which results in effective water use (reviewed in Blum 2009, Sinclair 2018). Variations in transpiration response to evaporative demand and soil water deficit among wheat genotypes have been reported both at the regional (Schoppach and Sadok 2012) and global scale (Tamang *et al.* 2019), with implications for environment-specific breeding.

Despite recent progress in identifying the variations in transpiration response in wheat under drought stress, not much has been done to investigate the contribution of wild relatives to water conservation in wheat. Wheat wild relatives that are adapted to stress-prone environments are a good alternative to introduce genetic diversity to broaden the gene pool of modern wheat cultivars (Ogbonnaya *et al.* 2013; Kishii 2019). One such wild relative is *Ae. tauschii*, the D genome progenitor of bread wheat. *Ae. tauschii* is adapted to arid and semi-arid regions and is thus a promising source for wheat improvement, especially for drought stress tolerance (Tsujimoto *et al.* 2015). Sohail *et al.* (2011) reported significant variation in drought tolerance traits among *Ae. tauschii* accessions under drought stress. To transfer this variation to bread wheat, synthetic hexaploid wheat lines developed by crossing *Ae. tauschii* with a durum wheat cultivar

were used (Tsujimoto *et al.* 2015). However, due to the wild morphology of the synthetic wheat lines, there was low correlation between their individual performances and those of their corresponding *Ae. tauschii* accessions under drought stress (Sohail *et al.* 2011). Therefore, to effectively utilize the variation in *Ae. tauschii* for wheat breeding, the synthetic wheat lines were crossed with a known bread wheat cultivar and the resulting population was referred to as multiple synthetic derivative (MSD) lines. Elbashir *et al.* (2017) reported high variation in heat tolerance-related traits among the MSD lines under heat stress in Sudan. Similarly, Itam *et al.* (2020) reported higher drought resilience-related traits in some MSD lines compared with their backcross parent (N61). They also found that although two of the MSD lines (MSD53 and MSD345) have higher drought tolerance efficiency (the ratio of grain yield under drought to that under well-watered condition) than N61, they possess contrasting drought resilience traits: MSD53 has high yield reduction (from 5095 to 3375 kg ha^{-1}, 33.7%), whereas MSD345 has low yield reduction (from 2031 to 1656 kg ha^{-1}, 18.4%) under drought stress (Itam *et al.* 2020a), suggesting differences in water conservation traits. However, the transpiration response of these lines in terms of $FTSW_{Th}$ which is regulated by the stomata is not yet known. Also, the overall stress response function of these lines compared with N61 has not been systematically investigated. In this study, the term "drought resilience" refers to the capacity of the wheat plant to resist damage and maintain productivity under drought stress.

The objective of this study is to characterize the water conservation traits of MSD53 and MSD345 using the $FTSW_{Th}$ and drought stress response function under dry-down conditions. The dry-down condition is commonly used for studying plant-water relations and involves a systematic reduction of irrigation until wilting point, while measuring the rate of transpiration in the plants (Sinclair and Ludlow 1986; Schoppach and Sadok 2012). The results indicate alternative water conservation strategies among the investigated genotypes and demonstrate the diversity of drought resilience mechanisms among the MSD lines that can be explored in wheat breeding programs to develop new cultivars with improved drought resilience.

3.2 Materials and Methods

3.2.1 Plant materials

The MSD lines were developed by crossing durum wheat (*T. turgidum* ssp. *durum*, cv. Langdon, AABB genomes) with *Ae. tauschii* (DD genome), and then crossing and backcrossing once with a bread wheat cultivar, N61 (AABBDD genomes) (Tsujimoto *et al.* 2015; Gorafi *et al.* 2018). This resulted in MSD lines containing a recombinant DD genome. The genomic constitution of the MSD lines is 75% N61 and 25% synthetic parent origin including *Ae. tauschii* and durum wheat (Gorafi *et al.* 2018). The MSD lines were repeatedly self-pollinated until fixation and are currently at the 8th filial generation (BC_1F_8). The two MSD lines used in this study were developed with *Ae. tauschii* accessions from Iran (MSD53) and Georgia (MSD345), and their pedigrees have been reported in Itam *et al.* (2020). I selected them because of their contrasting drought resilience (Itam *et al.* 2020a). For comparison, N61 was also investigated in this study.

3.2.2 Seed sowing and growth conditions

Seeds were cold-treated at 4°C for five days in Petri dishes to break dormancy, and then kept at room temperature for 24 h for acclimatization. Three seeds were sown into pots (1.5 L; 1.2 kg of dry soil per pot) containing Kanto loam volcanic soil (6% clay, 44% silt, 50% sand) with a bulk density of 0.84 g cm^{-3}. The seedlings were thinned at the 3rd leaf stage [Zadoks stage 13 (Zadoks *et al.* 1974)] to two plants per pot. Ten pots were used per genotype. The experimental setup and water retention curve of the soil are shown in Figure 3.1 and 3.2, respectively. The plants were grown in a greenhouse with an average day and night temperature of 33°C and 22°C, respectively. Plants were allowed to grow at 100% field capacity for 32 days before the onset of drought treatment, which followed the dry-down protocol (Sinclair and Ludlow 1986). The 100% field capacity is the amount of water held in the soil after excess water had drained away creating a sufficiently irrigated condition.

Before the dry-down experiment, all pots were overwatered and allowed to drain overnight. On the following morning, the pots were wrapped in polyethylene bags to prevent evaporation from the soil surface. To facilitate watering, a 10-mL pipette tip was inserted between the plant stem and the end of the polyethylene wrap (Fig. 3.1), and was secured with a twist tie. After wrapping, the initial weight of the pots was measured.

Nine pots were used per genotype, three pots were designated as well-watered and maintained at 100% field capacity, while the seven remaining pots were subjected to drought treatment. To designate pots for the well-watered condition, I ranked the mean transpiration rates of the nine pots for each genotype, and then chose three pots each from the high, middle, and low ranks. Water supply was withheld from the seven pots to induce drought stress. Pots were weighed daily (between 11:00 and 12:00am) and the amount of water lost was replaced for the well-watered pots to maintain 100% field capacity. To prevent rapid dehydration of the soil and ensure gradual drought stress, water was added to the drought-treated pots when necessary so that daily net water loss did not exceed 50 g. The pot weight difference between successive days was considered as the daily transpiration rate. Finally, the number of days taken to extract all the available water in the soil was recorded as duration.

3.2.3 Determination of $FTSW_{Th}$

The $FTSW_{Th}$ is the soil water content which triggers a drastic reduction in plant transpiration. To calculate the daily transpiration ratio (TR) of each pot and minimize day-to-day variations in transpiration rate, the transpiration rate for each pot was divided by the average transpiration rate for the three well-watered pots of the same genotype (Gholipoor *et al.* 2012).

To account for plant-to-plant variation, the TRs were normalized using the equation:

$$NTR = \frac{TR}{iTRave} \qquad (1)$$

where *NTR* is the normalized transpiration ratio of a particular genotype on a particular day, *TR* is the transpiration ratio, and *iTRave* is the average transpiration ratio of each genotype during the first three days of drought treatment, when the drought-treated pots still had a well-

watered moisture range (Devi *et al.* 2009). The *iTRave* values were 0.98, 1.00, and 1.09 for N61, MSD53, and MSD345, respectively (Table 3.1). Therefore, the NTR of each drought-stressed genotype was centered on 1.0 during the well-watered stage to make NTR values comparable among the three genotypes. The dry-down experiment continued until the NTR of all stressed plants fell below 0.12 (i.e., when the transpiration of drought-stressed plants was < 12% of that of well-watered plants). The weight difference between the initial and final weight (at NTR < 0.12) of each pot was referred to as total transpirable soil water. The fraction of transpirable soil water (FTSW) was calculated as follows:

$$FTSW = \frac{[daily\ weight - final\ weight]}{[initial\ weight - final\ weight]} \quad (2)$$

Finally, to estimate the $FTSW_{Th}$ for the decline in TR for each genotype, segmented linear regression analysis was performed using GraphPad Prism, version 8 (GraphPad Software Inc., San Diego, CA). The following model was applied:

$$NTR1 = a1FTSW + NTR0$$

$$NTR2 = a2(FTSW - FTSW_{Th}) + NTRatThreshold \quad (3)$$

where *NTR*0 is the NTR value at which the first line segment intersects the vertical axis; *a*1 is the slope of the first line segment, *a*2 is the slope of the second line segment, $FTSW_{Th}$ is the FTSW value at which the two line segments cross and *NTRatThreshold* is the NTR value at the crossing point.

3.2.4 Determination of drought stress response function

To quantitatively predict transpiration rate and growth under drought stress, I applied a widely used root water uptake model (Simunek *et al.* 2006), which uses Van Genuchten's stress response function. In this model, the rate of water uptake, S (s^{-1}), is calculated by multiplying the reduction coefficient for root water uptake α by the potential water uptake rate S_p (s^{-1}) (Feddes and Raats 2004):

$$S = \alpha * S_p \quad (4)$$

The reduction coefficient depends on suction at each depth. I assumed that root density is uniform throughout the root zone; under these conditions, the reduction coefficient equals NTR. I fitted data with a linear function below 4000 cm, where the data are distributed fairly linearly based on the model, and obtained threshold suctions at which the reduction coefficient starts to decrease below unity. Then, I determined the parameter values of Van Genuchten's stress response function (Van Genuchten 1987) as follows:

$$\alpha = NTR = \frac{1}{1+\left(\frac{h}{h_{50}}\right)^{p}} \quad (5)$$

where h is suction (cm), and h_{50} and p are fitting parameters; h_{50} is the suction at which water uptake is 50% of its potential rate and is a simple index of plant stress tolerance. The suction for each genotype was calculated using the average daily volumetric water content in the pots and the soil water retention curve (Fig. 3.2). The aim of this modelling was to confirm the earlier results obtained by $FTSW_{Th}$ and to project these results for potential characterization of water conservation traits in wheat.

3.3 Results

3.3.1 $FTSW_{Th}$

The mean total extracted water for N61, MSD53, and MSD345 was 525, 514, and 519 g, respectively, with no significant difference among the three genotypes (Table 3.2), indicating that water extraction capacity was similar among the three genotypes. However, the number of days taken to extract this water (referred to as duration below) differed among the genotypes. This difference was consistent with the differences in their transpiration rates (Table 3.2): the duration was longest for MSD345, which had the lowest TR, emphasizing the inverse relationship between TR and duration under drought conditions.

The NTRs remained approximately 1.0 until an $FTSW_{Th}$ was reached, and then decreased linearly (Fig. 3.3) due to decreasing transpiration. The slopes of the linear decrease ($S1_{NTR}$) were: 2.41 for N61, 1.70 for MSD53, and 2.65 for MSD345 (Fig. 3.3). The $FTSW_{Th}$ varied among the genotypes: from 0.32 in MSD345 to 0.52 in MSD53 (Fig. 3.3). This variation indicates the

differences in water conservation traits among the genotypes; MSD53 had an early response to drought stress compared to MSD345 Overall, these genotypic differences tend to positively correlate with TR; MSD345 had the lowest TR and lowest $FTSW_{Th}$ (Table 3.2).

3.3.2 Drought stress response function

The h_{50} values of the three genotypes ranged from 2917 cm (MSD53) to 5051 cm (MSD345), indicating the highest drought resilience of MSD345 (Fig. 3.4). Similarly, MSD345 had a higher threshold suction than MSD53 (Fig. 3.4), confirming the result for $FTSW_{Th}$ obtained from segmental linear regression (Fig. 3.3, Table 3.2).

3.4 Discussion

Introgressed wild alleles from *Ae. tauschii* have been recently used to increase genetic diversity and introduce desirable agronomic trait(s) into elite wheat germplasm (Ogbonnaya *et al.* 2013; Cox *et al.* 2017; Kishii 2019). The wheat MSD lines MSD53 and MSD345 were developed using two *Ae. tauschii* accessions adapted to the dry regions of Iran and Georgia, respectively (Tsujimoto *et al.* 2015; Gorafi *et al.* 2018). Under post-anthesis drought stress under field conditions, the drought tolerance efficiencies were 52.3% for N61, 66.2% for MSD53, and 81.5% for MSD345, indicating differences in drought resilience (Itam *et al.* 2020a). This implies that, although MSD53 had high grain yield under well-watered and drought conditions (5.09 t ha^{-1} and 3.38 t ha^{-1}, respectively) (Itam *et al.* 2020a), it had higher yield reduction compared with MSD345**.** The differences in drought tolerance efficiency (Itam *et al.* 2020a) imply that genotypes with high TR and $FTSW_{Th}$ have higher yield reduction compared with those with low TR and $FTSW_{Th}$ under drought stress. This negative trend between drought tolerance efficiency and $FTSW_{Th}$ may potentially prove useful in breeding for drought resilience and needs to be validated with a large sample size in future studies.

The trend between transpiration rate and FTSW indicates that plants with lower TRs (such as MSD345) have longer duration of normal physiological activities before they begin to respond to drought stress (Table 3.2). This trend needs validation in a large-scale study. The $FTSW_{Th}$ was

lower in MSD345 than in N61 and MSD53 (Fig. 3.3). The low TR value in MSD345 ensured a limited but sustained water flow that maintains a steady transpiration rate, thereby extending the period before the $FTSW_{Th}$ (Fig. 3.3C). Under drought, the transpiration rate is adjusted to match the water flow rate to the stomata to avoid desiccation (Sinclair 2018), a mechanism linked to aquaporin activity in root cells (Sadok and Sinclair 2010; Sadok 2017). In contrast, MSD53 had an early partial stomatal closure trait at high FTSW, which is linked to effective water use (Sinclair 2018). This trait increases wheat yields under drought (Sadok *et al.* 2019). Similar yield increases have been reported in sorghum (Kholová *et al.* 2014), lentil (Guiguitant *et al.* 2017), and soybean, especially in drier growing seasons (Sinclair *et al.* 2010), pointing to the universal nature of this trait in plants. Consistently, the drought stress response function (Fig. 3.4) showed that MSD345 is more drought resilient than MSD53 or N61, which may be attributed to its lowest TR and $FTSW_{Th}$.

The genotypic differences between the MSD lines indicated the presence of alternative water conservation strategies within the wheat MSD population (Gorafi *et al.* 2018). MSD345 achieved drought resilience by maintaining constant transpiration rate until its low $FTSW_{Th}$ was reached, whereas MSD53 had a high-$FTSW_{Th}$ strategy for conserving water under drought stress (Fig. 3.3B and C). Similar alternative strategies have been reported in sorghum genotypes under dry-down conditions (Gholipoor *et al.* 2012) and in wheat genotypes under different evaporative demands and soil water deficit (Schoppach and Sadok 2012; Sadok *et al.* 2019; Tamang *et al.* 2019). The alternative strategies in the two MSD lines may be attributed to different genomic contributions from their individual synthetic parents which contain genomic fragments from *Ae. tauschii*, and demonstrate the diversity of drought resilience mechanisms in *Ae. tauschii*. Worthy of note is the possible effect of the durum wheat cultivar (‘Langdon’) used for developing the synthetic parents. Overall, the diversity of the MSD lines is largely dependent on the diversity of the D genome due *Ae. tauschii* introgression (Gorafi *et al.* 2018). As expected, the diversity in water conservation traits affected yield, which is lower in MSD345 than in MSD53 under both

well-watered and drought conditions (Itam *et al.* 2020a), pointing to a possible trade-off between yield and drought resilience based on water conservation.

The choice between these synthetic wheat lines for further breeding will depend on breeders' target. In drylands, soil evaporation may substantially decrease the potential benefits of low TR and $FTSW_{Th}$, as these traits tend to conserve water within the soil. Genotypes with constitutively low TR and $FTSW_{Th}$ may have lower vegetative biomass and consequently lower yield. These traits, at least in the Sudan study, seemed to result in the plant not fully utilizing the available water. Sciarresi *et al.* (2019) have reported that the limited-TR trait only marginally increased wheat yield (by about 0.12 t ha^{-1}) in comparison with the increases (by 0.60 t ha^{-1}) due to enhanced root exploration traits in semiarid climate. In contrast, high TR early in the growing season may support vegetative growth, leading to high biomass, and subsequently, when drought occurs during grain filling, the high $FTSW_{Th}$ may be able to support grain yield. Plants with high $FTSW_{Th}$ may also produce more straw for livestock feed. Furthermore, the high TR and $FTSW_{Th}$-traits were ultimately beneficial under drought stress in Sudan (Itam *et al.* 2020a). This finding agrees with Sinclair 2017 (b) on the potential of the high $FTSW_{Th}$ trait for yield increase and the concept of effective water use (reviewed in Blum 2009, Sinclair 2018), but contradicts a recent simulation study in Tunisia (Sadok *et al.* 2019), which reported that high $FTSW_{Th}$ is wasteful and too conservative to enable yield gains in wheat under drought conditions. Therefore, to develop wheat lines with effective water use for specific locations, factors such as plant phenology and temporal phenomena need to be carefully considered (Sinclair 2018).

In conclusion, based on TR, $FTSW_{Th}$, and stress response function, MSD345 may be better suited for drylands, where soil water is always limited, whereas MSD53 may be better suited for areas with erratic rainfall where the plants can fully use their genetic potential under wet conditions and then quickly lower their transpiration rate in response to drying conditions. Under very dry conditions, MSD53 may fail completely, whereas MSD345 may survive, albeit with low yield. Since these wheat lines were developed by *Ae. tauschii* introgressions, this study shows the

benefits of the introgression in improving transpiration dynamics in wheat under two scenarios of water-limiting conditions (prolonged drought and erratic rainfall). Furthermore, the alternative water conservation traits from wheat wild relatives, which I identified and characterized in these lines using $FTSW_{Th}$ and drought stress response function, offers new options for increasing yield under water-deficit conditions.

Table 3.1 Transpiration ratio (TR) for Norin 61 (N61) and the two MSD lines under dry-down conditions

Genotype	iTR	iTRave	SD
N 61	0.974391	0.987899	0.165724
N 61	1.004759		
N 61	1.166201		
N 61	1.091048		
N 61	1.009614		
N 61	0.681382		
MSD 53	0.847874	1.009854	0.149643
MSD 53	0.878105		
MSD 53	1.110257		
MSD 53	1.097655		
MSD 53	0.840925		
MSD 53	1.088885		
MSD 53	1.205275		
MSD 345	1.082901	1.093527	0.252629
MSD 345	0.914826		
MSD 345	0.968332		
MSD 345	0.987531		
MSD 345	1.596816		
MSD 345	1.010754		

iTRave is the average transpiration ratio of each genotype during the first three days of drought treatment, when the drought-treated pots still had a well-watered moisture range. SD is the standard deviation of the mean for a minimum of six independent biological replicates.

Table 3.2 Segmented regression fit for normalized transpiration ratio (NTR) in response to decreasing fraction of transpirable soil water (FTSW) for two wheat multiple synthetic derivative lines and their backcross parent, Norin 61.

Genotype	Extracted water (g)	Transpiration rate (g plant^{-1} day^{-1})	Duration	FTSW threshold	Confidence interval (95%)	S.E.	Threshold suction (cm)
Norin 61	524.85±22.34^{a}	37.85±3.82^{a}	18.40±0.89^{c}	0.38	0.35–0.40	0.06	617
MSD53	513.64±11.42^{a}	39.32±5.28^{a}	16.28±1.25^{b}	0.52	0.48–0.57	0.08	333
MSD345	518.81±15.22^{a}	15.55±2.09^{b}	37.33±0.51^{a}	0.32	0.30–0.33	0.07	511

Different letters (column wise) indicate significant ($P < 0.05$) differences between genotypes according to Tukey's HSD test.

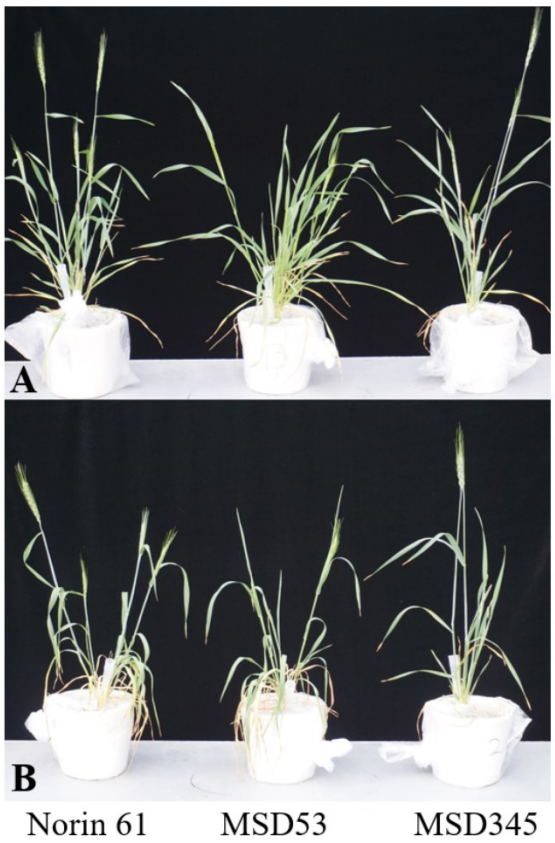

Figure 3.1 Experimental setup showing plants under different water regimes (A) well-watered plants, (B) drought-stressed plants. Photos were taken at 16 days after the beginning of the dry-down treatment.

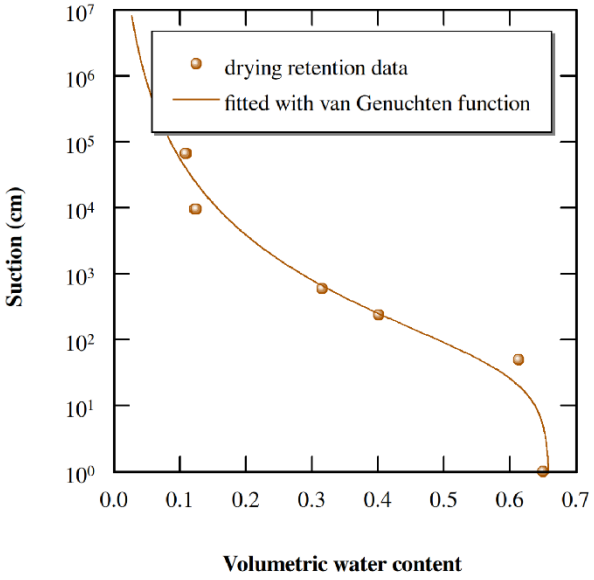

Figure 3.2 Water retention curve for Kanto loam soil.

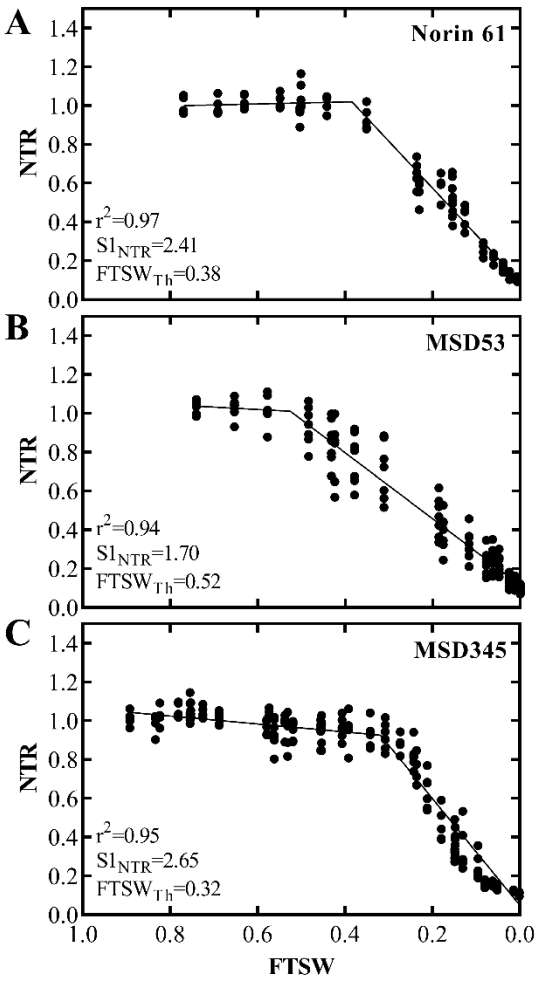

Figure 3.3 Normalized transpiration ratio (NTR) plotted against fraction of transpirable soil water (FTSW) for two wheat multiple synthetic derivative lines and their backcross parent, N61 under dry-down conditions. $S1_{NTR}$, slope 1; $FTSW_{Th}$, FTSW threshold for decrease in transpiration.

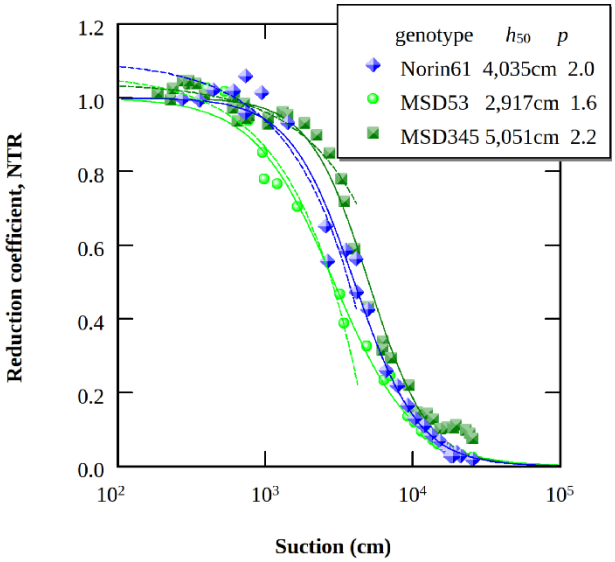

Figure 3.4 Stress response function of two wheat multiple synthetic derivative lines and their backcross parent, Norin 61, under dry-down conditions. Solid lines are curves fitted with equation 5; dashed lines are linear regression within 4000 cm.

Chapter 4

Metabolic and physiological responses to progressive drought stress in bread wheat

4.1 Introduction

Wheat (*T. aestivum*) is one of the most important staple-food crops and key sources of food calories especially to the ~4.5 billion people living in developing countries (Shiferaw *et al.* 2011). However, wheat yield is estimated to be reduced by ~6.0% per °C rise in global mean temperature, in concomitance with frequent exposures to prolonged drought episodes as a result of climate change (Zhao *et al.* 2017; Abdelrahman *et al.* 2019). Water availability is crucial for wheat production, and thus drought stress is considered a major factor affecting wheat yield losses (Yadav *et al.* 2019). With predicted increase in world population to 9.6 billion by 2050 (Godfray *et al.* 2010) agricultural water supply must be increased by ~17% to maintain agricultural productivity (Pennisi 2008). In addition, wheat demand is increasing in developing countries, and consumption rate in sub-Saharan Africa recently reached ~650 million tons per year (Mason *et al.* 2012), causing additional pressure on wheat demand. Thus, the generation of drought-tolerant wheat varieties with greater water-use efficiency is of the utmost priority, especially in the context of food sustainability. However, this requires a detailed understanding of wheat physiological and metabolic responses to drought stress.

Abscisic acid (ABA) biosynthesis is induced when plants respond to drought stress, and subsequently increased ABA binds to its receptor to initiate signal transduction, leading to stomatal closure and other cellular responses to stress (Cutler *et al.* 2010). By closing the stomata, transpiration is suppressed and plants are able to prevent water loss and maintain sufficient level of water under drought condition. A recent report on wheat drought tolerance indicates that wheat plants overexpressing ABA receptor (*TaPYL4*) improved seed production per L of supplied water in comparison with wild-type plants (Mega *et al.* 2019). Drought-responsive metabolites such as Pro were induced by ABA (Stewart and Voetberg 1985; Szabados and Savouré 2010), and the rate-limiting gene for Pro biosynthesis, *Δ1-pyrroline-5-carboxylate synthase* (*P5CS*), is also

controlled by the ABA-signalling pathway (Strizhov *et al.* 1997).

Metabolomics has become a powerful tool in the post-genomics era, enabling us to explore different aspects of the biological and physiological changes caused by environmental or genetic perturbations (Abdelrahman *et al.* 2019). In addition, metabolites come last in the omics cascade (that is, relatively close to the phenotype) and are therefore, a reliable tool for investigating abiotic stress responses in plants (Arbona *et al.* 2013). For example, branched chain amino acids (BCAAs), respiratory amino acids (Gly and Ser), and some of the tricarboxylic acid cycle-intermediates are known to be accumulated in *Arabidopsis thaliana*, rice (*O. sativa*), and barley (*H. vulgare*) in response to drought stress (Obata and Fernie 2012; Li *et al.* 2015; Templer *et al.* 2017). In wheat, accumulations of Pro, Trp, organic acids, phenolics, and sulphur-related metabolites (glutathione, Met, and Cys) have been reported under drought-stress conditions (Bowne *et al.* 2012; Valifard *et al.* 2012; Gregorová *et al.* 2015; Islam *et al.* 2015). However, there is limited knowledge on specific soil moisture conditions associated with particular metabolic profiles in wheat. To advance this knowledge, it is necessary to conduct a time-lapse study having many sampling points under progressive drought-stress conditions.

The objective of this study was to elucidate the physiological and metabolic responses of wheat N61 to progressive drought stress at the flowering stage, as a critical stage affecting grain yield (Boyer 1982). Wheat plants were subjected to progressive drought stress in a growth chamber by monitoring the conditions for 10 days. Then, the relationship between drought level based on soil water potential (SWP) and physiological responses such as canopy temperature (CT), reactive oxygen species (ROS), and carbon isotope composition ($\delta^{13}C$) were analysed. In parallel, metabolite changes and ABA-responsive gene expression under respective time points were analysed. Results (i) demonstrated a strong association between canopy temperature depression (CTD) and SWP, (ii) identified a threshold moisture content triggering maximum plant response, and (iii) drought response-related metabolite biomarkers. The findings provide comprehensive information on physiological and metabolic dynamics associated with drought stress tolerance in

wheat, which would be a major step for accelerating the development of wheat-tolerant varieties using biomarker-assisted selection.

4.2 Methods

4.2.1 Plant material and growth condition

A standard Japanese spring wheat cultivar, N61, was used for this study. N61 is a representative wheat genome (10+genome project, www.10wheatgenomes.com). Seeds were stratified at 4°C for 7 d, hardened at room temperature for 24 h, and then transferred to pots (f 7.5 cm x D 6.5 cm) containing commercial garden soil and maintained in a greenhouse for 30 d. The 30-d-old seedlings (4th-leaf-stage) were carefully transplanted into another soil medium prepared by watering dry commercial mixed soil (Oishii yasai wo sodateru tuchi, CAINZ, Japan) to field capacity with water containing 10 mL/L of liquid fertilizer (N P K 6. 10. 5, HYPONex, Japan). The medium was placed in rectangular pots (internal dimension = L 30 cm x W 18 cm x H 18 cm), with each pot containing three plants. A total of 16 pots containing 30-d-old plants were transferred to two climatic growth chambers (Espec, Japan). The growth chambers were maintained at 23°C (14-h light)/19°C (10-h dark), with relative humidity levels of 50% (light)/60% (dark), and a photosynthetic photon flux density of 900 μmol s^{-1} m^{-2}. To avoid spatial heterogeneity, turntables within the growth chambers ensured constant changes in plant positions (Fig. 4.1). The soil volumetric water content (SWC) was measured using moisture sensors (Em5b, Decagon devices, WA, USA), and the SWP was determined using the conversion equation:

$SWP = 1606.8 \times e^{-17.69*SWC}$ (Mega *et al.* 2019) (1)

4.2.2 Experimental design, drought treatment and sampling

The experiment was set up in a completely randomized design with the 16 pots being randomly assigned and subjected to either well-watered or progressive drought conditions. That is, each chamber had eight pots: four control and four drought pots. Progressive drought was initiated by withholding water at Zadok`s stage 65 (halfway into flowering (Zadoks *et al.* 1974)). Control pots were maintained at SWP −15 kPa. Flag leaf samples were collected at d 0 (before

the drought treatment), 2, 4, 6, 8, and 10 after withholding water (DT2, 4, 6, 8, and 10, respectively). Four plants were sampled from each condition, with four flag leaf samples taken from each plant. Sampling was performed between 11:00 am and 12:00 noon (~5 h into photoperiod) to account for diurnal fluctuations. All the samples were snap-frozen with liquid nitrogen, pulverized with MULTI-BEADS SHOCKER (Yasui Kikai, Japan), and stored at -80°C.

4.2.3 Canopy temperature measurement

Leaf thermal images were taken with an infrared camera (R500EX-Pro, NIPPON AVIONICS, Tokyo, Japan) on each sampling day just before flag leaf samples were collected. The images were taken laterally to minimize background effect due to the scanty nature of the plant canopy under severe drought stress. The thermal images were analysed using manufacturer's software (NS9500LT Version 2.7A, NIPPON AVIONICS). Twenty data points were randomly selected per image, and the average value was recorded as the CT. The CTD was determined by subtracting CT from ambient temperature.

4.2.4 Reactive oxygen species quantification

To estimate the extent of drought-induced oxidative stress, the ROS content was measured using a fluorogenic probe, 2,7-dichlorofluorescein (Cell Biolabs, San Diego, CA, USA) as described in Narayanan *et al.* (2016). Briefly, 50 mg of pulverized flag leaf samples were suspended in 1 ml of 1× phosphate-buffered saline (pH 7.4) and centrifuged at 10,000 ×g for 5 min. The supernatant (50 µL) was transferred to a black 96-well microplate and incubated for 5 min with a catalyst at room temperature. A freshly prepared dichlorodihydrofluorescein solution (100 µL) was added to each well and incubated for 45 min in the dark. After incubation, fluorescence from each well was read at 485 nm (excitation)/530 nm (emission) wavelengths using a microplate reader (SH-9000, Corona Electronic, Ibaraki, Japan). The amount of ROS was normalized using the sample fresh weight.

4.2.5 Carbon isotope analysis

The ^{13}C composition of flag leaves was analysed using an Elemental Analyser interfaced with a continuous-flow isotope ratio mass spectrometer (EA/IRMS; Thermo Fisher Scientific). Dried, pulverized flag leaf samples (1 mg) were filled into tin capsules (5 × 9 mm, LUDI Swiss) and placed in a combustion oven using an automatic sampler. Each sample was measured against standard CO_2 calibrated with an isotope standard. The accuracy of calibration was ± 0.066‰ SD. Finally, the ^{13}C composition was calculated as

$$\delta^{13}C = \left[\left(\frac{Rsample}{Rstandard}\right) - 1\right] \times 1{,}000, \qquad (2)$$

where R is the $^{13}C/^{12}C$ isotope ratios of samples and standards.

4.2.6 Metabolite analysis: sample preparation and quantification

In total, 50 mg of each pulverized flag leaf sample was freeze-dried and stored in a desiccator at room temperature for metabolite analysis. Later, 4 mg of each freeze-dried sample was treated with 500 µL of 50% methanol and centrifuged at 15,000 ×g at 4°C for 5 minutes. Then, to separate polar and non-polar metabolites, 450 µL of the supernatant was carefully mixed with an equal volume of chloroform, vortexed and centrifuged (15,000 ×g at 4°C for 5 min). In total, 400 µL of the resultant supernatant was filtered through a membrane (Amicon Ultra-0.5 mL, 3 kDa cutoff, Millipore, Billerica, MA, USA) and centrifuged (15,000 ×g at 4°C for 30 min). MiliQ water (400 µL) was added to the filter and centrifuged (15,000 ×g at 4°C for 30 min). The filtrate was then dried in a SpeedVac concentrator (Thermo Fisher Scientific, Waltham, MA, USA) at 45°C for 6 h. The concentrated dry sample was resuspended in 50% methanol (200 µL). A 50-µL aliquot was then transferred into another tube containing 450 µL of 50% methanol to form a 10-fold dilution. The resulting 500 µL solution was used for LC-MS metabolite quantification. In total, 94 metabolites were quantified using a triple quadrupole LC-MS/MS system (Agilent 6420, CA, USA), with a Discovery HS-F5 column (2.1 × 250 mm, 5 µm, Sigma-Aldrich, PA, USA). The metabolites were identified by MRM analysis. Product ions used to characterize each metabolite are shown in Table 4.1. The levels of metabolites in each leaf sample were normalized using sample dry weight. A quality control reference was established using

metabolite standard mixtures of different concentrations (0, 0.4, 2 and 10 ppm). Compounds having similar molecular masses or retention times were not included in the same mixture. The mobile phase consisted of 0.1% formic acid and acetonitrile as A and B solutions, respectively. A gradient flow with four A:B ratios was applied: (1) 100% A:0% B for 2 min, (2) 72% A:25% B for 8 min, (3) 65% A:35% B for 4 min, and (4) 5% A:95% B for 3 min. All the solvents and reagents used were of LC-MS grade.

4.2.7 Quantitative reverse transcription PCR (qRT-PCR) analysis

4.2.7.1 RNA extraction

Total RNA was isolated from flag leaves using RNeasy Plant Mini Kit (74904; Qiagen, Germany) according to the manufacturer's protocol. A total of 500 ng total RNA was reverse transcribed using ReverTra Ace qPCR RT Master Mix with gDNA remover according to the manufacturer's manual (Toyobo, Japan).

4.2.7.2 Primer design

Sequence homologs of three ABA-responsive genes were queried against the hexaploid wheat sequences obtained from the International Wheat Sequencing Consortium using the Phytozome database (http://www.phytozome.net). The genes are (1) an ABA-signalling regulator, *TaPP2C6*; (2) a late embryogenesis abundance protein, *TaLEA* (Mega *et al.* 2019); and (3) a Pro biosynthetic gene, *TaP5CS* (Maghsoudi *et al.* 2018). The sequences with the highest homology levels to the hexaploid wheat genome were selected. Primer sequences were designed using NCBI PrimerBlast (https://www.ncbi.nlm.nih.gov/tools/primer-blast/).

4.2.7.3 qRT-PCR for ABA-responsive genes

qRT-PCR was performed on a StepOnePlus Real Time PCR system (Life Technologies) using KOD SYBR qPCR Mix (Toyobo), and the gene-specific primer sets are shown in Table 4.2. The PCR program consisted of an initial temperature of 98°C for 2 min, followed by 40 cycles of 98°C for 10 s, 60°C for 10 s and 68°C for 30 s. A melting curve was constructed by increasing the temperature from 68°C to 99°C at a rate of 0.05°C s^{-1}. To calculate the copy number, a

standard curve was generated for the pMD20 plasmid containing the target DNA sequence. Four biological replicates were performed, and *TaActin* was used as an internal standard for normalization.

4.2.8 Statistical analyses

ANOVA, Student's *t*-tests, and *Z*-transformation of metabolic and physiological data were conducted using Microsoft Excel 2019. A principal component analysis (PCA) and graphical representations were made using the R program, version 3.5.2 (R Core Team 2018). The metabolite pathway and network analysis were conducted using Kyoto Encyclopedia of Genes and Genomes (KEGG; https://www.genome.jp/kegg/) and the literature. The cluster analysis was conducted using the Mass Profiler Professional software (MPP version 2.5, Agilent Technologies, CA, USA).

4.3 Results

4.3.1 Physiological effects of progressive drought stress in wheat

To evaluate drought-stress levels, the SWC was monitored using sensors, and the values were converted to SWP to ensure replicability in different soils. The SWP was maintained at −15.8 kPa in control pots but decreased continuously in drought-treated pots as the drought intensified. The steady decline in SWP ensured that plants were subjected to progressive drought stress. The SWP reduction rate was high during the early days of drought treatment (DT2, 4, and 6), decreasing from −45.1 kPa on DT2 to −385.1 kPa on DT6 (Fig. 4.2A and Table 4.3), but was low during day 8 and 10 (DT8 and 10, respectively), decreasing from −517.7 kPa on DT8 to −554.5 kPa on DT10 as the drought intensified.

To understand the CT changes in response to different drought levels, the thermal analysis of plants was performed under progressive drought stress as shown in Fig. 4.2B. Prior to drought treatment (d 0), the CTs of both drought-treated and well-watered plants were similar, and the CTDs were ~5°C (Table 4.3), indicating that plants were not under stress (Guendouz *et al.* 2013).

However, during DT2, drought-treated plants began to show slight increases in CT (Fig. 4.2B and C), and the CTDs were 5.3°C and 3.7°C for well-watered and drought-treated plants, respectively. The CT increased continuously, while the corresponding CTD decreased as the drought intensified. A sharp increase in CT was observed during DT8 as the SWP decreased to −517.7 kPa (Fig. 4.2A, C and Table 4.3). Overall, the greatest increases in CT were observed during DT8 and 10, with CTDs of 0.25°C and −0.62°C, respectively, while the corresponding well-watered control (WW8 and 10, respectively) had CTDs of 4.22°C and 3.34°C, respectively (Table 4.3). Consequently, there was a strong positive correlation between CTD and SWP ($r^2 = 0.95$, $P < 0.05$). This suggests that DT8 is a physiologically critical point. Using these soil and plant states, ROS, carbon isotope composition, metabolite changes, and ABA-responsive gene expression levels were analysed to better understand plant responses to progressive drought stress.

4.3.2 Gradual ROS accumulation under progressive drought stress

To investigate the oxidative stress effects of progressive drought stress, the ROS content was measured using flag leaf samples collected at each progressive drought point. The ROS contents of drought-treated samples increased significantly on DT8 and 10 (Fig. 4.2D). This suggests that at DT8 and 10, the ROS generation rate exceeded the plants' scavenging capability owing to severe drought stress. However, there were no significant changes during DT2, 4, and 6, indicating that there was no severe drought stress at these time points.

4.3.3 ^{13}C composition under progressive drought stress

Drought causes stomatal closure which affects photosynthetic carbon isotope discrimination (Farquhar *et al.* 1989). To evaluate the stress levels in plants under progressive drought conditions, the ^{13}C composition in flag leaf samples was investigated. The ^{13}C composition in drought-treated samples had higher values than the control conditions starting from DT4 (Fig. 4.2E). At DT8, the ^{13}C value was slightly higher but not significantly different from the control. Overall, this indicates that there was an alteration in carbon isotope discrimination in response to progressive drought stress.

4.3.4 ABA-responsive gene expression under progressive drought stress

ABA is well-known to be biosynthesized in response to drought stress. Endogenous ABA contents and ABA responsive genes are often utilized to confirm the effect of drought treatment. Therefore, transcript levels of ABA-responsive genes and endogenous ABA level with qRT-PCR and LC-MS, respectively were investigated. At first, LC-MS measurements indicated that ABA accumulated significantly from DT4 to 10, suggesting that ABA biosynthesis occurred starting from DT4 (Fig. 4.2F). Two ABA-responsive genes: the late embryogenesis abundance gene, *TaLEA* and the ABA-signalling negative regulator gene, *TaPP2C6* were previously reported in wheat under drought stress (Mega *et al.* 2019). Also, the Pro biosynthetic gene, *P5CS* was proposed as an ABA responsive gene in Arabidopsis (Strizhov *et al.* 1997). The expression levels of *TaLEA*, *TaPP2C6*, and *TaP5CS* significantly increased under drought-stress conditions, starting from DT4, indicating that these genes were upregulated in response to drought-induced ABA accumulation (Fig. 4.2G–I). This suggests that DT4 is the start point of ABA response.

4.3.5 Total metabolite profiling under progressive drought stress

To evaluate the metabolite changes involved in progressive drought responses, 94 metabolites were quantified using flag leaves of plants grown under well-watered and drought conditions. Subjecting the metabolite data to a PCA revealed the high variability in metabolite contributions to drought responses (Fig. 4.3A). PC1 (Dim 1) explained 36.9%, while PC2 (Dim 2) explained 11.6% of the variability. More than one-half of all metabolites, especially amino acids, nucleosides, and organic acids were affected by severe drought stress at DT8 and 10 (Fig. 4.3A–C and Table 4.4). All the well-watered samples (D0, WW2, 4, 6, 8, and 10) tended to cluster together, indicating that they had similar metabolite profiles. In addition, samples grown under mild drought conditions (DT2 and 4) clustered towards the well-watered samples (Fig. 4.3B and D). Two out of three samples at DT6 were located in the intermediate region between mild and severe drought (Fig. 4.3B and D), suggesting that DT6 is a transition state.

4.3.6 Metabolite changes at each drought level

Then, significantly up- and down-regulated metabolites (> twofold change, $P < 0.05$) were characterized by volcano plots under each drought condition. At DT2, there was no significant metabolite change, but starting from DT4, the number of upregulated metabolites increased along with drought intensity (Fig. 4.4A). In contrast, the numbers of downregulated metabolites were similar in a drought level-dependent manner. At DT4, DT6, DT8, and DT10, 9, 19, 28, and 38 metabolites, respectively, were upregulated, while 3, 3, 2, and 2 metabolites, respectively, were downregulated. In addition, correlation analyses among drought conditions indicated positive correlations (r = 0.66 and 0.51) among severe drought stress time points, DT8/WW8–DT10/WW10 and DT6/WW6–DT8/WW8, respectively, while low correlations (r = 0.25 and 0.20) were identified among severe and mild drought stress time points, DT4/WW4–DT6/WW6 and DT4/WW4–DT10/WW10, respectively (Fig. 4.4B). The correlations between the DT2 samples and the other samples were less than 0.2. This correlation analysis suggested that the drought levels from DT6 to 10 were more similar than those of DT2 to 4. This finding also indicated that drought stress rapidly increased between DT4 and 6, and, therefore, DT6 is likely a transition stage.

Among the 94 metabolites analysed, the 53 metabolites with the greatest accumulations (≥ twofold change, $P < 0.05$) were selected for further analyses. A hierarchical clustering analysis of the 53 metabolites showed an overview of their accumulation levels under different drought conditions (Fig. 4.5), with DT6 clustering between severe drought and control categories, which further indicated that DT6 is a transition state in the progressive drought responses.

Venn diagrams were used to reveal the condition-related specificities of the metabolites (Fig. 4.6). Five metabolites (Gly, taurine, hypoxanthine, lactic acid, and ornithine) were specifically upregulated at DT6, 3 (uracil, tyramine, and methionine-sulfoxide) at DT8, and 13 (malonic acid, putrescine, thymidine, uridine, Cys-Cys, deoxyuridine, betaine, serotonin, cytidine, 1-aminocyclopropane-1-carboxylic acid (ACC), tryptamine, indole-3-acetic acid, and allantoin) at DT10 (Fig. 4.6A). Among the DT10-specific metabolites, allantoin (119-fold), ACC (13-fold),

and tryptamine (12-fold) had the highest fold changes (Table 4.4 and 4.5). Similarly, some metabolites were upregulated at two different drought levels. For example, pyroglutamic acid was upregulated at DT6 and 8. Eight metabolites [2,4-dihydroxy-1,4-benzoxazin-3-one-glucoside, Asn, cadavarine, gamma-aminobutyric acid (GABA), malic acid, deoxyadenosine, arginosuccinic acid, and Tyr] were upregulated at DT8 and 10 (Table 4.5). Pyruvic acid and arginosuccinic acid were downregulated at DT4, succinic acid and shikimic acid at DT6, glyceric acid and ACC at DT8, and deoxyinosine and ferulic acid at DT10 (Fig. 4.6B). Interestingly, four metabolites (His, Val, Trp, and Ile) were consistently upregulated from DT4 to 10 (Fig. 4.6C and Table 4.4). These metabolites are probably drought-responsive and may be used as potential biomarkers.

4.3.7 Pathway analysis based on metabolite enrichment under progressive drought stress

Finally, metabolite pathway analysis was conducted. Most metabolites showed increasing trends under drought-stress conditions, although shikimic, ferulic, and glyceric acids showed decreasing trends (Fig. 4.7). Taken together, the major metabolic pathways affected in this study, based on pathway and network analyses, include the following: (i) aspartate (ii) pyrimidine, (iii) glycine and serine, (iv) arginine and proline, (v) urea cycle (vi) tryptophan and aromatic amino acid, (vii) BCAA, and (viii) purine metabolism (Fig. 4.7).

4.4 Discussion

CT is an important tool for studying plant physiological responses to drought stress, because it integrates many physiological responses into a single low-cost measurement (Mason and Singh 2014). In the present study, the CT of wheat increased, while the corresponding CTD decreased under progressive drought-stress conditions. The increase in CT supports previous reports in which drought caused stomatal closure, leading to increased respiration and reduced transpiration (Maes and Steppe 2012). This study indicates that the reduction in water consumption, especially during DT8 (−517 kPa), is responsible for the sharp rise in CT (Fig. 4.2B and C) and suggests that although ABA accumulation began in DT4, drastic stomatal closure occurred in DT8 in response to the drought stress (Fig. 4.2F). Consistently, increase in ABA-

responsive gene (*TaLEA*, *TaPP2C6* and *TaP5CS*) expressions were observed under drought conditions starting from DT4, indicating that ABA signalling was earlier upregulated in response to the drought stress (Fig. 4.2F–I). This confirms that physiological response to drought occurred after ABA biosynthesis. These results support the findings of Merlot *et al.* (2002) in which the use of CT values for the genetic dissection of ABA biosynthesis in Arabidopsis was validated. There was a strong correlation ($r^2 = 0.95$, $P < 0.05$; Table 4.3) between CTD and SWP. The CTD explained 95% of the changes in SWP resulting from drought stress. This implies that a simple CT reading can accurately ($P < 0.05$) predict the SWP or drought-stress level in wheat without disturbing the plant.

^{13}C composition analyses have been used to evaluate plant responses to drought stress (Farquhar *et al.* 1989). In this study, the higher value than the control in the ^{13}C composition of wheat at each point (Fig. 4.2E) suggested a change in the normal carbon isotope discrimination in response to drought stress. This indicated that stomatal closure was induced at various time points due to drought stress. Consequently, a continuous increase in CTs was observed alongside ABA-responsive gene expression levels, indicating that plants were subjected to progressive drought stress.

Abiotic stresses have profound effects on plant metabolism, and, as a result, metabolomics is a burgeoning research field. In this study, metabolomics analysis was utilized to dissect the metabolite changes in wheat in response to different drought levels during a 10-day progressive drought period. The most pronounced changes were increases in amino acids, organic acids, and nucleosides. Four amino acids (His, Val, Trp, and Ile) were consistently and rapidly upregulated from DT4 to 10 (from mild to severe drought), suggesting that they are drought biomarkers (Fig. 4.6B). Amino acid accumulations, such as BCAAs and aromatic amino acids, in drought-stressed plants have overall beneficial effects on the stress acclimation (Bowne *et al.* 2012; Sanchez *et al.* 2012; Michaletti *et al.* 2018). Organic acids, such as lactic, malic, and succinic acids, increased in response to drought stress. Although the roles of organic acids in drought response and

adaptation are not fully understood, they may accumulate owing to drought-induced perturbations of the tricarboxylic acid cycle (Bowne *et al.* 2012; Gregorová *et al.* 2015; Michaletti *et al.* 2018). Similarly, salicylic acid, a plant hormone, accumulated alongside ABA in response to drought stress starting from DT6 (Table 4.4). Salicylic acid, like ABA, is involved in stomatal regulation through Ca^{2+}-dependent protein kinases located downstream of the peroxidase-mediated ROS signalling pathway in Arabidopsis guard cells (Prodhan *et al.* 2018). Thus, ABA and salicylic acid may co-regulate stomatal closure in response to drought stress.

Pro, a well-known marker for drought response, accumulated starting from DT6 (Fig. 4.5, Table 4.4). Pro acts as an osmolyte, ROS scavenger, and molecular chaperone for stabilizing protein structures (Verbruggen and Hermans 2008; Szabados and Savouré 2010). Pro biosynthesis is dependent on the expression of the *P5CS* gene, and ABA stimulates Pro biosynthesis under drought-stress conditions (Stewart and Voetberg 1985; Strizhov *et al.* 1997). In this study, ABA accumulation was associated with *TaP5CS* expression, which began on DT4 (Fig. 4.2F and I) before the metabolic response (proline accumulation) at DT6 (Table 4.4). GABA also significantly accumulated on DT4, 8, and 10 (Table 4.4). GABA accumulation has been associated with the carbon–nitrogen balance and ROS scavenging (Bouché and Fromm 2004; Song *et al.* 2010). There is a possible correlation between GABA and Pro biosynthesis under drought-stress conditions.

The levels of BCAAs (Leu, Ile, and Val) increased significantly, starting from DT4, as the drought stress progressed. Previous studies suggested that BCAAs are an alternative source of energy in sugar-starved Arabidopsis (Taylor *et al.* 2004), and drought-stressed wheat (Bowne *et al.* 2012). Urano *et al.* (2009), in a dehydration experiment, reported high accumulations of BCAAs that were regulated at the transcript level by the BCAA biosynthesis enzyme, branched-chain aminotransferase (*BCAT2*). Thus, it is concluded that the high BCAA accumulation level is an adaptive response to drought stress.

His biosynthesis is tightly linked to nucleotide metabolism through 5-phosphoribosyl-1-pyrophosphate (Ohta *et al.* 2000), which is required for the *de novo* biosynthesis and salvaging of nucleotides, as well as for plant growth and biomass accumulation (Koslowsky *et al.* 2008). In recent studies, Das *et al.* (2017) and Michaletti *et al.* (2018) reported that drought stress stimulates the upregulation of major purine bases as a first step in activating nucleic acid protective mechanisms. Purine–His cross-pathway regulation has been reported in *Saccharomyces cerevisiae* (Rébora *et al.* 2005). In the present study, concomitant His and nucleoside accumulations were observed starting from DT6 (Fig. 4.7 and Table 4.4). Thus, His accumulation may be correlated with the biosynthesis and protection of nucleosides under drought-stress conditions. Although His biosynthesis is an energy-demanding process, consuming 41 ATP molecules per His molecule synthesized (Brenner and Ames 1971), plant cells may preferentially synthesize His as a protectant of purine nucleosides under severe drought-stress conditions.

Purine metabolism is the fundamental route for nitrogen recycling and remobilization in non-leguminous plants (Takagi *et al.* 2016). Allantoin, a nitrogen-rich intermediate of purine catabolism, stimulates ABA production and jasmonic acid homeostasis in Arabidopsis under stress conditions (Watanabe *et al.* 2014; Takagi *et al.* 2016), indicating that purine metabolism plays dual roles in plants during stress. In the present study, pyrimidine metabolites, such as thymidine, uridine, and cytidine, and the purine metabolite allantoin accumulated only at DT10 (Table 4.5 and Table 4.4), suggesting their involvement in severe drought responses. Allantoin increased by 120-fold, indicating an increase in nitrogen recycling, which is a survival mechanism under severe drought-stress conditions. At the same time, ABA increased by 23.8-fold (far more than the 9.6-fold at DT6), suggesting allantoin-stimulated ABA production, as previously reported (Watanabe *et al.* 2014; Takagi *et al.* 2016). We, therefore, concluded that nucleoside metabolism, especially allantoin accumulation, was not only involved in nitrogen recycling but also in the upregulation of ABA biosynthesis in response to severe drought stress.

Among the condition-specific compounds observed in this study, ACC was downregulated at DT4, 6, and 8, but upregulated at DT10 (13-fold change). ACC is the precursor of the phytohormone ethylene, and it also functions as a signal itself, independent from ethylene (de Poel and Van Der Straeten 2014). The accumulation pattern of ACC is largely associated with ABA, which increased by 23.8-fold at DT10 (Table 4.4). Exogenous ABA applications accelerate the ageing processes in rice and maize (Ray *et al.* 1983; He and Jin 1999; Sade *et al.* 2018). In particular, ABA reduces the chlorophyll content in barley (Yamburenko *et al.* 2013). The rice *NAC2* gene, which is involved in ABA biosynthesis, has been reported to activate chlorophyll degradation genes, thereby accelerating ageing (Shen *et al.* 2017; Mao *et al.* 2017). ACC upregulation at DT10 indicates an increase in ethylene signalling, which is correlated with accelerated ageing in response to severe drought-stress conditions. Thus, ABA may have stimulated senescence in wheat by cooperating with ethylene signalling in response to the severe drought stress. Interestingly, Asn, which accumulates in ageing leaves (Eason *et al.* 2000; Herrera-Rodríguez *et al.* 2006), also accumulated under severe drought conditions (DT8 and 10), suggesting drought-induced senescence. In a recent study, metabolites belonging to the aspartate pathway (including Asn, Ser, and Met) were reported as biomarkers for yield gap-based drought tolerance, accurately predicting more than 94% of drought tolerance in wheat (Yadav *et al.* 2019). However, in this study, only methionine (among the aspartate pathway metabolites) made a large contribution to the drought response (Fig. 4.3A) and may be effective as a biomarker. The discrepancies among the results may be caused by differences in experimental conditions.

Aromatic amino acids (Phe, Trp, and Tyr) are synthesized through the shikimate pathway and are precursors to a wide range of secondary metabolites, such as terpenoids, auxins, glycosides, and lignin intermediates (Vogt 2010). In free form, aromatic amino acids are targets of oxidation and have protective functions against ROS (Dubouzet *et al.* 2007). In this study, aromatic amino acids significantly accumulated under drought-stress conditions, starting from DT4 (Fig. 4.7 and Table 4.4). This early accumulation may have contributed to the ROS scavenging capacity of the plant

to prevent oxidative stress during the early stages of drought. Consequently, there was no significant ROS accumulation during the early drought stages. Significant ROS accumulations occur only when the plant scavenging capacity is overwhelmed by stress (Sharma *et al.* 2012). Therefore, aromatic amino acids may have played a protective role against early drought-induced oxidative stress. Similarly, serotonin, a Trp-derived metabolite, significantly accumulated only at DT10 and may be involved in severe drought responses. In a recent report, serotonin was identified as a stress defense molecule that delays senescence in rice (Kang *et al.* 2019). Hence, Trp metabolism was activated only at DT10 in response to drought-induced senescence and may be involved in anti-senescence activities. Interestingly, shikimic and ferulic acids decreased under drought-stress conditions (Fig. 4.7 and 4.8). Shikimic acid is the precursor of aromatic amino acids in the shikimate pathway, while ferulic acid is formed downstream of the shikimate pathway, starting with Phe and Tyr. The decrease in shikimic acid (upstream) and ferulic acid (downstream) suggest that the shikimate pathway was not responsible for the aromatic amino acid accumulations. We, therefore, conclude that the aromatic amino acid accumulations may have resulted from protein degradation under drought-stress conditions. These findings corroborate a recent report in which amino acid accumulations resulted from protein degradation in drought-stressed Arabidopsis (Huang and Jander 2017).

In summary, these findings indicate that the physiological phase-shift point of wheat under progressive drought stress is near DT6 (SWP = about -400kPa). In addition, metabolites were identified that play significant roles and are potential biomarkers for drought-stress responses. The condition-related specificities of these metabolites suggest a disruption in their respective pathways or relevant protein degradation induced by specific drought levels. However, these findings require validation, which can be achieved using a variety of genetic resources including drought-tolerant and drought-sensitive wheat lines (Huang *et al.* 2012; Krasileva *et al.* 2017), to establish the applicability of these biomarkers in diverse genotypes. Interestingly, a highly diverse population, known as multiple synthetic derivative lines, has been developed by making wild

introgressions using N61 as a background genotype (Gorafi *et al.* 2018). With the soon-to-be-released complete genomic sequence of N61 (10+ genome project, www.10wheatgenomes.com), the future of wheat breeding using the multiple synthetic derivative lines seems promising, and this study will serve as a reference guide. Thus, this study has extended the knowledge of metabolic and physiological dynamics in wheat in response to progressive drought stress. In the future, high-throughput analyses and validations of these findings will allow them to serve as effective tools in drought-tolerance breeding.

Table 4.1 Reaction monitoring conditions for detected metabolites.

Label	Compound name	Short name	Formula	Mw.	Solvent	Polarity	Precursor ion	Fragmentor 1	Fragmentor 2	Fragmentor 3	Product ion 1 (CE)	Product ion 2 (CE)	Product ion 3 (CE)	Retention Time
M1	Tartaric acid		C4H6O6	150.09	50% MeOH	Negative	149	100	100	100	72.8(20)	43.0(20)	87.1(20)	2.95
M2	Glyceric acid		C3H6O4	106.03	50% MeOH	Negative	107	90			75.1(9)			3.03
M3	Shikimic acid		C7H10O5	174.05	50% MeOH	Negative	172.9	100	100	120	136.8(15)	110.9(15)	93.1(15)	3.68
M4	Malic acid		C4H6O5	134.02	50% MeOH	Negative	133	90	90		115.0(9)	71.1(13)		3.74
M5	Pyruvic acid		C3H4O3	88.06	50% MeOH	Negative	87	100			43.2(5)			3.88
M6	Ascorbic acid	Vitamin C	C6H8O6	176.03	water	Negative	175	100	100		115(9)	87.1(21)		3.91
M7	2-oxoglutaric acid	α-Ketogrutaric acid	C5H6O5	146.11	50% MeOH	Negative	145	50			101.1(5)			4.16
M8	Lactic acid		C3H6O3	90.03	50% MeOH	Negative	89	30			43.2(9)			4.27
M9	Malonic acid		C3H4O4	104.01	50% MeOH	Negative	103	50	50		59.2(5)	41.2(33)		4.72
M10	Citric acid		C6H8O7	192.03	50% MeOH	Negative	191	90	90		111.0(9)	112.3(21)		5.08
M11	Isocitric acid		C6H8O7	192.03	50% MeOH	Negative	191	90	90		111.0(9)	112.3(21)		5.08
M12	Succinic acid		C4H6O4	118.03	0.1% Formic acid	Negative	117	60			73.1(9)			6.53
M13	DIBOA-Glc		C14H17NO9	343.288	50% MeOH	Negative	342.1	210	210	210	133.9(13)	180(5)	162(5)	12.37
M14	DIMBOA-Glc		C15H19NO10	373.314	50% MeOH	Negative	372.1	210	210	210	149(29)	164(9)	209.9(5)	12.6
M15	Vanillic acid		C8H8O4	168.04	50% MeOH	Negative	167	100			152.1(13)	89.9(21)		13.36
M16	DIBOA		C8H7NO4	181.145	MeOH	Negative	180	50	50	50	134(5)	108(9)	73.1(13)	13.32
M17	Gibberellin 3	GA3	C19H22O6	346.14	50% MeOH	Negative	345.1	150	150	150	143.1(33)	221.1(25)	239.1(13)	13.73
M18	Jasmonic acid	JA	C12H18O3	210.13	DMSO	Negative	209.12	130	130		59.1(9)	41.2(55)		19
M19	Sinapic acid		C11H12O5	224.07	0.1% Formic acid	Negative	223.1	110	110	110	208(9)	121(29)	164.1(13)	14.73
M20	4-hydroxybenzoic aldehyde		C7H6O2	122.04	50% MeOH	Negative	121	120			92.2(25)			14.6
M21	Ferulic acid		C10H10O4	194.06	50% MeOH	Negative	193.1	100			134.1(17)			14.9
M22	Vanillin		C8H8O3	152.05	50% MeOH	Negative	151	90			136(13)			15.12
M23	Abscisic acid	ABA	C15H20O4	264.32	50% MeOH	Negative	263.1	130	130	130	153.1(5)	219.1(9)	203.8(21)	17.32
M24	Salicylic acid (o-hydroxybenzoic acid)	SA	C7H6O3	138.12	50% MeOH	Negative	137	100	100	100	93.1(35)	65.2(35)	39.2(35)	18.83
M25	Taurine		C2H7NO3S	125.01	0.1% Formic acid	Positive	126	90	90	90	44.2(21)	86(5)	41.1(25)	2.605
M26	Cystine		C6H12N2O4S2	240.29	0.1% Formic acid	Positive	241	90	90	90	74.1(29)	119.9(17)	151.9(9)	2.773
M27	Asparagine	Asn	C4H8N2O3	132.12	0.1% Formic acid	Positive	133.1	80	80	80	87.1(5)	74.1(13)	28.3(29)	2.845
M28	Serine	Ser	C3H7NO3	105.09	0.1% Formic acid	Positive	106.1	70	70	70	42.2(25)	60.2(9)	88.1(5)	2.847
M29	Aspartic acid	Asp	C4H7NO4	133.11	0.1% Formic acid	Positive	134	70	70	70	74.1(13)	88.1(5)	43.2(25)	2.871
M30	Allantoin		C4H6N4O3	158.04	0.1% Formic acid	Positive	159	80	80	80	116.1(5)	61.2(5)	44.2(55)	2.961
M31	Glycine	Gly	C2H5NO2	75.07	0.1% Formic acid	Positive	76	20	20		30.3(5)	48.2(5)		2.908
M32	Cysteine	Cys	C3H7NO2S	121.16	0.1% Formic acid	Positive	122	60	60	60	43.2(33)	59.1(25)	76.1(13)	3.122
M33	Threonine	Thr	C4H9NO3	119.12	0.1% Formic acid	Positive	120.1	70	70	70	56.2(17)	74.1(9)	102(5)	3.102
M34	Methionine Sulfoxide		C5H11NO3S	165.05	0.1% Formic acid	Positive	166.1	80	80	80	56.2(25)	74.1(13)	75.1(5)	3.252
M35	Alanine	Ala	C3H7NO2	89.09	0.1% Formic acid	Positive	90.1	40	40	40	29.2(45)	44.2(9)	45.1(41)	3.225
M36	Glutamic acid	Glu	C5H9NO4	147.13	0.1% Formic acid	Positive	148.1	80	80	80	84.1(17)	56.2(33)	130(5)	3.275
M37	Citrulline		C6H13N3O3	175.1	0.1% Formic acid	Positive	176.1	80	80	80	70.2(25)	113.0(13)	159.0(5)	3.381
M38	Betaine		C5H11NO2	117.08	0.1% Formic acid	Positive	118.1	120	120	120	42.2(55)	58.2(33)	59.2(17)	3.505
M39	Ornithine		C5H12N2O2	132.09	0.1% Formic acid	Positive	133.1	80	80	80	43.2(37)	70.2(17)	116.0(5)	3.565
M40	Proline	Pro	C5H9NO2	115.13	0.1% Formic acid	Positive	116.1	90	90	90	28.3(41)	43.2(37)	70.2(17)	3.829
M41	Glutamine	Gln	C5H10N2O3	146.14	0.1% Formic acid	Positive	147.1	70	70	70	56.2(33)	84.2(17)	130(5)	3.021
M42	Lysine	Lys	C6H14N2O2	146.19	0.1% Formic acid	Positive	147.1	80	80	80	56.2(33)	84.2(17)	130(5)	3.808
M43	Histidine	His	C6H9N3O2	155.15	0.1% Formic acid	Positive	156.1	100	100	100	83.1(29)	93.1(25)	110(13)	3.924
M44	beta-Alanine		C3H7NO2	89.05	0.1% Formic acid	Positive	90.1	50	50	50	30.3(9)	45.2(45)	72.2(5)	4.014
M45	Argininosuccinic acid		C10H18N4O6	290.12	0.1% Formic acid	Positive	291.1	120	120	120	43.2(55)	70.2(37)	116(17)	4.382
M46	Arginine	Arg	C6H14N4O2	174.2	0.1% Formic acid	Positive	175.1	100	100	100	60.2(13)	70.2(25)	116(13)	4.455

Table 4.1 continued

Label	Compound name	Short name	Formula	Mw.	Solvent	Polarity	Precursor ion	Fragmentor 1	Fragmentor 2	Fragmentor 3	Product ion 1 (CE)	Product ion 2 (CE)	Product ion 3 (CE)	Retention Time
M47	Gamma-aminobutyric acid	GABA	C4H9NO2	103.12	0.1% Formic acid	Positive	104.1	70	70	70	43.2(17)	45.2(25)	87.1(9)	5.069
M48	Putrescine		C4H12N2	88.1	0.1% Formic acid	Positive	89.1	70	70		30.3(21)	72.2(5)		5.484
M49	Cholin		C5H14NO	104.11	0.1% Formic acid	Positive	105.1	110	110	110	61.2(17)	45.2(21)	46.2(25)	6.097
M50	Valine	Val	C5H11NO2	117.15	0.1% Formic acid	Positive	118.1	70	70	70	42.2(49)	55.2(21)	72.2(9)	6.553
M51	Methionine	Met	C5H11NO2S	149.21	0.1% Formic acid	Positive	150.1	80	80	80	56.2(17)	104(9)	133(5)	7.225
M52	Tyrosine	Tyr	C9H11NO3	181.19	0.1% Formic acid	Positive	182.1	80	80	80	91.1(33)	136(9)	165(5)	7.976
M53	Isoleucine	Ile	C6H13NO2	131.17	0.1% Formic acid	Positive	132.1	80	80	80	30.3(21)	44.2(25)	86.2(9)	8.715
M54	Leucine	Leu	C6H13NO2	131.17	0.1% Formic acid	Positive	132.1	70	70	70	30.3(17)	43.2(25)	86.2(5)	9.082
M55	Phenylalanine	Phe	C9H11NO2	165.19	0.1% Formic acid	Positive	166.1	80	80	80	77.1(45)	103(29)	120(9)	9.767
M56	Tryptophan	Trp	C11H12N2O2	204.23	0.1% Formic acid	Positive	205.1	90	90	90	118(29)	146(13)	188(5)	12.583
M57	Uracil		C4H4N2O2	112.03	50% MeOH	Positive	113.04	90	90	90	96(17)	401.(41)	70.1(17)	4.84
M58	Cytosine		C4H5N3O	111.04	50% MeOH	Positive	112.05	130	130	130	95.1(21)	40.2(45)	52.2(37)	4.81
M59	Pyro-glutamic acid		C5H7NO3	129.04	50% MeOH	Positive	130.05	90	90	90	84.1(13)	41.2(25)	56.2(29)	5.79
M60	Nicotinic acid		C6H5NO2	123.03	50% MeOH	Positive	124	130	130	130	80.1(21)	78.1(25)	53.2(33)	6
M61	Inosine		C10H12N4O5	268.08	50% MeOH	Positive	269.09	90	90	90	137(5)	110(45)	119(53)	7.07
M62	Deoxyinosine		C10H12N4O4	252.09	50% MeOH	Positive	253.1	50	50	50	137(5)	110(45)	119(41)	7.08
M63	Xanthine		C5H4N4O2	152.03	50% MeOH	Positive	153.04	90	90	90	110(17)	136(13)	55.2(37)	7.08
M64	Hypoxanthine		C5H4N4O	136.04	50% MeOH	Positive	137.05	130	130	130	110(21)	119(21)	55.2(37)	7.08
M65	Thymine		C5H6N2O2	126.04	50% MeOH	Positive	127.05	90	90		110(17)	54.2(25)		7.1 or 7.3
M66	Xanthosine		C10H12N4O6	284.08	50% MeOH	Positive	285.09	90	90	90	153(5)	136(37)	43.2(55)	7.1
M67	Guanosine		C10H13N5O5	283.09	50% MeOH	Positive	284.1	90	90	90	152(9)	135(41)	110(49)	7.08
M68	Nicotinamide adenine dinucleotide	NAD	C21H27N7O14P2	663.11	50% MeOH	Positive	664.1	170	170	170	136(53)	428(25)	524(17)	7.08
M69	Deoxyguanosine		C10H13N5O4	267.1	50% MeOH	Positive	268.11	90	90	90	152(5)	135(41)	110(41)	7.21
M70	Thymidine		C10H14N2O5	242.09	50% MeOH	Positive	243.1	50	50	50	127(9)	117(5)	109.9(37)	7.3
M71	Guanine		C5H5N5O	151.05	50% MeOH	Positive	152.06	130	130	130	135(21)	110(21)	43.2(33)	7.11
M72	Uridine		C9H12N2O6	244.07	50% MeOH	Positive	245.08	50	50	50	113(5)	96(41)	70.1(37)	7.07 or 7.27
M73	Cytidine		C9H13N3O5	243.09	50% MeOH	Positive	244.1	90	90	90	112(9)	95.1(49)	42.2(55)	7.27
M74	Adenosine		C10H13N5O4	267.1	50% MeOH	Positive	268.11	90	90	90	136(13)	119(55)	94.1(53)	7.73
M75	Deoxyuridine		C9H12N2O5	228.07	50% MeOH	Positive	229.08	50	50		112.9(15)	116.9(5)		7.07
M76	Deoxycytidine		C9H13N3O4	227.09	50% MeOH	Positive	228.1	50	50	50	112(5)	95.1(45)	42.2(55)	7.71
M77	Deoxyadenosine		C10H13N5O3	251.1	50% MeOH	Positive	252.11	90	90	90	136(9)	119(49)	43.2(37)	8.04
M78	Syringic acid		C9H10O5	198.05	50% MeOH	Positive	199.1	100	100	100	140(13)	125(33)	77.1(29)	9.22
M79	6-(γ,γ-dimethylallylamino) purine	IP	C10H13N5	203.12	100% MeOH	Positive	204.13	90	90	90	136(13)	41.2(41)	119(37)	12.58
M80	Indole-3-acetic acid	IAA	C10H9NO2	175.06	50% MeOH	Positive	176.07	90	90	90	130(13)	77.1(53)	103(37)	12.71
M81	Coumarin		C9H6O2	146.04	50% MeOH	Positive	147	130	130	130	91.1(25)	103.1(17)	39.2(53)	14.22
M82	Indole-3-butyric acid	IBA	C12H13NO2	203.09	50% MeOH	Positive	204.1	90	90	90	186(9)	130(25)	117(33)	15.23
M83	Adenine		C5H5N5	145.01	0.1N HCl	Positive	146.02	50	50		64.2(1)	104.9(1)		16.2
M84	Methyl-Jasmonate	MeJA	C13H20O3	224.14	50% MeOH	Positive	225.1	100	100	100	151(9)	133(13)	41.2(53)	16.3
M85	Hydroxy-L-proline		C5H9NO3	131.13	50% MeOH	Positive	132.1	90	90	90	41.2(33)	68.2(21)	86.2(13)	2.935
M86	1-Aminocyclopropanecarboxylic acid	ACC	C4H7NO2	101.05	water	Positive	102.1	50	50	50	56.2(9)	28.3(25)	61.2(5)	3.58
M87	Trigonelline		C7H7NO2	137.05	water	Positive	138.1	130	130	130	92.1(21)	94.1(21)	39.2(55)	4.3
M88	Spermidine		C7H19N3	145.16	water	Positive	146.2	90	90	90	72.2(13)	112.1(13)	30.3(37)	4.97
M89	5-Aminolevulinic acid		C5H9NO3	131.06	50% MeOH	Positive	132.1	80	80		55.1(21)	114.0(5)		5.517
M90	Cadaverine (1,5-Diaminopropane)		C5H14N2	102.12	50% MeOH	Positive	103.13	90	90	90	86.2(9)	41.2(25)	30.3(21)	6.93
M91	DIMBOA		C9H9NO5	211.05	50% MeOH	Positive	212.1	90	90	90	194(5)	166(5)	110(21)	10.05
M92	Tyramine		C8H11NO	137.08	water	Positive	138.1	50	50	50	121.1(9)	77.2(33)	51.2(53)	12.45
M93	Serotonin		C10H12N2O	176.09	50% MeOH	Positive	177.1	50	50	50	160.1(9)	115.1(33)	117.1(29)	14.25
M94	Tryptamine		C10H12N2	160.1	50% MeOH	Positive	161.11	50	50	50	144.1(5)	115.1(41)	117.1(25)	15.89

Table 4.2 Primer sets.

Gene name	Sequence
TaLEA_fw	GACAACACCATCACCACCAAGGACA
TaLEA_rv	TAATACAGAACCGGACACGAGGAGT
TaPP2C6_fw	ACGAGTGCCTGATCCTAGCCAG
TaPP2C6_rv	GGAGATGTTGTCCGAGCTGTTCTT
Taactin_fw	CCTCTCTGCGCCAATCGT
Taactin_rv	TCAGCCGAGCGGGAAATTGT
TaP5CS1-fw	TGGCCTTGTGAAAAGCAAAGA
TaP5CS1-rv	GCCTGTTACTGCCTCTTGGA
TaBCAT2-fw	GCCAGGTACGGAGAACAACA
TaBCAT2-rv	ATCCTTCCCACACAGCATCC

Table 4.3 Comparison of canopy temperature depression (CTD) and soil water potential (SWP).

Treatment days	SWP in WW (kPa)	CTD in WW (°C)	SWP in DT (kPa)	CTD in DT (°C)
0	−15.8	5.48	−17.0	5.38
2	−14.5	5.33	−45.1	3.77
4	−15.5	5.32	−185.0	2.99
6	−16.4	4.22	−385.1	2.48
8	−15.8	4.22	−517.7	0.25
10	−14.8	3.34	−554.7	-0.62

A strong positive correlation ($r^2 = 0.95$, $P < 0.05$) exists between CTD and SWP under drought-stress conditions. DT, drought-treatment; WW, well-watered control. CTD data represent means of three pots. SWP data represent means of four pots.

Table 4.4 Fold change (FC) of 53 significantly changed metabolites ($P < 0.05$, fold change >2).

Compound	DT2 FC	DT4 FC	DT6 FC	DT8 FC	DT10 FC
Hypoxanthine	ns	1.6351	2.6078	ns	ns
1-Aminocyclopropanecarboxylic acid (ACC)	ns	0.0833	0.1448	0.3861	13.2468
DIBOA-Glc	ns	ns	ns	6.1673	2.9572
Abscisic acid (ABA)	ns	ns	9.6320	ns	23.8238
Allantoin	ns	ns	ns	ns	119.5903
Arginine	ns	4.0602	ns	47.3579	14.8753
Argininosuccinic acid	ns	0.3458	ns	3.7386	9.9639
Asparagine	ns	ns	ns	16.5315	9.6051
b-Alanine	ns	ns	3.3970	14.8017	13.4725
Betaine	ns	0.6710	ns	ns	3.1168
Cadaverine	ns	ns	ns	4.1588	3.6471
Cystine	ns	ns	ns	ns	8.4083
Cytidine	ns	ns	ns	1.5405	2.8363
Deoxyadenosine	ns	ns	ns	3.6007	5.3102
Deoxycytidine	ns	ns	2.2076	3.1525	5.8807
Deoxyguanosine	ns	ns	2.0607	3.4213	4.4570
Deoxyinosine	ns	ns	ns	ns	0.3835
Deoxyuridine	ns	ns	ns	ns	6.3283
Ferulic acid	ns	ns	ns	ns	0.1360
Gamma-aminobutyric acid	ns	1.8276	ns	3.3775	6.9021
Glutamine	ns	5.8753	ns	24.4363	2.3231
Glyceric acid	ns	ns	ns	0.4517	0.6107
Glycine	ns	ns	2.5845	ns	ns
Histidine	ns	4.2293	6.8094	20.8998	4.9152
Indole acetic acid (IAA)	ns	ns	ns	ns	4.6393
Isoleucine	ns	5.2530	8.3584	25.4311	10.5347
Lactic acid	ns	ns	2.3128	ns	ns
Leucine	ns	5.0045	ns	25.0677	10.0035
Hydroxyproline	ns	ns	7.1435	8.3941	9.3807
Lysine	ns	5.8174	ns	16.4277	1.9646
Malic acid	ns	ns	ns	2.6991	2.3705
Malonic acid	ns	ns	ns	ns	4.5491
Methionine	ns	ns	7.2636	23.4312	6.7936
Methionine sulfoxide	ns	ns	ns	28.6361	ns
Ornithine	ns	ns	3.1170	ns	ns
Phenylalanine	ns	2.6715	ns	20.7436	12.1451
Proline	ns	ns	38.9031	109.6950	40.0525
Putrescine	ns	ns	ns	ns	2.0430
Pyro-gultamic acid	ns	ns	2.3954	4.1829	ns
Salisylic acid (SA)	ns	ns	67.0121	7.6769	5.7292
Serotonin	ns	ns	ns	ns	8.0528
Shikimic acid	ns	ns	0.1215	ns	ns
Succunic acid	ns	ns	0.3759	ns	ns
Taurine	ns	0.6058	3.4755	ns	ns
Threonine	ns	ns	2.3989	4.0643	3.0211
Thymidine	ns	ns	ns	ns	3.5722
Tryptamine	ns	ns	ns	ns	12.7032
Tryptophan	ns	3.8212	10.7873	58.6675	32.2124
Tyramine	ns	ns	ns	2.2495	1.7061
Tyrosine	ns	1.8942	ns	9.1628	2.8985
Uracil	ns	ns	ns	3.5963	ns
Uridine	ns	ns	ns	ns	2.7004
Valine	ns	3.1748	4.6581	12.4014	8.1055

Table 4.5 Metabolites specifically upregulated under severe drought conditions on days 8 and 10 (DT8 and DT10, respectively).

Metabolites	Label	Condition	Fold change	*P*-value
Uracil	M57	DT8	3.5	0.0189
Tyramine	M92	DT8	2.2	0.0020
Met-Sul	M34	DT8	28.6	0.0049
DIBOA-Glc	M13	DT8, DT10	6.1, 2.9	0.0013, 0.0004
Asn	M27	DT8, DT10	16.5, 9.6	0.0389, 0.0115
Cadaverine	M90	DT8, DT10	4.1, 3.5	0.0023, 0.0070
GABA	M47	DT8, DT10	3.3, 6.9	0.0001, 0.0000
Malic acid	M4	DT8, DT10	2.6, 2.3	0.0009, 0.0003
Deoxyadenosine	M77	DT8, DT10	3.6, 5.3	0.0034, 0.0003
Arg-Suc	M45	DT8, DT10	3.7, 9.9	0.0062, 0.0036
Tyr	M52	DT8, DT10	9.1, 2.8	0.0010, 0.0136
Malonic acid	M9	DT10	4.5	0.0316
Putrescine	M48	DT10	2	0.0134
Thymidine	M70	DT10	3.5	0.0017
Uridine	M72	DT10	2.7	0.0061
Cys-Cys	M26	DT10	8.4	0.0001
Deoxyuridine	M75	DT10	6.3	0.0007
Betaine	M38	DT10	3.1	0.0292
Serotonin	M93	DT10	8	0.0000
Cytidine	M73	DT10	2.8	0.0007
ACC	M86	DT10	13.2	0.0062
Tryptamine	M94	DT10	12.7	0.0071
IAA	M80	DT10	4.6	0.0041
Allantoin	M30	DT10	119.5	0.0096

DIBOA: 2,4-dihydroxy-1,4-benzoxazin-3-one; GABA: gamma-aminobutyric acid; ACC: 1-aminocyclopropane-1-carboxylic acid; IAA: indole-3-acetic acid

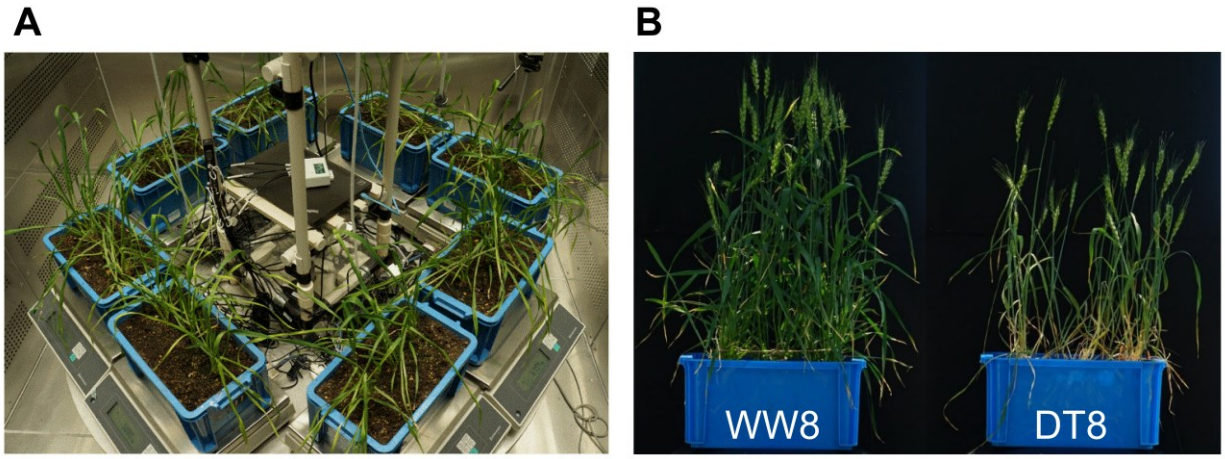

Figure 4.1 Setup of experiment. (A) Plants at nursery stage (B) Plants under control conditions day 8 (WW8, left) and under drought day 8 (DT8, right). Pots containing three plants each were placed on a turntable in a growth chamber. Soil moisture condition was monitored with soil moisture sensors.

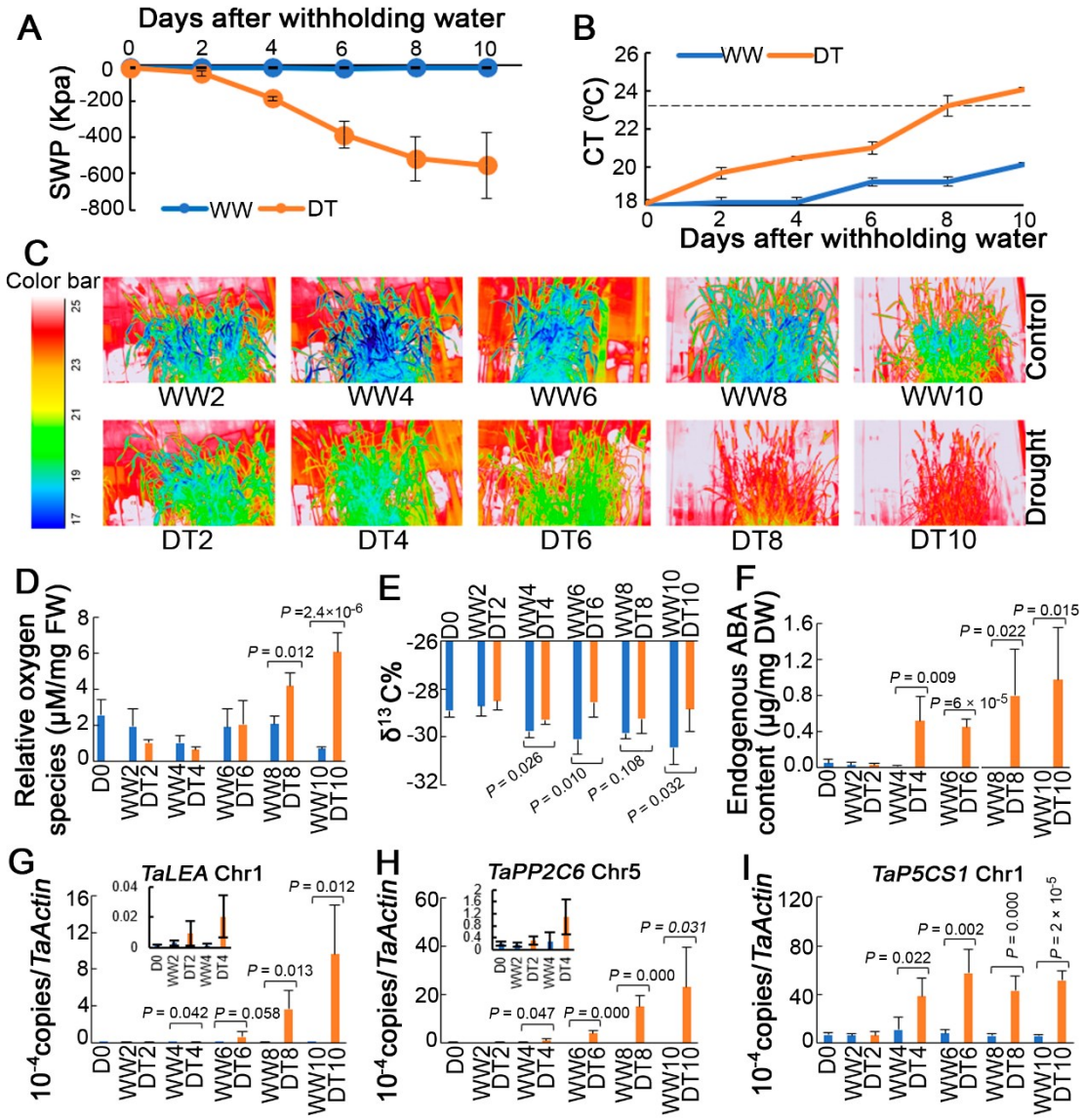

Figure 4.2 Physiological changes in wheat Norin 61 under progressive drought stress. (A) Decreasing soil water potential (SWP) under 10 days of progressive drought stress. Data represent mean ± standard deviation (SD) of four replicates. (B) Canopy temperature (CT) of plants under drought (DT) and well-watered (WW) conditions. Data represent mean ± SD of three biological replicates (one replicate consisted of three plants per pot) with 20 data points from each pot. Dashed line represents ambient temperature. (C) Thermal images of plants under different time points of DT and WW conditions. (D) Increase in reactive oxygen species in flag leaves of plants under DT in comparison with WW using spectrophotometry at 480 nm (excitation)/530 nm (detection). (E) Increase in carbon isotope composition ($\delta^{13}C$) in flag leaves of plants under DT compared with WW. (F) Increase in abscisic acid (ABA) concentration in flag leaves of plants under DT and WW conditions. Endogenous ABA contents were measured using LC-MS and calculated with ABA standard mixtures of different concentrations (0, 0.4, 2 and 10 ppm). (G–I) Relative expression of ABA-responsive genes in response to drought stress. Data represent mean ± SD of four biological replicates. Numbers represent days after withholding water. Inset bar graphs indicate each figure magnified for early treatment regions.

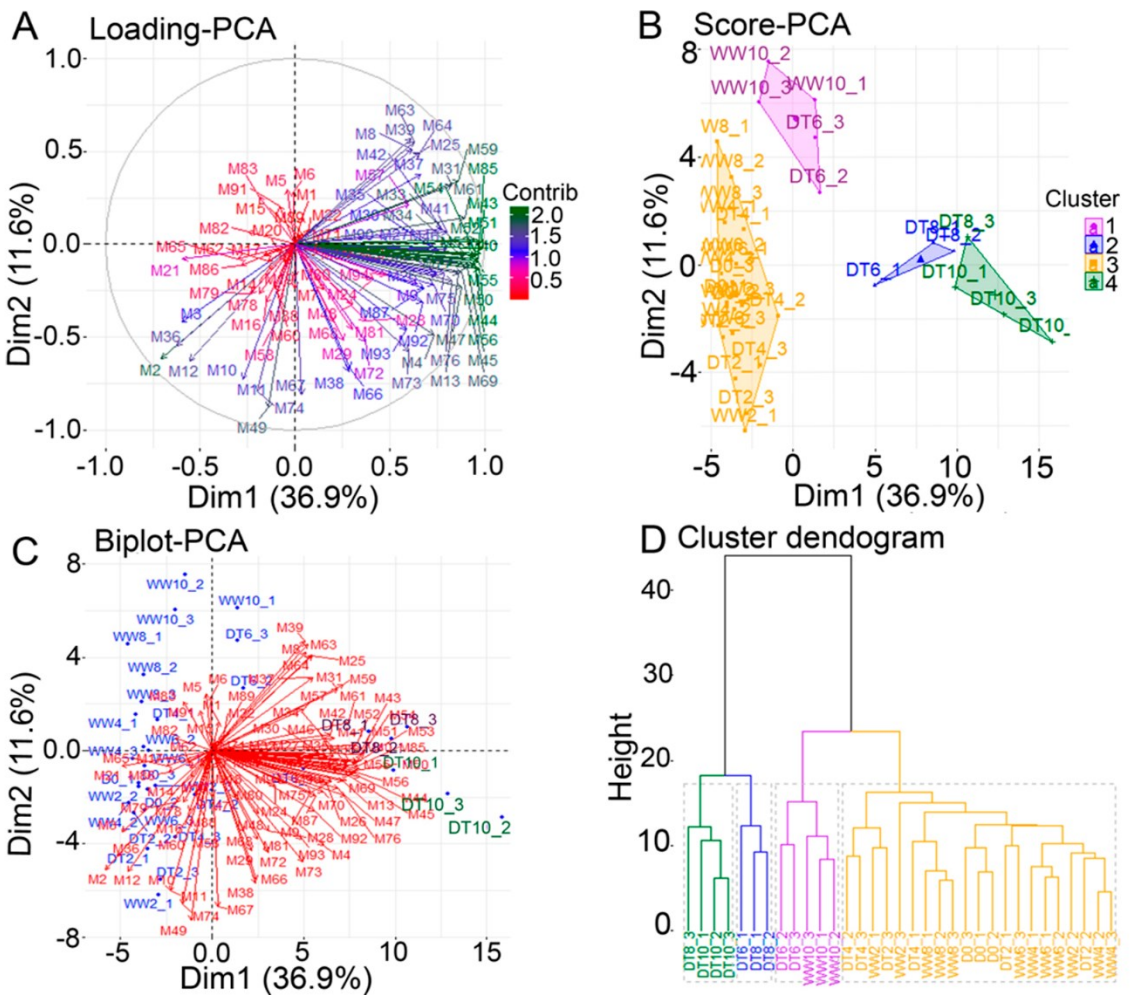

Figure 4.3 Principal component analysis (PCA) and dendrogram clustering of the interrelated effects of progressive drought (DT) stress and well-watered (WW) conditions on the metabolic profile of wheat Norin 61. (A) PCA loading plot of the metabolite (M) variables identified in wheat Norin 61 under different time points of drought (DT2, 4, 6, 8 and 10) and well-watered (WW2, 4, 6, 8 and 10) conditions. Metabolites with high contribution to PC1 and PC2 axes are shown in green. (B) PCA score plot of flag leaf samples collected from different DT and WW conditions according to their metabolite profiles. (C) PCA Biplot showing combined metabolite and condition trends (D) K-means cluster dendrogram further confirming the clustering of flag leaf samples based on metabolite profiles. DT10 and DT8 are clearly separated from well-watered samples, indicating severe drought stress. Data represent three biological replicates. Numbers following DT or WW represent days after treatment, while numbers following the underbars represent individual replicate numbers.

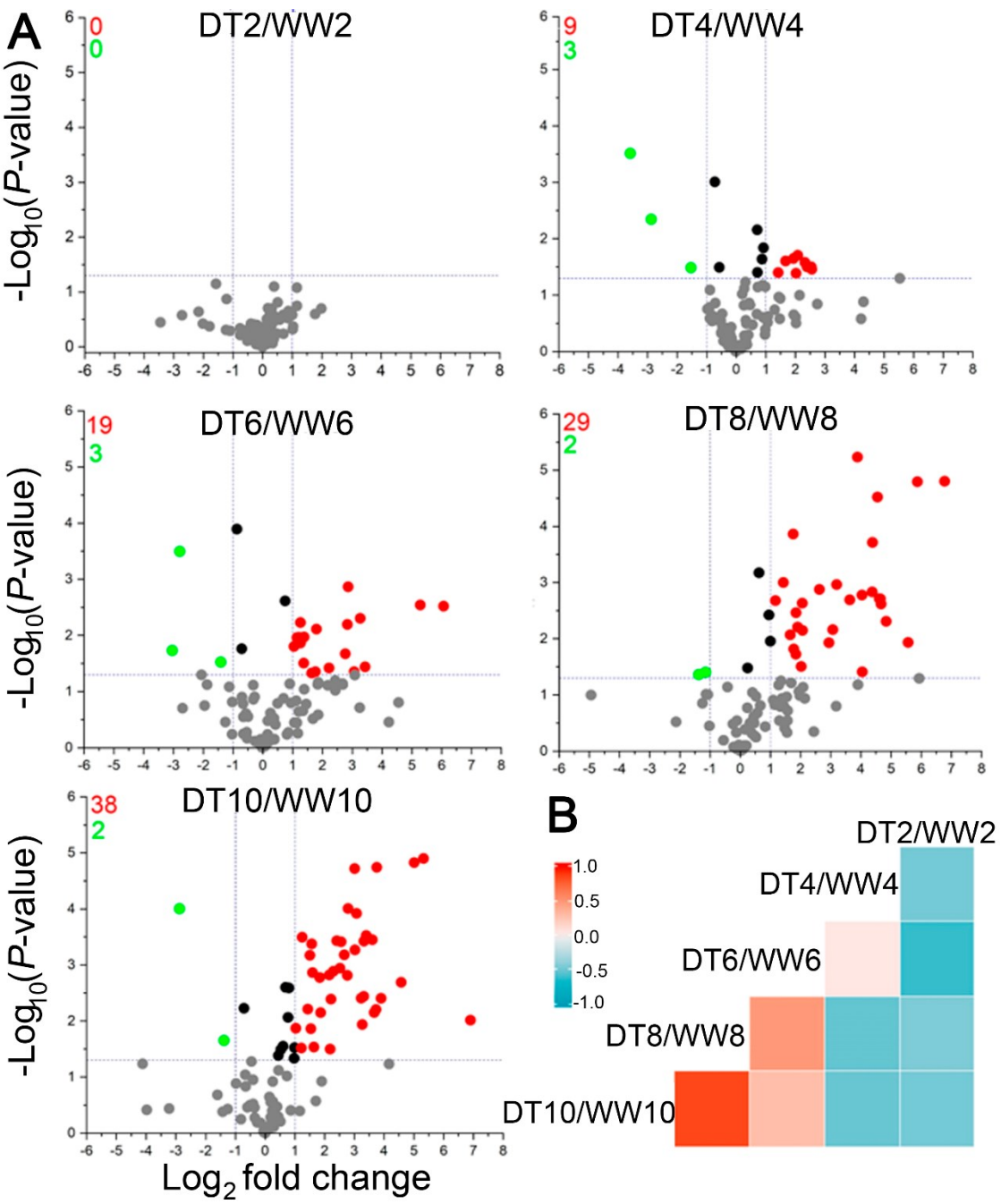

Figure 4.4 Metabolite trends in wheat Norin 61 under different drought levels (DT2, 4, 6, 8, and 10, respectively) relative to well-watered (WW) conditions. (A) Volcano plots of differentially accumulated metabolites. The threshold of significantly ($P < 0.05$) downregulated (green dots, fold change ≤ 0.5) and upregulated metabolites (red dots, fold change ≥ 2.0) are highlighted. (B) Treatment-treatment correlations in Norin 61 in response to DT versus WW at different time points.

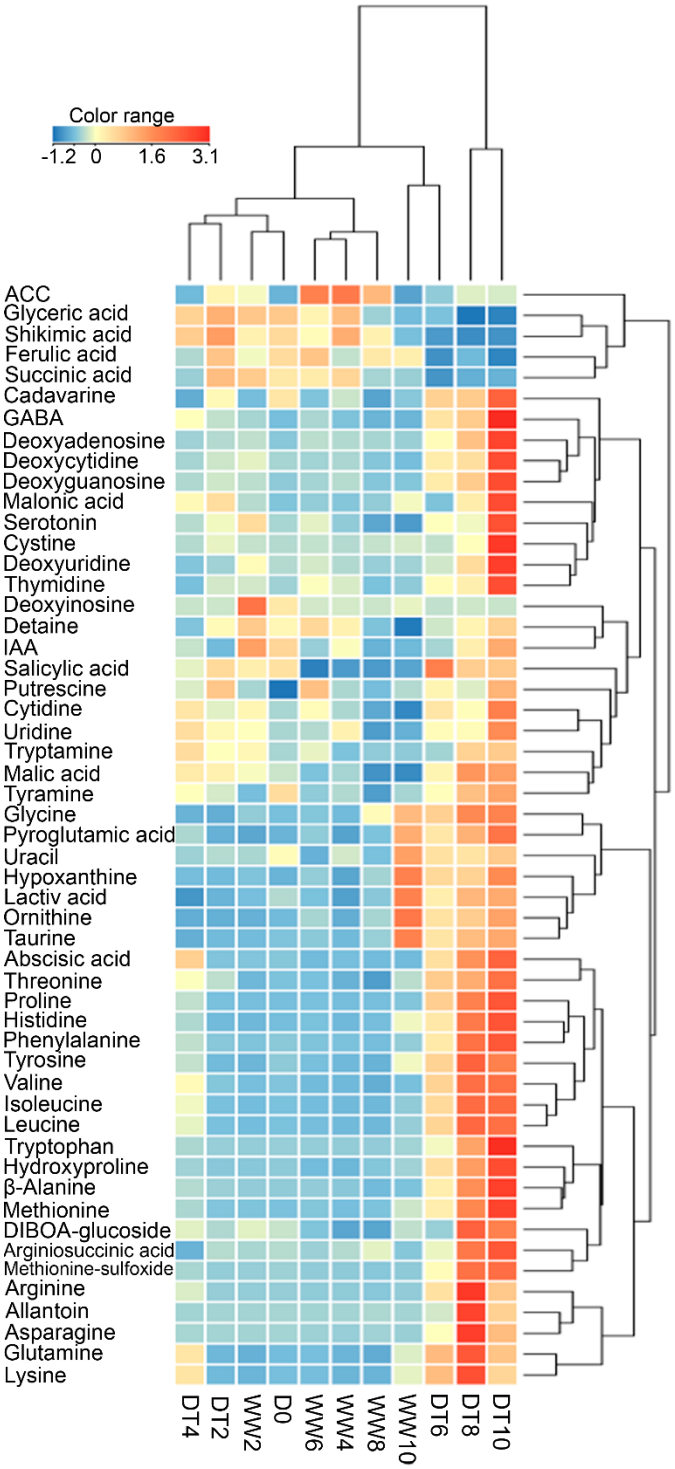

Figure 4.5 Hierarchical clustering of metabolite levels of Norin 61 in response to drought (DT) and well-watered (WW) conditions. The Z-score transformation of the mean values of 53 significantly ($P \leq 0.05$) increased (fold change ≥ 2.0) or decreased (fold change ≤ 0.5) metabolite intensities were used for hierarchical clustering. Data represent three independent biological replicates in each condition. Red fields indicate high accumulation rates, yellow and blue fields indicate low and very low accumulation rates, respectively.

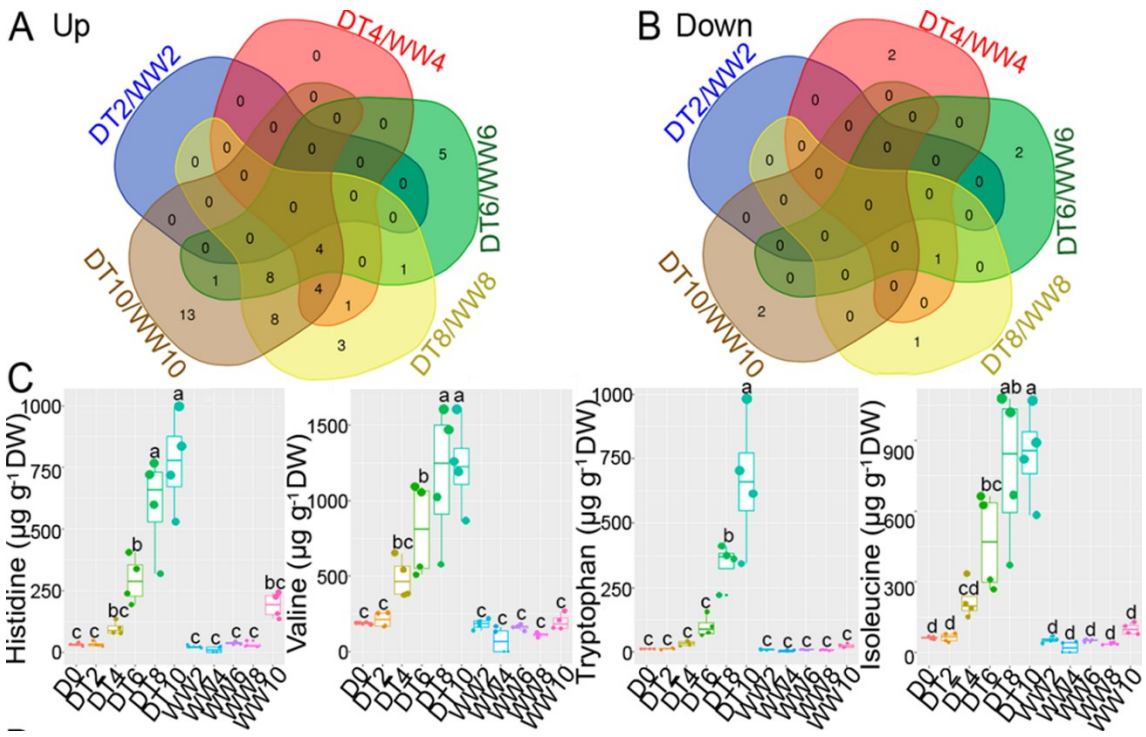

Figure 4.6 Metabolite dynamics in wheat Norin 61 after 2, 4-, 6-, 8-, and 10-days exposure to drought stress (DT2, 4, 6, 8, and 10, respectively) relative to well-watered (WW) conditions. (A-B) Venn diagram of unique and overlapped significantly increased ($P \leq 0.05$, fold change ≥ 2.0) and decreased ($P \leq 0.05$, fold change ≤ 0.5) metabolites in response to drought stress. (C) Box plot analysis of four commonly increased metabolites at DT4, 6, 8, and 10 relative to WW conditions. Different letters indicate significant difference ($P < 0.001$) according to Tukey's honesty significant difference (HSD) test.

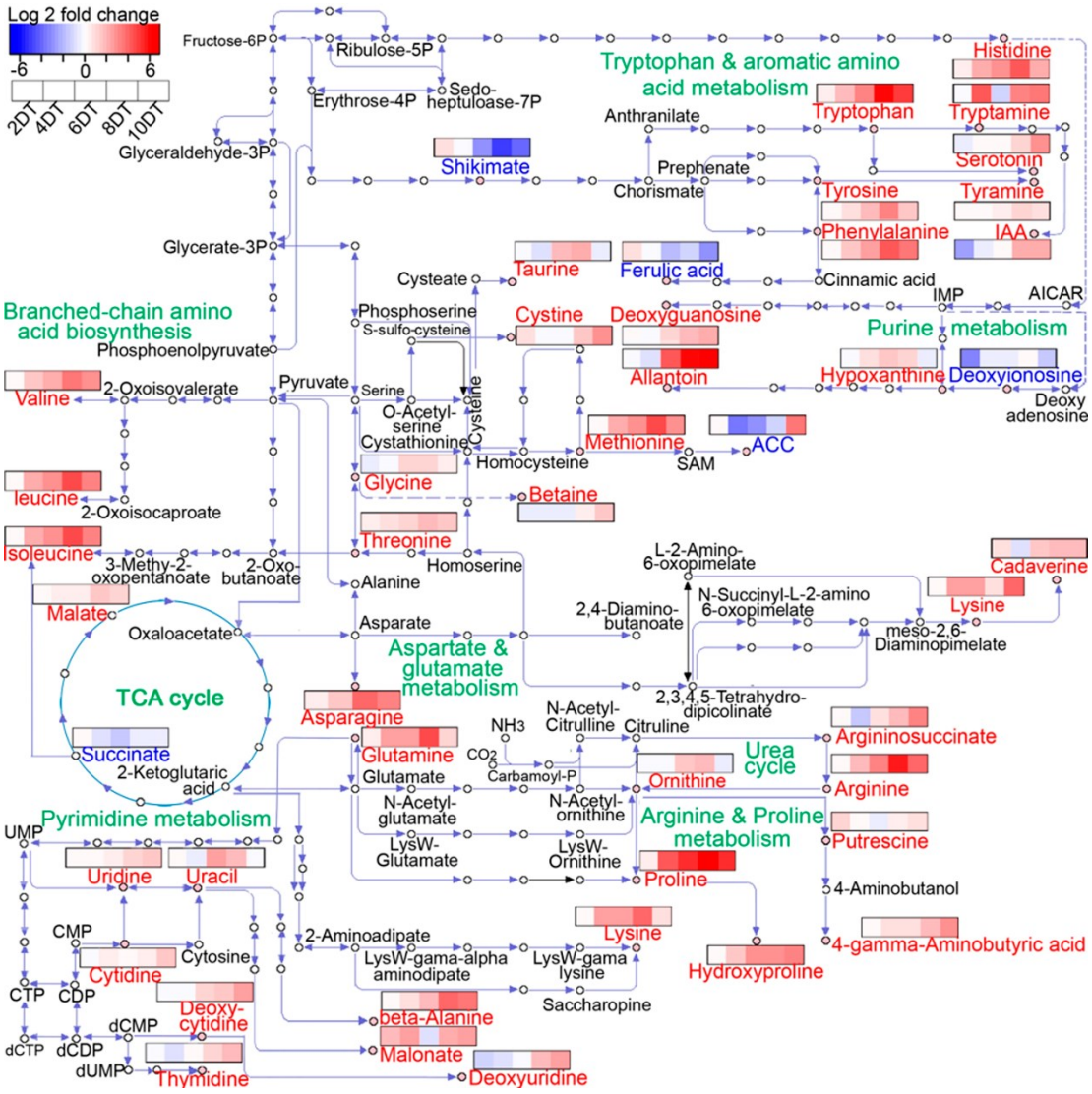

Figure 4.7 Metabolite changes in flag leaves of wheat Norin 61 during 10 days of progressive drought stress (DT2, 4, 6, 8 and 10). The proposed metabolic pathways are based on KEGG database (https://www.genome.jp/kegg/) and the literature. Metabolites with significant ($P \leq 0.05$) increase or decrease (fold change >2.0 or fold change ≤ 0.5, respectively) and are shown in the pathway. Colour bar indicates the $\log_2$ fold change.

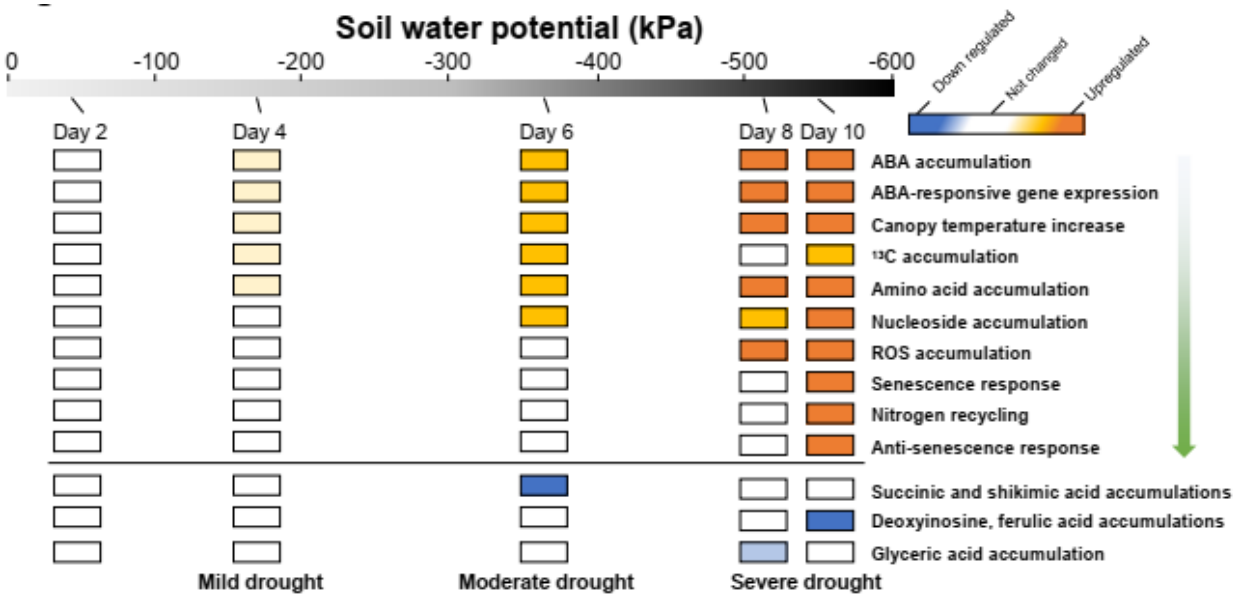

Figure 4.8 A schematic diagram of wheat Norin 61 response to progressive drought stress. Changes in physiological and metabolic traits were evaluated from experimental results. The arrow indicates the observed sequence of drought-responsive changes.

Chapter 5

Aegilops tauschii introgressions improve physio-biochemical traits and metabolite plasticity in bread wheat under drought stress

5.1 Introduction

Persistent drought and reductions in the quantity and quality of water resources are considered major environmental constraints affecting global wheat (*T. aestivum*) production (Pour-Aboughadareh *et al.* 2020). Drought episodes are not limited to dryland regions, but are also increasingly impacting European farmlands due to the current climate change scenario (Templer *et al.* 2017). Therefore, to maintain sustainable wheat productivity under water-deficit conditions, it is imperative to improve wheat drought resilience. Drought resilience or resistance has been categorized into four mechanisms: escape, avoidance, tolerance, and recovery (Luo 2010; Templer *et al.* 2017). Drought escape involves the reprogramming of plant phenology resulting in a short life cycle or increased developmental plasticity (Yue *et al.* 2006). Drought avoidance comprises physiological and morphological responses such as stomatal closure and root elongation that maintain high water status by improving water uptake and/or reducing water loss under dry conditions (Luo 2010). In contrast, drought tolerance refers to the capacity of plants to maintain cellular function under water-deficit conditions by improving osmotic adjustment, antioxidant capacity, and metabolic homeostasis (Templer *et al.* 2017). Finally, drought recovery refers to the plant's capability to resume growth and produce seeds after exposure to severe drought stress (Luo 2010).

Drought avoidance and drought tolerance are the two most important mechanisms for crop improvement (Yue *et al.* 2006). Drought-avoidant and drought-tolerant plants regulate key physiological, biochemical, and metabolic processes that help to avoid, reduce, or repair the damage from drought stress (Guo *et al.* 2018, 2020). These physiological and biochemical processes include regulation of transpiration rate (E) and stomatal conductance (g_{sw}) to improve water use efficiency (WUE), and increases in the activity of antioxidant enzymes such as

superoxide dismutase (SOD) and catalase to maintain reactive oxygen species (ROS) balance (Li *et al.* 2017). The metabolic processes involve accumulation of osmolytes, which enable osmotic adjustment; reprogramming of carbohydrate metabolism and the tricarboxylic acid cycle, which control energy flux; and induction of non-enzymatic antioxidants (polyphenols, Pro, serotonin, betaine, allantoin [All], ascorbic acid, and glutathione), which are involved in ROS homeostasis (Banu *et al.* 2009; Kaur *et al.* 2015; Nourimand and Todd 2016; Guo *et al.* 2020). These processes often affect normal plant functions, especially photosynthesis, as a trade-off for survival, leading to yield losses (Robredo *et al.* 2010). Despite these challenges, drought-resilient wheat genotypes with high yield under drought stress are necessary to meet increasing global wheat demands. Such wheat genotypes are not readily available within the narrow gene pool of elite bread wheat cultivars (Ogbonnaya *et al.* 2013). Wild relatives of wheat such as *Ae. tauschii*, obtained from dryland regions, have been used for broadening the gene pool of elite bread wheat, resulting in improved resilience to various abiotic stresses (Elbashir *et al.* 2017a; Gorafi *et al.* 2018; Kishii 2019). However, the mechanisms of stress resilience and the actual impacts of *Ae. tauschii* introgressions into bread wheat have not been fully understood.

The aim of this study was to evaluate the impact of *Ae. tauschii* introgressions in three wheat MSD lines under prolonged drought stress. The selected MSD lines had previously shown yield stability in various Sudanese fields under heat stress conditions (Elbashir *et al.* 2017a; b) and under post-anthesis drought stress. For comparison, the backcross parent of the MSD lines, the Japanese wheat cultivar (N61), was also investigated.

5.2 Materials and Methods

5.2.1 Plant Materials

Three wheat MSD lines (MNH5, MSD53, and MSD345) and their backcross parent, N61, were used in this study. The MSD lines were developed previously by crossing tetraploid durum wheat (AABB) with D-genome donor *Ae. tauschii* (DD) to produce synthetic hexaploids. Forty-

three synthetic hexaploid lines were crossed and backcrossed with N61 (AABBDD) to produce the MSD population that has been proposed as a platform to harness and utilize the genetic diversity of *Ae. tauschii* for wheat breeding (Tsujimoto *et al.* 2015; Gorafi *et al.* 2018). The pedigrees of the MSD lines and their yield performance under post-anthesis drought stress are shown in Table 5.1. The backcross parent of the MSD lines, N61, has a representative wheat genome adopted in the 10+wheat genome project (www.10wheatgenomes.com).

5.2.2 Experimental Design and Drought Treatment in the Field

The field experiment was designed in alpha lattice with two replications in Wad Medani, Sudan during the 2018/2019 growing season. The greenhouse experiment was also designed in alpha lattice with three replications in the same season. To control insect pests, seeds were treated with the insecticide Gaucho (imidacloprid, 35% WP, Bayer Crop Science, USA) at 1 g kg^{-1} before sowing. Weed control by hand-weeding was done twice. Drought stress was imposed by withholding water supply at 50% anthesis, while the well-watered condition was regularly irrigated until maturity. Grain yield was obtained as average grain weight per genotype.

5.2.3 Seed Sowing and Growth Conditions

Prior to sowing, seeds were kept at 4°C for 5 days to break dormancy, and then transferred to room temperature (22 ± 2°C) for 24 h. Germinated seeds from each genotype were sown in plastic trays (internal diameter = 44.3 × 33 × 16 cm) filled with compost and sand dune regosol (1:1, v: v) collected from Arid Land Research Center, Tottori, Japan. Plants (24 per tray; 6 replicates per genotype) were grown in a completely randomized design with an 8 × 9 cm^2 spacing between plants. All genotypes were grown in a growth chamber (Espec, Japan) at optimum temperature (25 /19°C day/night) and light period (14 /10-h light/dark), with a photosynthetic photon flux density of 950 µmol m^{-2} s^{-1} and controlled relative humidity level (40/50% light/dark). The soil water potential was monitored every 1 h using sensors (Teros21; Decagon Devices, Pullman, WA, USA) and data loggers (Em50; Decagon Devices).

5.2.4 Drought Treatment and Sampling

All seedlings from each genotype were grown for 21 days before imposing drought by withholding water from the drought trays, while the control trays were maintained at 100% field capacity. Samples were collected at the 5th leaf stage (Zadoks stage 15; (Zadoks *et al.* 1974)) when the soil water potential had decreased to −1000 kPa in the drought condition (Fig. 5.1). Whole shoots were harvested, snap-frozen in liquid nitrogen, and stored at −80°C for physiological, biochemical, and metabolome analyses.

5.2.5 Physiological Analysis

5.2.5.1 Determination of Relative Water Content (RWC)

The RWC of leaf samples from each genotype was determined from the middle section of fully expanded leaves collected from control and drought-treated plants. The leaves were cut into 2-cm segments and three segments per leaf were collected. RWC (Barrs and Weatherley 1962) was determined using the following equation: RWC % = [FW-DW]/([TW-DW]) ×100, where FW, TW, and DW are leaf fresh weight, turgid weight, and dry weight, respectively.

5.2.5.2 Measurement of Photosynthetic CO_2 Response

Photosynthetic CO_2 response was measured on fully expanded leaves using a LI-COR 6800 Portable Photosynthesis System (LI-COR Biosciences, Lincoln, NE, USA). A photosynthetic curve was developed using different ambient CO_2 concentrations (C_a): 0, 50, 100, 200, 400, 500, 800, 1000, 1500, and 2000 µmol mol^{-1}. Light intensity, leaf temperature, and relative humidity settings were similar to the growth chamber conditions mentioned above. CO2 assimilation rate (A), intercellular CO_2 concentration (C_i), g_{sw}, and E were obtained directly from the Portable Photosynthesis System, while maximum ribulose 1,5-bisphosphate carboxylase/oxygenase [Rubisco] carboxylation rate [V_{cmax}], photosynthetic electron transport rate [J], triose phosphate utilization rate [TPU], and leaf day respiration [R_d] were calculated using

curve-fitting equations (Sharkey *et al.* 2007; Bellasio *et al.* 2016). The intrinsic water use efficiency (iWUE) was calculated as the ratio of A to g_{sw} at 400 μmol mol^{-1} CO_2 (Bacon 2004).

5.2.6 Biochemical Analysis

5.2.6.1 Determination of Total Phenolic Content (TPC)

TPC was determined by the Folin–Ciocalteu method (Slinkard and Singleton 1977) using gallic acid as the standard. Freeze-dried leaf powder was accurately weighed and placed in 1.5-μL centrifuge tubes. Samples were extracted with 500 μL of 50% methanol for 30 min using a sonicator (AS ONE, Shanghai, China) and centrifuged at 6000 ×g for 6 min at 22 ± 2°C, and the supernatant was collected for further analysis. TPC was measured spectrophotometrically at 765 nm using a microplate reader (SH-9000; Corona Electronic, Ibaraki, Japan), and was expressed as gallic acid equivalents per sample dry weight (μg GAE mg^{-1} DW).

5.2.6.2 Determination of Trolox-Equivalent Antioxidant Capacity (TEAC)

TAC was measured using the DPPH radical assay described in Shimamura *et al.* (2014). Homogenized frozen leaf samples were extracted with 1 mL of 80% ethanol. Next, 25-μL extract aliquots were transferred into 96-well microplates and 80 μL of 0.1 M Tris-HCl buffer (pH 7.4) was added, followed by 100 μL of 0.1 mM freshly prepared DPPH solution. In addition, freshly prepared Trolox solutions (0, 20, 40, 60, and 80 mg L^{-1}) were treated in the same way as the samples. The absorbances of samples and standard were measured at 517 nm using a microplate reader (SH-9000). The percentage inhibition of the DPPH radical was calculated using the following equation: % inhibition = $[(A_{control} - A_{sample})/(A_{control} - A_{blank})] \times 100$, where $A_{control}$ = absorbance of ethanol + Tris-HCl buffer + DPPH solution, A_{sample} = absorbance of sample or standard + Tris-HCl buffer + DPPH solution, and A_{blank} = absorbance of ethanol + Tris-HCl buffer solution. The sample or standard concentration that caused a 50% reduction in the original concentration of the DPPH radical (defined as IC_{50}) was calculated from the percentage inhibition.

Finally, the antioxidant capacity of the samples was calculated as $IC_{50\ Trolox}/IC_{50\ sample}$ and expressed as TEAC.

5.2.6.3 SOD Assay

The SOD activity in the plant extracts was measured using an SOD Assay Kit-WST (lot# LG854; Dojindo, Kumamoto, Japan) following the manufacturer's instructions. The kit uses xanthine/xanthine oxidase to generate superoxide, which reduces WST-1 to a yellow formazan dye. SOD inhibits this reduction by scavenging the superoxide. To generate an SOD inhibition curve, serial dilutions of samples were made in the range of 1/5 to $1/5^5$. Absorbance was measured at 450 nm using a microplate reader (SH-9000), and SOD activity was calculated from the absorbances of blanks and samples.

5.2.7 Metabolite Analysis

5.2.7.1 Analysis of Amino Acids, Organic Acids, and Nucleotides

The metabolite sample preparation and analysis were conducted following the tandem liquid chromatographic–mass spectrometric (LC-MS/MS) method described in Itam *et al.* (2020). Briefly, 4 mg of freeze-dried sample was extracted with 500 µL of 50% methanol and centrifuged at 15,000 ×*g* for 5 minutes at 4°C. Then, 450 µL of the supernatant was mixed with an equal volume of chloroform, vortexed, and centrifuged at 15,000 ×*g* for 5 minutes at 4°C. Next, 400 µL of the supernatant was filtered through a membrane (Amicon Ultra-0.5 mL, 3-kDa cut off; Millipore, Billerica, MA, USA) and centrifuged. The filtrate was dried in a SpeedVac concentrator (Thermo Fisher Scientific, Waltham, MA, USA) at 45°C for 6 h. The dry extract was redissolved in 200 µL of 50% methanol, and an aliquot was diluted in 50% methanol by 10-fold for metabolite quantification. Metabolites were quantified using a triple quadrupole LC-MS/MS system (Agilent 6420; Agilent, Santa Clara, CA, USA), with a Discovery HS-F5 column (2.1 × 250 mm, 5 µm; Sigma-Aldrich, St. Louis, MO, USA). Quantification results were normalized by sample dry weight, and a quality control reference was developed using metabolite authentic standard

mixtures of different concentrations (0, 0.4, 2, and 10 ppm). All the solvents and reagents used were LC-MS grade.

5.2.7.2 Analysis of Glucose and Sucrose

The concentrations of glucose and sucrose were determined using HPLC (Prominence, Shimadzu, Kyoto, Japan) as described in Murata *et al.* (2012). This method is based on the fluorometric detection of reducing sugars using L-arginine as a detection agent (Mikami and Ishida 1983). Briefly, an aliquot of the resuspended dry extract was diluted by 10-fold in ddH_20. The solution was eluted with a gradient of 0.1 and 0.4 M potassium borate buffer (pH 8.0 and pH 9.0, respectively) for 90 min and heated at 150 °C under pressure with 1% L-arginine and 3% borate. Fluorescence was detected using a fluorescence detector (RF-10AXL, Shimadzu) set at 320 nm excitation and 430 nm emission wavelengths.

5.2.8 Statistical Analysis

Microsoft Excel 2019 was used for the ANOVA, Student's *t*-tests, and Z-transformations of metabolic and physiological data. The R program, version 3.5.2 63 (R Core Team 2018), was used for principal components analysis (PCA). The Mass Profiler Professional software (MPP version 2.5; Agilent Technologies) was used for clustering analysis. Genotype-genotype comparisons were conducted according to Tukey Honestly Significant Difference (HSD) test.

5.3 Results

5.3.1 Yield performance of the three MSD lines under post-anthesis drought stress

The average yield stability (drought tolerance efficiency) for all investigated genotypes was 59.75%. The three MSD lines showed higher drought tolerance efficiency than N61 under post-anthesis drought stress (Table 5.1). Under field conditions, MSD53 had high yield under control and drought conditions compared with N61, a local Sudanese cultivar (Imam) and MSD345. However, MSD53 had low drought tolerance efficiency compared with MSD345. Interestingly, N61 which had low yield under control and drought conditions also had low drought

tolerance efficiency compared with the three MSD lines (Table 5.1). Accordingly, these MSD lines were selected as drought-tolerant candidates.

5.3.2 Genotypic Variation in Photosynthetic Parameters and Leaf Relative Water Content of MSD lines and N61 under Drought Stress

To investigate the impact of D-genome introgressions from *Ae. tauschii* on physiological adaptation to drought stress, the photosynthetic changes and leaf RWCs of the three selected MSD lines and N61 were evaluated. Leaf RWC did not show any significant differences between the three MSD lines and N61 in response to drought stress, and the mean RWC of all investigated genotypes decreased by ~60% relative to the control conditions (Fig. 5.2A). On the other hand, the plot of A against C_i indicated that the three MSD lines exhibited higher photosynthesis rates than N61 under control conditions (Fig. 5.3). In particular, MNH5 and MSD345 showed significantly higher As than MSD53 and N61 (Fig. 5.3). However, under drought stress, A significantly decreased in all investigated genotypes, and there were no significant differences between the MSD lines and N61 (Fig. 5.2B). Although A was comparable among the MSD lines and N61 under drought stress, C_i showed an increasing trend in the MSD lines and was significantly higher in MSD345 than in N61, suggesting that MSD lines are able to maintain higher diffusion of CO_2 into the substomatal cavity under drought stress than N61 (Fig. 5.2C).

Next, I applied the data obtained from the photosynthetic CO_2 response to photosynthesis models (Sharkey *et al.* 2007; Bellasio *et al.* 2016) to identify the processes affecting leaf photosynthesis in the investigated genotypes in response to drought stress. MNH5 and MSD345 showed higher V_{cmax} values than MSD53 and N61 under control conditions, with MSD345 showing significantly higher values (Fig. 5.2D). However, V_{cmax} decreased to zero in all investigated genotypes under drought stress (Fig. 5.2D). Similarly, MNH5 and MSD345 showed significantly higher J than MSD53 and N61 under control conditions, whereas drought stress significantly decreased J in all four genotypes, with no significant differences among the drought-stressed genotypes (Fig. 5.2E). Consistently, the MSD lines showed higher TPU (ranging from

4.87 to 14.52 μmol m^{-2} s^{-1}) than N61 (3.80 μmol m^{-2} s^{-1}) under control conditions, particularly MNH5 and MSD345, whereas under drought stress, the TPU decreased (ranging from 1.97 to 8.14 μmol m^{-2} s^{-1}) in the MSD lines, but remained unchanged in N61 (Fig. 5.2F). Although TPU significantly decreased in the MSD lines under drought stress, the level of TPU in drought-stressed MSD345 was higher than that in N61 (Fig. 5.2F). Similarly, R_d was higher in MNH5 and MSD345 than in MSD53 and N61 under control conditions, but significantly reduced in all genotypes under drought stress (Fig. 5.4). The above results indicated that *Ae. tauschii* introgressions in the MSD lines improved several photosynthesis traits, including A, V_{cmax}, J, and TPU under control conditions compared with N61. Under drought stress, however, the values for these traits decreased in both MSD lines and N61, except for TPU in N61 which did not decrease under drought stress. Nevertheless, values for some photosynthesis traits such as C_i and TPU under drought conditions were higher in the MSD lines, especially MSD345, than in N61.

The E–C_a and g_{sw}–C_a curves showed higher E and g_{sw} in MNH5 and MSD345 than in MSD53 and N61 under control conditions (Fig. 5.5A and B). On the other hand, drought stress reduced E and g_{sw} in all investigated genotypes (particularly in the MSD lines) relative to control conditions (Fig. 5.5A and B). Although E and g_{sw} decreased under drought stress in all four genotypes, the three MSD lines tended to have lower E and g_{sw} than N61 under drought stress, suggesting that these MSD lines could reduce water loss under water-deficit conditions. The ability of the MSD lines to reduce water loss under drought conditions was also evident in the improved intrinsic water use efficiency (iWUE) in the MSD lines compared with N61 in response to drought stress. The iWUE of N61 was 151.3 μmol CO_2 mol H_2O^{-1} under control conditions, which was higher than that of the MSD lines (from 83.1 to 101.0 μmol CO_2 mol H_2O^{-1}; Fig. 5.5C). However, under drought stress, MNH5 and MSD345 showed an increase in iWUE of 1.52- and 1.57-fold relative to control conditions, whereas iWUE of MSD53 and N61 did not show any significant changes (Fig. 5.5C). This result provided additional evidence of the important

contributions of *Ae. tauschii* introgressions in improving WUE for drought adaptation in the MSD lines.

5.3.3 Genotypic Variation in TPC and TEAC of MSD lines and N61 under Drought Stress

Under control conditions, MNH5 and N61 exhibited significantly higher TPC than MSD53. However, under drought stress, all three MSD lines showed an increasing trend in TPC, whereas N61 showed a decreasing trend (Table 2). The effects of genotype (G), water regime (E), and G × E interaction were all significant for TPC.

In contrast, no significant differences were found in TEAC among the four genotypes under control conditions (Table 2). However, under drought stress, TEAC (ranging from 493.86 to 495.61 µg Trolox mg^{-1} FW) increased significantly in all three MSD lines (significantly in MNH5 and MSD345) but not in N61 (Table 2). The effects of genotype (G), water regime (E), and G × E interaction were all significant for TEAC (Table 2). As with TEAC, the SOD activity was similar among the MSD lines and N61 under control conditions. However, under drought stress, SOD activity significantly increased in the three MSD lines but not in N61 (Table 2).

5.3.4 Metabolite Changes in Response to Drought Stress

To evaluate metabolite homeostasis in response to drought stress, a targeted metabolomic analysis was conducted using LC-MS/MS and HPLC. A total of 37 metabolites were identified in the MSD lines and N61 and analysed by principal component analysis (PCA) to determine the interrelated effects of drought stress on the four genotypes (Fig. 5.6A and B). PC1 and PC2 explained 46.1% and 11.5%, respectively, of the total variation. PC1 separated the investigated genotypes based on drought or control conditions, while PC2 captured the genotypic variability (Fig. 5.6A and B). The PCA separated all investigated genotypes into five clusters: Clusters 1 and 2 contained MSD lines and N61, respectively, under control conditions, indicating that the metabolite profiles of the MSD lines were different from that of N61 even under control conditions (Fig. 5.6A and B). Cluster 3 primarily contained MSD345, cluster 5 primarily

contained both MNH5 and MSD53, and cluster 4 primarily contained N61, all under drought stress (Fig. 5.6A and B). The PCA results indicated that the MSD lines exhibited distinct metabolic profiles under both control and drought conditions compared with N61, which may be due to the *Ae. tauschii* introgressions in the MSD lines.

Under drought conditions, 16 of the 37 metabolites showed a decreasing trend while 17 showed an increasing trend in all investigated genotypes. Among the 17 increased metabolites, six metabolites, namely All, Leu, Phe, Pro, Tyr, and Val were observed only under drought conditions in both MSD lines and N61 (Fig. 5.6C). Four metabolites (adenine, γ-aminobutyric acid [GABA], His, and the polyamine putrescine) each specifically accumulated in an MSD line, but not in N61, in response to drought stress (Fig. 5.6C). Similar to the PCA results, the clustered heat map divided the investigated genotypes into two main clusters, one containing all genotypes grown under control conditions, and the other containing all genotypes grown under drought stress (Fig. 5.6D). The metabolite variables were also divided into two main clusters: one contained metabolites exhibiting a decreasing trend in the MSD lines and N61 under drought conditions, while the other contained metabolites that increased in the MSD lines or N61 under drought conditions (Fig. 5.6D). Interestingly, the drought-specific metabolites clustered together, while three out of four MSD line-specific metabolites also clustered together. These three metabolites are those found specifically in MSD345, whereas the non-clustered one (GABA) was specific to MSD53 (Fig. 5.6D). In addition, most of the detected amino acids showed an increasing trend in all four genotypes under drought stress, while organic acids showed a decreasing trend. Glucose and sucrose levels increased in MNH5 and MSD345 under drought stress, but decreased in N61. Also, glucose had a decreasing trend in MSD53 (Fig. 5.6D).

5.4 Discussion

Due to the polygenic nature of drought resilience and the genetic complexity of wheat, less progress has been made in developing drought-resilient varieties of wheat than of maize (*Z. mays*) or rice (*O. sativa*) (Khan *et al.* 2019). Wild relatives of wheat harbour many useful genes

and have the potential to survive well under climatic extremes. However, utilization of these wild relatives is hindered mainly by ploidy level differences and chromosomal barriers between cultivated and wild species. Careful selection is often needed to avoid cross-incompatibility and minimize linkage drag while maintaining high yield under drought stress (Kishii 2019). The introgression of wild alleles from *Ae. tauschii* into common wheat is one of the most efficient methods for increasing wheat genetic diversity and introducing desirable agronomic traits into elite germplasm (Cox *et al.* 2017; Gorafi *et al.* 2018). The MSD lines had been developed using *Ae. tauschii* accessions through the "synthetic derivative" approach (Fig. 1.1) (Tsujimoto *et al.* 2015; Itam *et al.* 2020a).

In the present study, the effects of drought stress on the biochemical, physiological, and metabolic plasticity of the MSD lines compared with N61 were investigated at the seedling stage. The MSD lines were developed in the background of N61 and are, therefore, comparable with N61 in this study. The "same-tray" method ensured that all investigated genotypes were exposed to the same level of drought stress as indicated by the decrease in soil water potential (Fig. 5.1). Moreover, the reduction of RWC in the tested lines under drought stress compared to the control conditions indicated that all investigated genotypes were exposed to severe drought stress (Fig. 5.2A). Photosynthetic parameters such as A, V_{cmax}, J, TPU, and R_d were significantly higher in MSD lines, especially MNH5 and MSD345, than in N61 under control conditions (Fig. 5.2B, 1D–F, S2), indicating that the D-genome introgressions from wild *Ae. tauschii* improved the photosynthetic capacity of the MSD lines under optimal conditions. On the other hand, the high TPU observed in MNH5 and MSD345 compared with MSD53 and N61 under drought stress (Fig. 5.2F) indicated that MNH5 and MSD345 were able to maintain the conversion of triose phosphates to sugars (Sharkey 1985). These high TPU levels were consistent with high glucose and sucrose contents in those genotypes, whereas the low TPU levels in MSD53 and N61 were consistent with the relatively low glucose and sucrose contents in the respective genotypes (Fig. 5.6D).

In general, drought-tolerant plants are known to maintain high TPU compared with drought-sensitive plants (Killi *et al.* 2017). A similar increase in TPU under drought stress has been reported in a wheat line containing introgressions from wild emmer wheat (*T. turgidum* ssp. *dicoccoides*), resulting in greater drought resilience and high yield components (Merchuk-Ovnat *et al.* 2016). High TPU under water-deficit conditions increases the level of inorganic phosphate concentration and ribulose 1,5-bisphosphate regeneration in the Calvin cycle, ultimately increasing photosynthesis (Sharkey 1985; Fabre *et al.* 2019). Additionally, TPU regulates the conversion of triose phosphates into sugars, which act as protective osmolytes and signalling molecules under drought and osmotic stresses (Sharma get al. 2019; Darko et al. 2019). MNH5 and MSD345 showed higher iWUE (Fig. 5.5C), as a common adaptive mechanism in drought-resilient wheat (Li *et al.* 2017). WUE at the leaf level is directly related to the physiological processes controlling the amount of carbon assimilated as biomass or grain produced per unit of water used by the plant (Hatfield and Dold 2019). Thus, iWUE as a consequence of reduced E or g_{sw} and a concomitant increase in A can boost wheat productivity during water-deficit conditions (Mega *et al.* 2019).

One of the mechanisms that enables plants to avoid oxidative-stress-induced damage is the production of phenolic compounds (Varela *et al.* 2016). The TPCs of wheat have been reported to increase in response to drought stress (Ma *et al.* 2014). Consistently, the TPCs of the MSD lines tended to increase in response to drought stress; however, the TPC levels were comparable between the MSD lines and N61 (Table 2), suggesting that there are no major genotypic differences between the MSD lines and N61 in terms of TPC. On the other hand, TEAC of all three MSD lines showed higher trend than that of N61 under drought stress (Table 2). In addition, SOD which catalyses the dismutation of the superoxide anion into hydrogen peroxide and molecular oxygen (Alscher *et al.* 2002), was significantly higher under drought stress in the MSD lines than in N61 (Table 2). Both TEAC and SOD activity suggested that the selected MSD lines

were able to maintain ROS homeostasis and subsequently reduced oxidative stress–induced damage under water-deficient conditions compared with N61.

The four metabolites (adenine, GABA, His, and putrescine) that specifically accumulated only in MSD lines (Fig. 5.6C) play important roles in stress response, antioxidant activities, osmoprotection, and nucleotide protection (Borrell *et al.* 1997; Ohta *et al.* 2000; Rébora *et al.* 2005; Das *et al.* 2017; Michaletti *et al.* 2018). Adenine, a purine nucleotide, has been reported to accumulate in drought-tolerant wheat under drought stress, indicating the activation of drought tolerance mechanisms to protect nucleic acid metabolism (Das *et al.* 2017; Michaletti *et al.* 2018). The improvements in nucleic acid metabolism were highly coordinated with the increase in the proteinogenic amino acid His, which is synthesized from 5-phosphoribosyl-1-pyrophosphate and tightly linked to nucleotide metabolism (Ohta *et al.* 2000). Due to purine–His cross-pathway regulation (Rébora *et al.* 2005), it has been suggested that His accumulation may be involved in nucleotide synthesis and protection under drought stress (Itam *et al.* 2020b). Also, the polyamine putrescine is a β-alanine precursor and an antioxidant reported in plants under abiotic stresses (Borrell *et al.* 1997; Gill and Tuteja 2010). Similarly, GABA accumulation has been associated with carbon–nitrogen balance and ROS scavenging (Bouché and Fromm 2004; Song *et al.* 2010). We, therefore, conclude that the MSD line-specific metabolites may play important roles in drought resilience in the MSD lines, and may be linked to contributions from *Ae. tauschii*. Additionally, the six metabolites that accumulated in all genotypes only under drought stress (All, Leu, Phe, Pro, Tyr, and Val; Fig. 5.6C and D) were identified as potential biomarkers for drought response. All is a nitrogen-rich intermediate of purine catabolism that stimulates abscisic acid production, jasmonic acid homeostasis, nitrogen recycling, and ROS scavenging in Arabidopsis under stress conditions (Watanabe *et al.* 2014; Takagi *et al.* 2016; Nourimand and Todd 2016). Also, Leu and Val are possible energy sources in drought-stressed wheat (Bowne *et al.* 2012), while Phe and Tyr are targets of oxidation and have protective functions against ROS (Dubouzet *et al.* 2007).

This study validates the initial selection of MNH5, MSD53, and MSD345 based on agronomic performance under field conditions (Elbashir *et al.* 2017a; b) (Table 5.1). This data suggest that MNH5 and MSD345 have isohydric (water-saving) traits; that is, they have the capacity to maintain low E and g_{sw} under drought conditions. This is evident in the low yield (but higher yield stability) and the relatively higher iWUE observed under drought stress (Table 5.1, Fig. 5.5C). In contrast, MSD53 has anisohydric (water-spending) traits, which are evident in its high yield and the low (and unchanged) iWUE under drought stress (Table 5.1, Fig. 5.5C). This further suggests that MSD53 may have mechanisms for avoiding drought stress in the field, enabling it to maintain high yield. Such drought avoidance mechanisms may be related to the root system. In a preliminary study on the root phenotypes of the MSD lines, MSD53 was found to have a wider root angle than MNH5 and MSD345, suggesting a higher capacity to absorb more water from a wide radius (data not included). This trait may have contributed to its high yield under field conditions in Wad Medani, Sudan (Table 5.1) and suggests adaptation to a specific type of drought environment, which may prove useful in drought breeding programs. Furthermore, an auxin-responsive transcription factor in the LATERAL ORGAN BOUNDARIES domain family, MORE ROOT from the D-genome of wheat (*TaMOR-D*), is conserved in *Ae. tauschii*, and has been reported to improve root system architecture, increase panicle length in rice, and increase yield in rice and Arabidopsis (Li *et al.* 2016). This transcription factor, among other favourable genes, may have been transferred into MSD53 from the *Ae. tauschii* accession used in the cross, which is adapted to the dry conditions of northern Iran. Future analysis of the root phenotypic plasticity and transcriptomics in the MSD lines under drought stress will further advance knowledge on the role of *Ae. tauschii* accessions in conferring drought resilience to bread wheat, and will create a platform for marker-assisted selection for drought-resilient genotypes. In summary, this study has shown the contributions of *Ae. tauschii* introgression to drought stress resilience of bread wheat through physiological, biochemical, and metabolite analysis. These

findings support the idea that actual drought adaptation can be assessed only when the whole system is considered in terms of yield potential, drought resilience, and WUE (Blum 2005).

In conclusion, the gains from *Ae. tauschii* introgression include high photosynthetic activity, SOD activity, and improved metabolite homeostasis in response to drought stress. This analysis suggests that MNH5 and MSD345 have water-saving traits, while MSD53 may be water-spending but drought-avoiding. The use of these genotypes for further breeding will depend on the target area and purpose of breeding. For example, the water-saving genotypes (MNH5 and MSD345) may be more useful in drylands with limited or non-reachable groundwater, such as the savannah regions of sub-Saharan Africa. In contrast, MSD53 will be potentially useful for drought avoidance breeding in areas with high groundwater content reachable with a robust root architecture, such as the Mediterranean region.

Table 5.1 Pedigrees of the three multiple synthetic derivative lines (MSD lines) and their yield performance under control and drought stress conditions compared with their backcross parent, Norin 61 (N61) and a Sudanese cultivar, 'Imam'

	Genotype	Pedigree	Origin of *Ae. tauschii* accession	GY_control (kg ha^{-1})	GY_drought (kg ha^{-1})	GY_DTE (%)
Greenhouse	MNH5	*T. durum* cv. Langdon × *Ae. tauschii* IG126387//N61	Turkmenistan	1646	1324	80.43
	N61			2785	1417	50.88
Field	MSD345	*T. durum* cv. Langdon × *Ae. tauschii* KU2829A//N61	Georgia	2031	1656	81.53
	MSD53	*T. durum* cv. Langdon × *Ae. tauschii* KU2156//N61	Iran	5094	3375	66.25
	N61			2626	1375	52.36
	Imam			3594	1775	49.38

GY_DTE, grain yield (GY)–based drought tolerance efficiency (GY_drought/GY_control * 100). Data were obtained from a post-anthesis drought stress field experiment in Wad Medani, Sudan, and from a greenhouse experiment in Tottori, Japan.

Table 5.2 Total phenolic content (TPC), antioxidant capacity, and superoxide dismutase (SOD) activity in the three multiple synthetic derivative lines (MSD lines) and their backcross parent, Norin 61, under control and drought stress conditions.

Water regime (E)	Genotype (G)	TPC (µg GAE mg^{-1} DW)	TEAC (µg Trolox eq. mg^{-1} FW)	SOD activity (%inhibition)
Control	MNH5	10.58 ± 0.23^{b}	486.63 ± 1.30^{d}	46.84 ± 2.35^{x}
	MSD345	8.03 ± 1.14^{ab}	488.76 ± 1.85^{de}	38.89 ± 5.42^{x}
	MSD53	6.82 ± 2.67^{a}	488.51 ± 1.68^{de}	42.00 ± 4.38^{x}
	Norin 61	11.18 ± 1.40^{b}	488.38 ± 3.57^{d}	46.58 ± 2.78^{x}
Drought	MNH5	10.97 ± 0.04^{b}	494.80 ± 0.99^{f}	72.34 ± 0.85^{y}
	MSD345	10.04 ± 0.38^{ab}	495.61 ± 1.92^{f}	71.04 ± 4.2^{y}
	MSD53	10.65 ± 0.28^{b}	493.86 ± 2.05^{ef}	75.72 ± 0.69^{y}
	Norin 61	10.50 ± 0.17^{b}	487.12 ± 0.56^{d}	48.25 ± 5.52^{x}
P-value*	G	< 0.05	< 0.05	< 0.01
	E	< 0.05	< 0.01	< 0.01
	G×E	< 0.05	< 0.01	< 0.01

[1] GAE mg^{-1} DW, gallic acid equivalent; TEAC, Trolox equivalent antioxidant capacity.

* Statistical significance for genotype (G), water regime (E), and their interaction (G × E). Within each column, values followed by the same letter were not significantly different ($P < 0.05$) according to the Tukey honestly significant difference (HSD) test.

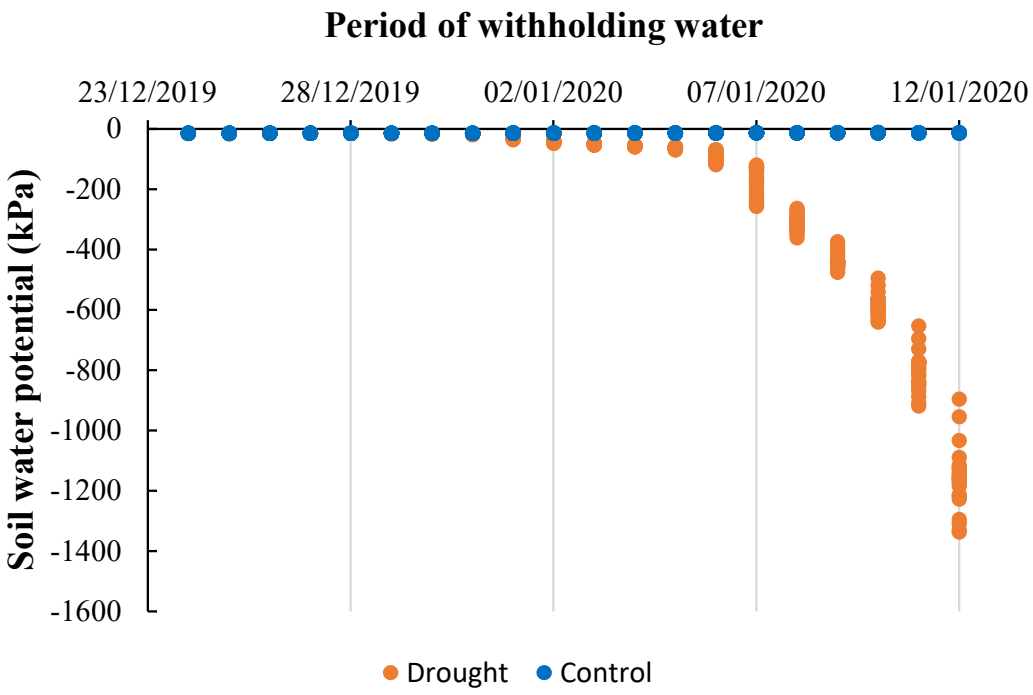

Figure 5.1 Decreasing soil water potential after withholding water. Data was recorded every 2 h during drought treatment.

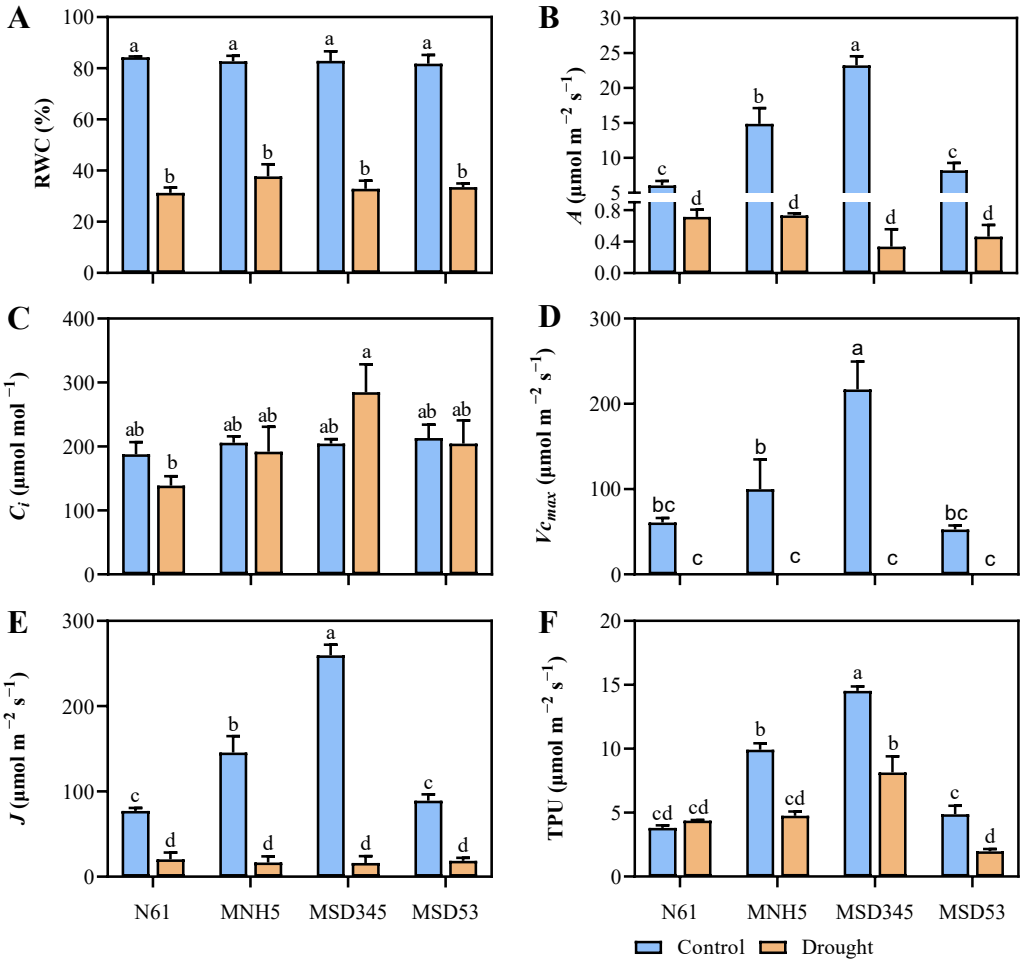

Figure 5.2 Comparative analyses of relative water content (RWC) and photosynthetic parameters of three multiple synthetic derivative lines and their backcross parent, Norin 61 (N61), under control and drought stress conditions. (A) RWC, (B) CO_2 assimilation rate (A), (C) intercellular CO_2 concentration (C_i), (D) maximum rubisco carboxylation rate (V_{cmax}), (E) electron transport rate (J), and (F) triose phosphate utilization (TPU). Data represent mean ± standard deviation of three independent biological replicates at 400 µmol mol^{-1} CO_2 concentration. Values marked with the same letter are not significantly different ($P < 0.05$) between genotypes and conditions according to the Tukey HSD test.

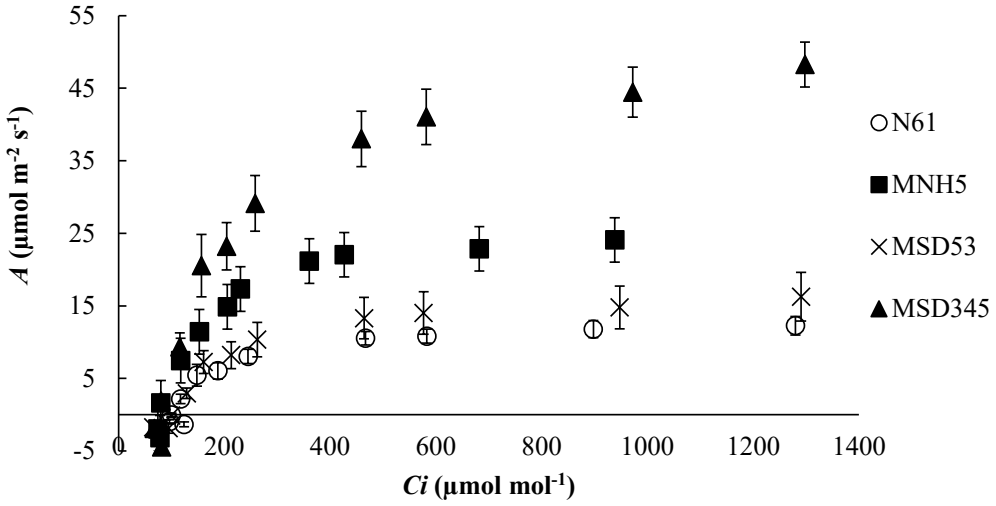

Figure 5.3 CO_2 response curve of the multiple synthetic derivative lines and their backcross parent, Norin 61 (N61) under control conditions. Data represent mean of three biological replicates. Error bars represent standard deviation.

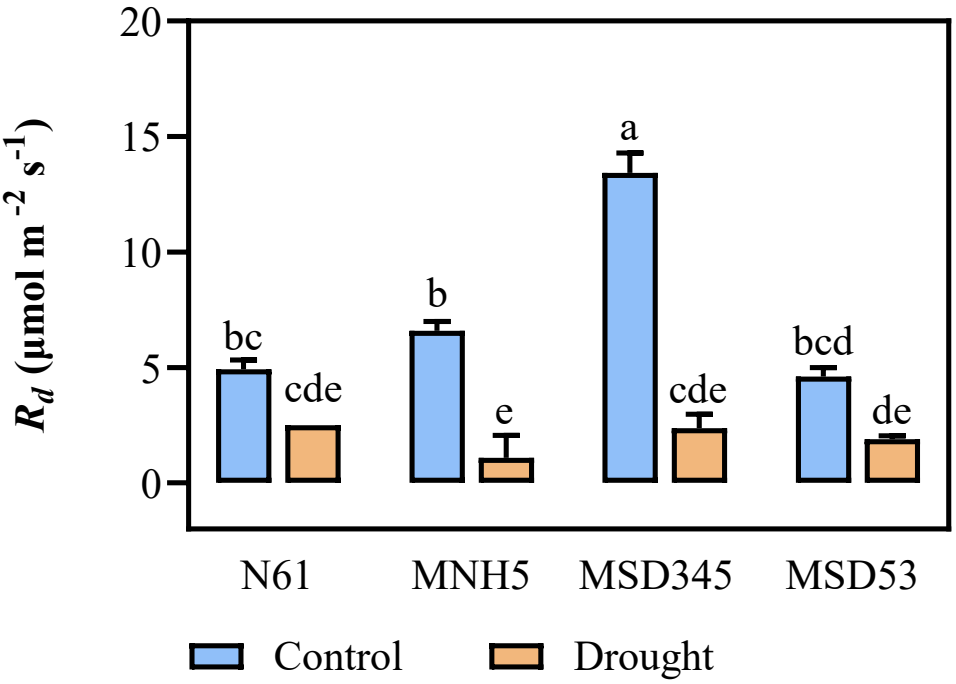

Figure 5.4 Leaf day respiration (Rd) of the multiple synthetic derivative lines and their backcross parent, Norin 61 under control and drought stress conditions. Data represent mean of three biological replicates at 400 µmol mol-1 CO_2 concentration. Error bars represent standard deviation. Values marked with the same letter are not significantly different ($P < 0.05$) between genotypes and conditions according to the Tukey HSD test.

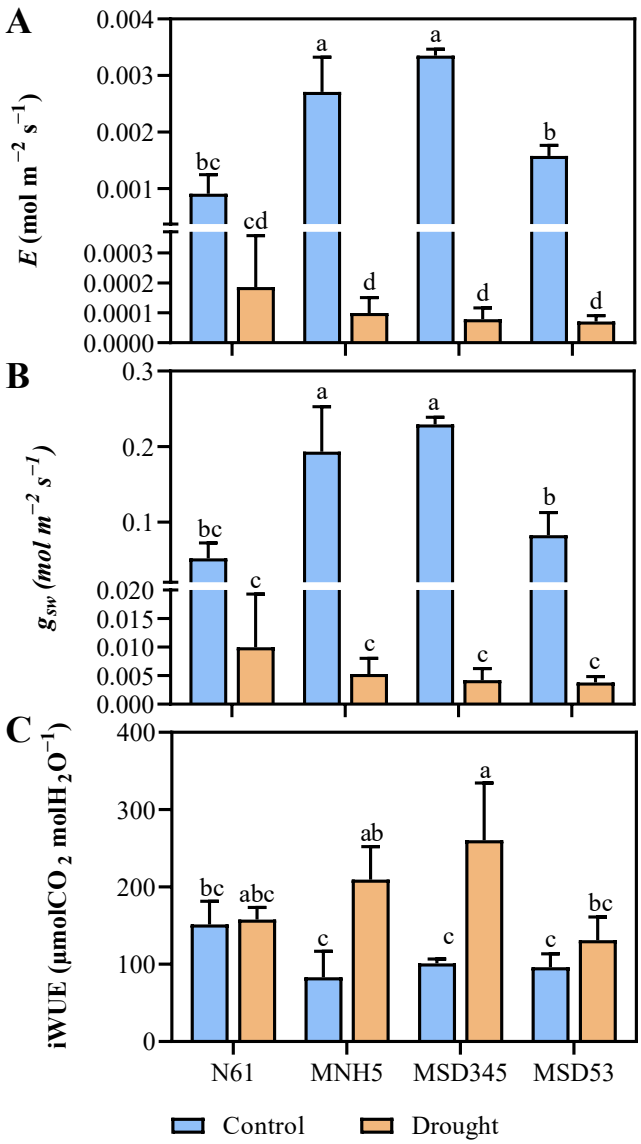

Figure 5.5 Changes in the transpiration rate (E), stomatal conductance (g_{sw}), and intrinsic water use efficiency (iWUE) of three multiple synthetic derivative lines (MSD lines) and their backcross parent, Norin 61, under control and drought stress conditions. (A) E, (B) g_{sw}, (C) iWUE. Data represent mean ± standard deviation of three independent biological replicates at 400 µmol mol^{-1} CO_2 concentration. Values marked with the same letter are not significantly different ($P < 0.05$) between genotypes and conditions according to the Tukey HSD test.

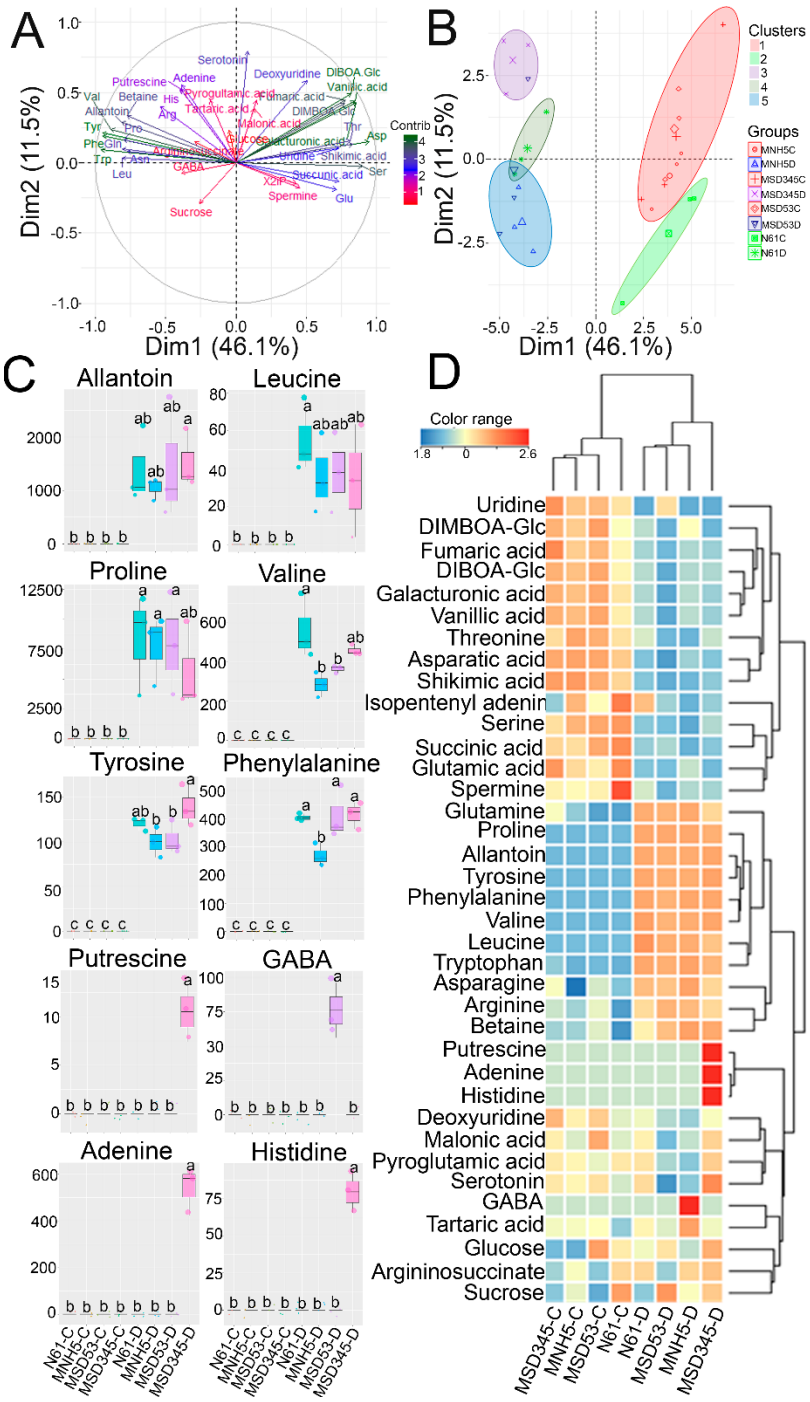

Figure 5.6 Principal component analysis (PCA) and accumulation of specific metabolites in the three multiple synthetic derivative lines (MSD lines) and their backcross parent, Norin 61, under control and drought stress conditions. Dim1 and Dim2 refer to PC1 and PC2, respectively. (A) Loading plot of the metabolite variables showing increasing metabolite contribution from red to green. (B) Score plot showing conditional and genotypic separation due to differences in metabolite profiles. (C) Drought-specific and MSD lines-specific metabolite accumulations. Values marked with the same letter are not significantly different ($P < 0.05$) between genotypes and conditions according to the Tukey HSD test. (D) Clustered heatmap of metabolite levels in the MSD lines and Norin 61 under control and drought conditions. The *Z*-score transformations of the mean metabolite concentrations were used to construct the heatmap. Accumulation rate: red, high; yellow, low; blue, very low. Data represent mean ± standard deviation of three biological replicates.

Chapter 6

General Discussion and Conclusion

As heat and drought stresses occur concurrently in actual field conditions, the common focus of studying them separately has limited opportunities for wheat improvement. Moreover, under the current climate change scenario and rising global population, breeding for combined stress resilience is a crucial step towards sustainable wheat productivity. In this study, a bread wheat diversity panel developed using 43 *Ae. tauschii* accessions, was evaluated: first under heat and combined heat-drought stress in Sudan, and then in greenhouses and growth chambers in Japan. The study expands our knowledge on the utilization of high diversity breeding panels for wheat improvement. Since this is the first detailed genomic study on combined heat and drought stress resilience in wheat under natural field conditions, the identified candidate genes, novel alleles and QTLs will potentially serve as a genomic landmark for breeding for improved adaptation to the combined stresses.

Additional screening of selected bread wheat lines (under a drought-rewatering-drought cycle) ensured that the lines are able to not only survive the erratic rainfall pattern common in natural field conditions, but to maintain high yield under prolonged drought spells nearing wilting point. This validated the results from the field study. High heritability values were obtained for some of the evaluated traits indicating that selection based on such traits can result in genetic gain for drought resilience. Since the selected lines have been evaluated under heat and drought stresses, they may serve as useful genetic resources for further breeding for climate-resilient wheat varieties.

Furthermore, using physiological parameters such as transpiration ratio (TR) and fraction of transpirable soil water ($FTSW_{Th}$), the water conservation traits of two selected wheat lines were characterized and suitable geographical locations recommended: MSD345 (low TR and $FTSW_{Th}$) is better suited for drylands, where soil water is always limited (such as the savannah regions of sub-Saharan Africa), whereas MSD53 (high TR and $FTSW_{Th}$) is better suited for areas with erratic

rainfall where the plants can fully use their genetic potential under wet conditions and then quickly lower their transpiration rate in response to drying conditions. Since these wheat lines were developed by *Ae. tauschii* introgressions, they reflect the benefits of the introgressions in improving transpiration dynamics in wheat under two water-limiting scenarios (prolonged drought and erratic rainfall). This offers new options for increasing yield under the two water-limiting scenarios. Additionally, the physiological phase-shift point of wheat under progressive drought stress was identified at soil water potential -400 kPa. Also, metabolites such as adenine, gamma aminobutyric acid, histidine, and putrescine were identified as potential biomarkers for drought resilience in wheat. Other potential gains from *Ae. tauschii* introgressions include high photosynthetic activity, SOD activity, and improved metabolite homeostasis in response to drought stress.

The sequence of studies in this thesis explored the heat and drought resilience diversity in bread wheat, the genomic regions (including loci, candidate genes and alleles) regulating this resilience, and the possible mechanisms involved. It also assessed the practicability of utilizing the diversity of *Ae. tauschii* for combined stress resilience breeding. To further understand the transpiration dynamics in this wheat population, the root phenotypic diversity is currently being explored. Also, recombinant populations are being developed using the selected bread wheat lines, and the identified genomic regions in this thesis will be used for marker-assisted selection among the recombinant populations. Taken together, this study has so far, presented genomic landmarks, genetic materials and in-depth physiological and metabolomic knowledge that will be harnessed to improve global wheat productivity.

Summary

Many studies have shown the potential of using *Aegilops tauschii* for breeding to enhance bread wheat productivity in drought- and heat-prone areas. However, the diversity in heat and drought resilience traits in bread wheat has not been fully explored. Also, there is a dearth of knowledge on the mechanism of combined heat and drought resilience, and a lack of genetic materials for combined stress resilience breeding. In this research, the heat and drought resilience diversity in bread wheat lines containing *Ae. tauschii* introgressions was explored; the genomic regions (including loci, candidate genes and alleles) regulating the resilience and the underlying physiological and metabolomic dynamics were highlighted. Also, the practicability of utilizing the diversity of *Ae. tauschii* for combined stress resilience breeding was assessed.

In Chapter 1, a wheat diversity panel containing *Ae. tauschii* introgressions was evaluated under heat (H) and combined heat-drought (HD) stress in Sudan to identify QTLs associated with resilience to the combined stress, and to assess the practicability of harnessing *Ae. tauschii* diversity for combined stress resilience breeding. Novel alleles and quantitative trait loci (QTLs) were identified on chromosomes 3D, 5D, and 7A controlling grain yield (GY), kernel number per spike (KPS), and thousand-kernel weight (TKW), and another on 3D (521–549 Mbp) controlling GY alone. A strong marker-trait association for GY stability was identified on chromosome 3D (508.3 Mbp) explaining 20.3% of the variation. Furthermore, leaf traits including canopy temperature (CT), normalized difference vegetative index (NDVI), and carbon-13 composition ($\delta^{13}C$) were controlled by five QTLs on 2D (23–96, 511–554, and 606–614 Mbp), 3D (155–171 Mbp), and 5D (407–413 Mbp), some of which were pleiotropic for GY and related traits. Most MTAs and QTLs were found in the D genome, indicating the potential of using *Ae. tauschii* diversity for wheat breeding. Further analysis revealed candidate genes, including *GA20ox*, regulating GY stability, and *CaaX prenyl protease 2*, regulating CT at the flowering stage, under H and HD stress. As this is the first such study, our results provide genomic landmarks for wheat breeding to improve adaptation to H and HD conditions under climate change.

In Chapter 2, twenty-four selected wheat lines, were evaluated under a drought-rewatering-drought cycle for two years in a greenhouse in Tottori, Japan. The objective was to validate the lines selected in Chapter 1. Drought was imposed by withholding water during flowering. The results revealed considerable genetic variability in physio-agronomic traits, reflecting the variation in introgressed segments. High heritability estimates (above 47%) were recorded for most traits, including days to 50% heading, plant height, and TKW, indicating the genetic control of these traits which may be useful for cultivar development. The trait-trait correlations within and between water regimes highlighted a strong association among the genetic factors controlling these traits. Some lines exhibited superior performance in terms of stress tolerance index and mean productivity compared with their backcross parent (N61) and elite cultivars commonly grown in hot and dry areas. Graphical genotyping revealed unique introgressed segments on chromosomes 4B, 6B, 2D, and 3D in some drought-resilient lines which may be linked to drought resilience. Therefore, these lines were recommended for further breeding to develop climate-resilient wheat varieties.

In Chapter 3, I used two classical physiological methods, the fraction of transpirable soil water threshold ($FTSW_{Th}$) and drought stress response function, to characterize the water conservation traits of two selected wheat lines (MSD53 and MSD345) which both contain introgressed segments from *Ae. tauschii* but differ in drought resilience. The lines and N61 were subjected to dry-down conditions. MSD53 had a higher $FTSW_{Th}$ for transpiration decrease than N61 and MSD345. In terms of drought stress response function, MSD53 had the lowest threshold suction, suggesting a lower drought resilience capacity compared with MSD345. However, MSD53 exhibited an effective-water-use trait whereas MSD345 exhibited a water-saving trait under dry-down conditions. These results are consistent with the reported higher GY of MSD53 in comparison with MSD345 under drought stress in Sudan, and demonstrate that high $FTSW_{Th}$ supports effective water use for improved agricultural productivity in drylands. The differences in water conservation traits between the two MSD lines may be attributed to variation in

introgressed segments, which can be further explored for drought resilience breeding. This study validates the results in Chapter 1 and 2.

In Chapter 4, my aim was to gain in-depth understanding of drought effect on wheat metabolism. I exposed wheat N61 plants to progressive drought stress [0 (before drought), 2, 4, 6, 8, and 10 days after withholding water] during the flowering stage and investigated physiological and metabolomic responses. Key abscisic acid-responsive genes, $\delta^{13}C$ and CT played major roles in wheat response to progressive drought stress. The CT depression was tightly correlated with soil water potential (SWP). Additionally, SWP at −517 kPa was identified as the critical point for increasing CT and inducing reactive oxygen species. Metabolome analysis identified four potential drought-responsive biomarkers, the enhancement of nitrogen recycling through purine and pyrimidine metabolism, drought-induced senescence based on 1-aminocyclopropane-1-carboxylic acid and Asn accumulation, and an anti-senescence response through serotonin accumulation under severe drought stress. These findings provide insights into the molecular, physiological and metabolite changes involved in drought response which are useful for wheat breeding programs developing drought-resilient wheat varieties.

In Chapter 5, the physiological and metabolic plasticity of three drought-resilient wheat lines and N61 were evaluated in response to drought stress at the seedling stage. The results suggested that the D-genome introgressions from *Ae. tauschii* to the lines improved their drought-adaptive traits. Specifically, MNH5 and MSD345 showed higher photosynthesis rates and triose phosphate utilization than N61 under control conditions, resulting in greater accumulation of glucose and sucrose in the shoots. However, under drought stress, MNH5 and MSD345 had higher intrinsic water use efficiency than MSD53 and N61. The total antioxidant capacity and superoxide dismutase activity increased in the three lines, whereas no significant changes were found in N61 in response to drought stress. Metabolome analysis identified six common drought-induced metabolites in all of the investigated genotypes. However, four metabolites (adenine, gamma

aminobutyric acid, histidine, and putrescine) each specifically accumulated in one resilient line in response to drought stress, suggesting that these metabolites are important for drought resilience.

Overall, this work has expanded current knowledge on the role of high diversity breeding panels for wheat breeding for heat and drought resilience. It has provided in-depth insights on important genomic regions, and metabolic and physiological dynamics in wheat in response to heat and drought stress. In the future, high-throughput analyses and validation of these findings will enable them to serve as effective tools for climate-resilience breeding.

Summary (Japanese)

多くの研究が、干ばつや高温に見舞われやすい地域でのコムギの生産性を高めるための育種に、タルホコムギ(*Aegilops tauschii*)を利用する可能性を示している。しかし、パンコムギ(*Triticum aestivum*)の高温や干ばつに強い形質の多様性については十分に検討されていない。また、高温と干ばつに対する複合的な回復力のメカニズムに関する知見も乏しく、複合的なストレス回復力育種のための遺伝素材も不足している。本研究では、タルホコムギを導入したパンコムギ系統における高温と乾燥に対する回復力の多様性を探り、回復力を制御するゲノム領域（遺伝子座、候補遺伝子、対立遺伝子を含む）と、その背景にある生理学的およびメタボロームの動態を明らかにした。また、タルホコムギの多様性を複合的なストレス耐性育種に利用することの実用性についても評価した。

第 1 章では、タルホコムギの導入遺伝子を含むコムギの多様性パネルをスーダンの高温・干ばつ複合ストレス下で評価し、複合ストレスへの耐性に関連する QTL を同定するとともに、複合ストレス耐性育種にタルホコムギの多様性を利用することの実用性を評価した。その結果、収量 (GY)、一穂粒数（KPS）、千粒重 (TKW)を支配する 3D、5D、7A 染色体上に新規対立遺伝子と QTL が、また GY のみを支配する 3D 染色体（521-549Mbp）上に新規対立遺伝子が同定された。3D 染色体（508.3Mbp）には、GY の安定性に関する強いマーカー・形質相関が確認され、変動の 20.3%を説明した。さらに、CT、NDVI、δ^{13}C などの葉の形質は、2D (23-96, 511-554, 606-614Mbp)、3D (155-171Mbp)、5D (407-413Mbp)上の 5 つの QTL によって制御されており、そのうちのいくつかは GY や関連形質に対して多面的発現をした。ほとんどの MTA や QTL は D ゲノムに見られ、タルホコムギの多様性をコムギの育種に利用できる可能性を示した。さらに解析を進めると、高温ストレス(H)および高温と干ばつストレス (HD)下において、GY の安定性を制御する GA20ox や、開花期のキャノピー温度を制御する CaaX プレニルプロテアーゼ 2 などの候補遺伝子が明らかになった。このような研究は初めてであり、今回の結果は、気候変動下の H および HD 条件への適応を改善するためのコムギ育種にゲノム上の試金石を投じるものである。

第 2 章では、選抜された 24 のコムギ系統を、鳥取の温室で 2 年間、干ばつ-灌水-干ばつのサイクルで評価した。その目的は、第 1 章で選抜した系統を検証することである。干ばつは、開花時に水を控えることで実施した。その結果、タルホコムギから導入された染色体断片の違いを反映して、生理農業形質にかなりの遺伝的変動が見られた。50%出穂日数、草丈、千粒重など、ほとんどの形質で高い遺伝率（47%以上）が記録されており、これらの形質が遺伝的に支配されていることを示しており、品種開発に役立つ可能性がある。灌水処理内および灌水処理間での形質相関は、これらの形質を支配する遺伝的要因の強い関連性を示した。いくつかの系統は、その戻し交配親や、高温・乾燥地域でよく栽培されているエリート品種よりも、ストレス耐性指数や平均生産性の点で優れた性能を示した。グラフィカルジェノタイピングの結果、干ばつに強い系統の中には、4B、6B、2D、3D 染色体上にユニークな導入セグメントが見られ、ここが干ばつ耐性に関連している可能性がある。気候変動に強いコムギ品種を開発するために、これらの系統を用いて、さらなる育種を行うことが推奨される。

第 3 章では、2 つの古典的な生理学的手法である、蒸散可能な土壌水分の閾値の割合（$FTSW_{Th}$）と干ばつストレス応答機能を用いて、タルホコムギの染色体断片を持ち、干ばつ耐性が異なる 2 つの選抜コムギ系統（MSD53 と MSD345）の保水形質を明らかにした。これらの系統とその戻し交配親（N61）を、途中で灌水を与えない処理条件に供した。MSD53 は、N61 や MSD345 に比べて、蒸散量減少時の $FTSW_{Th}$ が高かった。また、乾燥ストレス応答機能では、MSD53 が最も低い閾値吸引量を示し、効率的な水保存能力を持っていることが示唆された。これらの結果は、スーダンでの干ばつストレス下において、MSD53 が N61 や MSD345 と比較して高い収量を示したという報告と一致しており、高い $FTSW_{Th}$ が降雨の不安定な乾燥地での農業生産性向上のための効果的な水利用を支援することを示している。逆に、蒸散量と $FTSW_{Th}$ が低い MSD345 は、乾燥ストレスが長期化する乾燥地に適していると考えられる。このように、調査した遺伝子型間で保水形質が異なることは、第 1 章および第 2 章の結果を検証するものであり、干ばつに強い育種のためにさらに検討課題を与えるものである。

第 4 章では、乾燥がコムギの代謝に及ぼす影響について詳しく理解することを目的とした。コムギ N61 を開花期に段階的な乾燥ストレス（灌水停止、0 日、2 日、4 日、6 日、8 日、10 日）に曝し、生理的およびメタボロームの応答を調べた。その結果、主要なアブシジン酸応答遺伝子、炭素同位体組成、キャノピー温度（CT）が、乾燥ストレスに対するコムギの応答に大きな役割を果たしていた。CT の低下は、土壌水ポテンシャル（SWP）と密接な相関があった。さらに、SWP の-517kPa が、CT を上昇させ、活性酸素を誘発する臨界点であることが明らかになった。メタボローム解析の結果、干ばつに応答するバイオマーカーとして、プリンおよびピリミジン代謝による窒素リサイクルの促進、1-aminocyclopropane-1-carboxylic acid と Asn の蓄積による干ばつによる老化、セロトニンの蓄積による厳しい干ばつストレス下での抗老化反応の 4 つの可能性が確認された。これらの結果は、干ばつに強いコムギ品種の開発に役立つ、干ばつ応答に関わる分子的、生理的、代謝的変化についての知見を提供するものである。

第 5 章では、干ばつに強いコムギ 3 系統とその戻し交配親（N61）について、苗の段階での干ばつストレスに対する生理的・代謝的な可塑性を評価した。その結果、タルホコムギからの D ゲノム導入により、これらの系統の干ばつ適応形質が改善されることがわかった。具体的には、MNH5 と MSD345 は、対照条件下で N61 よりも高い光合成速度とトリオースリン酸の利用率を示し、その結果、グルコースとスクロースが新芽に多く蓄積された。しかし、乾燥ストレス下では、MNH5 と MSD345 は、MSD53 や N61 よりも高い内的水利用効率を示した。干ばつストレスに反応して、3 系統では総抗酸化力とスーパーオキシドディスムターゼ活性が上昇したが、N61 では有意な変化は見られなかった。メタボローム解析では、調査したすべての遺伝子型において、6 種類の共通した干ばつ誘発性代謝物が同定された。しかし、4 つの代謝物（アデニン、ガンマアミノ酪酸、ヒスチジン、プトレスシン）がそれぞれ乾燥ストレスに反応して 1 つの回復力のある系統で特異的に蓄積したことから、これらの代謝物が乾燥回復力に重要であることが示唆された。

全体として、本研究は、高温と干ばつに強いコムギの育種における高い多様性育種パネルの役割に関する現在の知識を拡大しました。また、重要なゲノム領域や、熱・

干ばつストレスに反応するコムギの代謝・生理動態について、詳細な知見を得ることができた。今後は、これらの知見をハイスループットで解析し、検証することで、気候変動に強い育種のための効果的なツールとして活用できるようになると考えられる。

References

Abdelrahman, M., D.J. Burritt, A. Gupta, H. Tsujimoto and L.-S.P. Tran (2019) Heat stress effects on source–sink relationships and metabolome dynamics in wheat. *J Exp Bot* erz296:. https://doi.org/10.1093/jxb/erz296

Abhinandan, K., L. Skori, M. Stanic, N.M.N. Hickerson, M. Jamshed and M.A. Samuel (2018) Abiotic stress signaling in wheat – An inclusive overview of hormonal interactions during abiotic stress responses in wheat. *Front. Plant Sci*. 9:734.

Alghabari, F., M.Z. Ihsan, A. Khaliq, S. Hussain, I. Daur, S. Fahad and W. Nasim (2016) Gibberellin-sensitive *Rht* alleles confer tolerance to heat and drought stresses in wheat at booting stage. *J Cereal Sci* 70:72–78. https://doi.org/10.1016/j.jcs.2016.05.016

Alscher, R.G., N. Erturk and L.S. Heath (2002) Role of superoxide dismutases (SODs) in controlling oxidative stress in plants. *J Exp Bot* 53:1331–1341. https://doi.org/10.1093/jexbot/53.372.1331

Alvarado, G., F.M. Rodríguez, A. Pacheco, J. Burgueño, J. Crossa, M. Vargas, P. Pérez-Rodríguez and M.A. Lopez-Cruz (2020) META-R: A software to analyze data from multi-environment plant breeding trials. *Crop J* 8:745–756. https://doi.org/10.1016/j.cj.2020.03.010

Arbona, V., M. Manzi, C. de Ollas and A. Gómez-Cadenas (2013) Metabolomics as a tool to investigate abiotic stress tolerance in plants. *Int J Mol Sci* 14:4885–4911. https://doi.org/10.3390/ijms14034885

Bacon, M.A. (2004) *Water use efficiency in plant biology*. Blackwell Publishing, Oxford, UK.

Banu, M.N.A., M.A. Hoque, M. Watanabe-Sugimoto, K. Matsuoka, Y. Nakamura, Y. Shimoishi and Y. Murata (2009) Proline and glycinebetaine induce antioxidant defense gene expression and suppress cell death in cultured tobacco cells under salt stress. *J Plant Physiol* 166:146–156. https://doi.org/10.1016/j.jplph.2008.03.002

Barrs, H., and P. Weatherley (1962) A re-examination of the relative turgidity technique for estimating water deficits in leaves. *Aust J Biol Sci* 15:413. https://doi.org/10.1071/BI9620413

Bellasio, C., D.J. Beerling and H. Griffiths (2016) An Excel tool for deriving key photosynthetic parameters from combined gas exchange and chlorophyll fluorescence: Theory and practice. *Plant Cell Environ*. 39:1180–1197

Benjamini, Y., and Y. Hochberg (1995) Controlling the False Discovery Rate: A practical and powerful approach to multiple testing. *J R Stat Soc Ser B* 57:289–300. https://doi.org/10.1111/j.2517-6161.1995.tb02031.x

Bennani, S., N. Nsarellah, M. Jlibene, W. Tadesse, A. Birouk and H. Ouabbou (2017) Efficiency of drought tolerance indices under different stress severities for bread wheat selection. *Aust J Crop Sci* 11:395–405. https://doi.org/10.21475/ajcs.17.11.04.pne272

Betts, N.S., C. Dockter, O. Berkowitz, H.M. Collins, M. Hooi, Q. Lu, R.A. Burton, V. Bulone, B. Skadhauge, J. Whelan, *et al.* (2020) Transcriptional and biochemical analyses of gibberellin expression and content in germinated barley grain. *J Exp Bot* 71:1870–1884. https://doi.org/10.1093/jxb/erz546

Blum, A. (2005) Drought resistance, water-use efficiency, and yield potential - Are they compatible, dissonant, or mutually exclusive? *Aust J Agric Res* 56:1159–1168.

https://doi.org/10.1071/AR05069

Borrell, A., L. Carbonell, R. Farràs, P. Puig-Parellada and A.F. Tiburcio (1997) Polyamines inhibit lipid peroxidation in senescing oat leaves. *Physiol Plant* 99:385–390. https://doi.org/10.1034/j.1399-3054.1997.990305.x

Bouché, N., and H. Fromm (2004) GABA in plants: Just a metabolite? *Trends Plant Sci.* 9:110–115.

Bowne, J.B., T.A. Erwin, J. Juttner, T. Schnurbusch, P. Langridge, A. Bacic and U. Roessner (2012) Drought responses of leaf tissues from wheat cultivars of differing drought tolerance at the metabolite level. *Molecular Plant*. pp 418–429

Boyer, J.S. (1982) Plant productivity and environment. *Science (80-)* 218:443–448. https://doi.org/10.1126/science.218.4571.443

Bracha-Drori, K., K. Shichrur, T.C. Lubetzky and S. Yalovsky (2008) Functional analysis of Arabidopsis postprenylation CaaX processing enzymes and their function in subcellular protein targeting. *Plant Physiol* 148:119–131. https://doi.org/10.1104/pp.108.120477

Bradbury, P.J., Z. Zhang, D.E. Kroon, T.M. Casstevens, Y. Ramdoss and E.S. Buckler (2007) TASSEL: Software for association mapping of complex traits in diverse samples. *Bioinformatics* 23:2633–2635. https://doi.org/10.1093/bioinformatics/btm308

Brenner, M., and B.N. Ames (1971) The histidine operon and its regulation. *Metab Regul* 349–387. https://doi.org/10.1016/b978-0-12-299255-1.50018-3

Colebrook, E.H., S.G. Thomas, A.L. Phillips and P. Hedden (2014) The role of gibberellin signalling in plant responses to abiotic stress. *J. Exp. Biol.* 217:67–75.

Cox, T.S., J. Wu, S. Wang, J. Cai, Q. Zhong and B. Fu (2017) Comparing two approaches for introgression of germplasm from *Aegilops tauschii* into common wheat. *Crop J.* 5:355–362.

Cutler, S.R., P.L. Rodriguez, R.R. Finkelstein and S.R. Abrams (2010) Abscisic acid: Emergence of a core signaling network. *Annu Rev Plant Biol* 61:651–679. https://doi.org/10.1146/annurev-arplant-042809-112122

Czyczyło-Mysza, I., I. Marcińska, E. Skrzypek, M. Chrupek, S. Grzesiak, T. Hura, S. Stojałowski, B. Myśków, P. Milczarski and S. Quarrie (2011) Mapping QTLs for yield components and chlorophyll a fluorescence parameters in wheat under three levels of water availability. *Plant Genet Resour Characterisation Util* 9:291–295. https://doi.org/10.1017/S1479262111000207

Daba, S.D., P. Tyagi, G. Brown-Guedira and M. Mohammadi (2020) Genome-wide association study in historical and contemporary U.S. winter wheats identifies height-reducing loci. *Crop J* 8:243–251. https://doi.org/10.1016/j.cj.2019.09.005

Darko, E., B. Végh, R. Khalil, T. Marček, G. Szalai, M. Pál and T. Janda (2019) Metabolic responses of wheat seedlings to osmotic stress induced by various osmolytes under iso-osmotic conditions. *PLoS One* 14:e0226151. https://doi.org/10.1371/journal.pone.0226151

Daryanto, S., L. Wang and P.A. Jacinthe (2016) Global synthesis of drought effects on maize and wheat production. *PLoS One* 11:e0156362. https://doi.org/10.1371/journal.pone.0156362

Das, A., P. Rushton and J. Rohila (2017) Metabolomic Profiling of soybeans (*Glycine max* L.) reveals the importance of sugar and nitrogen metabolism under drought and heat stress.

Plants 6:21. https://doi.org/10.3390/plants6020021

de Poel, B. Van, and D. Van Der Straeten (2014) 1-aminocyclopropane-1-carboxylic acid (ACC) in plants: More than just the precursor of ethylene! *Front Plant Sci* 5:1–11. https://doi.org/10.3389/fpls.2014.00640

Dixon, L.S., J. V Godoy and A.H. Carter (2019) Evaluating the utility of carbon isotope discrimination for wheat breeding in the pacific northwest. *Plant Phenomics* 2019:1–11. https://doi.org/10.34133/2019/4528719

Dodig, D., M. Zoric, B. Kobiljski, J. Savic, V. Kandic, S. Quarrie and J. Barnes (2012) Genetic and association mapping study of wheat agronomic traits under contrasting water regimes. *Int J Mol Sci* 13:6167–6188. https://doi.org/10.3390/ijms13056167

Dubouzet, J.G., A. Ishihara, F. Matsuda, H. Miyagawa, H. Iwata and K. Wakasa (2007) Integrated metabolomic and transcriptomic analyses of high-tryptophan rice expressing a mutant anthranilate synthase alpha subunit. *J Exp Bot* 58:3309–3321. https://doi.org/10.1093/jxb/erm179

Eason, J.R., J.W. Johnston, L. De Vré, B.K. Sinclair and G.A. King (2000) Amino acid metabolism in senescing Sandersonia aurantiaca flowers: Cloning and characterization of asparagine synthetase and glutamine synthetase cDNAs. *Aust J Plant Physiol* 27:389–396. https://doi.org/10.1071/pp99200

Eid, M.H. (2009) Estimation of heritability and genetic advance of yield traits in wheat (*Triticum aestivum* L.) under drought condition. *Int J Genet Mol Biol* 1:115–120.

Elbashir, A.A.E., Y.S.A. Gorafi, I.S.A. Tahir, A.M.A. Elhashimi, M.G.A. Abdalla and H. Tsujimoto (2017a) Genetic variation in heat tolerance-related traits in a population of wheat multiple synthetic derivatives. *Breed Sci* 67:483–492. https://doi.org/10.1270/jsbbs.17048

Elbashir, A.A.E., Y.S.A. Gorafi, I.S.A. Tahir, J.S. Kim and H. Tsujimoto (2017b) Wheat multiple synthetic derivatives: A new source for heat stress tolerance adaptive traits. *Breed Sci* 67:248–256. https://doi.org/10.1270/jsbbs.16204

Elhadi, G.M.I., N.M. Kamal, Y.S.A. Gorafi, Y. Yamasaki, K. Takata, I.S.A. Tahir, M.O. Itam, H. Tanaka and H. Tsujimoto (2021) Exploitation of tolerance of wheat kernel weight and shape-related traits from *Aegilops tauschii* under heat and combined heat-drought stresses. *Int J Mol Sci* 22:1830. https://doi.org/10.3390/ijms22041830

Elliott, J., D. Deryng, C. Müller, K. Frieler, M. Konzmann, D. Gerten, M. Glotter, M. Flörke, Y. Wada, N. Best, *et al.* (2014) Constraints and potentials of future irrigation water availability on agricultural production under climate change. *Proc Natl Acad Sci U S A* 111:3239–3244. https://doi.org/10.1073/pnas.1222474110

Elsheikh, E.R.A., B. Schultz, H.S. Adam and A.M. Haile (2015) Crop water productivity for sunflower under different irrigation regimes and plant spacing in Gezira Scheme , Sudan. *J Agric Environ Int Dev* 109:221–233. https://doi.org/10.12895/jaeid.20152.346

Fabre, D., X. Yin, M. Dingkuhn, A. Clément-Vidal, S. Roques, L. Rouan, A. Soutiras and D. Luquet (2019) Role of Triose Phosphate Utilization in photosynthetic response of rice to variable carbon dioxide levels and plant source-sink relations. *bioRxiv* 633016. https://doi.org/10.1101/633016

Fang, T., L. Lei, G. Li, C. Powers, R.M. Hunger, B.F. Carver and L. Yan (2020) Development and deployment of KASP markers for multiple alleles of Lr34 in wheat. *Theor Appl Genet*

133:2183–2195. https://doi.org/10.1007/s00122-020-03589-x

Farquhar, G.D., J.R. Ehleringer and K.T. Hubick (1989) Carbon isotope discrimination and photosynthesis. *Annu Rev Plant Physiol Plant Mol Biol* 40:503–537. https://doi.org/10.1146/annurev.pp.40.060189.002443

Feddes, R.A., and P.A.C. Raats (2004) Parameterizing the soil-water-plant root system. *In*: Feddes RA, de Rooij GH, and van Dam JC (eds) *Unsaturated-zone modeling: Progress, challenges and applications*, Wageningen. Kluwer Academic Publishers, Dordrecht, pp 95–141.

Fernandez, G.C.J. (1992) Effective selection criteria for assessing plant stress toerance. *In*: Kuo CG (ed) *Adaptation of food crops to temperature and water stress*. AVRDC, Taipei, Taiwan, pp 257–270.

Finlay, K.W., and G.N. Wilkinson (1963) The analysis of adaptation in a plant-breeding programme. *Aust J Agric Res* 14:742–754. https://doi.org/10.1071/AR9630742

Fischer, R.A., and R. Maurer (1978) Drought resistance in spring wheat cultivars. I. Grain yield responses. *Aust J Agric Res* 29:897–912. https://doi.org/10.1071/AR9780897

Food and Agriculture Organization of the United Nations (2020) FAO Cereal supply and demand brief | world food situation |: 05/03/2020. http://www.fao.org/worldfoodsituation/csdb/en/. Accessed 18 Feb 2021.

Gbegbelegbe, S., D. Cammarano, S. Asseng, R. Robertson, U. Chung, M. Adam, O. Abdalla, T. Payne, M. Reynolds, K. Sonder, *et al.* (2017) Baseline simulation for global wheat production with CIMMYT mega-environment specific cultivars. *F Crop Res* 202:122–135. https://doi.org/10.1016/j.fcr.2016.06.010

GCARD (2012) Breakout session P1.1 National Food Security – The Wheat Initiative – an international research initiative for wheat improvement. Uruguay.

Gholipoor, M., T.R. Sinclair and P.V.V. Prasad (2012) Genotypic variation within sorghum for transpiration response to drying soil. *Plant Soil* 357:35–40. https://doi.org/10.1007/s11104-012-1140-8

Gill, S.S., and N. Tuteja (2010) Polyamines and abiotic stress tolerance in plants. *Plant Signal Behav* 5:26–33. https://doi.org/10.4161/psb.5.1.10291

Godfray, H.C.J., J.R. Beddington, I.R. Crute, L. Haddad, D. Lawrence, J.F. Muir, J. Pretty, S. Robinson, S.M. Thomas and C. Toulmin (2010) Food security: The challenge of feeding 9 billion people. *Science (80-)* 327:812–818. https://doi.org/10.1126/science.1185383

Gorafi, Y.S.A., J.S. Kim, A.A.E. Elbashir and H. Tsujimoto (2018) A population of wheat multiple synthetic derivatives: an effective platform to explore, harness and utilize genetic diversity of Aegilops tauschii for wheat improvement. *Theor Appl Genet* 131:1615–1626. https://doi.org/10.1007/s00122-018-3102-x

Gregorová, Z., J. Kováčik, B. Klejdus, M. Maglovski, R. Kuna, P. Hauptvogel and I. Matušíková (2015) Drought-induced responses of physiology, metabolites, and PR proteins in *Triticum aestivum*. *J Agric Food Chem* 63:8125–8133. https://doi.org/10.1021/acs.jafc.5b02951

Guendouz, A., S. Guessoum, K. Maamri, M. Bendir and M. Hafsi (2013) Canopy temperature efficiency as indicators for drought tolerance in durum wheat (*Triticum durum* Desf.) in semi arid conditions. *J Chem Inf Model* 53:1689–1699. https://doi.org/10.1017/CBO9781107415324.004

Guiguitant, J., H. Marrou, V. Vadez, P. Gupta, S. Kumar, A. Soltani, T.R. Sinclair and M.E. Ghanem (2017) Relevance of limited-transpiration trait for lentil (*Lens culinaris* Medik.) in South Asia. *F Crop Res* 209:96–107. https://doi.org/10.1016/j.fcr.2017.04.013

Guo, R., L. Shi, Y. Jiao, M. Li, X. Zhong, F. Gu, Q. Liu, X. Xia and H. Li (2018) Metabolic responses to drought stress in the tissues of drought-tolerant and drought-sensitive wheat genotype seedlings. *AoB Plants* 10:1–13. https://doi.org/10.1093/aobpla/ply016

Guo, X., Z. Xin, T. Yang, X. Ma, Y. Zhang, Z. Wang, Y. Ren and T. Lin (2020) Metabolomics response for drought stress tolerance in chinese wheat genotypes (*Triticum aestivum*). *Plants* 9:520. https://doi.org/10.3390/plants9040520

Hanocq, E., M. Niarquin, E. Heumez, M. Rousset and J. Le Gouis (2004) Detection and mapping of QTL for earliness components in a bread wheat recombinant inbred lines population. *Theor Appl Genet* 110:106–115. https://doi.org/10.1007/s00122-004-1799-1

Hatfield, J.L., and C. Dold (2019) Water-use efficiency: Advances and challenges in a changing climate. *Front. Plant Sci*. 10:103

He, P., and J.Y. Jin (1999) Relationships among hormone changes, transmembrane Ca^{2+} flux and lipid peroxidation during leaf senescence in spring maize. *Acta Bot Sin* 41:1221–1225

Herrera-Rodríguez, M.B., J.M. Maldonado and R. Pérez-Vicente (2006) Role of asparagine and asparagine synthetase genes in sunflower (*Helianthus annuus*) germination and natural senescence. *J Plant Physiol* 163:1061–1070. https://doi.org/10.1016/j.jplph.2005.10.012

Huang, B.E., A.W. George, K.L. Forrest, A. Kilian, M.J. Hayden, M.K. Morell and C.R. Cavanagh (2012) A multiparent advanced generation inter-cross population for genetic analysis in wheat. *Plant Biotechnol J* 10:826–839. https://doi.org/10.1111/j.1467-7652.2012.00702.x

Huang, T., and G. Jander (2017) Abscisic acid-regulated protein degradation causes osmotic stress-induced accumulation of branched-chain amino acids in *Arabidopsis thaliana*. *Planta* 246:737–747. https://doi.org/10.1007/s00425-017-2727-3

Iizumi, T., I.-E.A. Ali-Babiker, M. Tsubo, I.S.A. Tahir, Y. Kurosaki, W. Kim, Y.S.A. Gorafi, A.A.M. Idris and H. Tsujimoto (2021) Rising temperatures and increasing demand challenge wheat supply in Sudan. *Nat Food* 2:19–27. https://doi.org/10.1038/s43016-020-00214-4

Islam, M., M.C. Begum, A.H. Kabir and M.F. Alam (2015) Molecular and biochemical mechanisms associated with differential responses to drought tolerance in wheat (*Triticum aestivum* L.). *J Plant Interact* 10:195–201. https://doi.org/10.1080/17429145.2015.1064174

Itam, M., M. Abdelrahman, Y. Yamasaki, R. Mega, Y. Gorafi, K. Akashi and H. Tsujimoto (2020a) *Aegilops tauschii* introgressions improve physio-biochemical traits and metabolite plasticity in bread wheat under drought stress. *Agronomy* 10:1–17. https://doi.org/10.3390/agronomy10101588

Itam, M., R. Mega, S. Tadano, M. Abdelrahman, S. Matsunaga, Y. Yamasaki, K. Akashi and H. Tsujimoto (2020b) Metabolic and physiological responses to progressive drought stress in bread wheat. *Sci Reports 2020 101* 10:1–14. https://doi.org/10.1038/s41598-020-74303-6

Itam, M.O., Y.S.A. Gorafi, I.S.A. Tahir and H. Tsujimoto (2021a) Genetic variation in drought resilience-related traits among wheat multiple synthetic derivative lines: insights for climate resilience breeding. *Breed Sci* (in press).

Jyostna Devi, M., T.R. Sinclair, V. Vadez and L. Krishnamurthy (2009) Peanut genotypic variation in transpiration efficiency and decreased transpiration during progressive soil drying. *F Crop Res* 114:280–285. https://doi.org/10.1016/j.fcr.2009.08.012

Kadam, S., K. Singh, S. Shukla, S. Goel, P. Vikram, V. Pawar, K. Gaikwad, R. Khanna-Chopra and N. Singh (2012) Genomic associations for drought tolerance on the short arm of wheat chromosome 4B. *Funct Integr Genomics* 12:447–464. https://doi.org/10.1007/s10142-012-0276-1

Kang, Z., M.A. Babar, N. Khan, J. Guo, J. Khan, S. Islam, S. Shrestha and D. Shahi (2019) Comparative metabolomic profiling in the roots and leaves in contrasting genotypes reveals complex mechanisms involved in post-anthesis drought tolerance in wheat. *PLoS One* 14:. https://doi.org/10.1371/journal.pone.0213502

Kaur, H., S. Mukherjee, F. Baluska and S.C. Bhatla (2015) Regulatory roles of serotonin and melatonin in abiotic stress tolerance in plants. *Plant Signal. Behav*. 10.

Khan, S., S. Anwar, S. Yu, M. Sun, Z. Yang and Z.Q. Gao (2019) Development of drought-tolerant transgenic wheat: Achievements and limitations. *Int J Mol Sci* 20:13. https://doi.org/10.3390/ijms20133350

Kholová, J., C.T. Hash, A. Kakkera, M. Koová and V. Vadez (2010) Constitutive water-conserving mechanisms are correlated with the terminal drought tolerance of pearl millet [*Pennisetum glaucum* (L.) R. Br.]. *J Exp Bot* 61:369–377. https://doi.org/10.1093/jxb/erp314

Kholová, J., T. Murugesan, S. Kaliamoorthy, S. Malayee, R. Baddam, G.L. Hammer, G. McLean, S. Deshpande, C.T. Hash, P.Q. Craufurd, *et al.* (2014) Modelling the effect of plant water use traits on yield and stay-green expression in sorghum. *Funct Plant Biol* 41:1019–1034. https://doi.org/10.1071/FP13355

Killi, D., F. Bussotti, A. Raschi and M. Haworth (2017) Adaptation to high temperature mitigates the impact of water deficit during combined heat and drought stress in C3 sunflower and C4 maize varieties with contrasting drought tolerance. *Physiol Plant* 159:130–147. https://doi.org/10.1111/ppl.12490

Kishii, M. (2019) An update of recent use of *Aegilops* species in wheat breeding. *Front Plant Sci* 10:585. https://doi.org/10.3389/fpls.2019.00585

Koslowsky, S., H. Riegler, E. Bergmüller and R. Zrenner (2008) Higher biomass accumulation by increasing phosphoribosylpyrophosphate synthetase activity in *Arabidopsis thaliana* and *Nicotiana tabacum*. *Plant Biotechnol J* 6:281–294. https://doi.org/10.1111/j.1467-7652.2007.00314.x

Krasileva, K. V., H.A. Vasquez-Gross, T. Howell, P. Bailey, F. Paraiso, L. Clissold, J. Simmonds, R.H. Ramirez-Gonzalez, X. Wang, P. Borrill, *et al.* (2017) Uncovering hidden variation in polyploid wheat. *Proc Natl Acad Sci U S A* 114:E913–E921. https://doi.org/10.1073/pnas.1619268114

Lê, S., J. Josse and F. Husson (2008) FactoMineR: An R package for multivariate analysis. *J Stat Softw* 25:1–18. https://doi.org/10.18637/jss.v025.i01

Li, B., D. Liu, Q. Li, X. Mao, A. Li, J. Wang, X. Chang and R. Jing (2016) Overexpression of wheat gene *TaMOR* improves root system architecture and grain yield in *Oryza sativa*. *J Exp Bot* 67:4155–4167. https://doi.org/10.1093/jxb/erw193

Li, X., L.M.F. Lawas, R. Malo, U. Glaubitz, A. Erban, R. Mauleon, S. Heuer, E. Zuther, J.

Kopka, D.K. Hincha, *et al.* (2015) Metabolic and transcriptomic signatures of rice floral organs reveal sugar starvation as a factor in reproductive failure under heat and drought stress. *Plant, Cell Environ* 38:2171–2192. https://doi.org/10.1111/pce.12545

Li, Y., H. Li, Y. Li and S. Zhang (2017) Improving water-use efficiency by decreasing stomatal conductance and transpiration rate to maintain higher ear photosynthetic rate in drought-resistant wheat. *Crop J* 5:231–239. https://doi.org/10.1016/j.cj.2017.01.001

Liu, C., S. Sukumaran, E. Claverie, C. Sansaloni, S. Dreisigacker and M. Reynolds (2019) Genetic dissection of heat and drought stress QTLs in phenology-controlled synthetic-derived recombinant inbred lines in spring wheat. *Mol Breed* 39:1–18. https://doi.org/10.1007/s11032-019-0938-y

Luo, L.J. (2010) Breeding for water-saving and drought-resistance rice (WDR) in China. *J. Exp. Bot*. 61:3509–3517.

Ma, D., D. Sun, C. Wang, Y. Li and T. Guo (2014) Expression of flavonoid biosynthesis genes and accumulation of flavonoid in wheat leaves in response to drought stress. *Plant Physiol Biochem* 80:60–66. https://doi.org/10.1016/j.plaphy.2014.03.024

Maes, W.H., and K. Steppe (2012) Estimating evapotranspiration and drought stress with ground-based thermal remote sensing in agriculture: A review. *J Exp Bot* 63:4671–4712. https://doi.org/10.1093/jxb/ers165

Maghsoudi, K., Y. Emam, A. Niazi, M. Pessarakli and M.J. Arvin (2018) P5CS expression level and proline accumulation in the sensitive and tolerant wheat cultivars under control and drought stress conditions in the presence/absence of silicon and salicylic acid. *J Plant Interact* 13:461–471. https://doi.org/10.1080/17429145.2018.1506516

Mao, C., S. Lu, B. Lv, B. Zhang, J. Shen, J. He, L. Luo, D. Xi, X. Chen and F. Ming (2017) A rice nac transcription factor promotes leaf senescence via ABA biosynthesis. *Plant Physiol* 174:1747–1763. https://doi.org/10.1104/pp.17.00542

Mason, N.M., T.S. Jayne and B. Shiferaw (2012) Wheat consumption in sub-Saharan Africa: Trends, drivers, and policy implication. *MSU Int Dev Work Pap* 1–29

Mason, R., and R. Singh (2014) Considerations when deploying canopy temperature to select high yielding wheat breeding lines under drought and heat stress. *Agronomy* 4:191–201. https://doi.org/10.3390/agronomy4020191

Matsuoka, Y., and S. Nasuda (2004) Durum wheat as a candidate for the unknown female progenitor of bread wheat: An empirical study with a highly fertile F1 hybrid with *Aegilops tauschii* Coss. *Theor Appl Genet* 109:1710–1717. https://doi.org/10.1007/s00122-004-1806-6

Mau, Y.S., A.S.S. Ndiwa, S.S. Oematan and J.E.R. Markus (2019) Drought tolerance indices for selection of drought tolerant, high yielding upland rice genotypes. *Aust J Crop Sci* 13:170–178. https://doi.org/10.21475/ajcs.19.13.01.p1778

Mega, R., F. Abe, J.S. Kim, Y. Tsuboi, K. Tanaka, H. Kobayashi, Y. Sakata, K. Hanada, H. Tsujimoto, J. Kikuchi, *et al.* (2019) Tuning water-use efficiency and drought tolerance in wheat using abscisic acid receptors. *Nat Plants* 5:153–159. https://doi.org/10.1038/s41477-019-0361-8

Merchuk-Ovnat, L., T. Fahima, T. Krugman and Y. Saranga (2016) Ancestral QTL alleles from wild emmer wheat improve grain yield, biomass and photosynthesis across enviroinments in modern wheat. *Plant Sci* 251:23–34. https://doi.org/10.1016/j.plantsci.2016.05.003

Merlot, S., A.-C. Mustilli, B. Genty, H. North, V. Lefebvre, B. Sotta, A. Vavasseur and J. Giraudat (2002) Use of infrared thermal imaging to isolate Arabidopsis mutants defective in stomatal regulation. *Plant J* 30:601–609. https://doi.org/10.1046/j.1365-313X.2002.01322.x

Messina, C.D., T.R. Sinclair, G.L. Hammer, D. Curan, J. Thompson, Z. Oler, C. Gho and M. Cooper (2015) Limited-transpiration trait may increase maize drought tolerance in the US corn belt. *Agron J* 107:1978–1986. https://doi.org/10.2134/agronj15.0016

Michaletti, A., M.R. Naghavi, M. Toorchi, L. Zolla and S. Rinalducci (2018) Metabolomics and proteomics reveal drought-stress responses of leaf tissues from spring-wheat. *Sci Rep* 8:5710. https://doi.org/10.1038/s41598-018-24012-y

Mikami, H., and Y. Ishida (1983) Post-column fluorometric detection of reducing sugars in high performance liquid chromatography using arginine. *Bunseki Kagaku* 32:E207–E210. https://doi.org/10.2116/bunsekikagaku.32.6_E207

Murata, N., F. Iwanaga, A. Maimaiti, S. Imada, N. Mori, K. Tanaka and N. Yamanaka (2012) Significant improvement of salt tolerance with 2-day acclimatization treatment in *Elaeagnus oxycarpa* seedlings. *Environ Exp Bot* 77:170–174. https://doi.org/10.1016/j.envexpbot.2011.11.019

Mwadzingeni, L., H. Shimelis and T.J. Tsilo (2017) Variance components and heritability of yield and yield components of wheat under drought-stressed and non-stressed conditions. *Aust J Crop Sci* 11:1425–1430. https://doi.org/10.21475/ajcs.17.11.11.pne548

Narayanan, S., P.J. Tamura, M.R. Roth, P.V.V. Prasad and R. Welti (2016) Wheat leaf lipids during heat stress: High day and night temperatures result in major lipid alterations. *Plant Cell Environ* 39:787–803. https://doi.org/10.1111/pce.12649

Nourimand, M., and C.D. Todd (2016) Allantoin increases cadmium tolerance in Arabidopsis via activation of antioxidant mechanisms. *Plant Cell Physiol* 57:2485–2496. https://doi.org/10.1093/pcp/pcw162

Obata, T., and A.R. Fernie (2012) The use of metabolomics to dissect plant responses to abiotic stresses. *Cell. Mol. Life Sci.* 69:3225–3243.

Ogbonnaya, F.C., O. Abdalla, A. Mujeeb-Kazi, A.G. Kazi, S.S. Xu, N. Gosman, E.S. Lagudah, D. Bonnett, M.E. Sorrells and H. Tsujimoto (2013) Synthetic hexaploids: Harnessing species of the primary gene pool for wheat improvement. *Plant Breed Rev* 37:35–122. https://doi.org/10.1002/9781118497869.ch2

Ohta, D., K. Fujimori, M. Mizutani, Y. Nakayama, R. Kunpaisal-Hashimoto, S. Münzer and A. Kozaki (2000) Molecular cloning and characterization of ATP-phosphoribosyl transferase from Arabidopsis, a key enzyme in the histidine biosynthetic pathway. *Plant Physiol* 122:907–14.

Pask, A., J. Pietragalla and D. Mullan (2012) Physiological breeding II: A field guide to wheat phenotyping. CIMMYT, Mexico City.

Pearce, S., A.K. Huttly, I.M. Prosser, Y.D. Li, S.P. Vaughan, B. Gallova, A. Patil, J.A. Coghill, J. Dubcovsky, P. Hedden, *et al.* (2015) Heterologous expression and transcript analysis of gibberellin biosynthetic genes of grasses reveals novel functionality in the GA3ox family. *BMC Plant Biol* 15:130. https://doi.org/10.1186/s12870-015-0520-7

Pennisi, E. (2008) The blue revolution, drop by drop, gene by gene. *Science (80-)* 320:171–173. https://doi.org/10.1126/science.320.5873.171

Pinto, R.S., and M.P. Reynolds (2015) Common genetic basis for canopy temperature depression under heat and drought stress associated with optimized root distribution in bread wheat. *Theor Appl Genet* 128:575–585. https://doi.org/10.1007/s00122-015-2453-9

Pour-Aboughadareh, A., A. Etminan, M. Abdelrahman, K.H.M. Siddique and L.S.P. Tran (2020) Assessment of biochemical and physiological parameters of durum wheat genotypes at the seedling stage during polyethylene glycol-induced water stress. *Plant Growth Regul* 92:81–93. https://doi.org/10.1007/s10725-020-00621-4

Pradhan, G.P., P.V.V. Prasad, A.K. Fritz, M.B. Kirkham and B.S. Gill (2012) Effects of drought and high temperature stress on synthetic hexaploid wheat. *Funct Plant Biol* 39:190–198. https://doi.org/10.1071/FP11245

Prasad, P.V.V., S.R. Pisipati, I. Momčilović and Z. Ristic (2011) Independent and combined effects of high temperature and drought stress during grain filling on plant yield and chloroplast EF-Tu expression in spring wheat. *J Agron Crop Sci* 197:430–441. https://doi.org/10.1111/j.1439-037X.2011.00477.x

Prodhan, M.Y., S. Munemasa, M.N.E.N. Nahar, Y. Nakamura and Y. Murata (2018) Guard cell salicylic acid signaling is integrated into abscisic acid signaling via the Ca^{2+}/CPK-dependent pathway. *Plant Physiol* 178:441–450. https://doi.org/10.1104/pp.18.00321

Qaseem, M.F., R. Qureshi, H. Shaheen and N. Shafqat (2019) Genome-wide association analyses for yield and yield-related traits in bread wheat (*Triticum aestivum* L.) under pre-anthesis combined heat and drought stress in field conditions. *PLoS One* 14:e0213407. https://doi.org/10.1371/journal.pone.0213407

Qin, X., J.H. Liu, W.S. Zhao, X.J. Chen, Z.J. Guo and Y.L. Peng (2013) Gibberellin 20-Oxidase Gene *OsGA20ox3* regulates plant stature and disease development in rice. *Mol Plant-Microbe Interact* 26:227–239. https://doi.org/10.1094/MPMI-05-12-0138-R

R Core Team (2018) *R: A language and environment for statistical computing. R foundation for statistical computing*. Vienna, Austria, pp 201. https://doi.org/10.1108/eb003648

Rasheed, A., W. Wen, F. Gao, S. Zhai, H. Jin, J. Liu, Q. Guo, Y. Zhang, S. Dreisigacker, X. Xia, *et al.* (2016) Development and validation of KASP assays for genes underpinning key economic traits in bread wheat. *Theor Appl Genet* 129:1843–1860. https://doi.org/10.1007/s00122-016-2743-x

Ray, S., W.A. Mondal and M.A. Choudhuri (1983) Regulation of leaf senescence, grain-filling and yield of rice by kinetin and abscisic acid. *Physiol Plant* 59:343–346. https://doi.org/10.1111/j.1399-3054.1983.tb04212.x

Rebetzke, G.J., A.G. Condon, G.D. Farquhar, R. Appels and R.A. Richards (2008) Quantitative trait loci for carbon isotope discrimination are repeatable across environments and wheat mapping populations. *Theor Appl Genet* 118:123–137. https://doi.org/10.1007/s00122-008-0882-4

Rebetzke, G.J., M.H. Ellis, D.G. Bonnett, A.G. Condon, D. Falk and R.A. Richards (2011) The *Rht13* dwarfing gene reduces peduncle length and plant height to increase grain number and yield of wheat. *F Crop Res* 124:323–331. https://doi.org/10.1016/j.fcr.2011.06.022

Rébora, K., B. Laloo and B. Daignan-Fornier (2005) Revisiting purine-histidine cross-pathway regulation in *Saccharomyces cerevisiae*: A central role for a small molecule. *Genetics* 170:61–70. https://doi.org/10.1534/genetics.104.039396

Reynolds, M., M. Tattaris, C.M. Cossani, M. Ellis, K. Yamaguchi-Shinozaki and C. Saint Pierre

(2015) Exploring genetic resources to increase adaptation of wheat to climate change. *In*: Ogihara Y., S. Takumi and H. Handa (eds) *Advances in wheat genetics: from genome to field*. Springer Japan, Tokyo, pp 355–368

Robredo, A., U. Pérez-López, M. Lacuesta, A. Mena-Petite and A. Muñoz-Rueda (2010) Influence of water stress on photosynthetic characteristics in barley plants under ambient and elevated CO_2 concentrations. *Biol Plant* 54:285–292. https://doi.org/10.1007/s10535-010-0050-y

Rosielle, A.A., and J. Hamblin (1981) Theoretical aspects of selection for yield in stress and non-stress environment. *Crop Sci* 21:943–946. https://doi.org/10.2135/cropsci1981.0011183x002100060033x

Royo, C., D. Villegas, L.F. García del Moral, S. Elhani, N. Aparicio, Y. Rharrabti and J.L. Araus (2002) Comparative performance of carbon isotope discrimination and canopy temperature depression as predictors of genotype differences in durum wheat yield in Spain. *Aust J Agric Res* 53:561–569. https://doi.org/10.1071/AR01016

Rutkoski, J., J. Poland, S. Mondal, E. Autrique, L.G. Pérez, J. Crossa, M. Reynolds and R. Singh (2016) Canopy temperature and vegetation indices from high-throughput phenotyping improve accuracy of pedigree and genomic selection for grain yield in wheat. *G3 Genes, Genomes, Genet* 6:2799–2808. https://doi.org/10.1534/g3.116.032888

Sade, N., M. Del Mar Rubio-Wilhelmi, K. Umnajkitikorn and E. Blumwald (2018) Stress-induced senescence and plant tolerance to abiotic stress. *J Exp Bot* 69:845–853. https://doi.org/10.1093/jxb/erx235

Sadok, W. (2017) Wheat. In: Sinclair TR (ed) *Water-conservation traits to increase crop yields in water-deficit environments: Case studies*. Springer, Cham, Switzerland, pp 85–92

Sadok, W., R. Schoppach, M.E. Ghanem, C. Zucca and T.R. Sinclair (2019) Wheat drought-tolerance to enhance food security in Tunisia, birthplace of the Arab Spring. *Eur J Agron* 107:1–9. https://doi.org/10.1016/j.eja.2019.03.009

Sadok, W., and T.R. Sinclair (2010) Genetic variability of transpiration response of soybean [*Glycine max* (L.) Merr.] shoots to leaf hydraulic conductance inhibitor $AgNo_3$. *Crop Sci* 50:1423–1430. https://doi.org/10.2135/cropsci2009.10.0575

Saghai-Maroof, M.A., K.M. Soliman, R.A. Jorgensen and R.W. Allard (1984) Ribosomal DNA spacer-length polymorphisms in barley: mendelian inheritance, chromosomal location, and population dynamics. *Proc Natl Acad Sci U S A* 81:8014–8018. https://doi.org/10.1073/pnas.81.24.8014

Sanchez, D.H., F. Schwabe, A. Erban, M.K. Udvardi and J. Kopka (2012) Comparative metabolomics of drought acclimation in model and forage legumes. *Plant, Cell Environ* 35:136–149. https://doi.org/10.1111/j.1365-3040.2011.02423.x

Sansaloni, C., C. Petroli, D. Jaccoud, J. Carling, F. Detering, D. Grattapaglia and A. Kilian (2011) Diversity Arrays Technology (DArT) and next-generation sequencing combined: genome-wide, high throughput, highly informative genotyping for molecular breeding of Eucalyptus. *BMC Proc* 5:P54. https://doi.org/10.1186/1753-6561-5-s7-p54

Schmidt, J., P.J. Tricker, P. Eckermann, P. Kalambettu, M. Garcia and D. Fleury (2020) Novel alleles for combined drought and heat stress tolerance in wheat. *Front Plant Sci* 10:1–14. https://doi.org/10.3389/fpls.2019.01800

Schoppach, R., D. Fleury, T.R. Sinclair and W. Sadok (2017) Transpiration sensitivity to

evaporative demand across 120 years of breeding of australian wheat cultivars. *J Agron Crop Sci* 203:219–226. https://doi.org/10.1111/jac.12193

Schoppach, R., and W. Sadok (2012) Differential sensitivities of transpiration to evaporative demand and soil water deficit among wheat elite cultivars indicate different strategies for drought tolerance. *Environ Exp Bot* 84:1–10. https://doi.org/10.1016/j.envexpbot.2012.04.016

Sciarresi, C., A. Patrignani, A. Soltani, T. Sinclair and R.P. Lollato (2019) Plant traits to increase winter wheat yield in semiarid and subhumid environments. *Agron J* 111:1728–1740. https://doi.org/10.2134/agronj2018.12.0766

Sharkey, T.D. (1985) O_2-insensitive photosynthesis in C3 plants. *Plant Physiol* 78:71–75. https://doi.org/10.1104/pp.78.1.71

Sharkey, T.D., C.J. Bernacchi, G.D. Farquhar and E.L. Singsaas (2007) Fitting photosynthetic carbon dioxide response curves for C3 leaves. *Plant, Cell Environ* 30:1035–1040. https://doi.org/10.1111/j.1365-3040.2007.01710.x

Sharma, A., B. Shahzad, V. Kumar, S.K. Kohli, G.P.S. Sidhu, A.S. Bali, N. Handa, D. Kapoor, R. Bhardwaj and B. Zheng (2019) Phytohormones regulate accumulation of osmolytes under abiotic stress. *Biomolecules* 9

Sharma, P., A.B. Jha, R.S. Dubey and M. Pessarakli (2012) Reactive oxygen species, oxidative damage, and antioxidative defense mechanism in plants under stressful conditions. *J Bot* 2012:1–26. https://doi.org/10.1155/2012/217037

Shen, J., B. Lv, L. Luo, J. He, C. Mao, D. Xi and F. Ming (2017) The NAC-type transcription factor OsNAC2 regulates ABA-dependent genes and abiotic stress tolerance in rice. *Sci Rep* 7:40641. https://doi.org/10.1038/srep40641

Sherval, M., L.E. Askew and P.M. McGuirk (2014) Manifestations of drought. *In*: Michalos A.C. (ed) *Encyclopedia of quality of life and well-being research*. Springer Netherlands, Dordrecht, pp 3756–3761

Shiferaw, B., B.M. Prasanna, J. Hellin and M. Bänziger (2011) Crops that feed the world 6. Past successes and future challenges to the role played by maize in global food security. *Food Secur*. 3:307–327

Shimamura, T., Y. Sumikura, T. Yamazaki, A. Tada, T. Kashiwagi, H. Ishikawa, T. Matsui, N. Sugimoto, H. Akiyama and H. Ukeda (2014) Applicability of the DPPH assay for evaluating the antioxidant capacity of food additives – inter-laboratory evaluation study. *Anal Sci* 30:717–721. https://doi.org/10.2116/analsci.30.717

Shimelis, H., and R. Shiringani (2010) Variance components and heritabilities of yield and agronomic traits among cowpea genotypes. *Euphytica* 176:383–389. https://doi.org/10.1007/s10681-010-0222-z

Shimizu, K.K., D. Copetti, M. Okada, T. Wicker, T. Tameshige, M. Hatakeyama, R. Shimizu-Inatsugi, C. Aquino, K. Nishimura, F. Kobayashi, *et al.* (2021) De novo genome assembly of the Japanese wheat cultivar Norin 61 highlights functional variation in flowering time and fusarium-resistant genes in East Asian genotypes. *Plant Cell Physiol* 62:8–27. https://doi.org/10.1093/pcp/pcaa152

Simunek, J., M.T. Van Genuchten and M. Sejna (2006) *The HYDRUS software package for simulating two- and three-dimensional movement of water, heat, and multiple solutes in variably-saturated media, user manual, Version 1.0*. Prague, Czech Republic.

Sinclair, T.R. (2017a) Limited-transpiration rate under elevated atmospheric vapor pressure deficit. *In*: Sinclair (ed) *Water-conservation traits to increase crop yields in water-deficit environments: case studies*. Springer, Cham, Switzerland, pp 11–16.

Sinclair, T.R. (2017b) Early partial stomata closure with soil drying. *In*: Sinclair TR (ed) *Water-conservation traits to increase crop yields in water-deficit environments: case studies*. Springer, Cham, Switzerland, pp 5–9

Sinclair, T.R. (2018) Effective water use required for improving crop growth rather than transpiration efficiency. *Front Plant Sci* 9:1442. https://doi.org/10.3389/fpls.2018.01442

Sinclair, T.R., and M.M. Ludlow (1986) Influence of soil water supply on the plant water balance of four tropical grain legumes. *Aust J Plant Physiol* 13:329–341. https://doi.org/10.1071/PP9860329

Sinclair, T.R., C.D. Messina, A. Beatty and M. Samples (2010) Assessment across the united states of the benefits of altered soybean drought traits. *Agron J* 102:475–482. https://doi.org/10.2134/agronj2009.0195

Slinkard, K., and V.L. Singleton (1977) Total phenol analysis: automation and comparison with manual methods. *Am J Enol Vitic* 28:49–55

Sohail, Q., T. Inoue, H. Tanaka, A.E. Eltayeb, Y. Matsuoka and H. Tsujimoto (2011) Applicability of *Aegilops tauschii* drought tolerance traits to breeding of hexaploid wheat. *Breed Sci* 61:347–357. https://doi.org/10.1270/jsbbs.61.347

Song, H., X. Xu, H. Wang, H. Wang and Y. Tao (2010) Exogenous γ -aminobutyric acid alleviates oxidative damage caused by aluminium and proton stresses on barley seedlings. *J Sci Food Agric* 90:1410–1416. https://doi.org/10.1002/jsfa.3951

Stewart, C.R., and G. Voetberg (1985) Relationship between stress-induced ABA and proline accumulations and ABA-induced proline accumulation in excised barley leaves. *Plant Physiol* 79:24–27. https://doi.org/10.1104/pp.79.1.24

Strizhov, N., E. Ábrahám, L. Ökrész, S. Blickling, A. Zilberstein, J. Schell, C. Koncz and L. Szabados (1997) Differential expression of two *P5CS* genes controlling proline accumulation during salt-stress requires ABA and is regulated by ABA1, ABI1 and AXR2 in Arabidopsis. *Plant J* 12:557–569. https://doi.org/10.1111/j.0960-7412.1997.00557.x

Sukumaran, S., S. Dreisigacker, M. Lopes, P. Chavez and M.P. Reynolds (2014) Genome-wide association study for grain yield and related traits in an elite spring wheat population grown in temperate irrigated environments. *Theor Appl Genet* 128:353–363. https://doi.org/10.1007/s00122-014-2435-3

Sukumaran, S., M.P. Reynolds and C. Sansaloni (2018) Genome-wide association analyses identify QTL hotspots for yield and component traits in durum wheat grown under yield potential, drought, and heat stress environments. *Front Plant Sci* 9:81. https://doi.org/10.3389/fpls.2018.00081

Szabados, L., and A. Savouré (2010) Proline: a multifunctional amino acid. *Trends Plant Sci* 15:89–97. https://doi.org/10.1016/j.tplants.2009.11.009

Takagi, H., Y. Ishiga, S. Watanabe, T. Konishi, M. Egusa, N. Akiyoshi, T. Matsuura, I.C. Mori, T. Hirayama, H. Kaminaka, *et al.* (2016) Allantoin, a stress-related purine metabolite, can activate jasmonate signaling in a MYC2-regulated and abscisic acid-dependent manner. *J Exp Bot* 67:2519–2532. https://doi.org/10.1093/jxb/erw071

Tamang, B.G., R. Schoppach, D. Monnens, B.J. Steffenson, J.A. Anderson and W. Sadok

(2019) Variability in temperature-independent transpiration responses to evaporative demand correlate with nighttime water use and its circadian control across diverse wheat populations. *Planta* 250:115–127. https://doi.org/10.1007/s00425-019-03151-0

Taylor, N.L., J.L. Heazlewood, D.A. Day and A.H. Millar (2004) Lipoic acid-dependent oxidative catabolism of α-keto acids in mitochondria provides evidence for branched-chain amino acid catabolism in Arabidopsis. *Plant Physiol* 134:838–848. https://doi.org/10.1104/pp.103.035675

Templer, S.E., A. Ammon, D. Pscheidt, O. Ciobotea, C. Schuy, C. McCollum, U. Sonnewald, A. Hanemann, J. Förster, F. Ordon, *et al.* (2017) Metabolite profiling of barley flag leaves under drought and combined heat and drought stress reveals metabolic QTLs for metabolites associated with antioxidant defense. *J Exp Bot* 68:1697–1713. https://doi.org/10.1093/jxb/erx038

Tounsi, S., K. Feki and F. Brini (2019) Abiotic stress signaling in wheat crop. *In*: Hasanuzzaman M, Nahar K, and Hossain M (eds) *Wheat production in changing environment*s. Springer, Singapore, pp 261–282.

Tricker, P.J., A. Elhabti, J. Schmidt and D. Fleury (2018) The physiological and genetic basis of combined drought and heat tolerance in wheat. *J Exp Bot* 69:3195–3210. https://doi.org/10.1093/jxb/ery081

Tsujimoto, H. (2021) Gene-mining asian wheat to feed the population in the 21st century. *Plant Cell Physiol* 62:1–2. https://doi.org/10.1093/pcp/pcaa158

Tsujimoto, H., Q. Sohail and Y. Matsuoka (2015) Broadening the genetic diversity of common and durum wheat for abiotic stress tolerance breeding. *In*: Ogihara Y., S. Takumi and H. Handa (eds) *Advances in wheat genetics: from genome to field.* Springer Japan, Tokyo, pp 233–238

Turner, S. (2018) qqman: an R package for visualizing GWAS results using Q-Q and manhattan plots. *J Open Source Softw* 3:731. https://doi.org/10.1101/005165

Urano, K., K. Maruyama, Y. Ogata, Y. Morishita, M. Takeda, N. Sakurai, H. Suzuki, K. Saito, D. Shibata, M. Kobayashi, *et al.* (2009) Characterization of the ABA-regulated global responses to dehydration in Arabidopsis by metabolomics. *Plant J* 57:1065–1078. https://doi.org/10.1111/j.1365-313X.2008.03748.x

Valifard, M., A. Moradshahi and B. Kholdebarin (2012) Biochemical and physiological responses of two wheat (*triticum aestivum* L.) cultivars to drought stress applied at seedling stage. *J Agric Sci Technol* 14:1567–1578

Van Genuchten, M.T. (1987) A numerical model for water and solute movement in and below the root zone. Riverside, California.

Varela, M.C., I. Arslan, M.A. Reginato, A.M. Cenzano and M.V. Luna (2016) Phenolic compounds as indicators of drought resistance in shrubs from Patagonian shrublands (Argentina). *Plant Physiol Biochem* 104:81–91. https://doi.org/10.1016/j.plaphy.2016.03.014

Verbruggen, N., and C. Hermans (2008) Proline accumulation in plants: a review. *Amino Acids* 35:753–759. https://doi.org/10.1007/s00726-008-0061-6

Vogt, T. (2010) Phenylpropanoid biosynthesis. *Mol Plant* 3:2–20. https://doi.org/10.1093/mp/ssp106

Watanabe, S., M. Matsumoto, Y. Hakomori, H. Takagi, H. Shimada and A. Sakamoto (2014)

The purine metabolite allantoin enhances abiotic stress tolerance through synergistic activation of abscisic acid metabolism. *Plant, Cell Environ* 37:1022–1036. https://doi.org/10.1111/pce.12218

World Health Organization (2018) The state of food security and nutrition in the world 2018: building climate resilience for food security and nutrition. Food & Agriculture Org. Rome

Yadav, A.K., A.J. Carroll, G.M. Estavillo, G.J. Rebetzke and B.J. Pogson (2019) Wheat drought tolerance in the field is predicted by amino acid responses to glasshouse-imposed drought. *J Exp Bot* 70:4931–4948. https://doi.org/10.1093/jxb/erz224

Yamburenko, M. V., Y.O. Zubo, R. Vanková, V. V. Kusnetsov, O.N. Kulaeva and T. Börner (2013) Abscisic acid represses the transcription of chloroplast genes. *J Exp Bot* 64:4491–4502. https://doi.org/10.1093/jxb/ert258

Yaqoob, M. (2016) Estimation of Genetic Variability, heritability and genetic advance for yield and yield related. *J Agric Res* 54:1–14

Yousaf, M.J., A. Hussain, M. Hamayun, A. Iqbal, M. Irshad, A. Ahmad and I.-J. Lee (2019) Phytohormonal cross-talk modulate *Bipolaris sorokiniana* (Scc.) interaction with *Zea mays*. *bioRxiv* 847061. https://doi.org/10.1101/847061

Yu, J., G. Pressoir, W.H. Briggs, I.V. Bi, M. Yamasaki, J.F. Doebley, M.D. McMullen, B.S. Gaut, D.M. Nielsen, J.B. Holland, *et al.* (2006) A unified mixed-model method for association mapping that accounts for multiple levels of relatedness. *Nat Genet* 38:203–208. https://doi.org/10.1038/ng1702

Yue, B., W. Xue, L. Xiong, X. Yu, L. Luo, K. Cui, D. Jin, Y. Xing and Q. Zhang (2006) Genetic basis of drought resistance at reproductive stage in rice: Separation of drought tolerance from drought avoidance. *Genetics* 172:1213–1228. https://doi.org/10.1534/genetics.105.045062

Zadoks, J.C., T.T. Chang and C.F. Konzak (1974) A decimal code for the growth stages of cereals. *Weed Res* 14:415–421. https://doi.org/10.1111/j.1365-3180.1974.tb01084.x

Zampieri, M., A. Ceglar, F. Dentener and A. Toreti (2017) Wheat yield loss attributable to heat waves, drought and water excess at the global, national and subnational scales. *Environ Res Lett* 12:064008. https://doi.org/10.1088/1748-9326/aa723b

Zanke, C.D., J. Ling, J. Plieske, S. Kollers, E. Ebmeyer, V. Korzun, O. Argillier, G. Stiewe, M. Hinze, K. Neumann, *et al.* (2014) Whole genome association mapping of plant height in winter wheat (*Triticum aestivum* L.). *PLoS One* 9:e113287. https://doi.org/10.1371/journal.pone.0113287

Zhang, X., H. Feng, C. Feng, H. Xu, X. Huang, Q. Wang, X. Duan, X. Wang, G. Wei, L. Huang, *et al.* (2015) Isolation and characterisation of cDNA encoding a wheat heavy metal-associated isoprenylated protein involved in stress responses. *Plant Biol* 17:1176–1186. https://doi.org/10.1111/plb.12344

Zhao, C., B. Liu, S. Piao, X. Wang, D.B. Lobell, Y. Huang, M. Huang, Y. Yao, S. Bassu, P. Ciais, *et al.* (2017) Temperature increase reduces global yields of major crops in four independent estimates. *Proc Natl Acad Sci U S A* 114:9326–9331. https://doi.org/10.1073/pnas.1701762114

List of publications

Chapter 1

Title: Genomic analysis of heat and combined heat–drought resilience in bread wheat under field conditions

Authors: Itam, M. O., Mega, R., Gorafi, Y. S. A., Yamasaki, Y., Tahir, I. S. A., Akashi, K. and Tsujimoto, H

Journal: under review

Chapter 2

Title: Genetic variation in drought resilience-related traits among wheat multiple synthetic derivative lines: insights for climate resilience breeding

Authors: Itam, M. O., Gorafi, Y. S. A., Tahir, I. S. A. and Tsujimoto, H.

Journal: Breeding Science

Published online: August 2021

Chapter 3

Title: Transpiration response of two bread wheat lines differing in drought resilience and their backcross parent under dry-down conditions

Authors: Itam, M. O., Wahbi, A., Fujimaki, H. and Tsujimoto, H.

Journal: Accepted in Breeding Science (September, 2021)

Chapter 4

Title: Metabolic and physiological responses to progressive drought stress in bread wheat

Authors: Itam, M., Mega, R., Tadano, S., Abdelrahman, M., Matsunaga, S., Yamasaki, Y., Akashi, K. and Tsujimoto, H.

Journal: Scientific Reports 10 (17189): 1–14.

Published online: October 2020

Chapter 5

Title: *Aegilops tauschii* introgressions improve physio-biochemical traits and metabolite plasticity in bread wheat under drought stress

Authors: Itam, M., Abdelrahman, M., Yamasaki, Y., Mega, R., Gorafi, Y., Akashi, K. and Tsujimoto, H.

Journal: Agronomy 10 (1588): 1–17.

Published online: October 2020